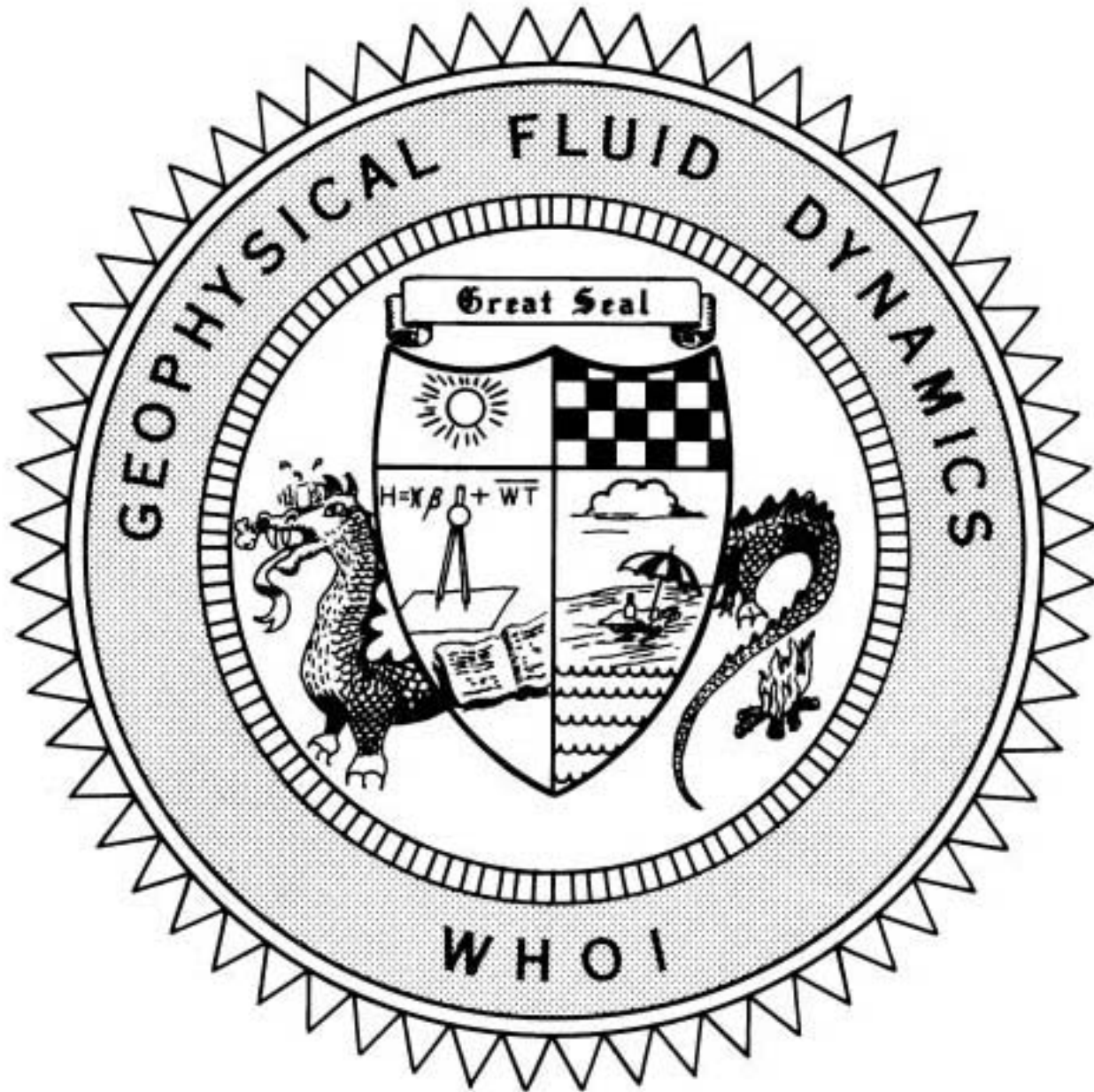# 1979

VOLUME I

COURSE LECTURES

SEMINARS

ABSTRACTS OF SEMINARS

WHOI-79-84

1979 SUMMER STUDY PROGRAM
IN
GEOPHYSICAL FLUID DYNAMICS
THE WOODS HOLE OCEANOGRAPHIC INSTITUTION

NOTES ON POLAR OCEANOGRAPHY

By

Melvin E. Stern, Director
and
Florence K. Mellor, Editor

WOODS HOLE OCEANOGRAPHIC INSTITUTION
Woods Hole, Massachusetts 02543

November 1979

TECHNICAL REPORT

Prepared for the Office of Naval Research under
Contract N00014-79-C-0671

Approved for Distribution

_____
Charles D. Hollister
Dean of Graduate Studies

1979 SUMMER STUDY PROGRAM

in

GEOPHYSICAL FLUID DYNAMICS

at

THE WOODS HOLE OCEANOGRAPHIC INSTITUTION

NOTES ON POLAR OCEANOGRAPHY

EDITOR'S PREFACE

VOLUME I

The emphasis in this year's GFD program has been somewhat different from the past. We have tried to expose a theoretically oriented audience to the new body of observations pertaining to the Arctic and Antarctic circulation. We have, however, not departed from our traditional goal of encouraging broad based inquiries into the field of Geophysical Fluid Dynamics. We would like to believe that the breadth of interest and enthusiasm exhibited in these reports will stimulate future work in Polar Oceanography and Fluid Dynamics.

The Steering Committee of GFD is particularly grateful to Dr. Michael McCartney to the point where they record much more closely what he said rather than the students' interpretation of his lectures. In that sense this volume departs from the records of the programs of previous years. Mrs. Florence Mellor has assembled all of the reports, and particular thanks for unstinting help also goes to Mr. A. L. Peirson of W.H.O.I. Without the sympathetic understanding of Dr. Ralph Cooper, and the financial support of ONR, NASA, and NOAA this year's GFD program would have been in the "doldrums" and not in "high latitudes"!

Melvin E. Stern

CONTENTS OF VOLUME I

COURSE LECTURES ON POLAR OCEANOGRAPHY

by

Michael S. McCartney
Woods Hole Oceanographic Institution

SEMINARS and ABSTRACTS OF SEMINARS

CONTENTS OF VOLUME I (continued)

v

CONTENTS OF VOLUME I (continued)

Page No.

CONTENTS OF VOLUME I (continued)

CONTENTS OF VOLUME II: LECTURES OF THE FELLOWS

COURSE LECTURES

By

Michael S. McCartney

Woods Hole Oceanographic Institution

Lecture #1.   GLOBAL OCEANS

1.   Regions of the World Oceans

Usually the world's oceans are divided into different regions; tropical, subtropical, subpolar and polar regions. A decision of what area belongs to what region is made through looking at near surface characteristics (fronts or convergences). The ocean area north of the Arctic front ($\sim 60^O$N) and south of the Antarctic front ($\sim 60^O$S) is called polar. The adjacent area down to the Subtropical Convergence ($\sim 45^O$N or $\sim 45^O$S) is the subpolar region (Fig. 1, Defant, 1961). Fronts (large temperature gradients) do not always coincide with the convergences. The polar oceans cover 10% of the world's ocean surface, whereas polar and subpolar oceans cover 26%. These areas are characterized by a net heat loss.

At high latitudes the ocean is covered with sea ice. The sea ice cover exhibits a pronounced annual cycle, the amplitude of which is strongly longi-tudinal dependent. Large amplitudes are to be found in the Weddell Sea and Ross Sea (Antarctica) and in the Davis Strait, East Greenland Sea and Barents Sea (Arctic). Sea ice has a strong effect on the air–sea interaction. It acts as a thermal insulator and decreases the momentum transport. On the other hand, it produces cold and highly saline water in wintertime due to brine ex-pulsion. This dense water is a major source of Arctic and Antarctic deep and bottom water.
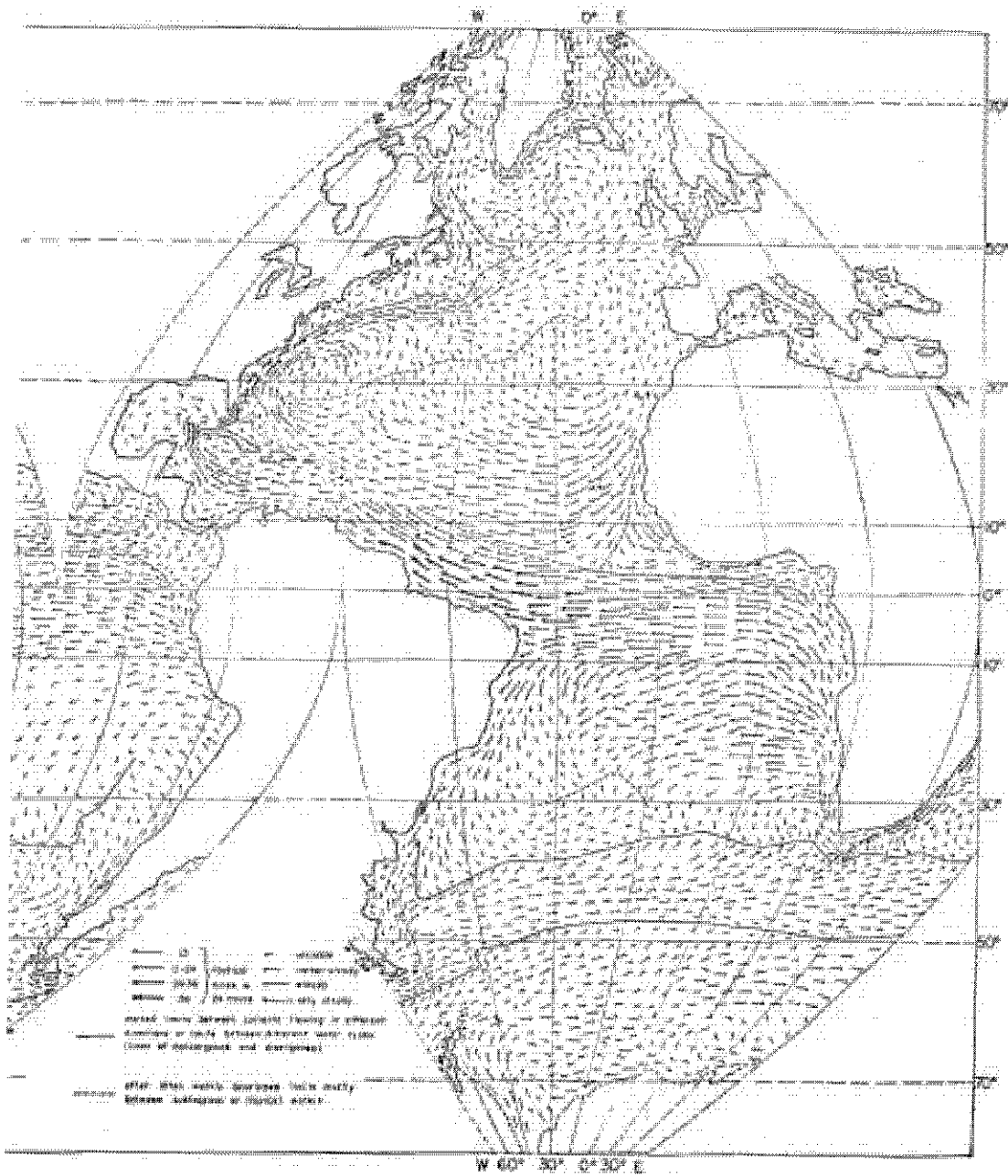
Fig. 1. Surface currents of the Atlantic Ocean during northern hemisphere winter, from Defant (1961, Plate 8, after Schott's work of the 1930's).

The geography, which has a strong effect on sea ice variation and ocean circulation, is totally different for South and North Pole. The Arctic Ocean is surrounded by continents and there is only one major (shallow) out-flow region of the Greenland–Iceland–Scotland ridge. The Bering Strait and the Barents Sea are too shallow (< 100m) to account for large water mass exchange. Therefore, the interaction of the Arctic Basin with the North Atlantic and the North Pacific is only weak.

At the South Pole the Antarctic continent is surrounded by an open ocean. The sea ice can move freely and the annual cycle is larger than in the landlocked Arctic Basin. Exchanges of upper layer water between the subtropical gyres to the north and the circumpolar stream are unobstructed. The surrounding circumpolar ridges prevents the cold water of the Weddell Sea and the Ross Sea of going north easily. But there are some holes in the ridge system where the Antarctic Bottom Water leaks out. The influence of this dense water $(-0.4^{\circ}C$, S = 34.66 o/oo) is recognized in all three oceans.

2. Water Characteristics of the World Oceans

77% of ocean water has a temperature of less than $4^{\circ}C$. The salinity of this water mass ranges from 34.2 o/oo to 35.2 o/oo (shaded area in Fig. 2). It is of polar and subpolar origin and most of this volume is found below the main thermocline in the three major oceans.

23% of the ocean water is warmer than $4^{\circ}C$. This "central water" is located within the main thermocline in the world's major basins.

In the world ocean volumetric T–S diagram, (Fig. 2), the central water forms the three warm branches. The old thermocline idea (cold water upwelling balancing diffusion of heat downward) could explain these ridges. They would be interpreted as the result of vertical mixing of warm subtropical water

(18° water in the Atlantic) and cold polar water (Labrador Sea Water, Antarctic Intermediate Water), which is advected equatorward through the deep ocean circulation. In such a two point mixing scheme, one would have to be able to rationalize the maintenance of the end member water-type pools.

Since it is easier to move than to mix water masses in the deep ocean, temperature, salinity and O_2 provide useful tags to trace the movement of deep ocean water masses. This has been done since the middle of the last century. The overall interpretation of the structure of the meridional circulation that emerged has not changed very much since the 1930's. It is instructive to reexamine the historical development of this traditional interpretation.

3. Deep Atlantic Circulation (Historical Review)

A valuable hypothesis on the deep ocean circulation was introduced by A. von Humboldt (1814). He found that the temperatures in the deeper layers of the oceans at low latitudes were too low to be explained through local sinking of surface waters that were cooled during wintertime. He assumed a deep ocean current coming from the poles to the equator, whereas a surface current flows from the equator to the poles. The driving forces of this circulation he suggested to be the density differences due to temperature differences. Salinity differences did not play an important role in Humboldt's image of this circulation.

E. Lenz (1847) found that the temperatures in the deeper tropical oceans were lower than at the same level in the subtropics. Therefore, he concluded that the north-south deep ocean current turns to the surface at the equator. He assumed a Hadley cell type of ocean circulation with sinking cold water at the poles, deep advection to the tropics, upwelling at the equator and a poleward surface current.
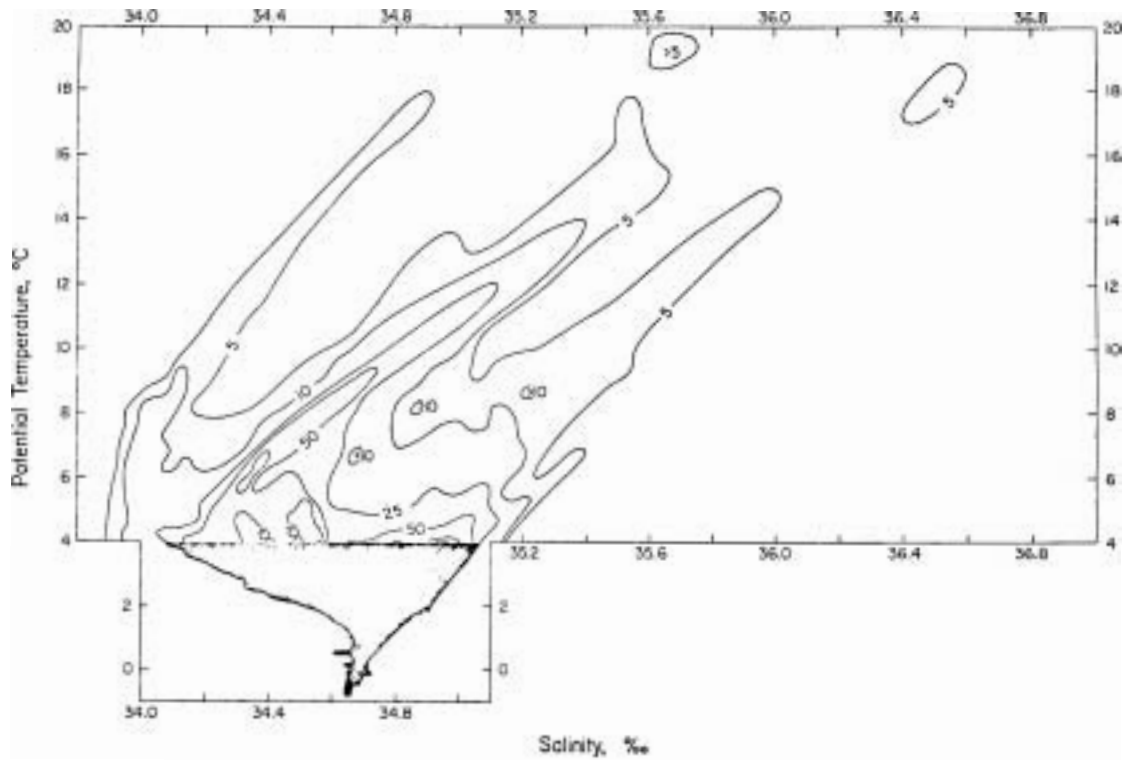
Fig. 2. A contoured volumetric potential temperature–salinity diagram prepared by L. V. Worthington. The contour values are the volumes in $10^3 km^3$ found in each class of $0.1^\circ C$ and $.01\%$. Contours are not shown for the water colder than $4^\circ C$, which includes 77% of the World Ocean volume. The right diagonal branch is the North Atlantic, with an isolated mode at $18^\circ C$. The left diagonal branch is the North Pacific. The middle branch is the west of the World Ocean, diminished by the Subantarctic Mode Water of McCartney (1977).
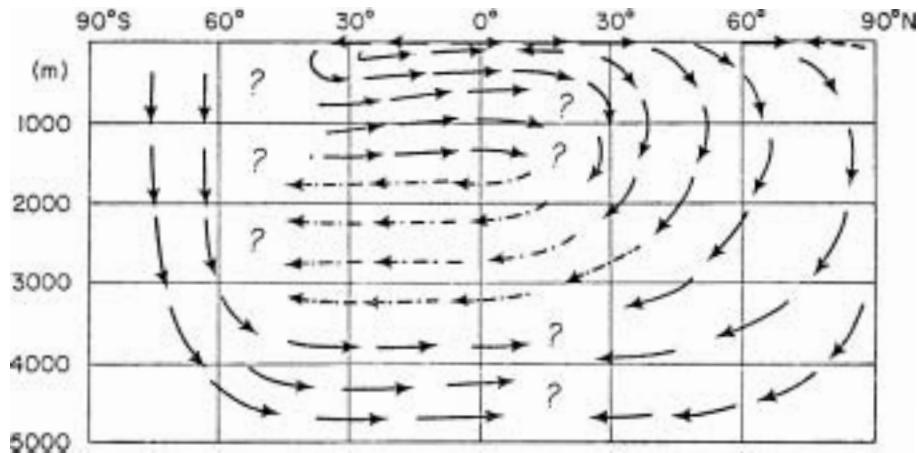
Fig. 3. The meridional circulation of the Atlantic Ocean from the discussions by Buchanan (1885) and Buchan (1895) of the CHALLENGER Expedition data. The sketch was made by Merz and Wust (1922) as their interpretation of the texts of the earlier papers.

Half a century later Buchanan(1885) and Buchan (1895) found from the
CHALLENGER data that the salinity distribution in the tropics is in contradic-
tion with the Lenz type of ocean circulation. There seems to be no strong
vertical movement of ocean water at the equator, and they found flow across
the equator, so that the oceanic hemispheres were not isolated.

Merz and Wüst(1922) drew a meridional picture of Buchanan's and
Buchan's interpretation of the CHALLENGER observations (Fig. 3). The main
characteristics were downwelling over the entire North Atlantic (> 20°N)
and in the Southern Ocean (> 60°S), whereas mainly horizontal flow occurs
in the tropical Atlantic and the subtropical region of the South Atlantic.
The three sets of question marks are interesting, because we would still have
to insert them today; what happens at $15^{\circ} - 20^{\circ}$N in the Atlantic, where
the fresh water of South Atlantic origin encounters the salty waters of the
North Atlantic? How do the North Atlantic Deep Water components originating
in the North interact with the Antarctic Bottom Water flowing into the North
Atlantic from the south? What happens at the southern hemisphere Polar Front:
what is the ultimate fate of the southward flowing North Atlantic Deep Water
and how is Antarctic Intermediate Water formed?

Brennecke(1909, 1921) obtained meridional sections from both sides
of the Atlantic. His interpretations of the two sections are repeated here
(Fig. 4).

In the earlier section(east side, Fig. 4a) he adhered to the Lenz
hemispheric meridional cell interpretation at the equator, and indicated a
general northward movement in the upper 2000 meters as the eastern limb of the
subtropical anticyclone. The later section (West Side, Fig. 4b) shows the
recognition of transequatorial flows, convection in the subantarctic zone at

Surface Currents of the Atlantic Ocean

Deep Circulation (East side of the Atlantic Ocean)
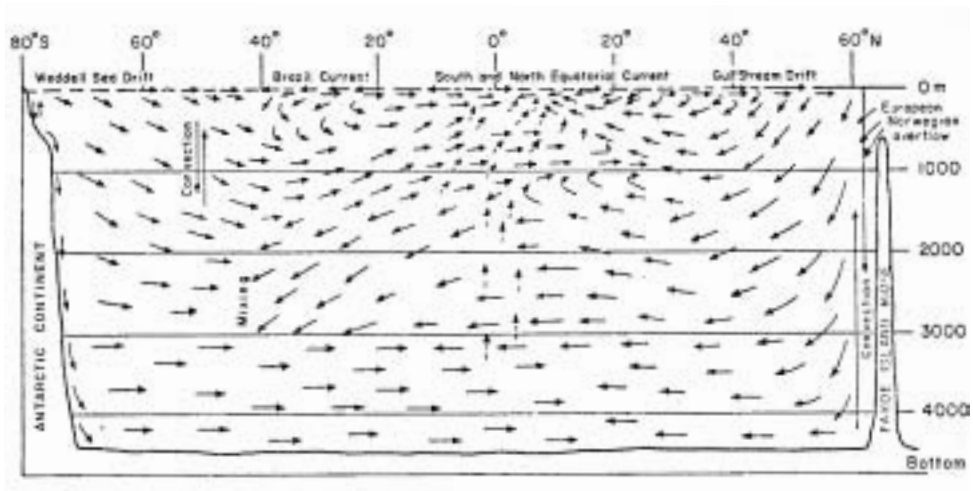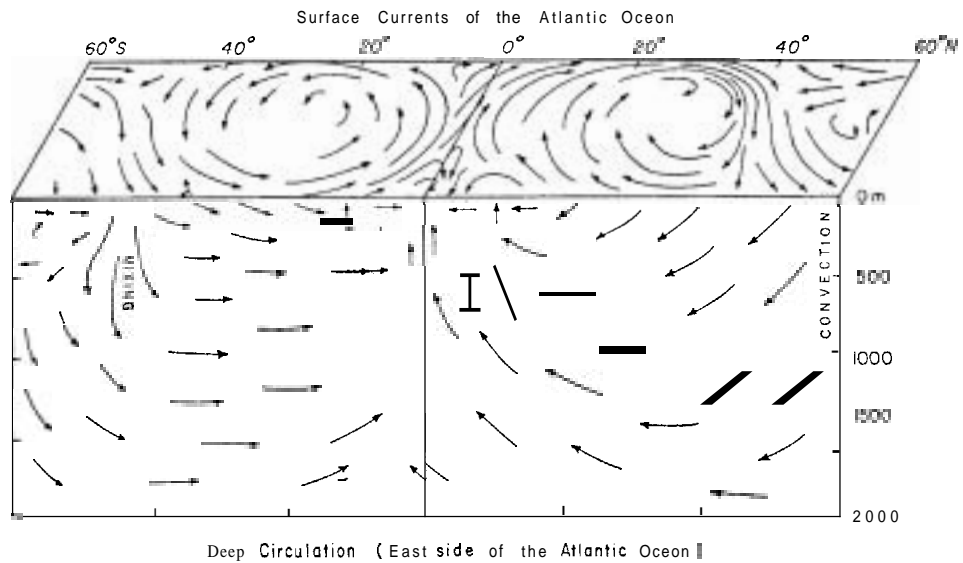
Fig. 4. Brennecke's interpretation of the Atlantic circulation.
(a) East side of Atlantic, using the Planet expedition data (Brennecke, 1907).
(b) West side of Atlantic, using the Deutschland expedition data (Brennecke, 1921).

50°S, the need for mixing between the pools of North Atlantic Deep Water and Circumpolar Deep Water, and the participation of Norwegian Sea overflows in determining the characteristics of the deep North Atlantic. On the basis of the existence of low salinity Intermediate Water in the southwest of the South Atlantic subtropical layers, the concept of a shallow gyre was hypothesized, with a level of no motion near 500 meters. This is a crucial step in the evolving meridional circulation picture. At Antarctica, an early representation of continental slope Bottom Water formation is indicated.

This picture was detailed further by Wüst (1935) using the data of the German Atlantic Expeditions (1925-1927). His salinity distribution for the western Atlantic Ocean (Fig. 5) shows a pronounced salinity minimum "tongue" that starts from the surface at 50°S heading down to a depth of 1000 m at which it remains until it reaches 20°N. This Antarctic Intermediate Water (or Subantarctic Intermediate Water as Wüst called it) is characterized by a salinity minimum and O_2 maximum. The surfacing of the low salinity tongue at 50° - 60°S was taken as evidence that the Antarctic Intermediate Water is formed right at the surface at the Antarctic Convergence. The second feature of this figure is the southward movement of high saline North Atlantic Deep Water beneath the Antarctic Intermediate Water. Three cores were recognized in the layer: an upper salinity maximum derived from the Mediterranean Influence, and two oxygen maxima derived from northern polar water influence.

In 1933 Sverdrup completed the picture of what is going on at the Antarctic Convergence from DISCOVERY II data from the Drake Passage region. His method as well as Wüst's was a meridional cell core layer study. This technique is shown in Fig. 6. McCartney (1979) has described the method as
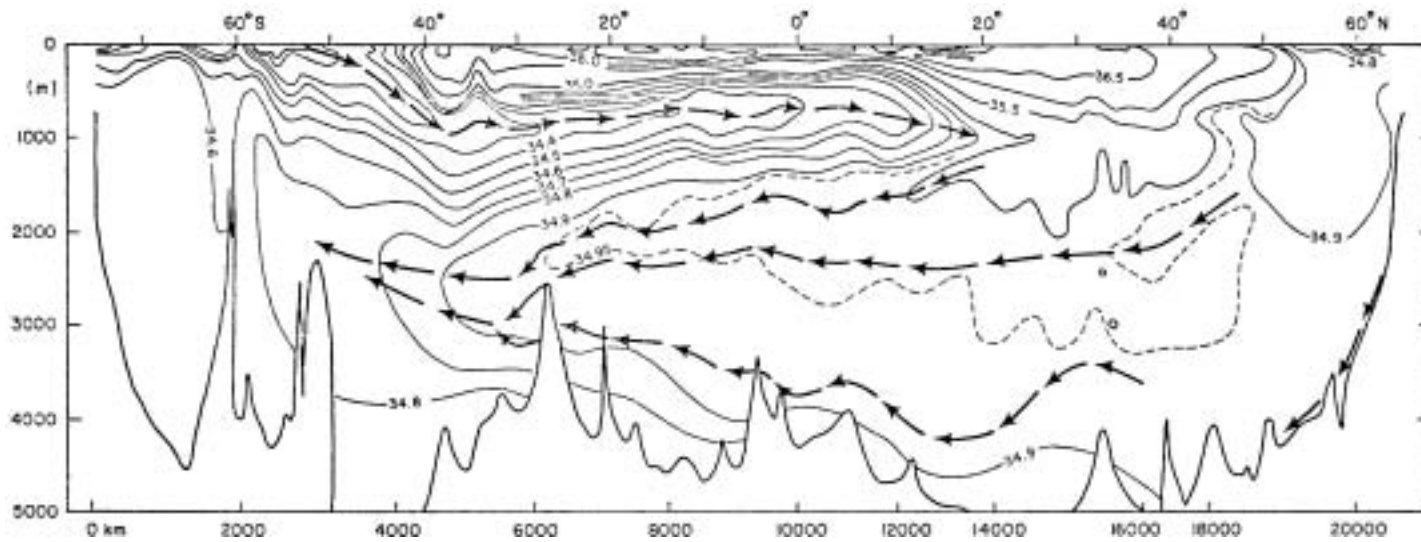
Fig. 5.   Salinity section, western Atlantic (Wust, 1935).   The four sets of arrows represent the vertical salinity minimum, salinity maximum, upper oxygen maximum, and lower oxygen maximum that Wust used to define the Subantarctic Intermediate Water, the Upper, Middle, and Lower North Atlantic Deep Water, respectively, from top to bottom.   The direction of the arrows indicates the direction of spreading of the water mass.
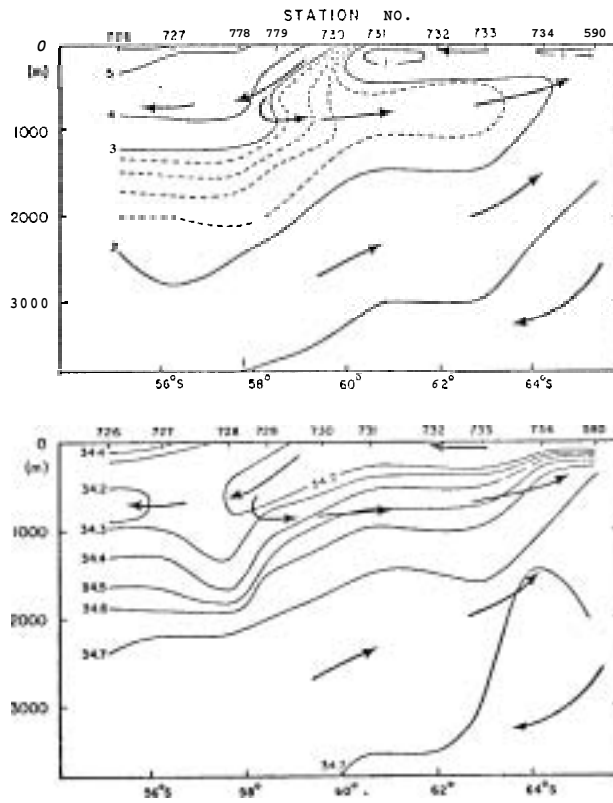
Fig. 6.   An example of Sverdrup's (1933) technique of inference of meridional flow components from core layers.
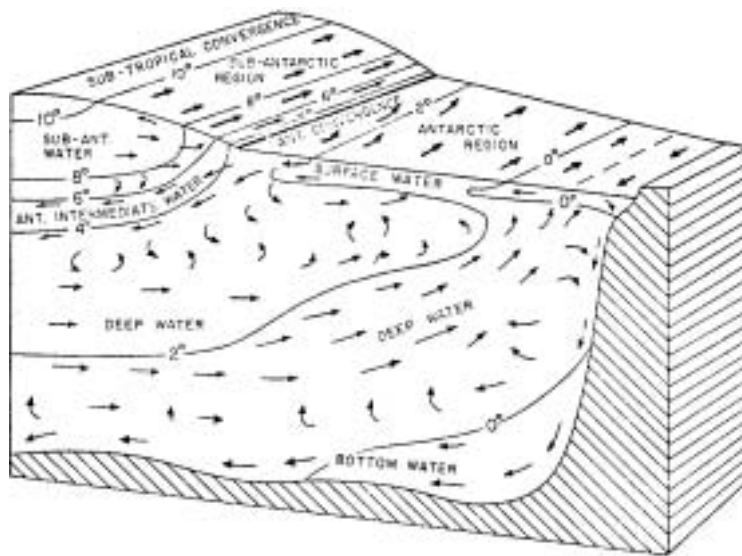
Fig. 7.   Figure 164 from Sverdrup, Johnson and Fleming (1942).

follows: "It is assumed that the axis of the meridional flow lies at the center of a layer of some extreme property, with the flow sense being directed away from the region of greatest extreme in the property. In Fig. 6 several different cores are used. The salinity minimum axis is used to define the actual Antarctic Intermediate Water flow, with the sinking between Stations 729 and 730 being defined from salinity alone. An intermediate return current has been inferred from the temperature field alone -- the inversions at Stations 729 and 730, and the axis of warm intermediate layer south of Station 730. The shallow minimum temperature layer is used to infer northward movement of Antarctic Surface Water towards the convergence. Finally, the deep salinity maximum is used to infer a southward rising flow of deep water."

The final stage of development of the traditional meridional cell concept was the extrapolation to the circumpolar ocean of the scheme Sverdrup had constructed from the Drake Passage data. Figure 7 is an often repeated figure(164 from Sverdrup, Johnson & Fleming, 1942) depicting the meridional flow in the Southern Ocean. The actual temperature field corresponds to that south of Australia. It indicates that the Antarctic Intermediate Water is formed at the Antarctic Convergence by mixing northward flowing low salinity Antarctic Surface Water with southward flowing higher salinity Subantarctic Water. The resulting denser Antarctic Intermediate Water sinks and flows northward underneath the Subantarctic Water. At a still deeper level, Deep Water is moving southward rising to the surface in the Antarctic region where it is cooled and partly enriched with salt from the sea ice brine expulsion. This highly dense water is the major source of the Antarctic Bottom Water that is sinking in a narrow region down the continental shelf and moving northward at the bottom of the ocean.

The focus, since this figure was published, has been on the nature of the supposed convergences mixing process. We will later address the more fundamental issues of whether this picture is correct either locally at any meridian or globally as a zonal average, and what processes control the formation of Antarctic Intermediate Water.

<div align="center">REFERENCES</div>

Brennecke, W., 1909. Ozeanographie. Forschungsreise S.M.S. "Planet" 1906/07, 3, x–154 p.

Brennecke, W., 1921. Die ozeanographischen Arbeiten der Deutschen Antarktischen Expedition 1911–1912. Arch dtsch. seewarte, 39, 1, VI–216 p.

Buchan, A., 1895. Report on oceanic circulation, based on the observations made on board H.M.S. Challenger, and other observations. Rep. Voy. Challenger 1873–76, Summary, 2, Appendix (Physics and Chemistry, pt. 8), 38 p.

Buchanan, J. Y., 1885. Narrative of the cruise of H.M.S. Challenger. Rep. Voy. Challenger 1873–76, Narrative, 1, 2, pp. 948–1003.

Defant, A., 1961. Physical Oceanography. Oxford: Pergamon Press.

Lenz, E. von, 1847. Bericht über die ozeanischen temperature in verschiedenen Tiefen. Bull., Cl. hist. phil. Acad. Sci., Petersburg 3, suppl.11–12.

McCartney, M. S., 1979. On the formation and circulation of Antarctic Intermediate Water.

Merz, A. and G. Wust, 1922. Die atlantische vertikalzirkulation. Z. Ges. Erdk. Berl, 102, 1–35.

Sverdrup, H. U., 1933. On vertical circulation in the ocean due to the action of the wind with application to conditions within the Antarctic circumpolar current. Discovery Reports 7, 139–170.

Sverdrup, H. U., M. W. Johnson, and R. H. Fleming, 1942. The Oceans: their physics, chemistry, and geobiology. Prentice–Hall, 1087 p.

Wust, G., 1935. The stratosphere of the Atlantic Ocean. Scientific results of the German Atlantic expedition of the research vessel "Meteor" 1925–27, 6, 1, 109–288.

FURTHER READING

Cochrane, J. D., 1958. The frequency distribution of water characteristics in the Pacific Ocean. Deep-sea Res., 5, 111–127.

Deacon, G.E.R., 1933. A general account of the hydrology of the South Atlantic Ocean. Discovery Reports, 7, 171–238.

Deacon, G.E.R., 1937. The hydrology of the Southern Ocean. Discovery Reports, 15, 1–124.

Merz, A., 1925. Die atlantische Hydrophie und die Planlegung der Deutschen Atlantischen Expedition. S. B. preuss. Akad. Wiss., 21, 562–586.

Montgomery, R. B., 1958. Water characteristics of Atlantic Ocean and of world ocean. Deep-Sea Res., 5, 134–148.

Pollak, M. J., 1958. Frequency distribution of potential temperatures and salinities in the Indian Ocean. Deep-Sea Res., 5, 128–133.

Schott, G., 1902. Oceanographic und Maritime Meteorologie. Wiss. Ergebn. 'Valdivia', 1, XII–404 p.

Notes Submitted by
Peter Lemke

Lecture #2.   SUBTROPICAL GYRES ONE

Subtropical gyres have historically generated much interest and research. As a result, much has been written on the topic, especially with respect to the North Atlantic.

Probably the most obvious feature of the North Atlantic Subtropical Gyre is the Gulf Stream (Fig. 1). South of the stream lie the closed contours of the interior of the gyre (the Sargasso Sea) and much recent discussion has centered on just how big this interior is.

There is a poleward shift of the center of the isopycnal depression that marks the gyre (Figs. 2A–F), which moves from $25^{\circ}N$ at $\sigma_t = 26.5$ to $38^{\circ}N$ at $\sigma_t = 27.8$. There is a very thick lens of heated water filling this depression that was first noted by the Challenger expedition (Fig. 3).
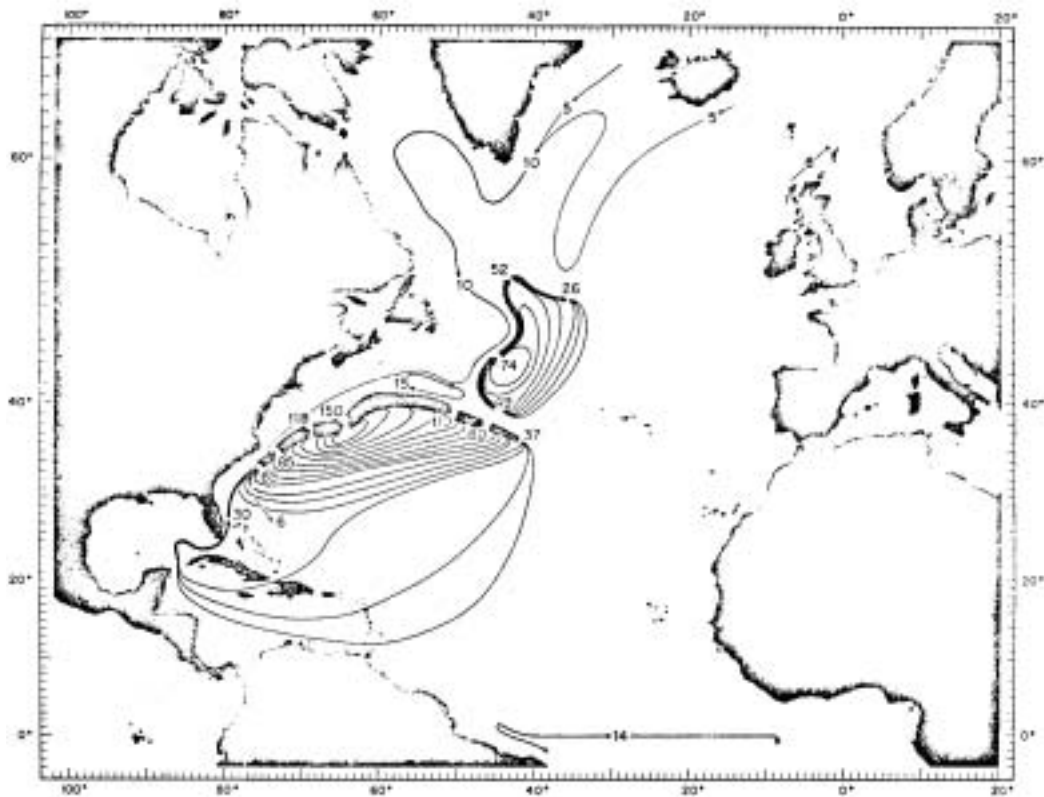
Fig. 1.   Circulation diagram for the total top to bottom
          circulation in the North Atlantic (Worthington, 1976,
          Fig. 42).
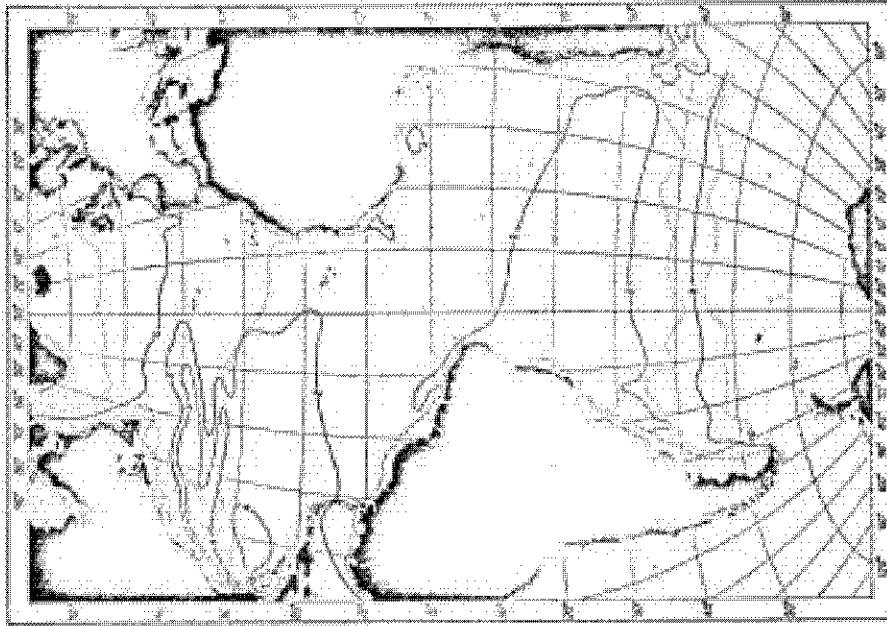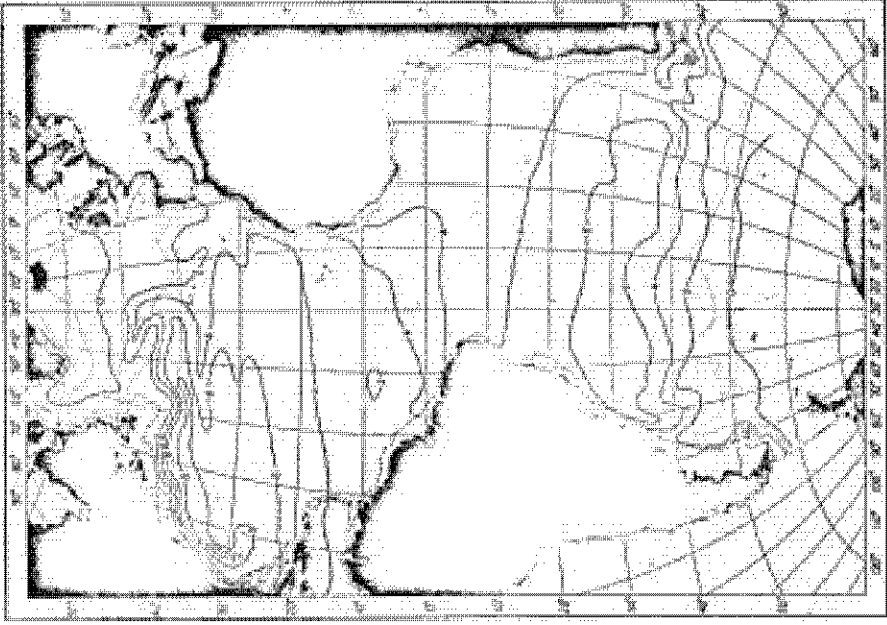
Fig. 2. Topography of density surfaces in the Atlantic
(Montgomery and Pollak, 1947).
= 27.0   C = 27.2   D = 27.4   E = 27.6   F = 27.8
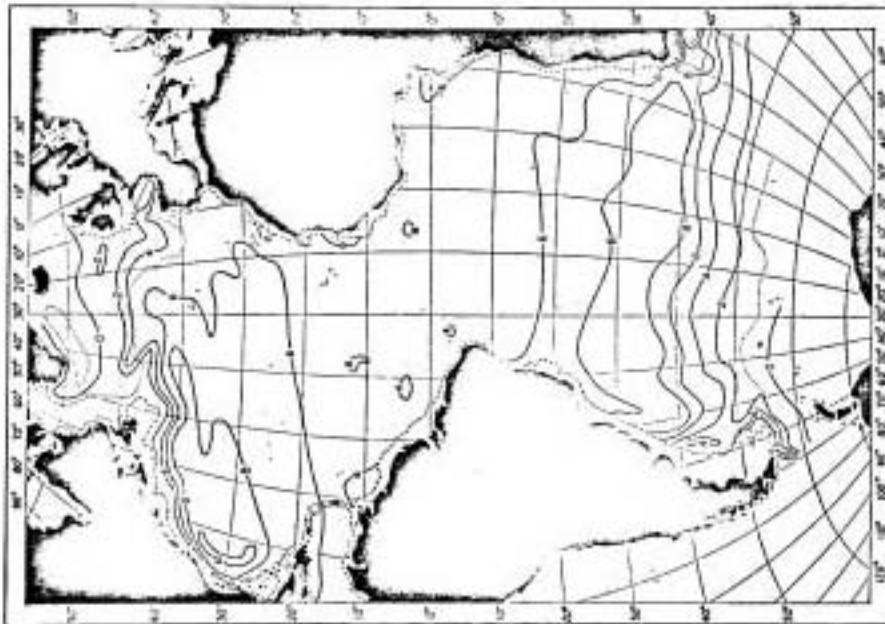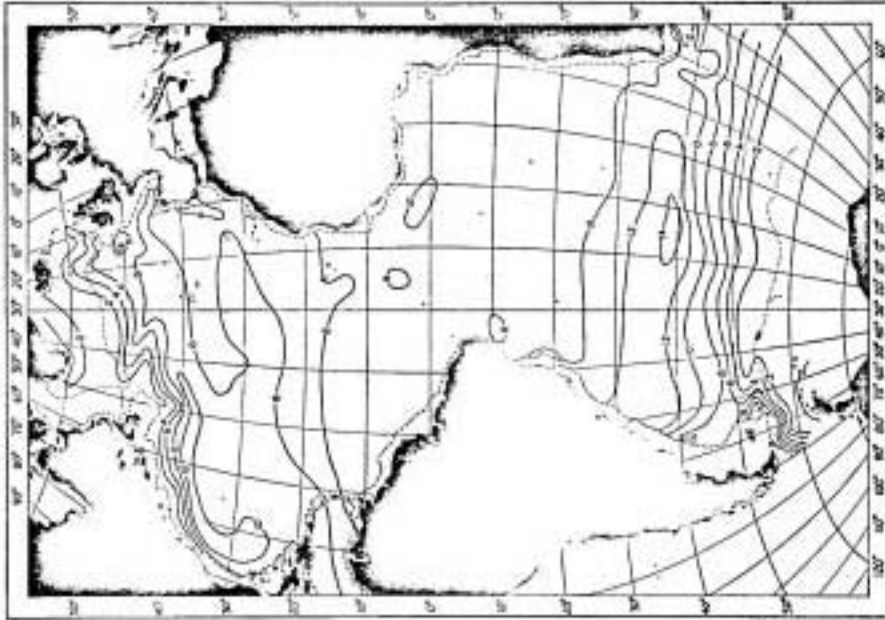
E
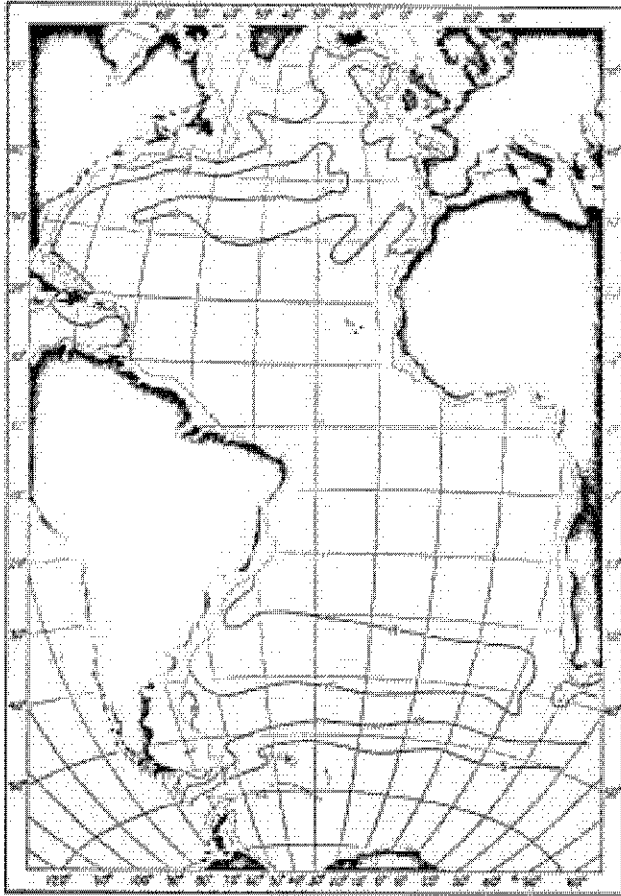
F
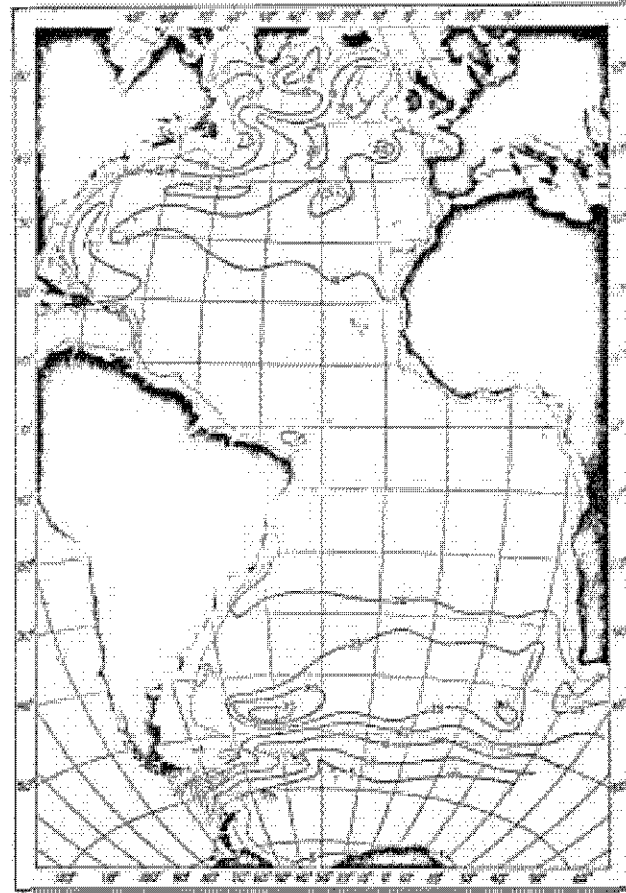
A high salinity field matches the temperature and is also quite thick. This may be contrasted with the South Atlantic Subtropical gyre where the high salinity and temperature layer is relatively thin. This added to the initial impression of early investigators that the South Atlantic gyre circulation is restricted to the uppermost water.

Atlantic

There is a nearly linear T–S relation as you go from the warmest Subtropical Waters to the cold deep waters within the Sargasso Sea (Fig. 4). Iselin (1936) considered this linear relation and postulated that it was due to the vertical mixing between two disparate water types. But, in order to explain why the T–S relation was curved at all, he was forced to include lateral mixing of fresh or salty water.

By 1939 he had changed his mind and postulated that the water types at intermediate depths have been formed at the surface. Subsequent sinking along a surface of constant density gave the observed characteristics. For supporting evidence he noted that the T–S relation along a meridian in the center of the North Atlantic is very similar to the vertical T–S curve between the 20° and 8° isotherms. This theory was later modified in Sverdrup, Johnson and Fleming (1942) to include the effects of lateral and vertical mixing (Fig. 5).

Heat Budget

Using bulk aerodynamic formulas for surface heat flux as a function of temperature, humidity, and other parameters, the surface heat budget can be calculated and contoured (Fig. 6). Large heat losses to the atmosphere can be seen on the western side of the gyre where warm water is carried north by the Gulf Stream. Conversely, there is a heat gain on the eastern side of the
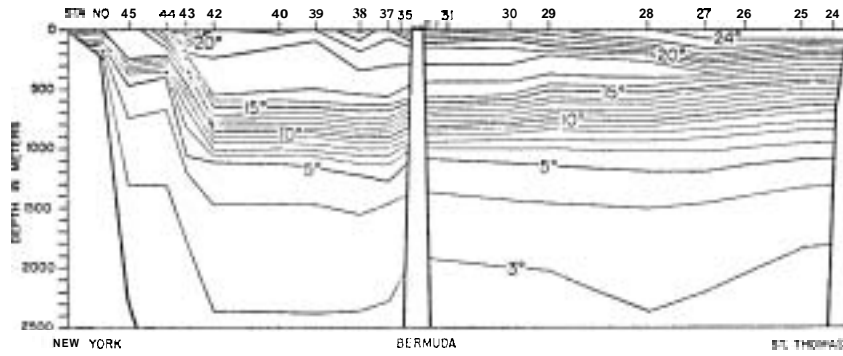
Fig. 3. The Eighteen Degree Water thermostad of the
         Sargasso Sea as discovered by the CHALLENGER
         Expedition in 1873. (Worthington, 1976, Fig. 32).
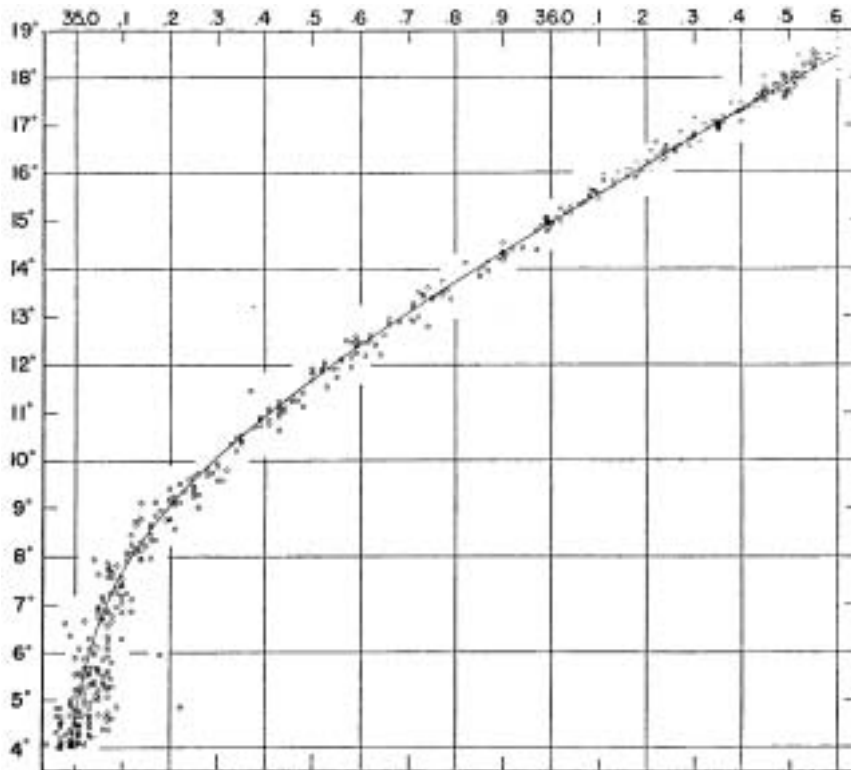
Fig. 4. The temperature-salinity correlation in the northwest
         Atlantic. (Iselin, 1936).
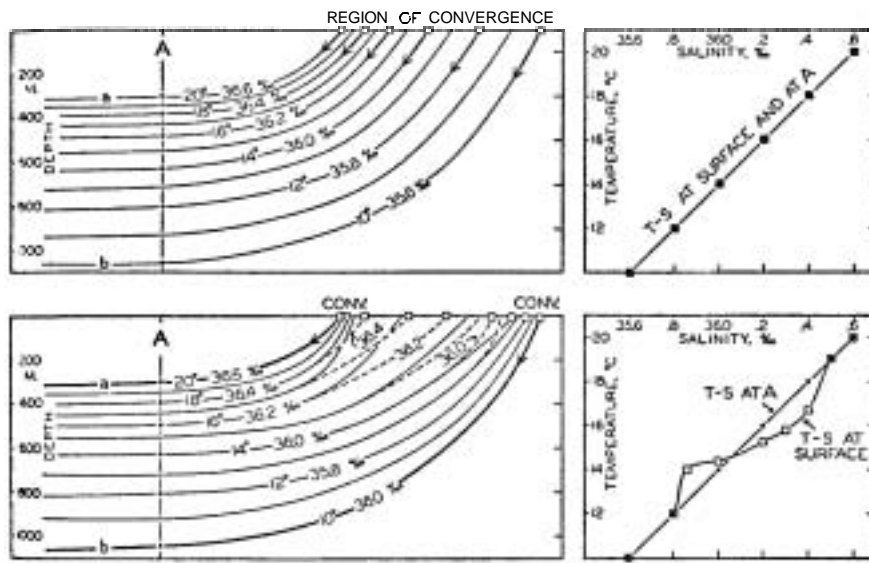
Fig. 5.   Production of temperature-salinity correlation by
          sinking along density surfaces. (Sverdrup, Johnson,
          Fleming, 1942, Fig. 36).
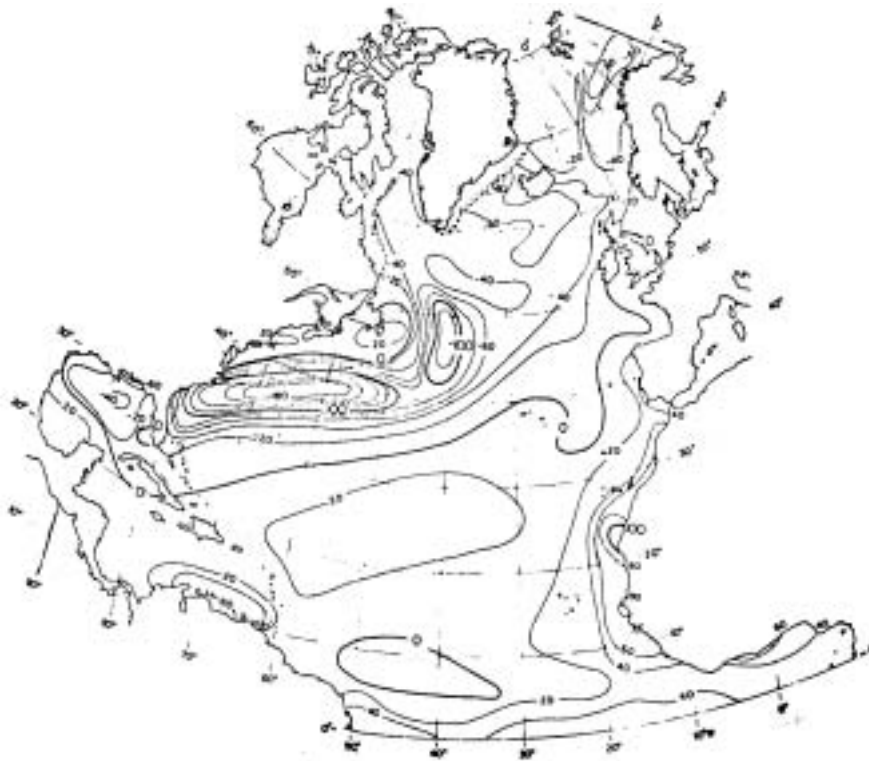
Fig. 6.   Net annual air-sea heat exchange in the North Atlantic
          Ocean after Bunker and Worthington, 1976.

gyre where the return flow of cold water is southward. There are also large
seasonal cycles superimposed on this mean picture.

These heat exchanges are quite significant and can change near-surface
densities substantially. This makes drawing a closed gyre, using density
measurements, quite difficult.

Further complicating the situation is the evaporation/precipitation budget
which changes sign at 40°N (Fig. 7).   However, overall, gyres seem to gain
fresh water due to precipitation.

18° Water

South of the Gulf Stream and above the main thermocline there is a thick
layer of nearly isotherm and isohaline water with a temperature near 18°
(Fig. 3). It is ubiquitous throughout the Sargasso Sea and shows up as an
isolated high volume "mode" in a temperature-salinity volumetric chart
(Lecture 1, Fig. 2). There is a temptation to explain the T-S character-
istics of water at intermediate depths by using this 18° water as a "parent"
in a vertical mixing process:
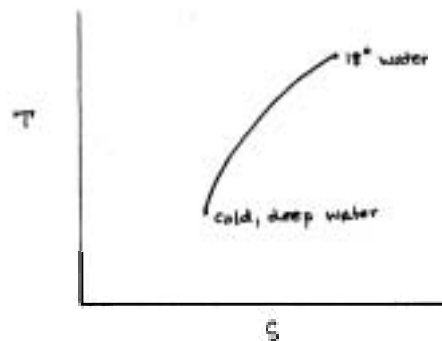
But, one is again left with the task of explaining why the line is curved
at all.

The importance of 18° water lies, not in its possible role as a parental water type, but rather because it is an archetype of a large, more common, process. Anywhere in the subtropics one sees a similar vertical temperature and salinity structure: a large isothermal and isohaline layer just above the main thermocline and capped off by a thin layer of warmer water. How did it get there?

Worthington (1972a) looked at the warm water recirculation in the North Atlantic and noted that on an annual basis more heat is lost to the atmopshere than is carried in by the Gulf Stream. He surmised that warm water must be pulled in at the surface (Fig. 8). He saw 18° water as being formed by winter convective overturning south of the Gulf Stream and subsequent meridional motion along the 18° isotherm. The meridional cell was completed by northward movement of the heated water to be cooled at the surface in the formation region. His view, then, was that 18° water is not formed locally, but involved significant advective effects.

Warren (1972) proposed a thermocline model that did not rely on horizontal advection at all, but rather saw 18° water as being the "natural" preferred temperature of the wintertime mixed layer. He imposed three artificial constraints on the model: the depth and slope of the main thermocline and the slope of the seasonal thermocline. The nature of the internal adjustment of the model is such that for fixed seasonal cycles of meteorological variables, the model settles into a limit cycle with an embedded 18° water layer, and a seasonal heat storage only in the seasonal thermocline. In this limit cycle there is no net annual heat flux.

His model cycled back and forth between a "cooling" and "heating" phase. During the cooling phase he would calculate the net heat loss to the atmosphere for each month and vertically mix enough of the surface water to vent
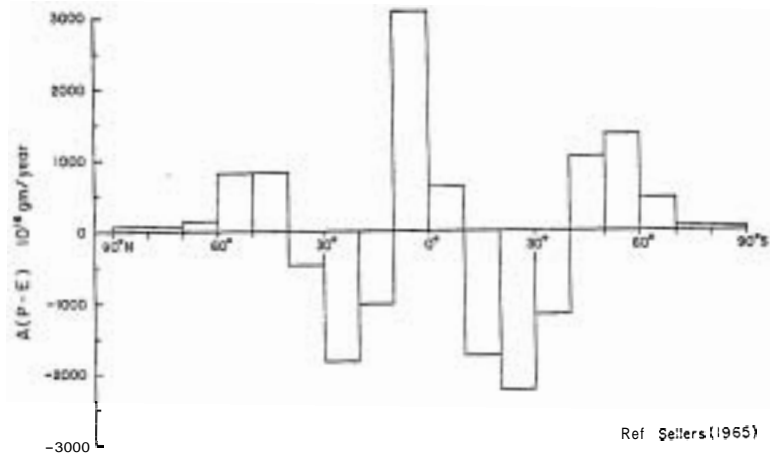
Fig. 7. Total evaporation-precipitation difference in
latitude bands.
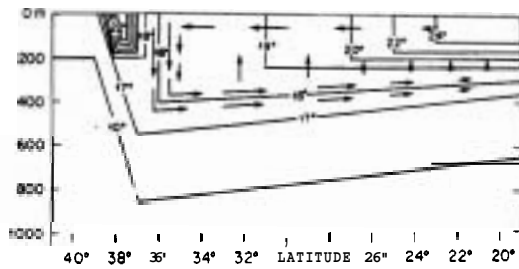
Fig. 8. An interpretation of the meridional motion accompanying
the formation of Eighteen Degree Water in late winter
(Worthington, 1977a).

that much excess heat while keeping the slope of the seasonal thermocline constant. Before the limit cycle is reached, erosion of the main thermocline occurs (Fig. 9a).

During the heating part of the seasonal cycle, the heat is stored in a growing seasonal thermocline of fixed slope (Fig. 9c). Each month the seasonal thermocline is deepened enough to match the observed influx of excess heating. He cycled the model through about 10 years after which it stabilized into a limit cycle with a winter deep mixed layer of 18° water. Given the assumption of fixed main thermocline depth, and fixed seasonal meteorology, then the mode water temperature is completely defined. Further-more, it is formed locally, leaving open the question of the role of horizon-tal advection, and in the limit cycle has zero net annual heat flux. Certainly the mode water's existence is due to the homogenization during cooling. Ad-vection may just modify the temperature structure of the mode.

Deep 18° mixed layers have been observed (Fig. 10). The two upper curves are from slope water while the two lower curves are from the center of the gyre. The KNORR cruise was in the fall of 1975 and shows a very slight pooling of 18° water. However, the RESEARCHER cruise was in the spring of 1977, immediately after a particularly severe winter. A thick isothermal pool of nearly 18° water was observed at RESEARCHER station 33, within the Sar-gasso Sea. Furthermore, an earlier XBT cast (not shown) which was made a few days before RESEARCHER 33 showed the isothermal pool extending right up to the surface.

Transport of the Gulf Stream

The transport of the Gulf Stream varies seasonally with the highest trans-port in the winter and lower values in the summer (Fig 11). Worthington (1972b) has suggested that intrusions of cold polar air causes vertical
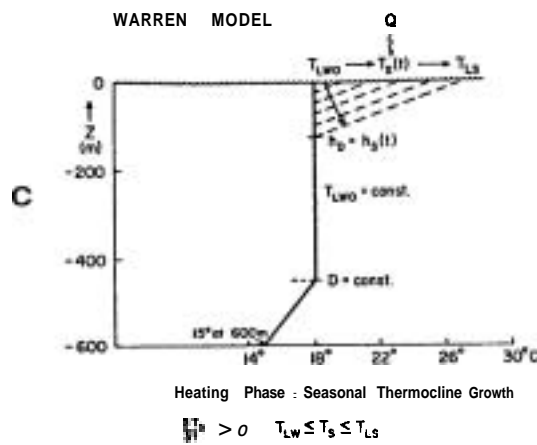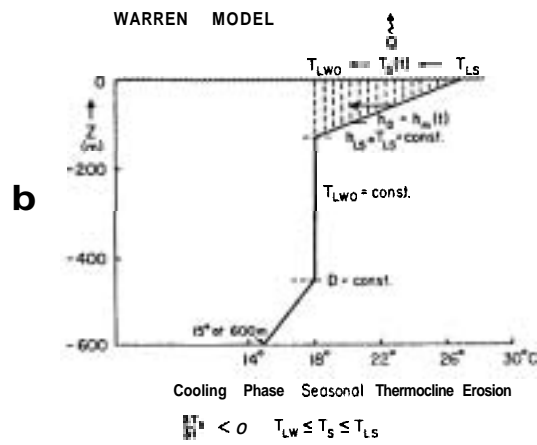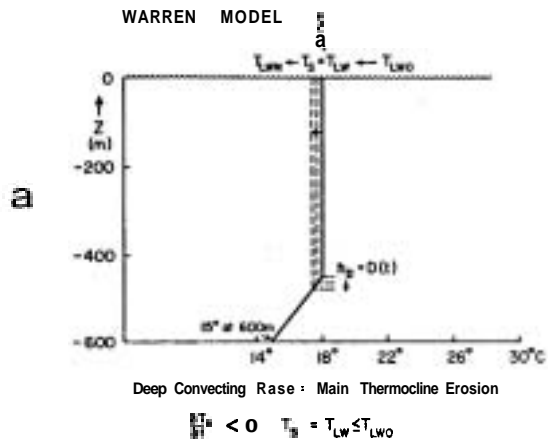
Fig 9 Temperature structure changes during the three phases of Warren's (1972) local formation model for Eighteen Degree Water.
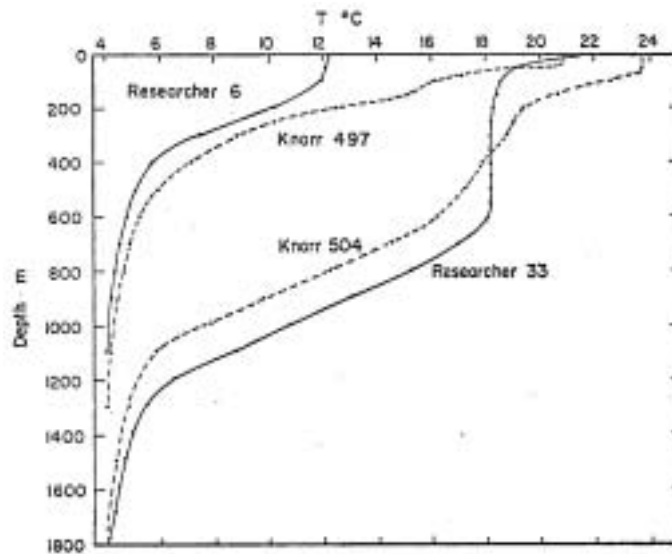
Fig. 10.   Comparison of stations from either side of the
           Gulf Stream for a mild winter (KNORR stations in
           1975) and a vigorous winter (RESEARCHER stations
           in 1977).
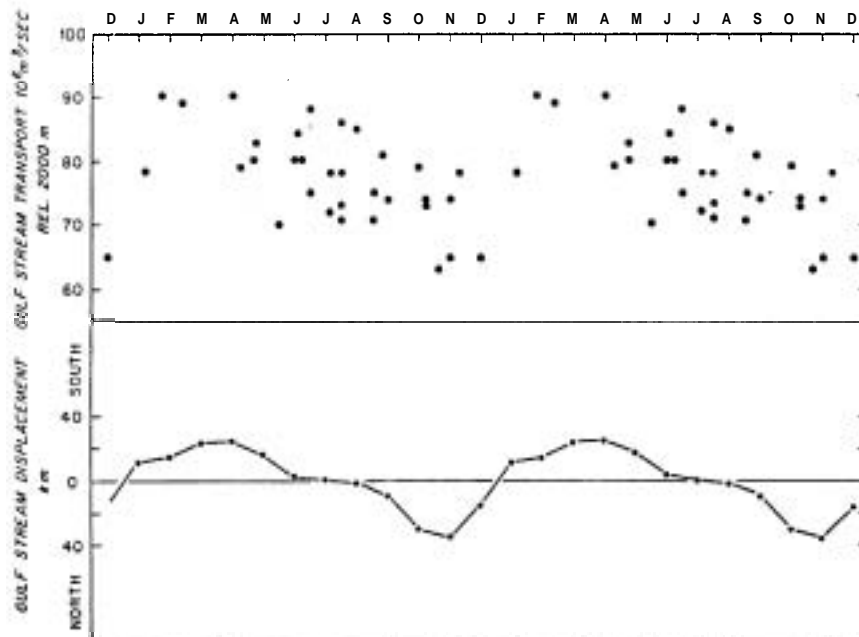
Fig. 11.   Monthly variability of Gulf Stream transport and
           position (Worthington, 1976, Fig. 44).

convective mixing and formation of 18° water south of the Gulf Stream and depression of the thermocline. The resulting increased slope of the thermocline would increase the baroclinic transport. Figure 10 shows this effect, while the transport values are shown on Fig. 11.

Leetmaa and Bunker (1978) have calculated the expected transport of the Gulf Stream by using wind stress curl. They found that their estimates matched geostrophically calculated estimates south of the latitude of maximum wind stress curl but was a poor fit to the north.

REFERENCES

Bunker, A. F. and L. V. Worthington, 1976. Energy exchange charts of the North Atlantic Ocean. Bull. Am. Meteor. Soc., 57, (6).

Iselin, C. O'D., 1936. A study of the circulation of the western North Atlantic. Pap. Phys. Oceanogr., 4(4), 101 p.

Leetmaa, A. and A. F. Bunker, 1978. Updated charts of the mean annual wind stress, convergences in the Ekman layers, and Sverdrup transports in the North Atlantic. J.M.R., 36(2), 311-322.

Montgomery, R. B. and M. J. Pollak, 1942. Sigma-T surfaces in the Atlantic Ocean. J. Mar. Res., 5, 20-27.

Sverdrup, H. U., Johnson, M. W., and Fleming, R. H., 1942. "The Oceans, Their Physics, Chemistry, and General Biology". Prentice-Hall, Englewood Cliffs, New Jersey.

Warren, Bruce A., 1972. Insensitivity of subtropical mode water characteristics to meteorological fluctuations. Deep-Sea Res., 19, 1-19.

Worthington, L. V. and W. R. Wright, 1970. North Atlantic Ocean atlas of potential temperature and salinity in the deep water, including temperature, salinity and oxygen profiles from the ERIKA DAN cruise of 1962. Woods Hole Oceanographic Institution Atlas Series, 2, 58 plates.

Worthington, L. V., 1972a. Negative oceanic heat flux as a cause of water mass formation. J. Phys. Oceanogr. 2, 205-211.

Worthington, L. V., 1972b. Anticyclogenesis in the oceans as a result of outbreaks of continental polar air. In: Studies in Physical Oceanography --A tribute to Georg Wust on his 80th birthday, A. L. Gordon, editor, Gordon and Breach, New York, 1, 169-178.

SUPPLEMENTARY REFERENCES

Bunker, A. F., 1976. Computations of surface energy flux and annual air–sea interaction cycles of the North Atlantic Ocean. Monthly Weather Review, 104, 9.

Fuglister, F. C., 1960. Atlantic Ocean atlas of temperature and salinity profiles and data from the International Geophysical Year of 1957–58. Woods Hole Oceanographic Institution Atlas Series, 1, 209 p.

Iselin, C. O'D., 1939. The influence of vertical and lateral turbulence on the characteristics of waters at mid–depths. Trans. Amer. Geophys. Un., 14–417.

Seitz, R. C., 1967. Thermostad, the antonym of thermocline. J. Mar. Res., 25, 203.

Worthington, L. V., 1959. The 18° water in the Sargasso Sea. Deep–Sea Kes., 5, 297–305.

Worthington, L. V., 1976. On the North Atlantic circulation. The Johns Hopkins Oceanographic Studies, No. 6 (Monograph).

Worthington, L. V., 1977. Intensification of the Gulf Stream after the winter of 1976–77. Nature, 270, 5636, 415–417.

Wright, W. R., 1934. Schichtung und Zirkulation des Atlantischen Ozeans. Die Stratosphäre des Atlantischen Ozeans. Wiss. Ergebn. dtsch. atlant. Exped. 'Meteor', 6, Teil 1, 109–228.

<div align="right">
Notes Submitted by
Thomas Keffer
</div>

Lecture #3.   SUBTROPICAL GYRES TWO

One method of possibly confirming aspects of the meridional cell interpretation of the $18°$ water circulation utilizes the β-spiral concept of Stommel and Schott (1977) and Schott and Stommel, 1978). Relative velocity spirals follow directly from thermal wind calculations for a field where the direction of horizontal density gradient changes with depth. Their papers point out the functional relation between these calculated horizontal velocity vector rotations and the vertical velocity field and subsurface heating and cooling. Subsurface heating or downward vertical velocity give

spirals with shallow level velocities to the left of the velocity at deeper levels – the same sense of rotation as an Ekman spiral. Subsurface cooling or upward vertical velocity give spirals of the opposite sense. To apply this to the 18° water circulation, note that practically all the Sargasso Sea gyre sketched out by Worthington (1976, see Figure 5 below) lies within the negative annual heat flux regions of Bunker and Worthington (1976)(see Fig. 5 in lecture 2). Thinking of the 18o water level as the bottom of the infiuence of this cooling, then a cooling spiral motion should be found and shows westward return flow of the gyre. The surface water should move north relative to the 18° water, while the 18° water itself should move south relative to the main thermocline water. The upper part of this system sounds like Worthington's meridional cell. What's more is that the intensity of the relative meridional cell is proportional to the instantaneous cooling through the seasonal cycle, and the southern boundary of the northward flowing surface water also shifts seasonally.

Mathematically, the expression for the vertical rotation of the horizontal velocity vector is: $\dfrac{\partial \theta}{\partial z} - \dfrac{g}{f \rho_o}\left(\dfrac{1}{U^2(z)}\right)\left(w \rho_z - (\dot{\rho})\right)$

where $U(z)$ = horizontal velocity in polar coordinates

$(\dot{\rho})$ = in situ cooling or heating: the vertical distribution of the effort of air–sea exchanges.

Because the 18° water has a ρ_z which goes to zero in the winter and is a minimum the rest of the year, it is possible that this water forms a vertical regime boundary. The main question, however, is how much of an angle can exist between 18° water and the meridional mean (i.e. is relative meridional advection or gyre advection more important). So far velocity vectors along $55^O W$ confirm the high velocities of the Gulf Stream return flow and hint

at some rotation at 600m relative to 1000m of the above indicated sense (Schmitz, 1979).

$$\beta - \text{Spiral (Peter Killworth)}$$

The original concept for the β - spiral developed from a desire to be able to deduce the total absolute velocity field from temperature salinity data. The main equations of the β - spiral which accomplish this goal can be developed from the following five basic equations:

Geostrophy (should hold providing there are a minimum number of eddies present):

(1) $-fv = -p_x/p_o$

(2) $fu = -p_y/p_o$

Hydrostatic motion:

(3) $p_z = -g\rho$

Zero divergence:

(4) $u_x + v_y + w_z = 0$

Density is conserved following the particle:

(5) $\underset{\sim}{u} \cdot \nabla \rho = 0$

From these equations the thermal wind equations can be derived by first differentiating the geostrophic equations with respect to z, yielding:

(6) $-fv_z + p_{xz}/p_o = 0$

(7) $fu_z + p_{yz}/p_o = 0$

Then subtracting from equation (6) $\quad \frac{\partial}{\partial x}(g\rho + p_z) = 0$

or $\quad g\rho_x + p_{zx} = 0$

and subtracting from equation (7) $\quad \frac{\partial}{\partial y}(g\rho + p_z) = 0$

or

This yields the thermal wind equations:

(8) $f v_z = -g \rho_x / \rho_0$

(9) $f u_z = g \rho_y / \rho_0$

These express a relationship between the horizontal density gradients and the vertical velocity gradients. If u, v is therefore known somewhere (e.g. at the surface, u_s and v_s) then they can be obtained everywhere. Everything is now known except w which can be obtained by rearranging the geostrophic equations into terms of u and v, then substituting these values into the zero divergence equation (4) which yields:

(10) $\beta v = f w_z$

More formally, divide equation (5) by ρ_z and differentiate with respect to z .

$$\left(\frac{u \rho_z}{\rho_z} \right)_z + \left(\frac{v \rho_z}{\rho_z} \right)_z + w_z = 0$$

yielding:

$$u_z \left(\frac{\rho_x}{\rho_z} \right) + u \left(\frac{\rho_{xz}}{\rho_z} - \frac{\rho_x \rho_{zz}}{\rho_z^2} \right) + v_z \left(\frac{\rho_y}{\rho_z} \right) + v \left(\frac{\rho_{yz}}{\rho_z} - \frac{\rho_y \rho_{zz}}{\rho_z^2} + \frac{\beta}{f} \right) = 0$$

rearranging:

(11)

$$u \left(\frac{\rho_{xz}}{\rho_z} - \frac{\rho_x \rho_{zz}}{\rho_z^2} \right) + v \left(\frac{\rho_{yz}}{\rho_z} - \frac{\rho_y \rho_{zz}}{\rho_z^2} + \frac{\beta}{f} \right) = - \left(u_z \frac{\rho_x}{\rho_z} + v_z \frac{\rho_y}{\rho_z} \right)$$

where the terms within the parantheses are knowns.

This is Stommel and Shott's deduced equation and there are now as many equations as layers examined, so the problem is overdetermined. Therefore, by substituting u_s and v_s for u and v this will now yield mean surface veloci-ties which can then be used in the thermal wind equations to obtain u and v at any depth (resulting in the spiral). Finally, from equations (10), w can be

determined.   These equations can be used with any conservative property and need not be restricted to ρ .

Transportation Controversy of the Gulf Stream System

All of the old schemes used to calculate the Gulf Stream transport have in common the use of an intermediate level of no motion depth, resulting in values of 50 to 60 Sverdrups (Fig. 1).   These are all obtained by vertically integrating from the level of no motion to the surface.   The calculations differed by only a factor of two from linear Sverdrup interior transport predictions (Fig. 2 and Lecture 2 Fig. 1), which could be rationalized by weak nonlinear effects and/or under estimating the wind stress curl.   The idea of an intermediate level of no motion in the Sargasso Sea survived until about 1960 at which time Fuglister (1963), using deep floats, found nontrivial speeds in the direction of the stream much deeper than the assumed level of no motion.   This suggested higher transports.   Estimates based on transport float data indicate that the Gulf Stream builds up to well over 100 Sverdrups down-stream of Cape Hatteras.   A second phase in theoretical modelling has ensued in an attempt to explain this high transport.   The observational evidence of the big Gulf Stream is summarized in Worthington's (1976) monograph.   His Subtropical Gyre transport is 150 Sverdrups (Fig. 3) and is restricted laterally to the western central North Atlantic.   Independent measurements by moored instruments seem to be confirming Worthington's transport distribution in this western gyre.   The two gyre aspect is still unresolved.

In the other ocean basins, transports are not well known as of present although large scale eddies observed in the Brazil and Australian Currents, and the Circumpolar Current, are similar in structure to those of the Gulf Stream suggesting similar dynamical processes may be at work also.   This
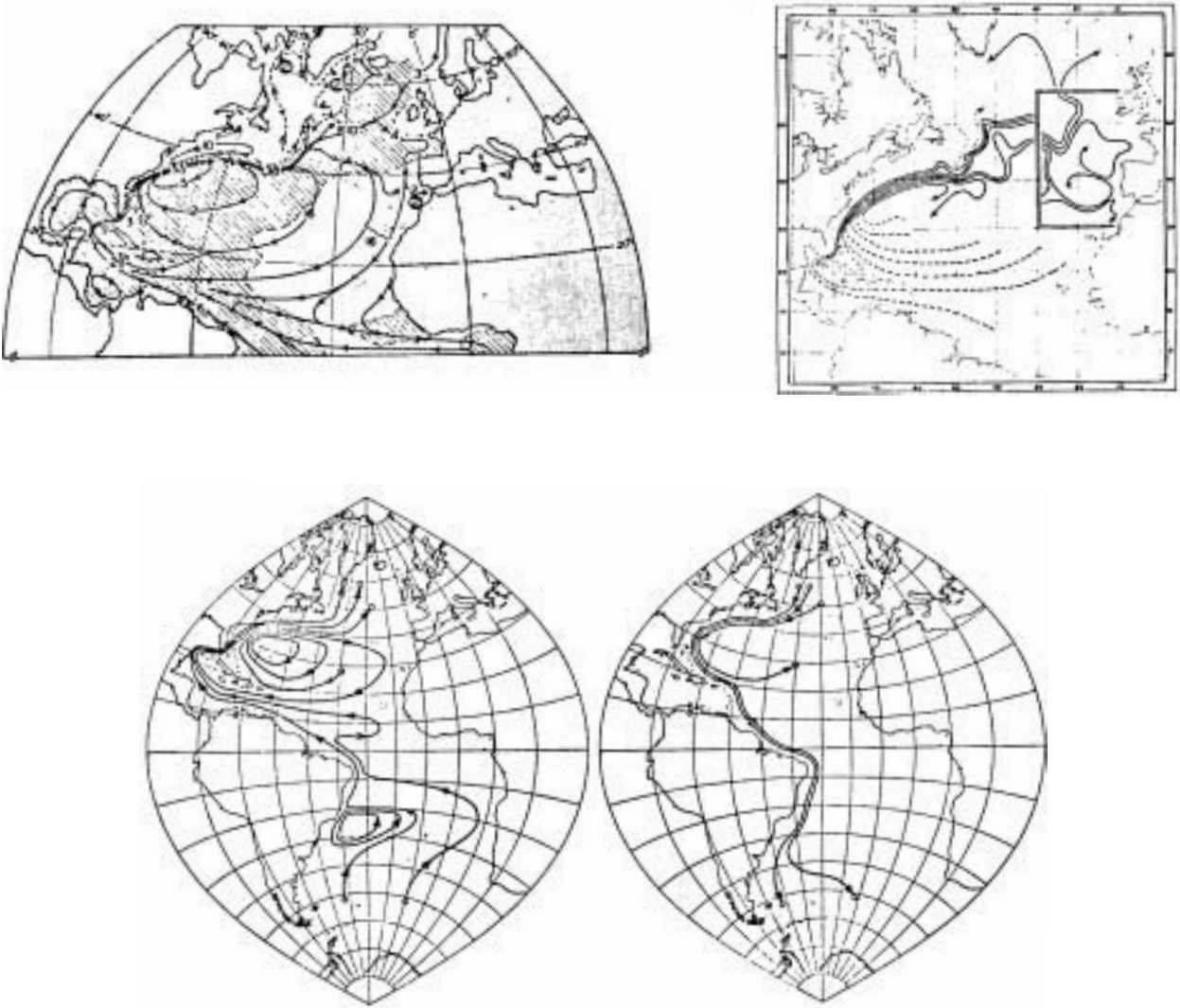
Fig. 1, Transport circulation diagram for the North Atlantic
Ocean (Worthington, 1976, Fig. 17).
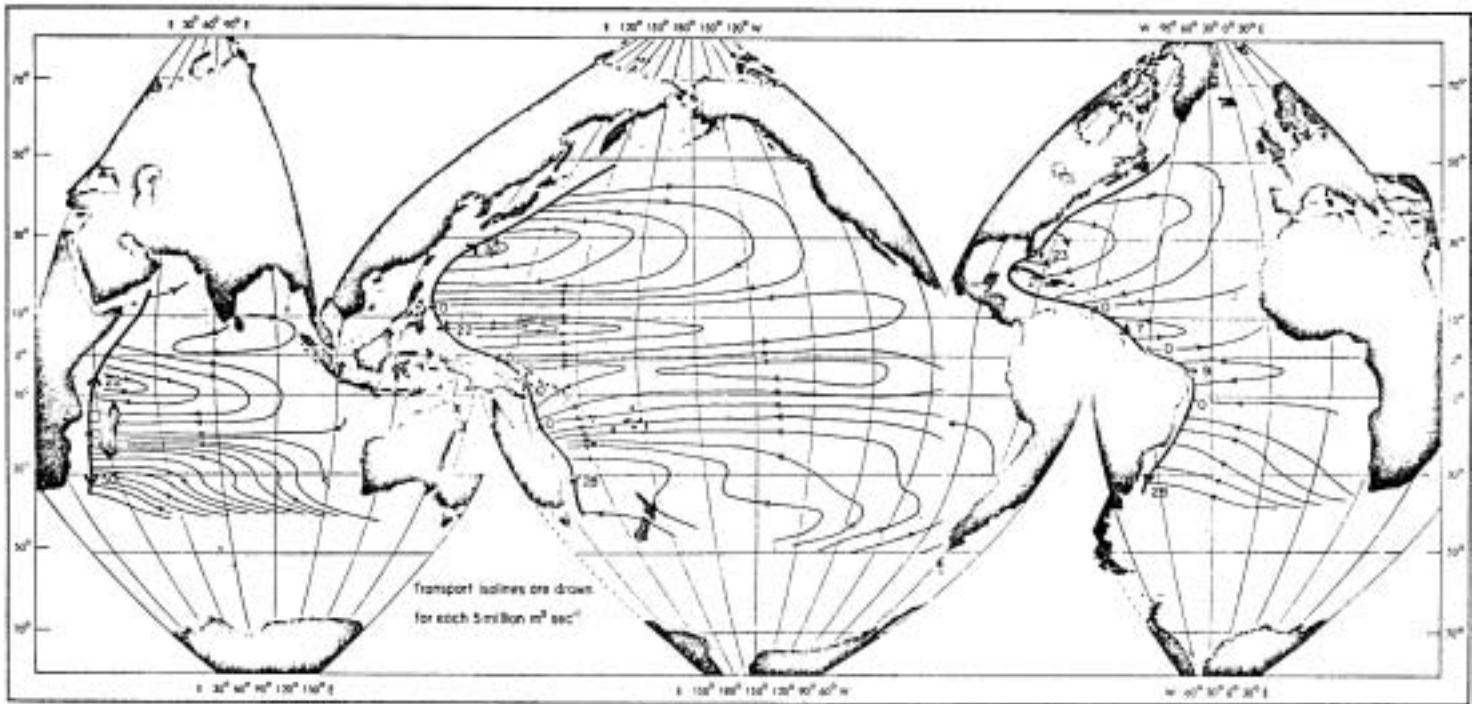
Fig. 2. Sverdrup transport and required western boundary
currents as calculated by Welander (1959), using
annual mean wind stress.
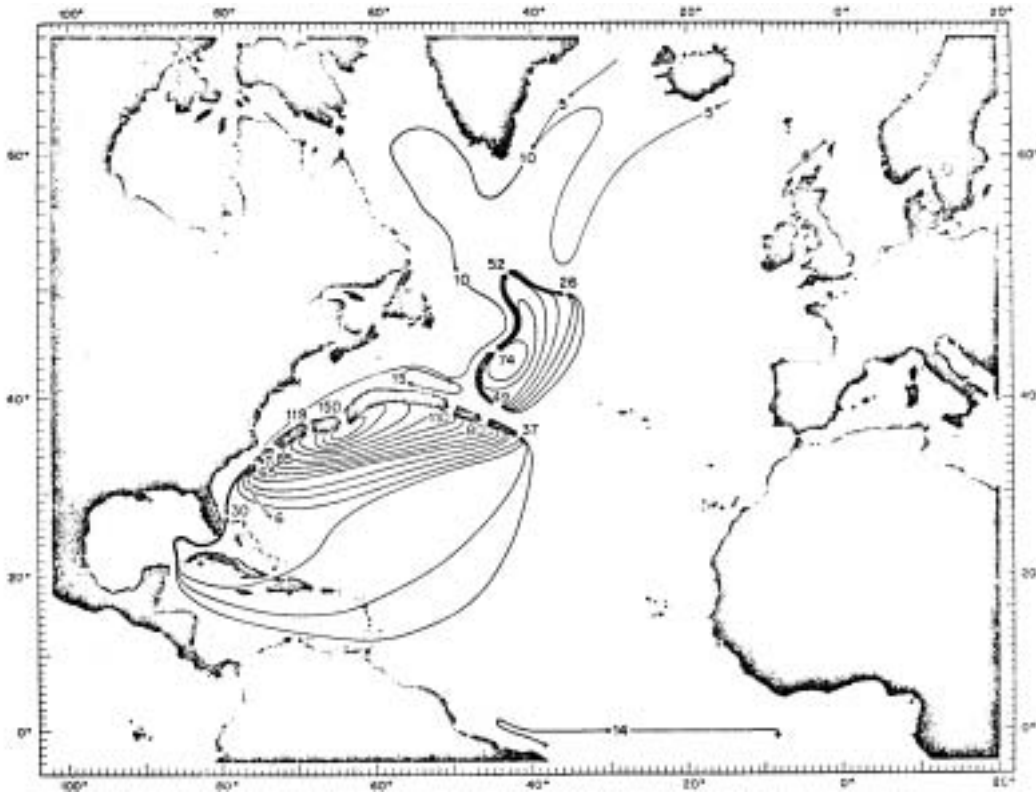
Fig. 3. Circulation diagram for the total top-to-bottom
circulation in the North Atlantic Ocean (Worthington,
1976, Fig. 42).

suggests that the wind driven estimates (like Fig. 2) may be in error there also.   Theoretical modeling (Rhines, and Holland) is giving in situ nonlinear dynamics that drives the deep Gulf Stream, and the compact recirculation gyre.

Another question concerning the Gulf Stream gyre system is whether or not the presence of the Mediterranean salt tongue (Figs. 4 and 5) is consistent with a large Gulf Stream return flow on the eastern side of the North Atlantic. Worthington says no, and this is a crucial step in arguing for the gyre shown in Fig. **3.**   This consistency has been tested by several simple advection-diffusion models (Richardson and Mooney, 1975).   Prescribing a simple closed circulation gyre, basin wide (Fig. *6*) and instead of modelling, using a point salt flux for the Mediterranean outflow area, (using specified salt boundary condition at the eastern boundary of the basin) the problem is reduced to a two dimensional advection-diffusion equation.

So $\quad \underline{u} \cdot \nabla_{H} S = \frac{1}{P} \nabla_{H}^{2} S$

where P = Peclet Number = $\dfrac{V L}{K_H}$

$S(y)$ is prescribed at the eastern boundary

$S = 0$ at the other boundaries

Results from these models (Fig. 6 and 7) show that for a Peclet number of 0 a symmetrical distribution results and for values around 10-30 the observed salt tongue shape is approached.

Richardson and Mooney's calculation for the gyre of Fig. 6 are shown in Fig. 7 and a Peclet number of 10 to 30 looks about right.   The proper questions may not be addressed by this procedure.   In the model the salt diffuses in the east end and out the other three sides.   We can reformulate the question as follows.   Given the shape of the tongue, the value of the Peclet number and
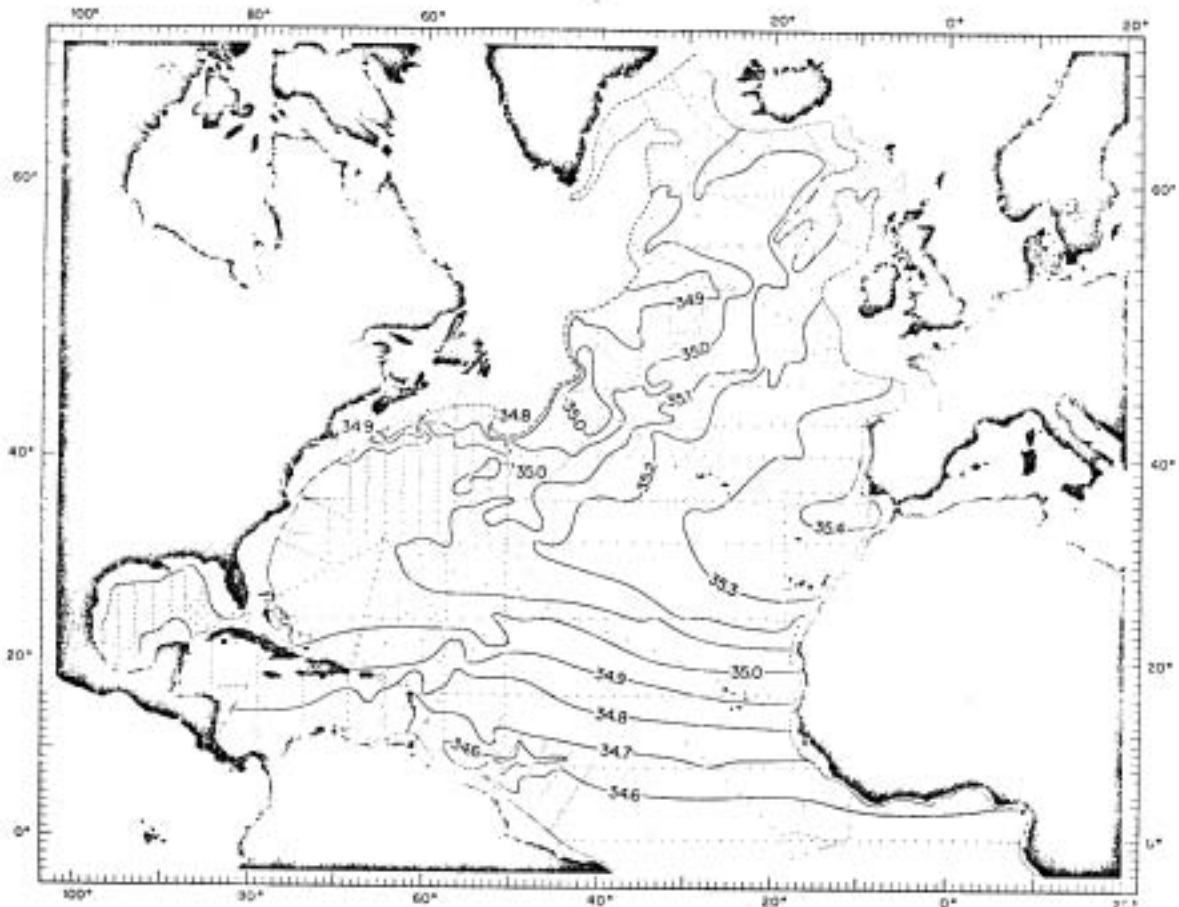
Fig. 4. Salinity at 6°C in the North Atlantic (Worthington, 1976, Fig. 23).
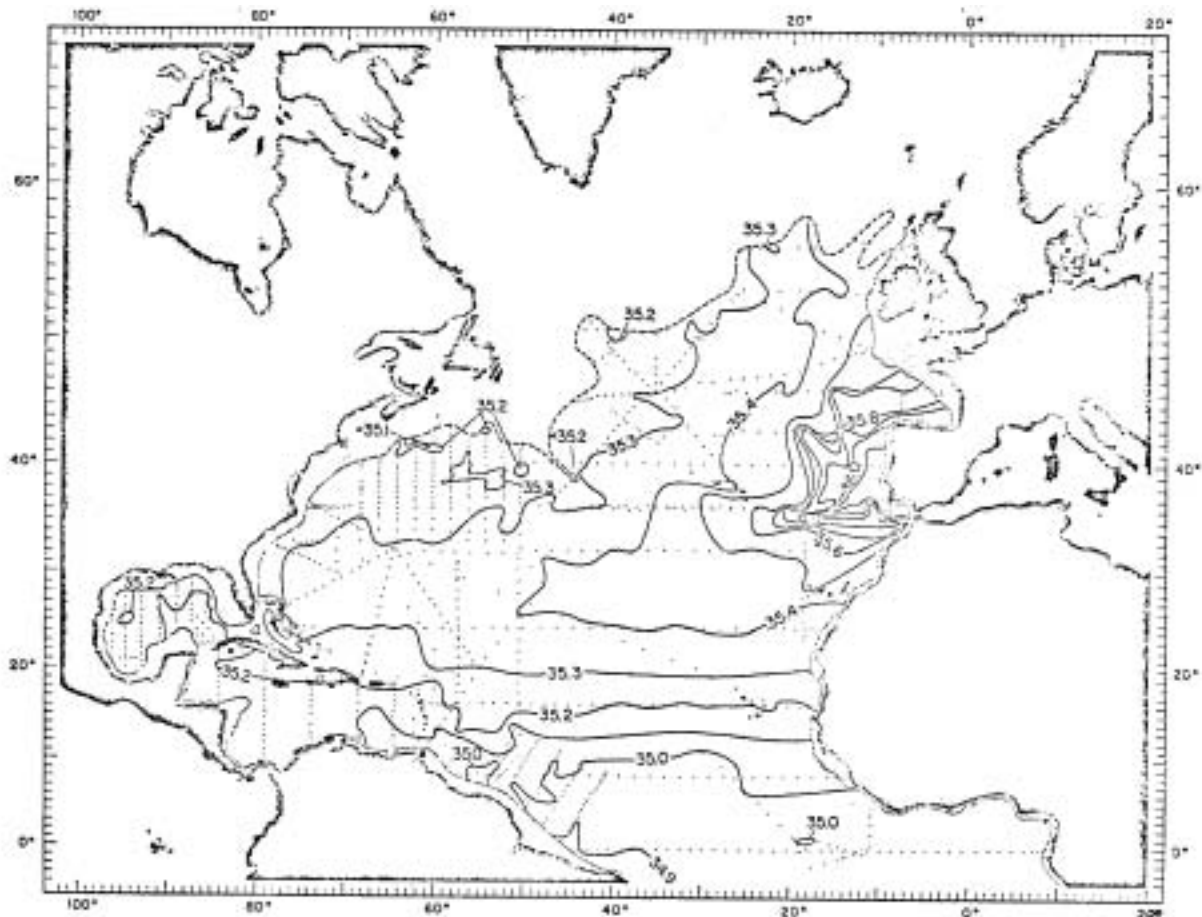
Fig. 5. Salinity at 10°C in the North Atlantic (Worthington, 1976, Fig. 25).
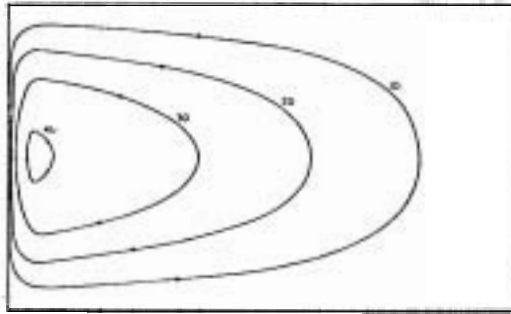
Fig. 6. Transport streamliner used in the advective-diffusion model of the Mediterranean salt tongue of Richardson and Mooney (1975).
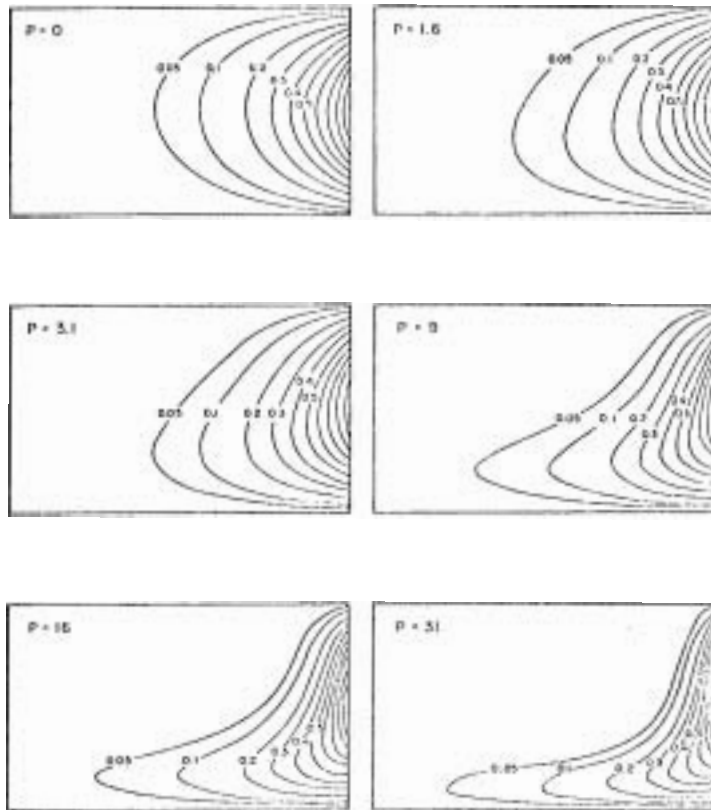
Fig. 7. Salinity anomaly contour for various values of the Peclet number, as calculated by Richardson and Mooney (1975).

the <u>observed</u> flux of salt from Gibraltar (transport times salinity anomaly), what is the transport magnitude of the gyre? The flux gives K_h in the Peclet number definition, the shape choosing procedure gives the Peclet number, and therefore, a V is predicted to be consistent with the flux. Joyce (1979, in press) uses this procedure to estimate a mid thermocline transport of only 5 to 10 Sverdrups, which is much smaller than the observed western gyre the transport. This would seem to support the Worthington (1976) contention that the gyre closes outside the Mediterranean tongue.

TEXT REFERENCES

Fuglister, F. C., 1963. Gulf Stream 60, <u>Progr. Oceanogr.</u> <u>1</u>, 265–373.

Joyce, T. M., 1979. On the Mediterranean Outflow in the North Atlantic Part 1. 2–D advective diffusive model with a mid–ocean ridge. JMR (in press)

Richardson, P. L. and K. Mooney, 1975. The Mediterranean outflow – a simple advection diffusion model. <u>JPO</u> <u>5</u> (3), 476–482.

Schmitz, W. J., Jr., 1979. Weakly depth–dependent segments of the North Atlantic circulation. <u>JMR</u> (in press)

Stommel, H. M. and F. Schott, 1977. The Beta spiral and the determination of the absolute velocity field from hydrographic station data. <u>DSR</u>, <u>24</u>, 325–329.

Worthington, L. V., 1976, On the North Atlantic Circulation, <u>John Hopkins Ocean. Studies 6.</u>

Worthington, L. V., 1977. The intensification of the Gulf Stream after the winter of 1976–1977. <u>Nature, 207</u> (5636), 415–419

SUPPLEMENTARY REFERENCES

Bunker, A. F., 1976. Computations of surface energy flux and annual air–sea interaction cycles of the North Atlantic Ocean. <u>Monthly Weather Review</u>, <u>104</u> (9), 1122–1140.

Bunker, A. F. and L. V. Worthington, 1976. Energy exchange charts of the North Atlantic Ocean. <u>Bull. Am. Meteor. Soc.</u>, <u>57</u> (5), 670–678.

Bye, J.A.T. and G. Veronis, 1979. A correction to the Sverdrup transport.
    <u>JPO</u>, 649-651.

Gill, A. E., 1968. A linear model of the Antarctic Circumpolar Current. <u>JEM</u>,
    <u>32</u> (3), 465-488.

Knauss, John A., 1969. A note on the transport of the Gulf Stream. <u>Deep-Sea
    Res</u>., Suppl. to Vol. 16, 117-123.

McCartney, M. D. and L. V. Worthington, 1979. Anomalous water mass
    distribution at 55°W in the North Atlantic in 1977. <u>JMR</u> (in press).

Schott, F. and H. M. Stommel, 1978. Beta spirals and absolute velocities in
    different oceans. <u>Deep-Sea Res</u>., <u>25</u>.

Welander, P., 1976. A Zonally uniform regime in the oceanic circulation. <u>JPO</u>
    <u>6</u> (2), 121-124.

<div align="right">
Notes Submitted by
Douglas Martinson
</div>

Lecture 4   THE POLAR - SUBPOLAR INFLUENCE ONE

Introduction

The passage of water which has been influenced by the intense cooling of

the polar regions can be traced in some form and at some depth throughout a

major portion of the world's oceans. This progression of the polar water

properties is most strikingly revealed in studies of western boundary currents

and of the circulation patterns of the deep water. This overall circulation

pattern corresponds closely to that deduced from thermohaline circulation

models. Stommel and Robinson (1959) proposed an ocean thermocline model in

which heat was added to the top and distributed downwards by some mixing

process, represented by a constant eddy thermometric conductivity. To main-

tain a steady state in the model a continuous upwards flux of cold water into

the underside of the thermocline is required. This implies that there must be

sources of cold water in the system to maintain mass continuity. The con-

sequences of such sources on the interior flows have been studied by Stommel

and Arons (1960a, b), who considered a uniformly distributed sink at the sur-
face (corresponding to the base of the thermocline) and concentrated sources
in the interior. They showed that a concentrated source in the polar regions
led, in the Northern hemisphere, to a strong western boundary current along
the eastern side of a meridional barrier, the direct action of the Coriolis
force on the released fluid. The return flow from the western boundary cur-
rent to the distributed sink is in a poleward direction. This follows
directly from the vorticity equation

$$\beta v \quad f w_z$$

Integrating this from the bottom of the ocean ($w = 0$) to the base of the
thermocline ($w > 0$), yields $\int v \, dz > 0$ since w is always positive in the
model, hence v is always positive (poleward).

The systematic application of this model to the world's oceans implies the
circulation patterns of Fig. 1, taken from Stommel (1958), where the major
sources have been placed in the Greenland and Weddell Seas. The boundary cur-
rents required to close the circulation are indicated by heavy lines.

The North Atlantic

The circulation system of the North Atlantic can be described in broad
terms as a northward flow in the upper levels followed by a southward return
flow in the deep water. The southward return flow encounters a northward flow
of Antarctic Bottom Water where, after some mixing North Atlantic Deep Water
is formed, a water mass comprising a large percentage of the waters of the
Atlantic Ocean, characterized by salinity of 34.9 to 35.0 o/oo and poten-
tial temperature between $1.8°$ and $4°C$.

The North Atlantic Deep Water is considered to be a mixture of five basic
sources (Worthington, 1976) as follows:

Norwegian Sea overflow through Denmark Strait.

Norwegian Sea overflow through Iceland–Scotland passage.

Inflow of Antarctic Bottom Water.

Laborador Sea Water.

Mediterranean Sea Water.

The first two are already predominantly "pure" North Atlantic Deep Water at
the overflows. The salinity in potential temperature surface charts of
Worthington and Wright(1970) illustrate most graphically the spreading and
interplay of these five.

The main transport features of the deep water currents are shown in the
accompanying diagram taken from Worthington(1976, Fig. 2). The water masses
shown are those lying below $4^{\circ}C$ and transports of the Gulf Stream are the
result of calculations from density measurements with the geostrophic and
hydrostatic relationships augmented where available by direct current measure-
ments. The positions of the latter are marked on the diagram by asterisks,
and these direct measurements help to establish reference level values for the
geostrophic calculations. In certain locations it is necessary to invoke en-
trainment of water from higher temperature levels to maintain mass continuity;
such positions are marked by circled cross symbols, ⊕ . In a like manner the
upwelling of fluid to the upper layers is marked by circled dot symbols ⊙
The numbers marked on the flow lines indicate mass transport in Sverdrup
units (1 Sv = $10^{6}m^{3}$/sec).

The southward flow has its origins in the Norwegian and Iceland Sea areas,
and later work(Aagaard, GFD, 1979) suggests that the water mass flowing over
the sill of the Denmark Strait does not originate in the Norwegian Sea as sug-
gested by Worthington, but obtains its characteristics from the Iceland Sea,
with small quantities of Norwegian Sea water in erratic pulses. The main flux
of Norwegian Sea Water flows over the sills of the Iceland-Scotland passage

Fig. 1. Schematic theoretical pattern of deep circulation in the world ocean (Stommel, 1958).
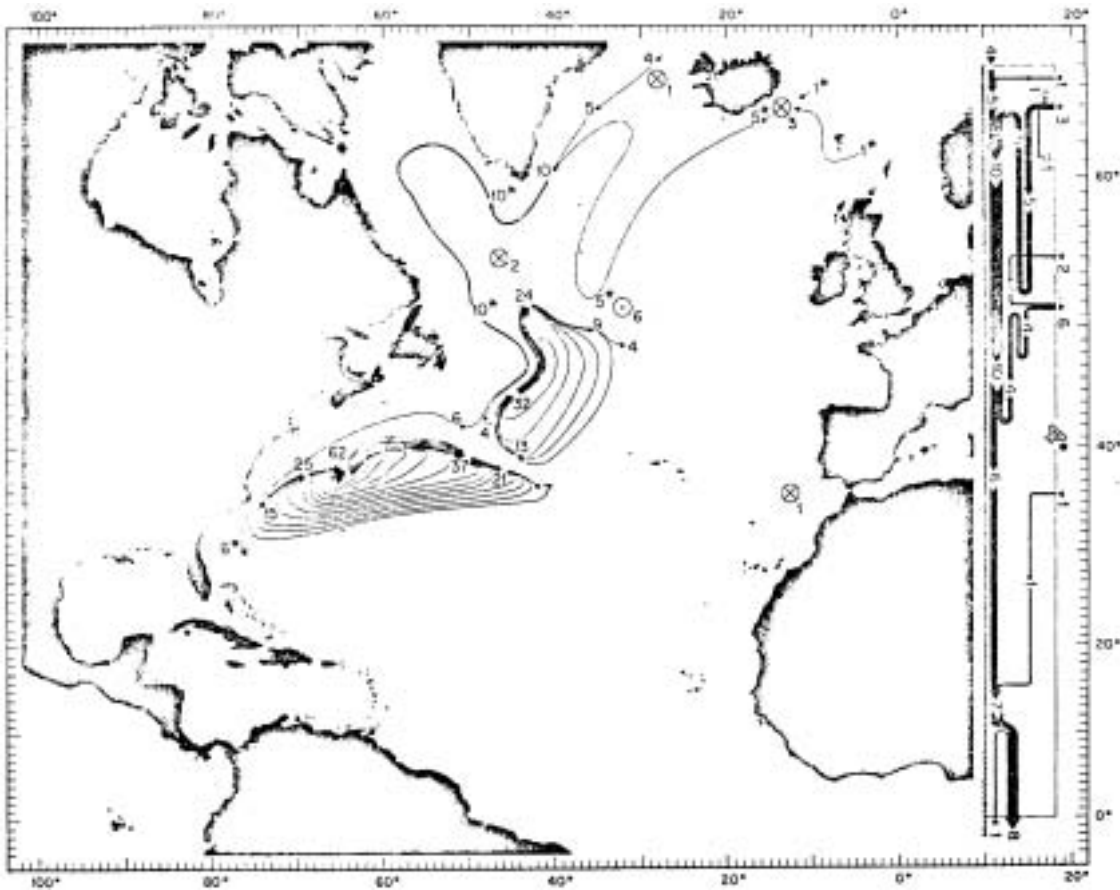
Fig. 2. Circulation diagram and box model for the deep
$(3 < 4.0^{\circ}C)$ circulation in the North Atlantic
(Worthington, 1976, Fig, 11).

entraining a large quantity of water from the upper layer. These two streams join close to the southern tip of Greenland, enter the Labrador Sea and turn south. The surface waters of the Labrador Sea are a source of low salinity and density which can be entrained by the underlying outflows from the Norwegian Sea.

Passing further south this deep current encounters the two anticyclonic gyres, losing some of its water to the northernmost of the two, the rest continuing along the coast of Florida. The distinct and separate gyres are distinguished by Worthington on the basis of these temperature, salinity and silicate characteristics, the latter being the more sensitive indicator for deep water masses. The southward moving flows now meet Antarctic Bottom Water and together complete the mixture of the North Atlantic Deep Water.

This description of the overall circulation system comprises data from many sources extending over many years and describes the ocean under what might be called 'normal' conditions. It presents a picture of continuous formation and transport of the various source waters. On closer inspection, and as more data becomes available, it becomes apparent that this relatively placid picture may be misleading, as there is evidence of large scale dis-tortions of the flow patterns which are identified with sudden formation events.

A large scale distortion of the Sargasso Sea circulation system was observed in July 1977 (McCartney and Worthington, 1979) when the axis of the Gulf Stream moved 200 km south. The evidence for these changes is found in a comparison of data from cruises #60 and #66 of the Research Vessel KNORR. The data is presented in Figs. 3a and b which compares sections of temperature, salinity anomaly and silicate anomaly taken along longitude 55oN. The KNORR Cruise #60 is regarded as 'normal', with the Gulf Stream

located at 41°N. (This axis is defined as 15°C water lying at 200 m).
Negative salinity anomalies at 18°C extend southwards; this '18O water'
is a conspicuous feature of the gyre at this latitude.   Below the main
thermocline, a positive salinity anomaly representative of the Mediterranean
outflow intrudes from the south.   At the northern end, negative salinity
anomalies above 10° mark the slope water.   The silicate anomalies are a
more sensitive indicator in the deeper waters and the negative anomalies at
the northern end of the section are attributed to Denmark Strait overflow
water.   To the south lies positive silicate anomaly water which Worthington
(1976) uses to define the southern boundary of the deep return flow of the
Gulf Stream, on the grounds that this return flow does not acquire excess
silicate and hence does not mix with the deep high silicate water.

Compare this now with the data from KNORR Cruise #66, also shown on Figs.
3a and b.   The axis of the Gulf Stream has moved 200 km to the south.   A
striking feature of the salinity anomaly distribution is the four regions of
low salinity cold water below the thermocline, and their properties, -.106
o/oo salinity anomaly, 3.52°C temperatuure and 6.51 ml/l of oxygen identify
them as Laborador Sea Water.   A large intrusion of positive salinity anomaly
water is found to the south at the base of the thermocline; water with this
Mediterranean characteristic spreads unevenly across the section much further
north than normal.   The Gulf Stream as a whole is transporting more saline
water than usual.

McCartney and Worthington attribute these changes to formation events in
the source waters characterizing the distortion, in the case of 18° Water
and Laborador Sea Water.   In particular, 18° Water has been known to have
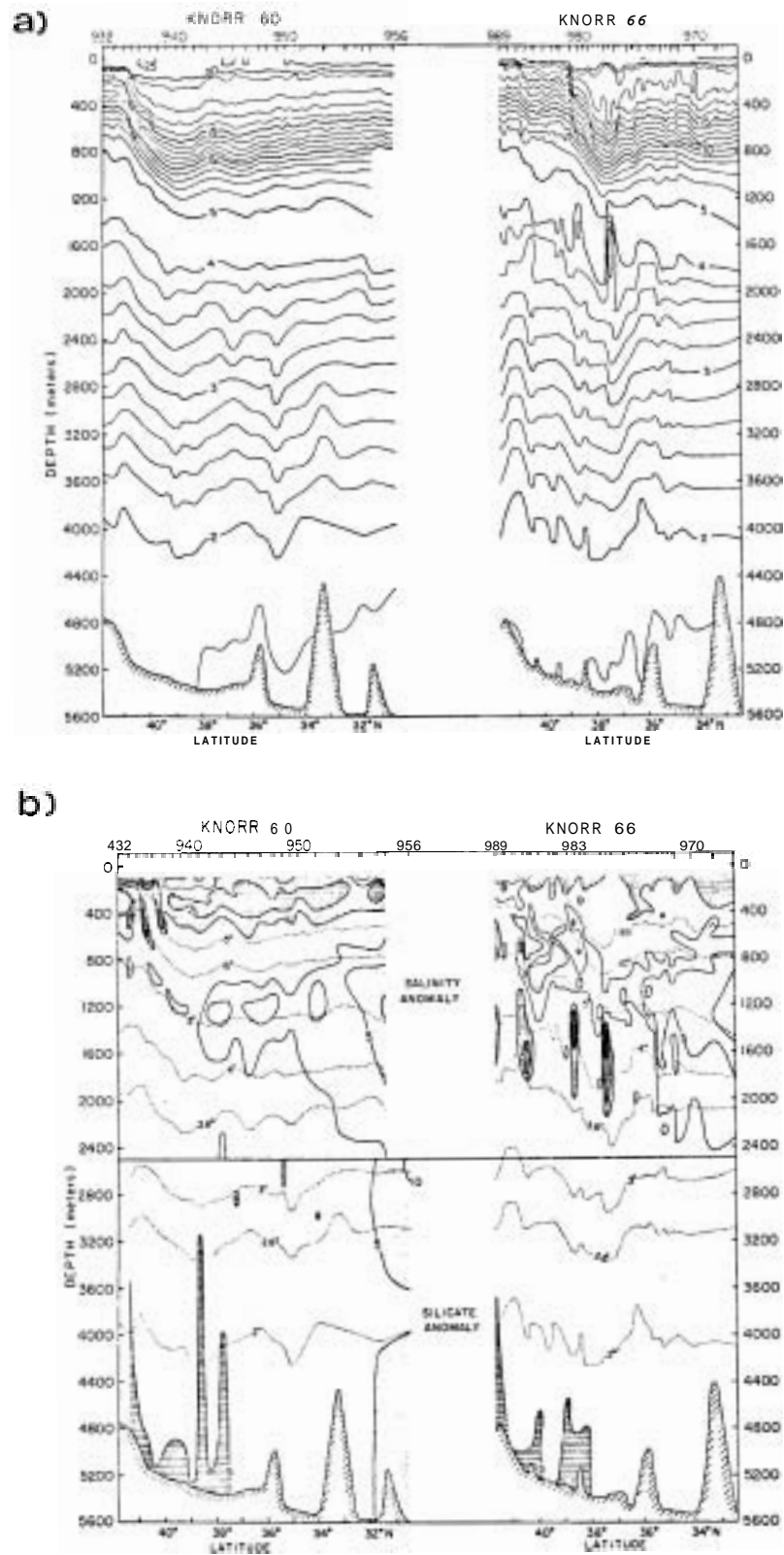
Fig. 3. Comparison of sections along 55°W in October 1976 and
August 1977. a) Potential temperature. b) Salinity
anomaly (Z < 2500m) and silicate anomaly (Z ≥ 2500m).
McCartney, Worthington and Raymer, 1979).

convectively overturned in the winter 1976 to 1977 (Worthington, 1977) and also a convective formation in the Labrador Sea in March 1976 (Gascard, GFD, 1979).

It is noted that similar changes were seen in 1956 (Fuglister, 1960).

The Southern Oceans

The theory of Stommel and Arons predicted deep northward flowing currents along the western boundaries of the southern continents and the Scorpio expedition of 1967 verified some of these predictions. Two sections were taken across the southern Pacific at 28° and 43^OS, each spanning the South Pacific from the eastern coast of Australia to South America. A notable feature was a large clockwise gyre in the southwest Pacific Basin with an intense northward flowing deep western boundary current along the Kermadoe Ridge at Lat. 28^OS, Long. 180^OW and at the base of the Chatham Rise, 43^OS, 168^OW. A similar, but weaker current system, was found in the Bellingshausen Basin off the coast of Chile. No deep boundary current was found along the western Australian boundary as the Tasman Sea is blocked to the north at depth (Warren, 1973).

Figure 4 shows the locations of the two Scorpio sections across the Pacific, together with calculated geostrophic velocities in the region of the Kermadac trench. The alternating regions of weak flow to the east are not considered to be significant. The western boundary current is well defined in both sections. Similar northward flowing western boundary currents are found in the Indian Ocean off Madagascar (warren, 1974). Figure 5 shows sections off Madagascar, and again geostrophic flow contours indicate well developed western boundary currents.
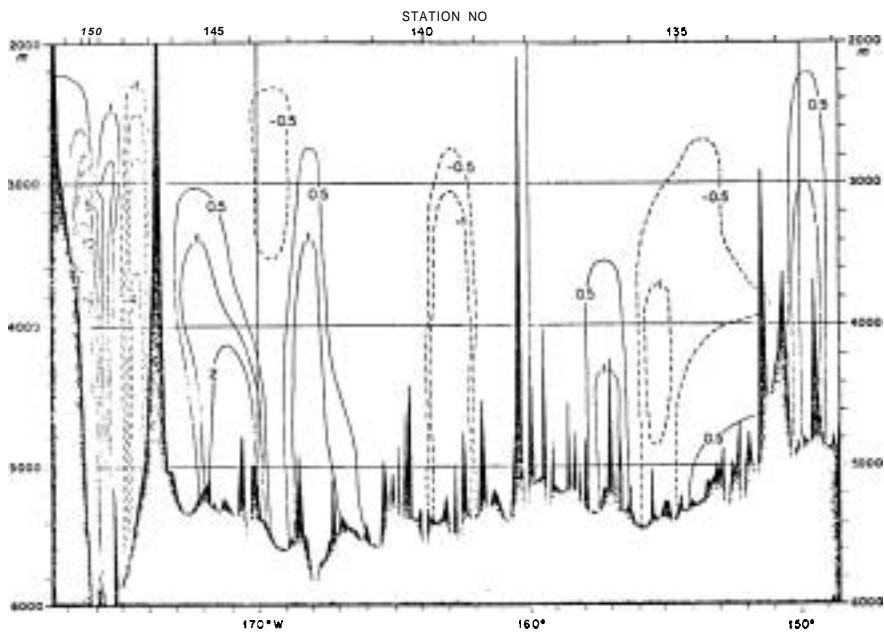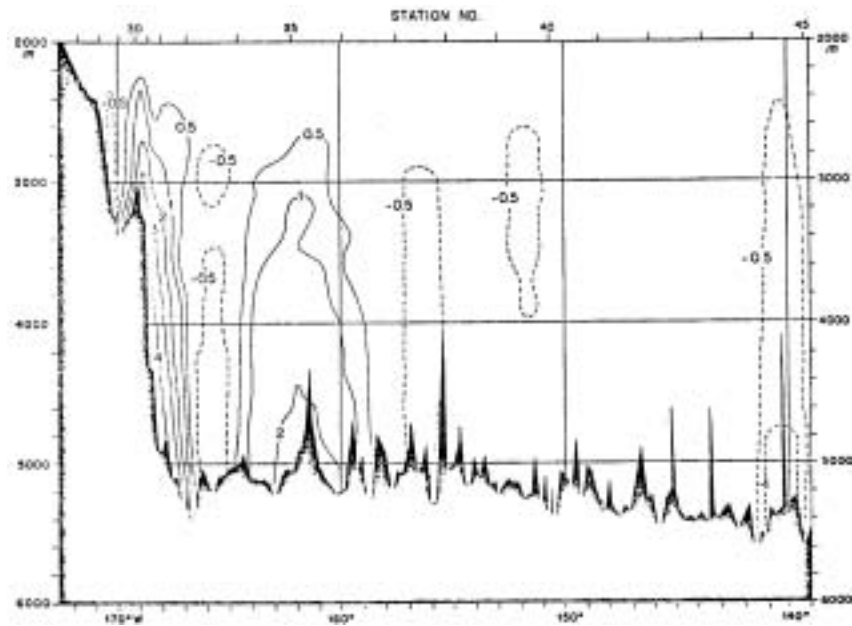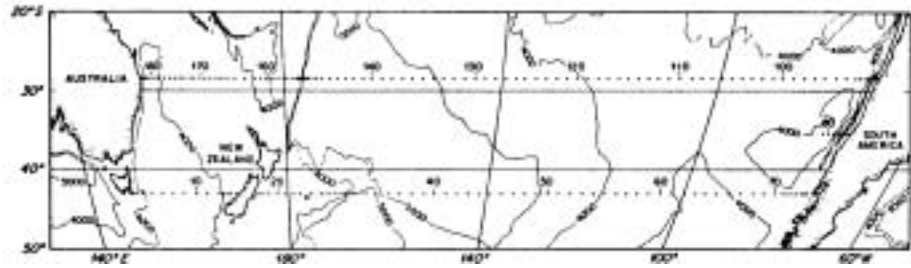
Fig. 4. Sections showing existence of western intensified
deep motion boundary currents in the South Pacific
Ocean (Warren, 1973).
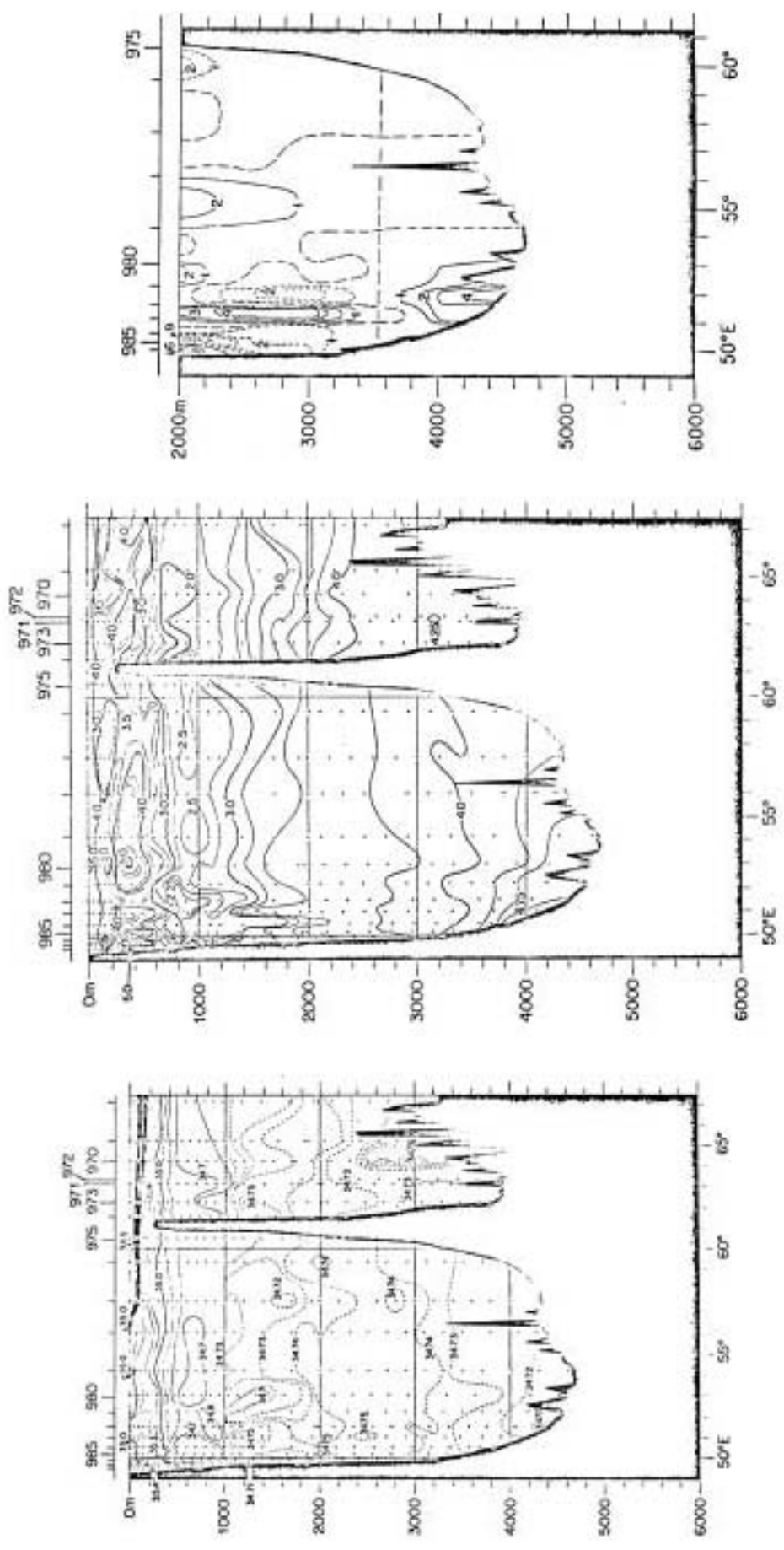
Fig. 5. Sections showing existence of western intensified deep western boundary
currents in the South Indian Ocean (Warren, 1974).

The northward flowing boundary currents transport water of Antarctic origin into the world's oceans, and as an extreme example the southward flowing western boundary current down the coast of South America transports water of Arctic origin south of the equator where **it** is eventually carried east by the circumpolar current and can be identified in the Indian Ocean and Pacific Ocean. This global impact of North Atlantic Deep Water is documented by Reid and Lynn (1971). The polar and subpolar regions thus not only influence the water properties of most of the world's oceans but provide the driving forces for the deep circulation patterns.

We will always have severe data interpretation problems. The signal we often want is how much water flows through a given section; this will generally be a small fraction of the larger recirculating gyre flow. When we make a current measurement, say a deep Swallow float in a deep western boundary current, we measure the total transport. How do we split out the gyre component and the through flow component?

REFERENCES

Aagaard, K., 1979. Northern contributions to the deep circulation. GFD, 1979.

Fuglister, F. C., 1960. Atlantic Ocean atlas of temperature and salinity profiles and data from the International Geophysical Year of 1957–1958. Woods Hole Oceanographic Institution Atlas Series, 1, 209 pp.

Gascard, J. C., 1979. Deep water formation in the Mediterranean and Labrador Seas. Preconditioning – Mixing processes and spreading.

McCartney, M. S. and L. V. Worthington, 1979. Anomalous water mass distribution at $55°W$ in the North Atlantic in 1977. Jour. Mar. Res. (in press).

Reid, J. L. and R. J. Lynn, 1971. On the influence of the Norwegian–Greenland and Weddell Seas upon the bottom waters of the Indian and Pacific Oceans. Deep–sea Kes., 18, 1063–1088.

Robinson, A. and H. Stommel, 1959. The ocean thermocline and the associated thermohaline circulation. Tellus Xl, 3, 295–308.

Stommel, Henry, 1958. The abyssal circulation. Deep-sea Res., 5, 80-82.

Stommel, H. and A. B. Arons, 1960b. On the abyssal circulation of the world ocean. II. An idealized model of the circulation pattern and amplitude in oceanic basins. Deep-sea Res., 6(3), 217-233.

Stommel, H. and A. B. Arons, 1960c. On the abyssal circulation of the world ocean. I. Stationary planetary flow pattern on a sphere. Deep-Sea Res., 6(2), 140-154.

Warren, B. A., 1973. Transpacific hydrographic sections at Lats. 43°S and 28°S: the Scorpio Expedition - Part II: Deep Water. Deep-Sea Res., 20(1), 9-38.

Warren, B. A., 1974. Deep flow in the Madagascar and Macarene Basins. Deep-Sea Res., 21(1), 1-21.

Worthington, L. V., 1970. The Norwegian Sea as a Mediterranean Basin. Deep-Sea Res., 17, 77-84.

Worthington, L. V., 1976. On the North Atlantic circulation. The Johns Hopkins Oceanographic Studies, 6, 110 pp.

Worthington, L. V., 1977. Intensification of the Gulf Stream after the winter of 1976-77. Nature, 270, 5636, 415-417.

ADDITIONAL READING

Fuglister, F. C., 1960. Atlantic Ocean atlas of temperature and salinity profiles and data from the International Geophysical Year of 1957-1958. Woods Hole Oceanographic Institution Atlas Series, 1, 209 pp.

McCartney, M. S. and L. V. Worthington, 1979. Anomalous water mass distribution at 55°W in the North Atlantic in 1977. J.M.R. (in press).

Reid, J. L. and R. J. Lynn (1971). On the influence of the Norwegian-Norwegian-Greenland and Weddell Seas upon the bottom waters of the Indian and Pacific Oceans. Deep-Sea Res., 18, 1063-1088.

Richardson, P. L., 1977. On the cross-over between Gulf Stream and western boundary undercurrent. Deep-Sea Res., 24, 139-159.

Stommel, Henry, 1958. The abyssal circulation. Deep-Sea Res., 5, 80-82.

Stommel, H. and A. B. Arons, 1960. On the abyssal circulation of the world ocean. I. Stationary planetary flow pattern on a sphere. Deep-Sea Res., 6,(2), 140-154.

Stommel, H. and A. B. Arons, 1960. On the abyssal circulation of the world ocean. II. An idealized model of the circulation pattern and amplitude in oceanic basins. Deep-Sea Res., 6(3), 217-233.

Swallow, J. C. and L. V. Worthington, 1961. An observation of a deep counter-current in the western North Atlantic. Deep-sea Res., 8, 1-19.

Veronis, G., 1973. Model of world ocean circulation: I. Wind-driven, two-layer. Jour. Mar. Res., 31(3), 228-288.

Veronis, G., 1976. Model of world ocean circulation: II. Thermally driven, two-layer, Jour. Mar. Res., 34(2), 199-216.

Veronis, G., 1978. Model of world ocean circulation: III. Thermally and wind driven. Jour. Mar. Res., 36(1), 1-44.

Warren, Bruce A., 1970. General circulation of the South Pacific. In Scientific Exploration of the South Pacific, W. S. Wooster, ed., Nat. Acad. Sci., Washington, p. 33-49.

Warren, B. A., 1971. Antarctic deep water contribution to the world ocean. Res. in the Antarctic, Am. Assoc. Adv. Sci., 631-643.

Warren, B. A., 1973. Transpacific hydrographic sections at Lats. 43°S and 28°S: the Scorpio Expedition - Part II: Deep Water. Deep-Sea Res., 20(1), 9-38.

Warren, B. A., 1974. Deep flow in the Madagascar and Macarene Basins. Deep-Sea Res., 21(1), 1-21.

Worthington, L. V., 1969. An attempt to measure the volume transport of Norwegian Sea overflow water through the Denmark Strait. Deep-Sea Res. Supp. to 16, 421-432.

Worthington, L. V., 1970. The Norwegian Sea as a Mediterranean basin. Deep-Sea Res., 17, 77-84.

Worthington, L. V. and W. R. Wright, 1970. North Atlantic Ocean atlas of potential temperature and salinity in the deep water, including temperature, salinity and oxygen profiles from the Erika Dan cruise of 1962, Woods Hole Oceanographic Institution Atlas Series, 2, 58 plates.

Worthington, L. V., 1976. On the North Atlantic circulation. The Johns Hopkins Oceanographic Studies, 6, 110 pp.

Wüst, W. R., 1957. Stromgeschwindigkeiten und Strommengen in den Tiefen des Atlantischen Ozeans. Wiss. Ergebn. dtsch. atlant. Exped. 'Meteor', 6, Teil 2, 262-420.

Notes Submitted by
David Topham

Lecture #5.   POLAR - SUBPOLAR INFLUENCE TWO

1. Introductory Remarks and Summary

The consideration of the "Polar Influence" was concluded briefly with
discussions of the Antarctic Bottom Water-North Atlantic Deep Water transi-
tion on the $2^{0}C$ isotherm and the possible importance of meridional water
mass exchange ("leakage" from the circumpolar system) at depth southeast of
New Zealand, where the horizontal transition between these water masses at
3000 db is conspicuously sharp. We next considered the large-scale circula-
tion of the North Atlantic, poleward of the main anticyclonic gyre. Observed
distributions of conservative (i.e. internally source-free) tracers(salinity,
temperature, homogeneity index), indirect evidence of local winter convective
overturning, and the previously described scheme of circulation in lower lati-
tudes are synthesized to produce a general picture of the large-scale water
mass properties and transports. The picture includes a cyclonic gyre between
the northern branch of the subtropical gyres and the margins of the polar
basin. A steady-state calculation of advective transfer of internal energy
across a parallel, balanced by the negative surface energy balance poleward of
the parallel, yields a volume transport estimate in order-of-magnitude agree-
ment with independent estimates.

Attention is turned to the water mass structure and exchanges in the
Southern Hemisphere. Observational evidence is cited for the importance of
thermostad layers, particularly the Subantarctic Mode Water (SAMW), as tracers
around the entire circumpolar current system. Other data are shown which indi-
cate the circulation of this water mass within the subtropical gyre systems of
the South Atlantic and Pacific, with "injections" of SAMW occurring near their

southwestern edges. A highly simplified dynamical argument that relates the planetary vorticity to the vertical stability of the water column is consistent with the idea of a closed circulation of SAMW around the subtropical southern hemisphere gyres.

2. Conclusion of "The Polar Influence"

Recent GEOSECS data may be regarded as an update of Wüst's western South Atlantic sections. GEOSECS T-S diagrams show a pronounced kink where two approximately linear T-S curves with different slopes intersect (Broeker, et al, 1976). The intersection is found consistently around the circumpolar current system at the $2^{o}C$ isotherm, and is taken to be an indicator of the transition from warmer, saltier NADW above to colder, fresher AABW below (Fig. 1, see also: Gordon and Rodman, 1977; Craig, et al. 1972). The observational evidence that this transition occurs around the entire circumpolar current system illustrates nicely the eastward spreading of NADW from its entry in the Atlantic. In the horizontal plane (on the 3000 db surface) southeast of New Zealand the temperature distribution reveals a particularly sharp boundary between warmer and colder water masses, in the form of a northward protrusion (about $1^{o}C$) of AABW along the southeastern margin of the Campbell Plateau alongside a southward protrusion of warmer ($1.5^{o}C$) water only 5 degrees of longitude to the east (Fig. 2). The warmer water may be related to NADW which has come around the continent and is currently circulating in the Pacific gyre system, although Gordon (1967) would probably classify this as South Pacific Deep Water. In any case, the sharpness of this transition betwen the nearly zonal circumpolar deep current and the nearly meridional deep western boundary current is suggestive of mass and property exchanges between the systems, particularly in view of the tongue-like protrusions of temperature. We may
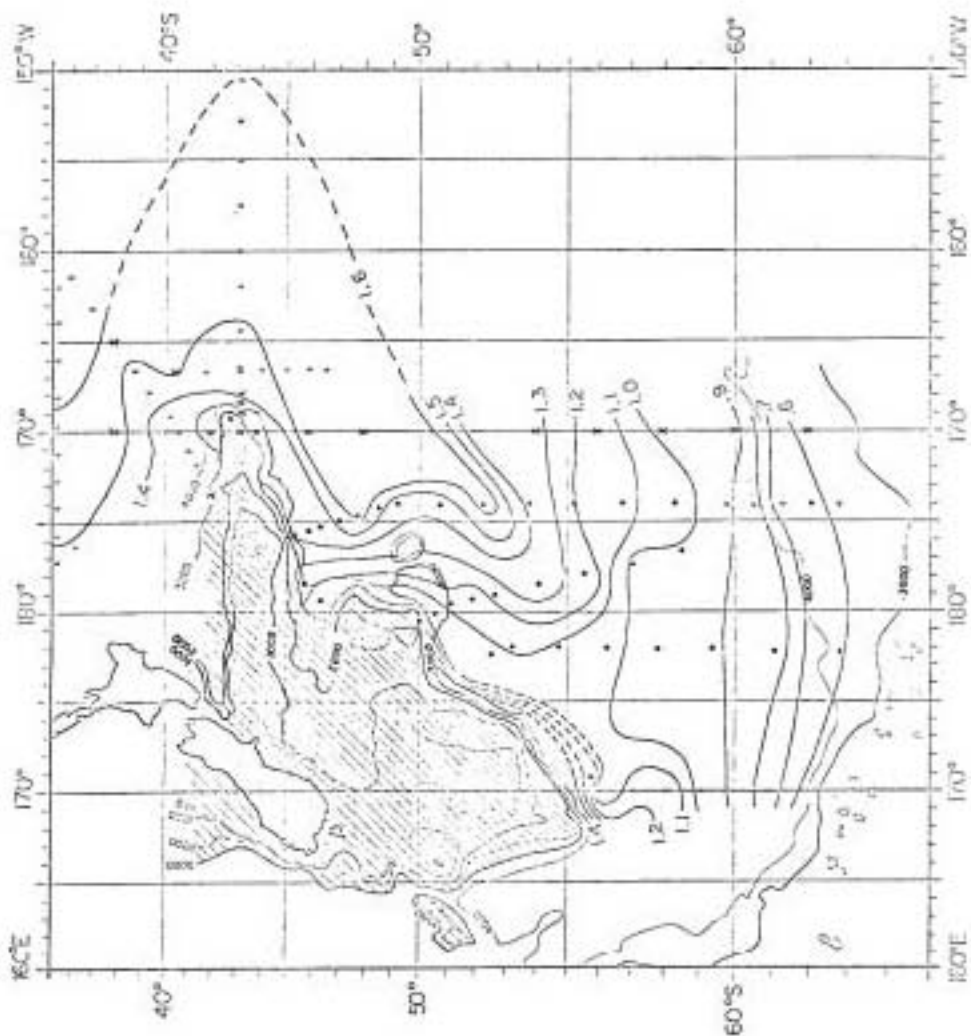
Fig. 2   Horizontal temperature distribution on the 3000 db pressure surface off New Zealand.
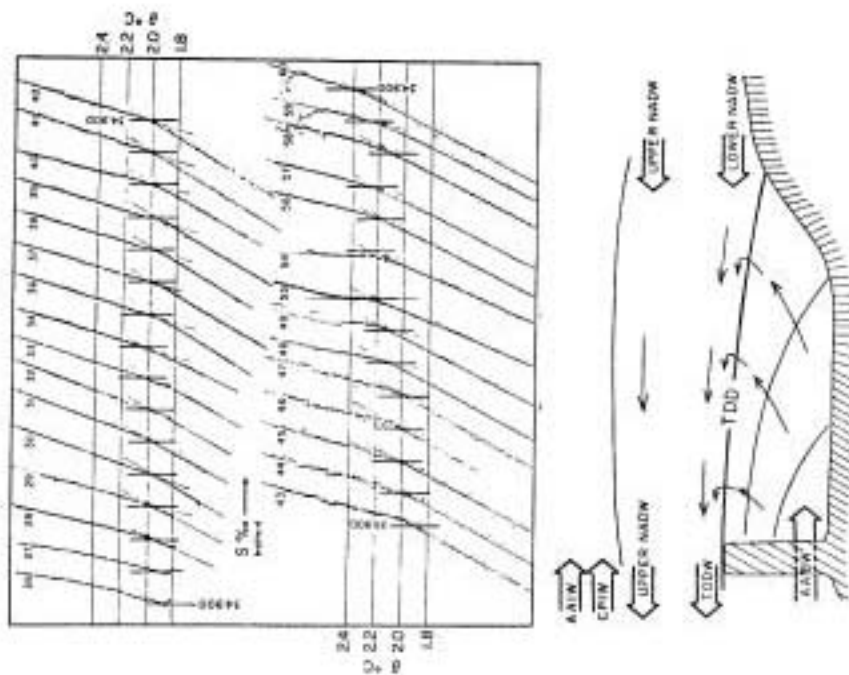
Fig. 1.   0-S plots for the deep waters in the western basin of the Atlantic (from Broeker, et al., 1976).

think of such an exchange as a localized "leakage" of the circumpolar system into the lower-latitude gyre system.

3. The Subpolar North Atlantic

We begin our consideration of the region with a look at a summer temperature section which extends directly across the return-flow area in Worthington's Northern gyre system (Worthington, 1976, p. 75), Fig. 3. The section is capped by a warmed seasonal thermocline, below which we find a thermostad layer about $14.5^{o}C$, which layer is particularly thick in the southwestern part of the section. The deepest $14^{o}C$ layer overlies a substantial depression of the main thermocline. No $18^{o}C$ water is evident here. The deep pool of $14^{o}C$ water and associated thermocline depression are perhaps indicative of recent vertical convection and homogenization of the temperature field in the layer, although horizontal advection must surely play some role in such a process. The depression of isotherms, if associated with a depression of isopycnals, implies increasingly anticyclonic geostrophic flow around the deep $14^{o}C$ pool as one moves upward through the water column, leading to Worthington's designation "anticyclogenesis" for the process (whatever it is) responsible for the deep thermostad. Figure 4 shows the location of three more North Atlantic temperature sections and their positions relative to Worthington's Northern gyre for waters with $12^{o}C < T < 17^{o}C$. Sections 7 and 9 (Fig. 5) show the spatially abrupt eastern terminus of the $18^{o}C$ water (here it is nearer $17^{o}C$, recall that the thermostad extends far to the southwest into the Sargasso-Gulf Stream system), with the $14^{o}C$ water to the east. Notice that the latter pool appears to be laterally less extensive than the $18^{o}C$ water. Worthington (1976) associates the domed isotherms (and presumably isopycnals) near station 331 with a thermocline-level low

pressure trough which separates southeastward flow of 17°C water in the Sargasso-Gulf Stream system on the left ("out" of the paper in Fig. 5) from northwestward flow of 14°C water on the right in the Northern Gyre ("into" the paper). The abrupt termination eastward of the 14°C water led to the notion of a tightly closed, compact Northern Gyre in Worthington's circulation diagrams. On Fig. 6 we see the water properties on a section just poleward of the main return flow area in the Northern Gyre. The seasonal thermocline is absent, of course, on this late winter section, and the prominent thermostad layer has a temperature of 11°C, terminating to the east after a limited (400 km) extent. We recall the volumetric T-S diagram presented in earlier lectures (Lecture 1, Fig. 2) for the world ocean, wherein the North Atlantic Central Water masses extended as a high volume linear envelope, with a gap between the nose of the ridge and the isolated mode at 18°C. The 14°C and 11°C modes represent other, less pronounced, volumetric maxima as we move down the axis of the Central Water ridge towards lower T and S. Thus we have identified some of the important volumetric modes in the main thermocline waters of the North Atlantic, and we have a notion of their possible origin, namely the late-winter convective overturning in the various gyre systems. We note that Masuzawa (1969) also located 18°C mode water in the Kuroshio Gyre system of the North Pacific.

Poleward of about 50°N we enter a region of roughly cyclonic surface currents. Given the juxtaposition of surface westerly winds on the equator-ward side of the (atmospheric) Icelandic low pressure system and easterlies on the poleward side, we might expect a cyclonic current pattern because the west-to-east component of the surface wind stress decreases with increasing latitude. Observed tracer fields, such as the salinity on isothermal sur-
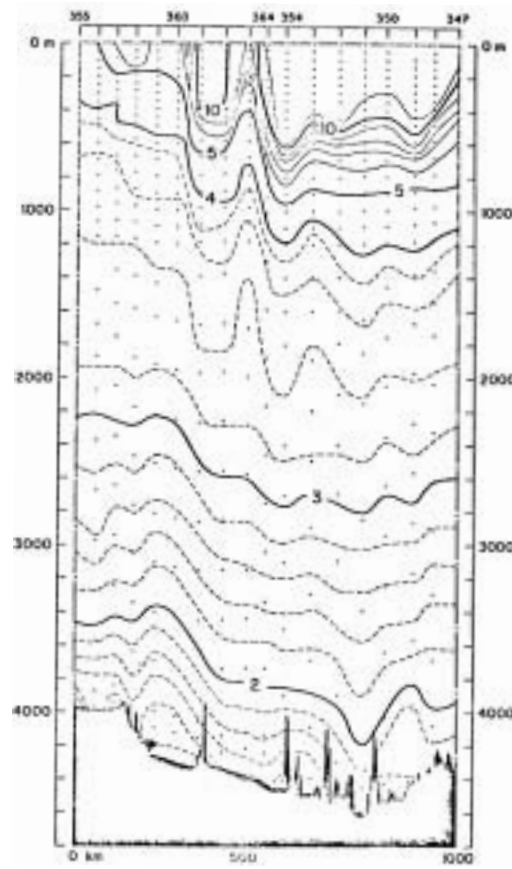
SECTION 12   Northwest Corner
Atlantis II Cruise 9 March - April 1964

Fig. 6.   Temperature section 12.
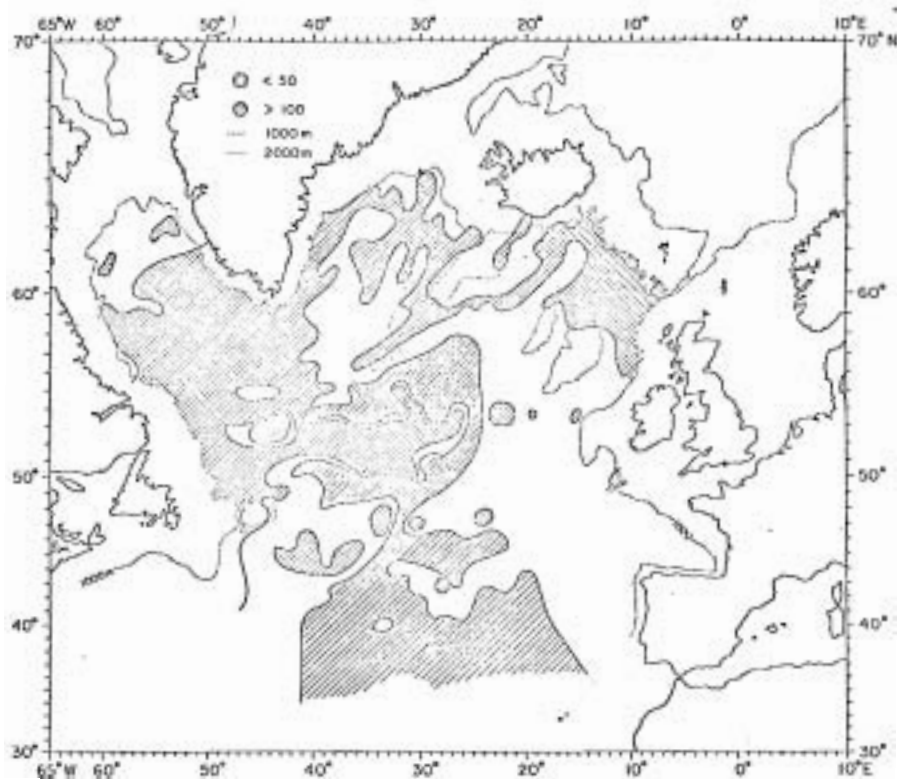
Fig. 7.   Brunt-Väisälä period on the level of its maximum: upper waters
of sub-polar N. Atlantic.
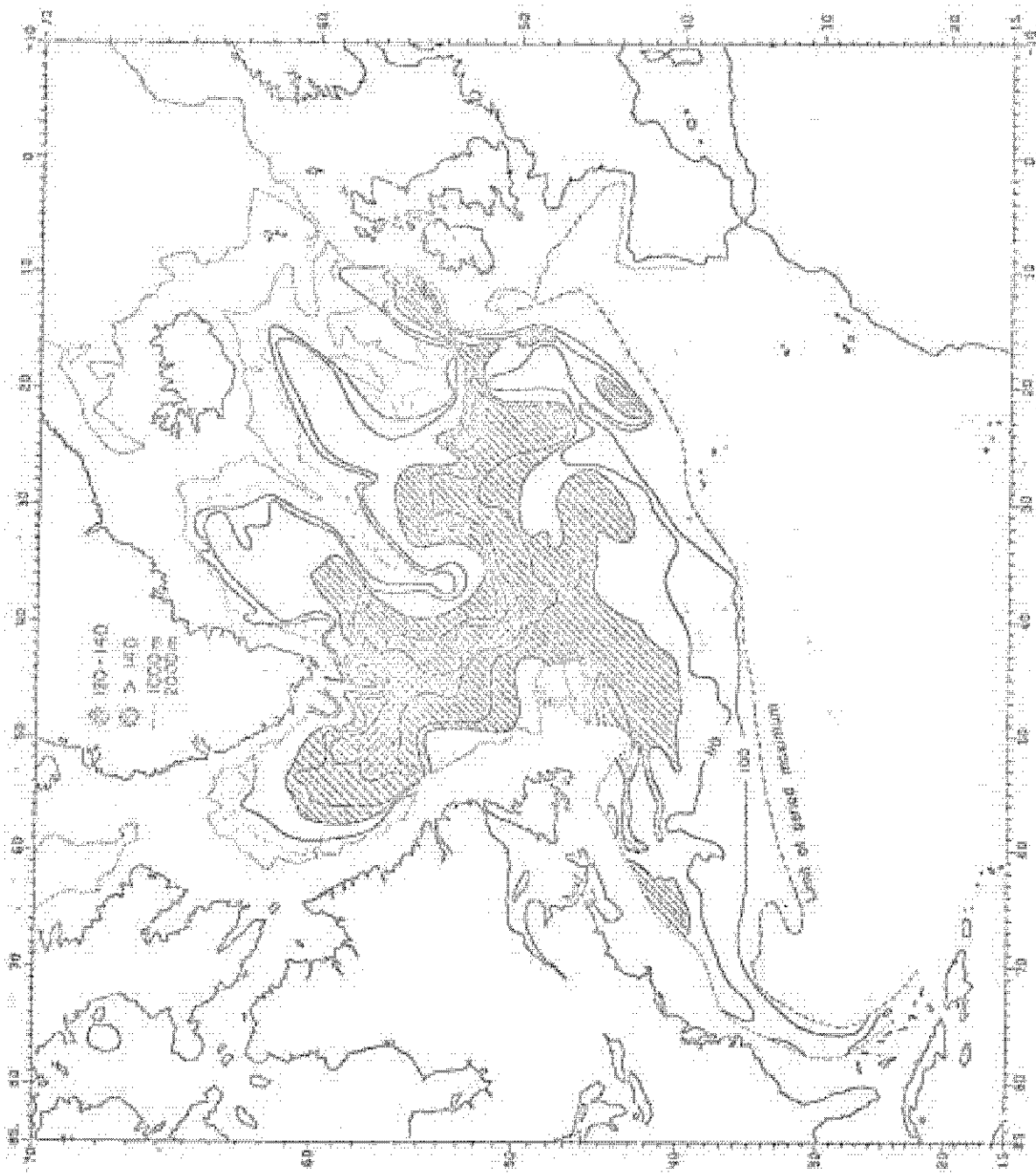
Fig. 8. Brunt-Väisälä period on the level of its maximum: deep waters of sub-polar N. Atlantic

faces, show some indication of tongue-like protrusions of extrema which form a partial loop in the cyclonic sense from the Faroe-Shetland Channel, west past Iceland, through the Irminger Sea and around Kap Farvel into the Labrador Sea. Large-scale water mass analyses in the past have indicated that pycnostadal layers (i.e. layers wherein the local buoyancy period is a vertical maximum) dominate the water mass transport. In Fig. 7 we present the value of the buoyancy period on the level of its maximum value in the upper 1000 m (Figs. 7, 9, 10 and 11 from McCartney and Talley, 1979). Highly homogeneous waters (long period) can be traced around a cyclonically-curved path from the Faroe-Shetland Channel region, westward with a meander across the Reykjanes Ridge, then on into the Irminger and Labrador Seas again. The end product of this cyclonic path is cold, low-salinity Labrador Sea Water. A plot of the same quantity in the 1000-2000 m layer (Fig. 8, from McCartney and Talley, 1979) suggests that the homogeneous Labrador Sea water mass spreads eastward across the basin at depth. This water mass has relatively low temperatures ($3.5^{o}C$) and salinities (34.4 o/oo) compared to other North Atlantic water, and we may consider its renewal by plotting temperature soundings from stations along our cyclonic mode water path (Fig. 9 shows station locations; Fig. 10 shows the soundings). The soundings are representative of late winter conditions when the results of winter cooling and any associated convection should be evident. A well-mixed layer 500 or more meters deep is ubiquitous, below which is found the main thermocline. The mixed-layer temperatures decrease steadily from $18^{o}C$ to around $4^{o}C$ as we move from the Sargasso Sea around to the Irminger Sea. The basal thermocline temperatures (not shown) tend to converge on the value $3.5^{o}C$ for these soundings, the value being characteristic of Labrador Sea Water. Figure 11 shows a deep mixed layer for late February southwest of
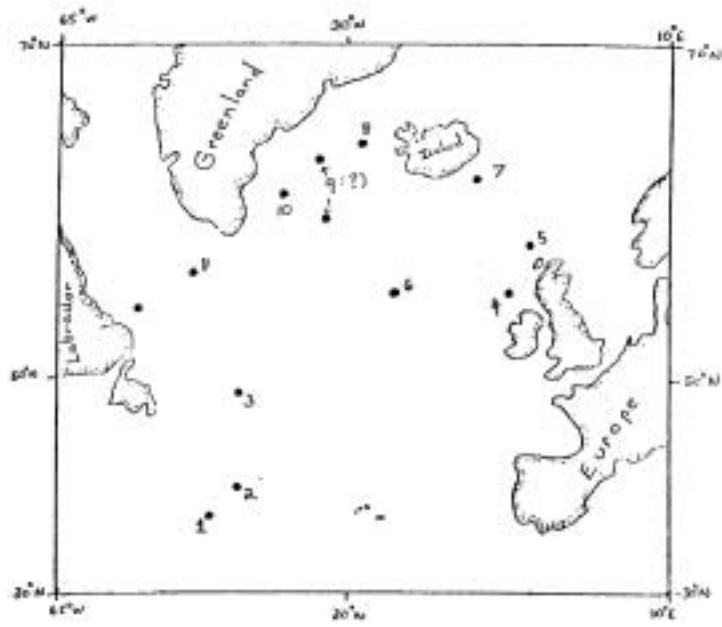
Fig. 9. Location of Late Winter Ncrth Atlantic stations.
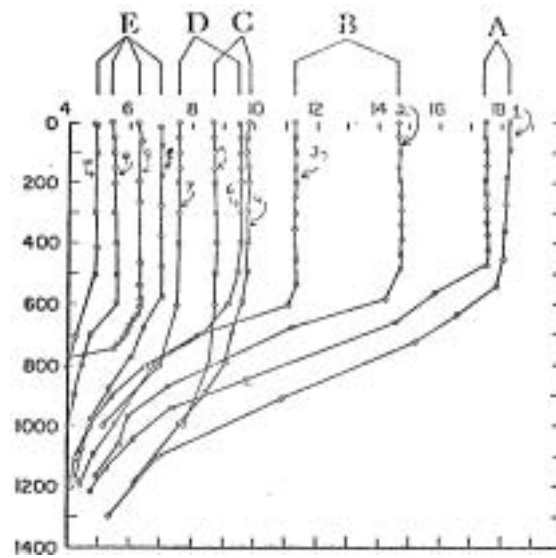
10. Representative Late winter stations from the North Atlantic.
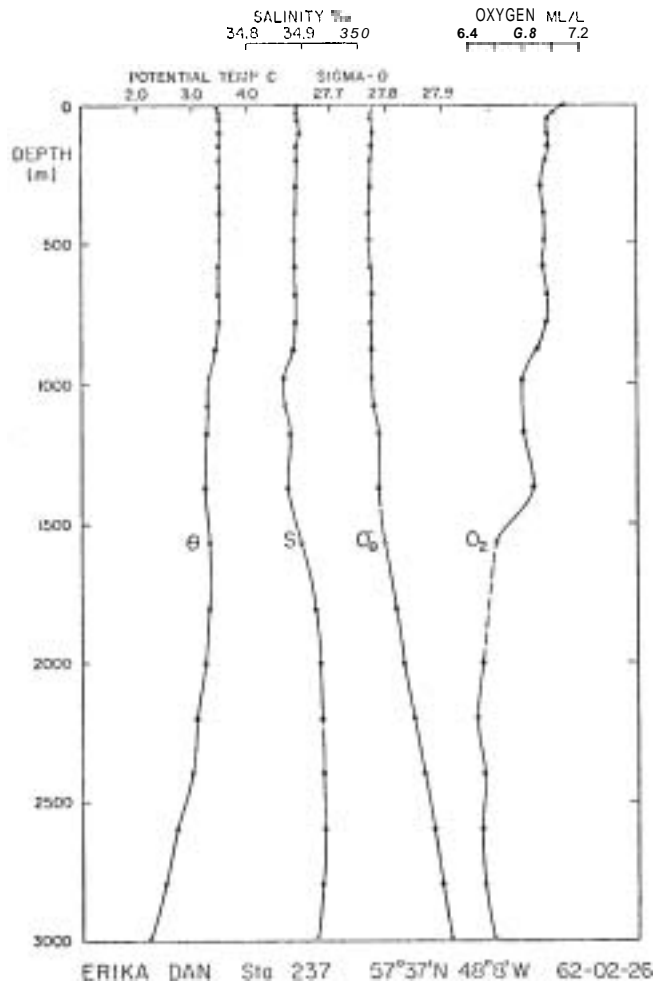
Fig. 11. Sounding in Labrador Sea indicating deep mixing.
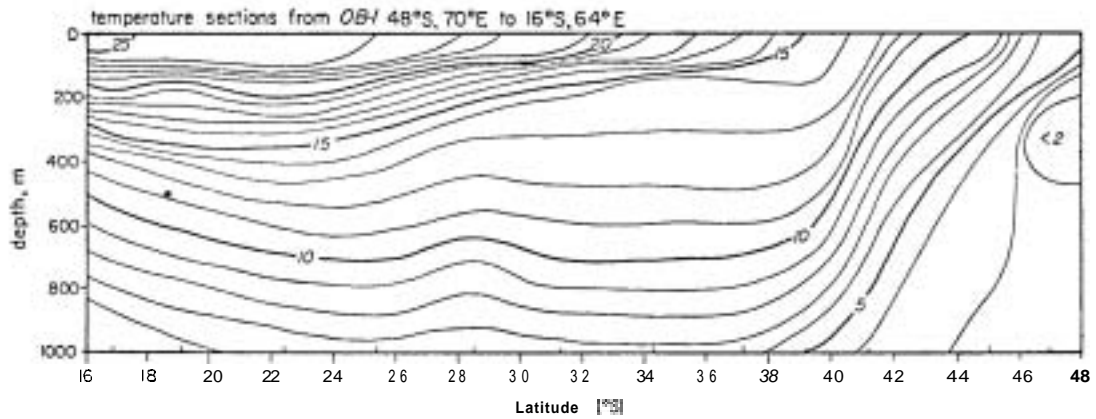
Fig. 12. Southern Ocean temperature section from OB-1.

Kap Farvel. The upper 800 meters are very well ventilated, having a uniformly high oxygen concentration of about 6.9 ml/liter, indicative of very recent contact with the atmosphere. Potential temperature, salinity and density curves are also fairly uniform down to 1500 m and below. It is suggested that the convective event(s), implied by such a sounding, are the formation events for Labrador Sea Water. Note that the mixed-layer temperature here is 3.5°C, as we would expect for Labrador Water renewal. It we attempt to explain the relatively high oxygen concentrations which are maintained in the thermocline waters of the North Atlantic, where the static stability greatly inhibits contact with the surface, we may consider deep convective renewal in the Labrador Sea as the source, with advection of the highly homogeneous waters at depth (e.g. Fig. 8). A simple thermodynamic calculation, assuming that warm water of uniform, representative temperature enters to the east, cools in the north, then exits through the Labrador Sea at 4°C, can be made from rough estimates of the surface energy loss over the northern region and the area over which the loss occurs. The transport of water required to maintain a steady-state for such a system is about 10 Sv, in rough agreement with current meter estimates of the total transport out of the Labrador Sea and the Norwegian overflow combined.

4. Subantarctic Mode Water (SAMW)

Typical summer temperature sections from around the Southern Ocean show extensive thermostad layers situated on the equatorward side of the Antarctic polar front zone, separated from the surface by a seasonal thermocline. Figure 12 shows a 13°C thermostad in the South Indian Ocean, with the pronounced frontal temperature gradient to the south. McCartney (1977) calls these water masses the Subantarctic Mode Water (SAMW). The frontal zone at 200 m is stippled on Fig. 13. Starting in the western South Atlantic the front spirals east

Fig. 14. Thermostad "strength" vs temperature and longitude for the zonal sections on Figure 13 (after McCartney, 1977)
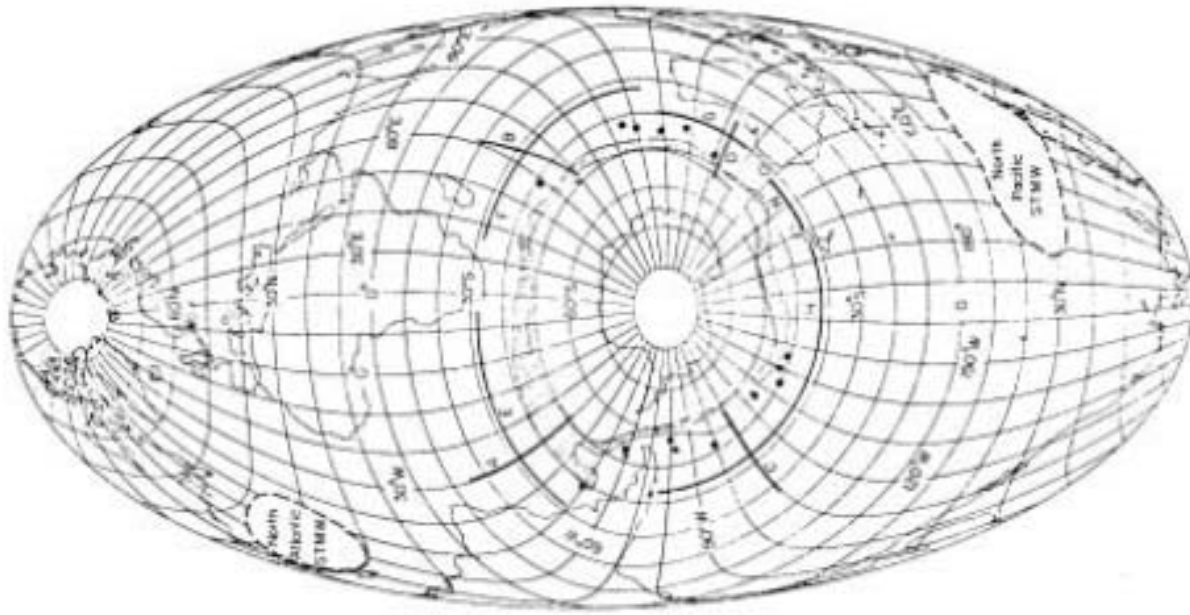
Fig. 13. Location map of the subantarctic front, late-winter stations and circumpolar sections.

and south around the continent until, after passing through Drake Passage, it "jumps" northward in a wide zone near the Brazil-Falkland Confluence. The inverse vertical temperature gradient $\triangle z / \triangle T$ is an index of the strength, or homogeneity, of a thermostad. The extensive zonal sections E, F, G, and H in Fig. 13 were used to calculate $\triangle z / \triangle T$ for various temperature layers at each longitude, roughly following the circumpolar current system from the confluence eastward. The results are shown in Fig. 14, where we see a continuous decrease in SAMW temperature as we move eastward with the current. The sections used for this graph were well equatorward of the formation zone, so the SAMW here is "capped" beneath a seasonal thermocline. The figure also suggests that important processes are to be looked for in the vicinity of the confluence zone east of Drake Passage, where we must somehow renew the warm end of the SAMW axis in the steady state. The longitudinal temperature gradient in the Mode water on Fig. 14 averages about $1^o C/3000$ km, similar to the value for North Atlantic subtropical mode water $(18^o C, 14^o C)$, and perhaps suggests other similarity in structure or process between the two oceans. We again look to the late winter stations for clues regarding the formation of the modes. First, we examine a meridional sequence of winter temperature soundings on 128° east (Fig. 15). Station E873 is located at the frontal zone. Equatorward of this station we can see deep mixed layers with temperatures between 8° and $9^o C$ in a zone which was determined to be about 4° of latitude in width. Further towards the equator the winter mixing has failed to penetrate as deeply, and summer observations in the region show that no thermostad remains for these shallow mixed layers once the summer heating produces the seasonal thermocline. Late winter soundings in the mode water regions all around Antarctica (Fig. 16) indicate a similar convective
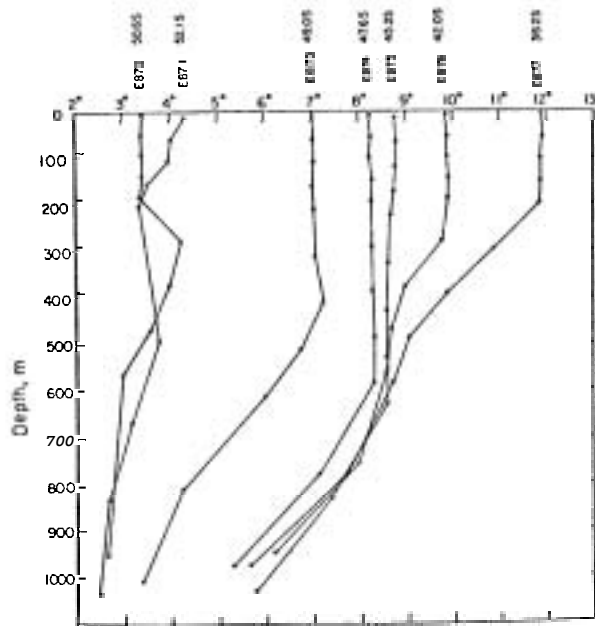
Fig. 15. Winter temperature soundings south of Australia (on 128°E).
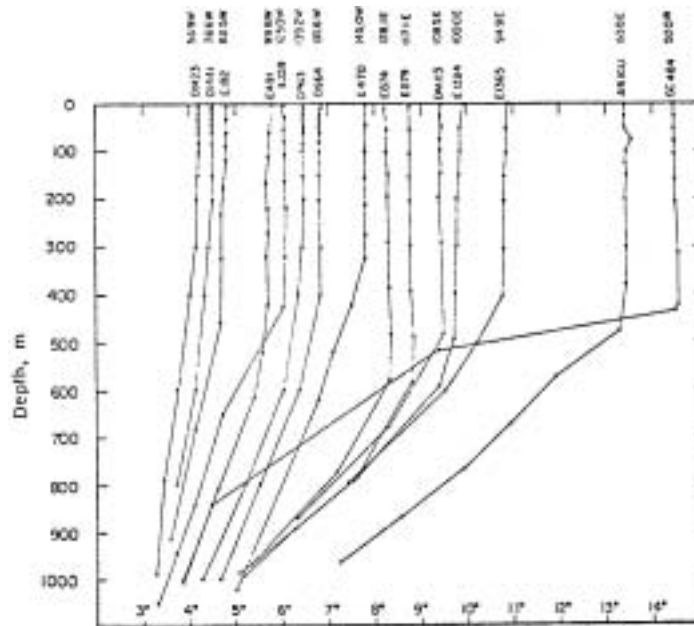
Fig. 16. Winter temperature soundings from stations (dots) shown on Figure 13.

origin for the SAMW. The T-S envelopes for all of these winter stations are shown on Fig. 17 and represent the formation zone T-S characteristics of the Mode water. In Fig. 18 we have the T-S data for SAMW found beneath the summer thermocline, which data were used to construct the SAMW axis on Fig. 14. Figure 17 and 18 practically overlay, lending credence to the postulated SAMW formation mechanism of convective overturning in a definite latitude band which, however, will vary with longitude. As McCartney (1977) points out, these thermostads make ideal tracers after they are isolated from the ocean's surface by the seasonal thermocline. The point was raised that the formation mechanism appears similar to that of North Atlantic SAMW, but the thermal forcing in the two regions must differ because the continent–ocean distribution in the north leads to frequent, intense "outbreaks" of cold, continental air, but the Southern Ocean does not have such large continents. However, Zillman's (1972) calculations of convective and evaporative energy fluxes from ocean to atmosphere for the Southern Ocean indicate order–of–magnitude agreement with the Northern Hemisphere values, suggesting that similar thermal forcing may indeed obtain. Surface heat fluxes over the South Indian and South Atlantic (Fig. 5) have been computed by Bunker (unpublished). In the South Atlantic the maximum surface heat loss contour overlies the SAMW formation zone, and a reasonable spatial correspondence is also found in the Indian Ocean. These results support the notion of similar formation processes for Mode waters in Northern and Southern Hemispheres.

We now examine the possible significance of SAMW in the Subtropical Gyre circulation of the Southern Ocean. Volumetric T-S diagrams for the South Pacific and Indian Oceans (Figs. 19 and 20) are overlaid on the T-S curves of the pycnostad layers (defined again by a vertical maximum in the buoyancy
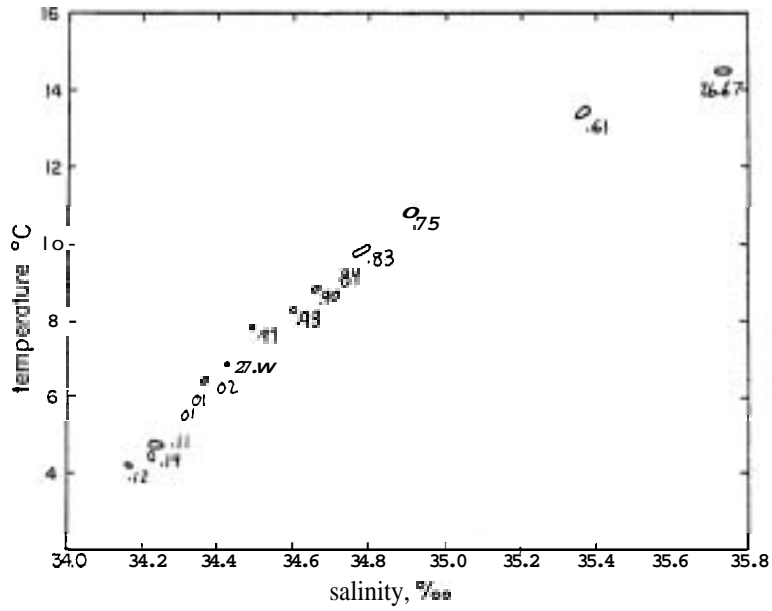
Fig. 17. T-S envelopes for SAMW formation region.
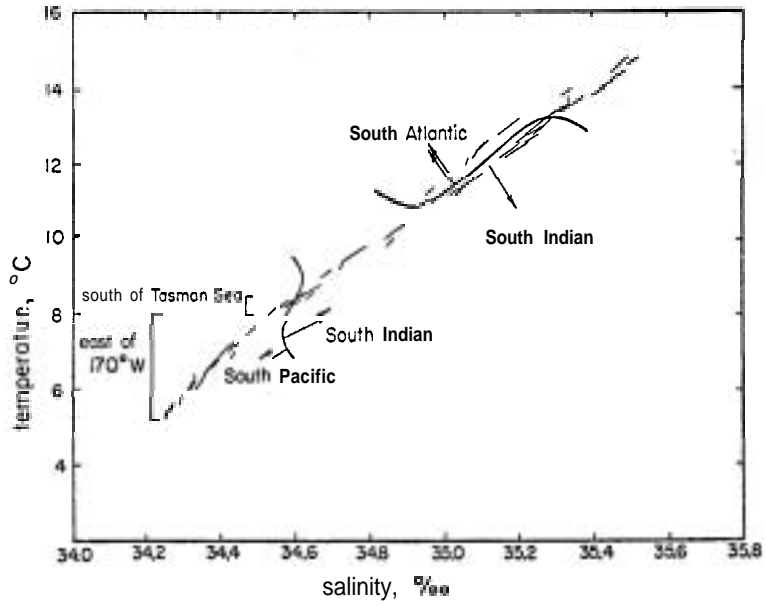
Fig. 18. T-S curves for SAMW capped below summer thermoclines.
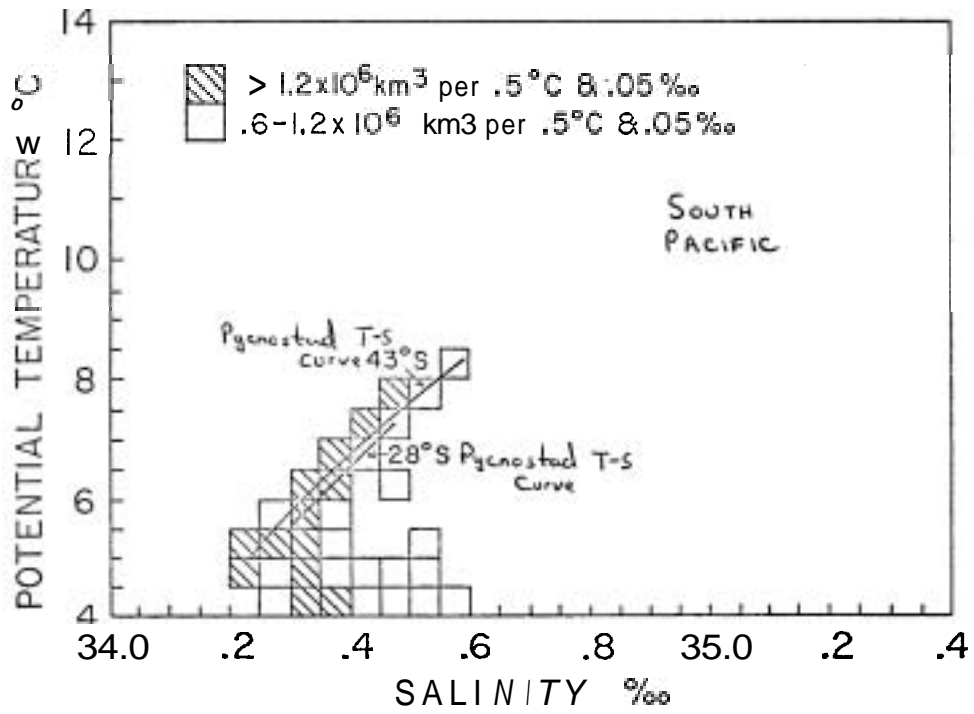
Fig. 19. Volumetric T–S diagram for the South Pacific.
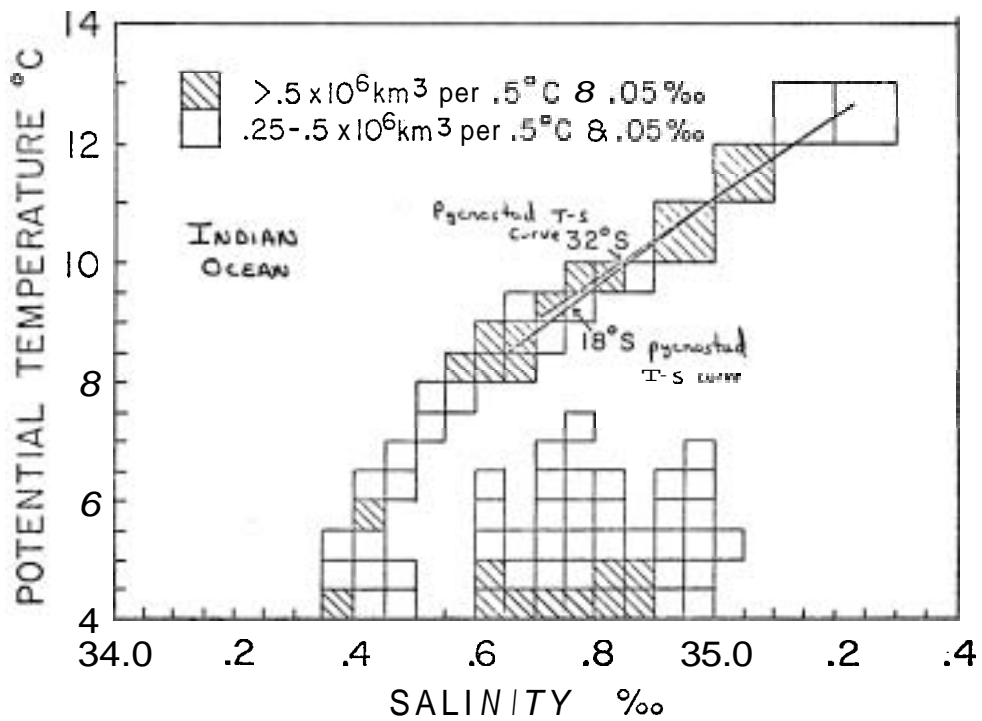
Fig. 20. Volumetric T–S diagram for the Indian Ocean.
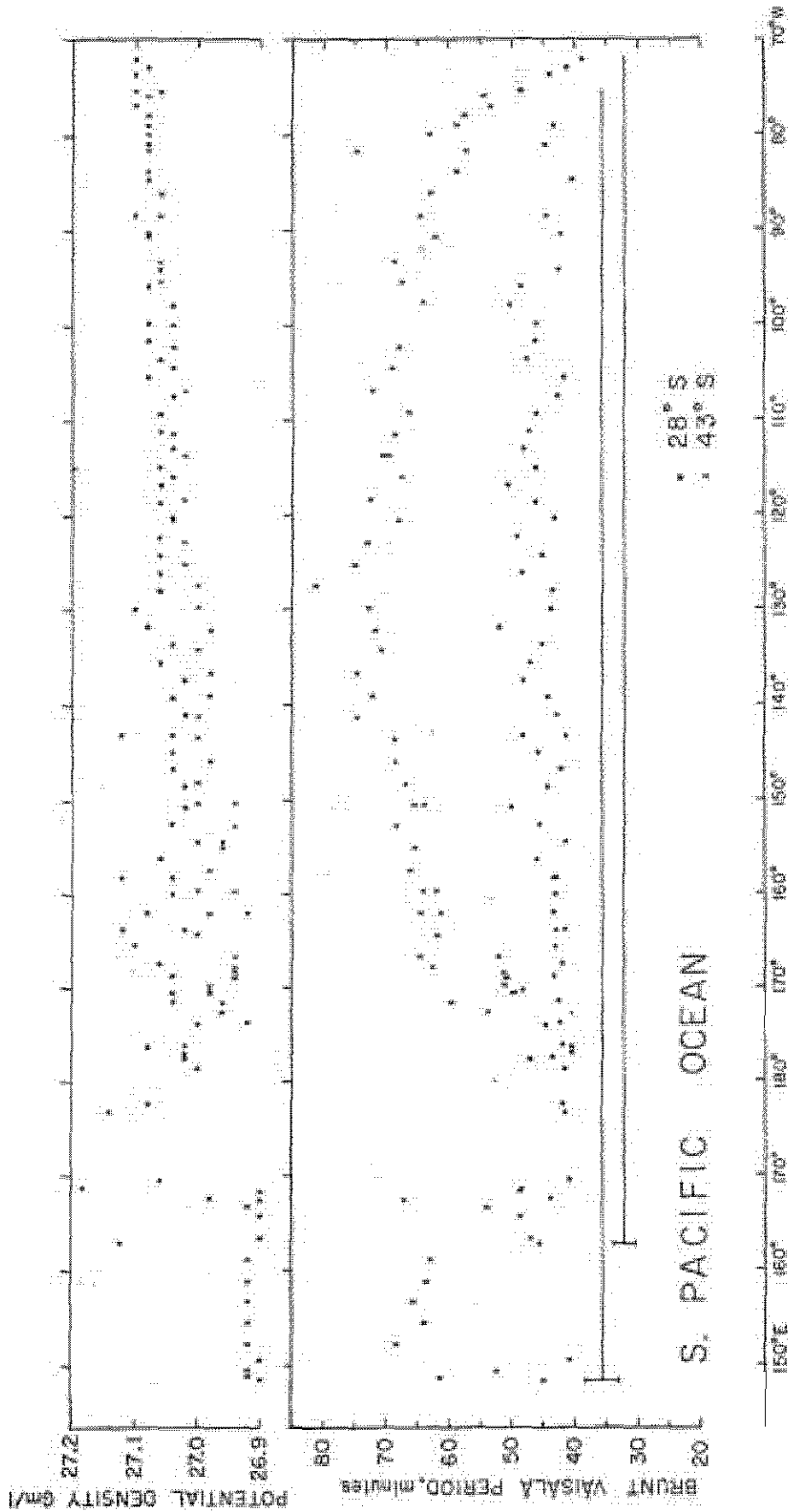
Fig. 21. Potential density and Brunt-Väisälä period at latitudes 28°S and 43°S across the South Pacific Ocean, on the level of maximum period.
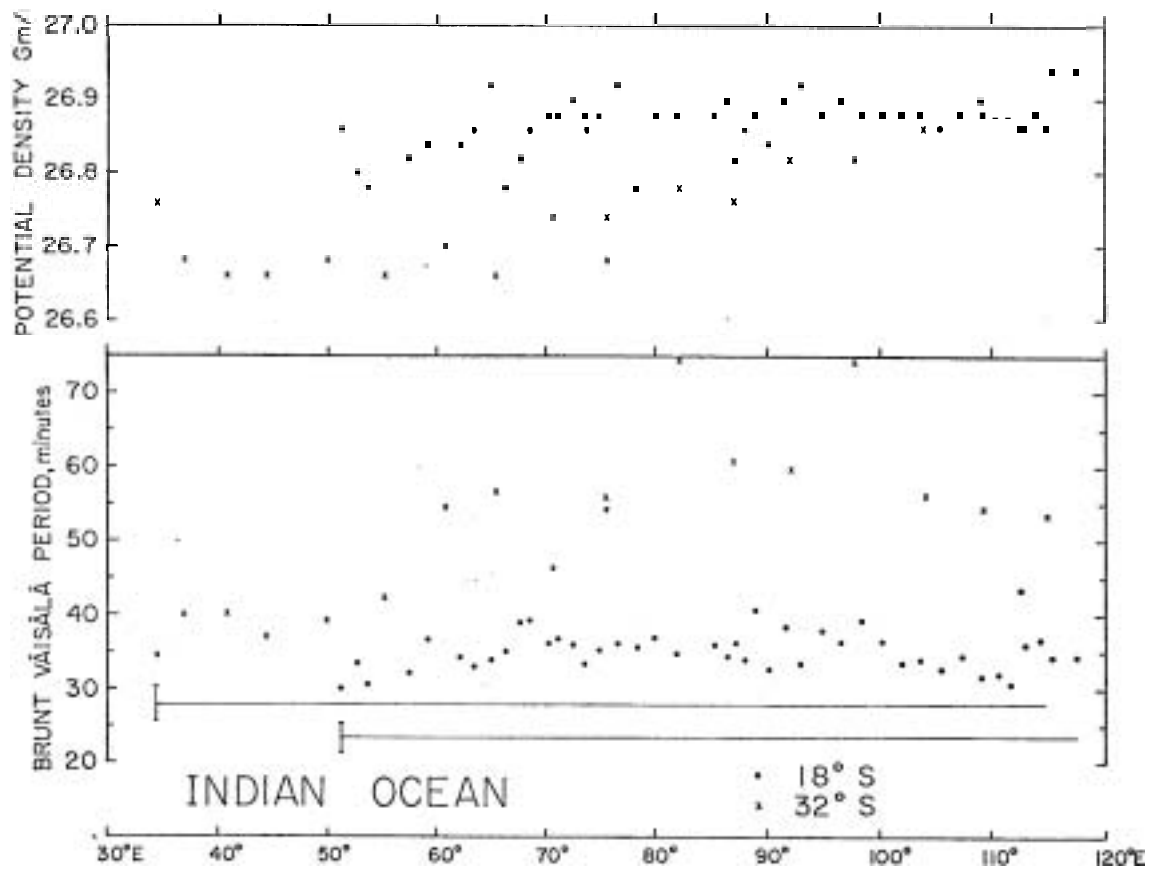
Fig. 22. Potential density and Brunt Väisälä period at latitudes $18°S$ and $32°$ across the Indian Ocean, on the level of maximum period.

period) found in the respective gyres (with poleward and equatorward branches plotted). The good correspondence between the volumetric maxima and the pycnostad T–S curves in the gyres shows that Mode Water could indeed be circulating around these gyres. If we plot the buoyance period of the Mode Water against longitudes we move west–to–east along the poleward side of the gyre and then east–to–west along the equatorward side, we see that the static stability $\left|\frac{\partial \rho}{\partial z}\right|$, which varies inversely with the buoyancy period, <u>is larger on the equatorward side</u> (Fig. 21 and 22, from McCartney, 1979a). This observation is consistent with the $\left|\frac{\partial \rho}{\partial z}\right|$ distribution expected from conservation of potential vorticity $f\frac{\partial \rho}{\partial z}$ in a highly simplified flow (see Appendix), lending further support to the notion of SAMW circulation in the gyres.

The transport of SAMW from the circumpolar current into the gyres is probably associated with the "jump" in frontal position at the Brazil–Falkland confluence area. McCartney (1977) states that SAMW with low T–S values enters Drake Passage from the SE Pacific and turns north with the Falkland current at intermediate depth. A strong pycnocline separates this flow from the $14^{\circ}C$ (locally formed) SAMW above (Lecture 6, Fig. 7) which moves SE as part of the Brazil Current. The cold fresh SE Pacific SAMW enters the gyre system here with T–S characteristics very similar to those of Antarctic Intermediate Water. McCartney notes that this process is a substantial deviation from the "classical" concept of Wust and Deacon, wherein Antarctic Surface Water and Subantarctic Surface Water mix and sink along the entire polar front zone around the continent, forming AIW as a mixture.

<div align="center">REFERENCES</div>

Broecker, W. S., T. Takahashi and Y. H. Li, 1976. Hydrography of the Central Atlantic. I. The two–degree discontinuity. <u>Deep–sea Res</u> , 23, 1083–1104.

Craig, H., Y. Chung and M. Fiadeiro, 1972. A benthic front in the South Pacific. Earth and Planetary Science Letters, 16, 50–65.

Gordon, A. L., 1967. Oceanography of Antarctic Waters. Antarctic Res. Ser., 169–203.

Gordon, A. L. and M. R. Rodman, 1977. Southern Ocean temperature gradient near 2°C. A Voyage of Discovery, M. Angel (ed.), 85–102.

Masuzawa, J., 1969. Subtropical Mode Water. Deep–Sea Res., 16, 463–472.

McCartney, M. C., 1977. Subantarctic mode water. A Voyage of Discovery, M. Angel (ed.), Pergamon, 103–119.

McCartney, M. C., 1979a. The subtropical recirculation of subantarctic mode water in the South Pacific and South Indian Oceans. Sub Judis.

McCartney, M. C. and L. Talley, 1979. The upper water thermostad family of the subpolar North Atlantic Ocean. (In preparation)

Talley, L. and M. C. McCartney, 1979. The circulation of Labrador sea water. (In preparation)

Worthington, L. V., 1976. On the North Atlantic Circulation. The Johns Hopkins Oceanographic Studies, 6, 110 p.

Zillman, J. W., 1972. Solar radiation and sea–air interaction south of Australia. Antarctic Oceanology II - New Zealand Sector, D. Hayes (ed.), 11–40.

APPENDIX

Consider a rapidly rotating, stratified, incompressible, "Boussinesq", hydrostatic fluid in steady–state motion. Let the flow have a low Rossby number, characteristics of the time average, large–scale oceanic gyres, leading to dominance of the geostrophic balance and the following familiar vorticity equation:

$$v\beta = f\frac{\partial w}{\partial z}$$

where $\beta = \frac{\partial f}{\partial y}$

and $\quad \dfrac{\partial w}{\partial z} = -\left(\dfrac{\partial u}{\partial x} + \dfrac{\partial v}{\partial y}\right)$

has been used from the conservation of mass equation. Since $f = f(y)$ we can write the vorticity equation in the form:

$$\frac{\Delta f}{dt} - f \frac{\partial w}{\partial z} = 0 \qquad (1)$$

where $\quad \dfrac{d}{dt} = u\dfrac{\partial}{\partial x} + v\dfrac{\partial}{\partial y} + w\dfrac{\partial}{\partial z}$

The constraints of geostrophy and hydrostatic balance imply the thermal wind relationships between the density field and the vertical shear of the horizonal velocity components:

$$\frac{\partial v}{\partial z} = -\frac{g}{f\rho_0}\frac{\partial \rho}{\partial x}$$

$$\frac{\partial u}{\partial z} = \frac{g}{f\rho_0}\frac{\partial \rho}{\partial y}$$

(ρ_0 = average density for use as an inertia (2) in Boussinesq eqs)

In an incompressible flow the density is conserved on a trajectory, in the absence of diffusion, internal sources or other diabatic influences (perhaps rather restrictive assumptions for treatment of long-term average water mass movements), so that:

$$u\frac{\partial \rho}{\partial x} + v\frac{\partial \rho}{\partial y} + w\frac{\partial \rho}{\partial z} = 0 \qquad (3)$$

Solving for $-w$ gives us

$$-w = \frac{1}{p_z}\left(u\, p_x \; + \; v\, p_y\right)$$

(subscripts denote differentiation with respect to the indicated variable x,y,or z). Thus

$$-\frac{\partial w}{\partial z} = \left(u\,\frac{p_x}{p_z} + v\,\frac{p_y}{p_z}\right)_z$$

and

$$-\frac{\partial w}{\partial z} = \frac{1}{p_z}\left(u_z p_x + v_z p_y\right) + u\left(\frac{p_x}{p_z}\right)_z + v\left(\frac{p_y}{p_z}\right)_z \tag{4}$$

Substituting for u_z and v_z from equation (2), we see that the leading term on the right hand side of (4) is zero. Carrying through the derivative operation on the second and third terms yields

$$-\frac{\partial w}{\partial z} = u\left(\frac{p_{xz}}{p_z} - \frac{p_x\, p_{zz}}{p_z^2}\right) + v\left(\frac{p_{yz}}{p_z} - \frac{p_y\, p_{zz}}{p_z^2}\right)$$

so that

$$-p_z\frac{\partial w}{\partial z} = u\left(p_z\right)_x + v\left(p_z\right)_y - \frac{p_{zz}}{p_z}\left(u\, p_x + v\, p_y\right)$$

Now substitute for $u\, p_x + v\, p_y$ from equation (3) to get

$$-p_z\frac{\partial w}{\partial z} = u\left(p_z\right)_x + v\left(p_z\right)_y + \frac{p_{zz}}{p_z}\left(w\, p_z\right) = \frac{d}{dt}\left(p_z\right)$$

Using the above relation in equation (1) gives us

$$\rho_z \frac{df}{dt} - f \frac{d(\rho_z)}{dt} = 0$$

$$\Rightarrow \frac{d}{dt}\left(f \frac{\partial \rho}{\partial z}\right) = 0$$

The quantity $f \frac{\partial \rho}{\partial z}$ is conserved for a fluid particle along its trajectory. Physically, the particle is required to stretch or shrink as the local Coriolis parameter f varies during meridional excursions. Since we require motion on density surfaces, we get a corresponding increase or decrease in the stability $\frac{\partial \rho}{\partial z}$ as the parcel moves (see Fig. next page). If our assumed flow field is a valid approximation to long-term mean conditions in the major ocean-ic gyres, then we would expect to see a large buoyancy period (i.e. a small $\left|\frac{\partial \rho}{\partial z}\right|$) in high latitudes where f is large, and vice versa in low latitudes. Recall from Figure 22 that this seems to be the case in the gyre circulation, which might be taken as an indication that the parcel trajectories are indeed "closed" within a gyre if we a priori are confident that our dynamics are applicable.
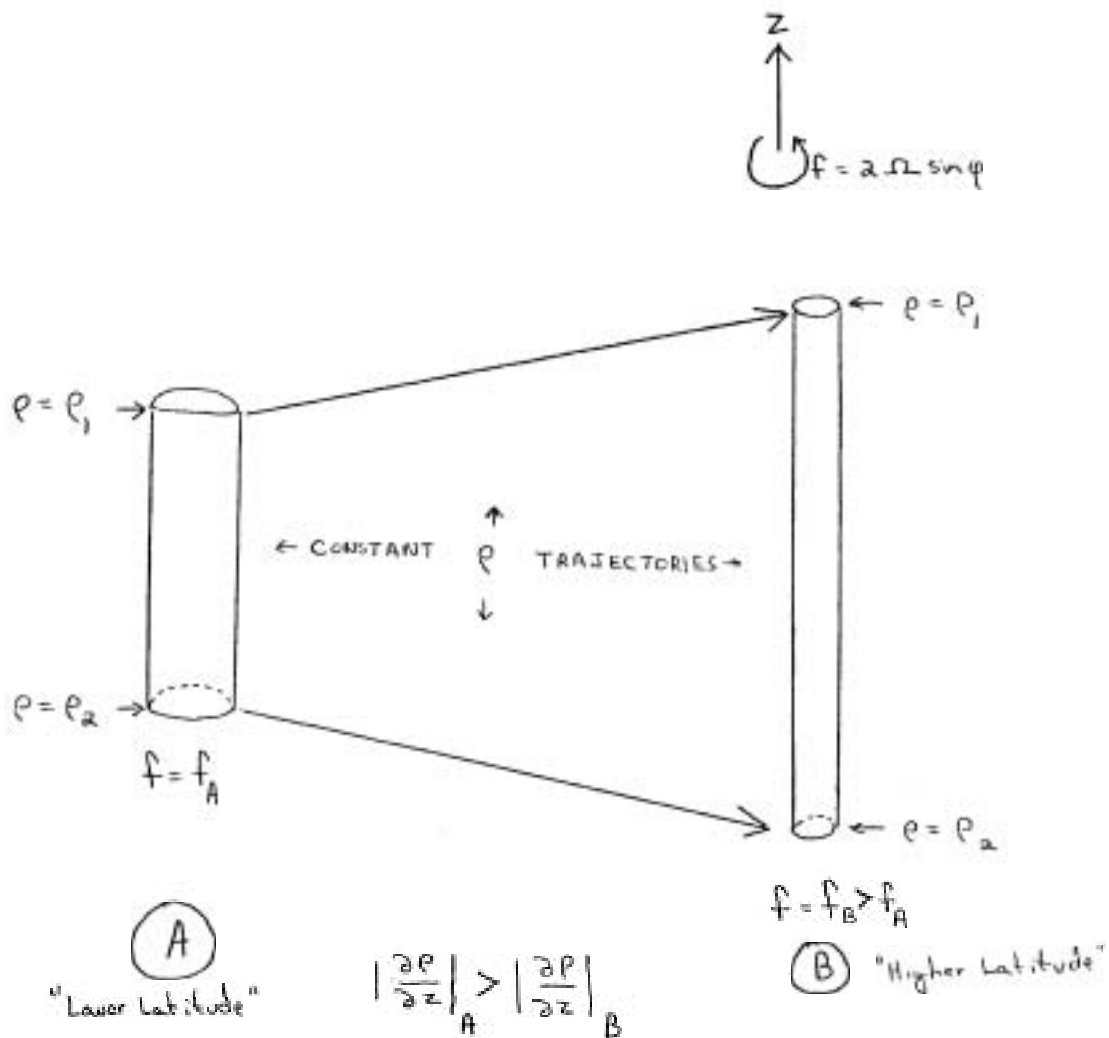
The vortex must "stretch" to conserve its absolute angular momentum about a vertical axis when f increases, because as its moment of inertia decreases, $-\nabla \cdot \underline{u} = \frac{\partial w}{\partial z}$ implies vertical extension. Trajectories constrained to <u>stretch</u> <u>on constant</u> ρ surfaces must then change the stability $\frac{\dot{\partial \rho}}{\partial z}$

Notes Submitted by
Richard Moritz

Lecture #6   ANTARCTIC INTERMEDIATE WATER: FORMATION AND INFLUENCE

Introduction

Around Antarctica, moving from the continent northward, we meet three different surface waters separated by two fronts: the Antarctic Surface Water, the Polar Front, the Polar Frontal Zone Water, the Subantarctic Front or Zone of convergence, and finally the Subantarctic Surface Water. The situation, however, may not be so simply depicted, the vertical structure is of great importance. A vertical north-south section off Antarctica was presented in Lecture 1. The arrows show the meridional flow components that traditionally are supposed to exist. The evolution of this concept was discussed in Lecture 1 (Fig. 1).

The traditional scheme may be described as follows: The excess of precipitation over evaporation, and the melting of ice, produce at high latitudes cold fresh water masses. Winter mixing by convection deepens this surface layer into a real mass of water of homogeneous properties, the Antarctic Water. Moving southward, the warmer but saltier circumpolar deep water upwells to meet the Antarctic Water. Despite their different properties, the two water masses have almost the same density; as a result the Antarctic Water is divided in two parts: the Bottom Water sinking along the shelf break and the Antarctic Surface Water moving north into and through the polar front zone. This second part mixes with Subantarctic Water, sinks and forms the so-called Antarctic Intermediate Water (AAIW). This newly formed water behaves like a tongue of fresh water and flows northward at depths of 600 - 1100 meters. Its influence in the three great basins (Atlantic, Indian and Pacific Oceans) can be traced

up to the Equator, and across **it** in the Atlantic and Pacific Oceans. The extent and the importance of that influence, as well as the nature of the formation process, is the purpose of this lecture.

Properties of the Antarctic Intermediate Water (AAIW)

By definition AAIW is low in salt, and generally **it** is oxygen rich. Its temperature ranges between 4 and 6°C; its density range is correspondingly narrow. Observations show that these properties are advected long distances with only slight erosion by mixing and therefore constitute good tracers. AAIW is comparatively homogeneous at depths of a few hundred meters to around 1000 m. While moving equatorward, a slight mixing increases to salinity and consumption of oxygen reduces the concentration, but nevertheless the salt deficiency and the high oxygen concentration are observed as far as the Equator (in the South Pacific Ocean, for instance). On a volumetric T–S diagram (Lecture 1, Fig. 2) AAIW ($\theta \sim 5^o$C, S $\sim$ 34.2 o/oo to 34.4 o/oo in the South Pacific) forms a high volume class, and for this reason may be called a Mode.

AAIW is found all around the Subantarctic zone. McCartney (1977) plotted the calculated thermostad strength $\Delta z / \Delta \theta$ as a function of temperature and longitude around Antarctica (see Lecture 5). This graph clearly shows a high constant thermostad strength (high homogeneity) at 4°–5^oC, the tem–perature of AAIW.

Figure 1 shows a variation of that graph, and also displays the variations of potential temperature and salinity for Subantarctic Mode Water around Antarctica. These two properties sharply increase at the exit of Drake Passage due to the influence of the Brazil Current, then monotonically decay eastward. These variations around the world may be explained by simple circulation model, as **it** will be shown later.
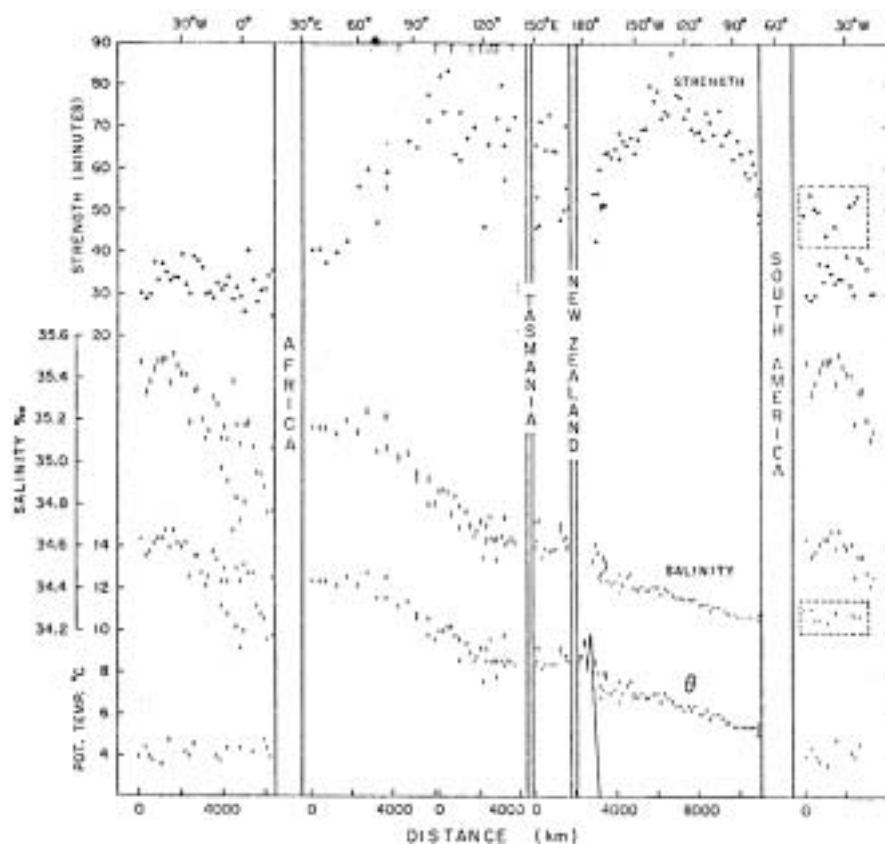
Fig. 1. Variations of AAIW properties around Antarctica.
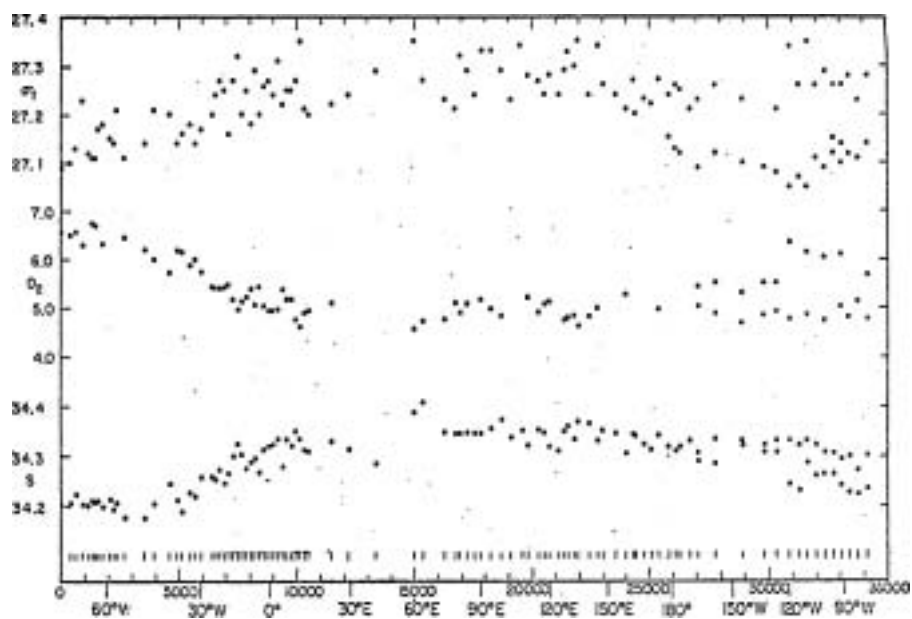
Fig. 2

Figure 2 shows the location of a circumpolar sequence of Subantarctic zone stations and the AAIW properties along that sequence. The lowest salinity, highest oxygen values are found near the Drake Passage.

Evidence of AAIW

Charts of the South-Pacific show the influence of AAIW north of the polar front zone (55°S) to the Equator (Johnson, 1943, Fig. 3.). The thickness attributable to AAIW ranges from 1200 m at 55°S down to 600 m at the Equator. North of the Equator, AAIW overlaps a tongue of low salinity water coming from the North Pole, lateral mixing processs complicates the picture, and AAIW can no longer be traced.

From density data, geotrophic currents may be calculated at the core of the AAIW (determined on the σ_θ = 27.10 surface, and calculated relative to 2500 meters). The resulting streamlines show that, in the South Pacific, AAIW circulates around an anticyclonic gyre between 55°S and 20°S. North of this small cyclonic and anticyclonic gyres are found. AAIW circulates along these gyres and passes from gyre to gyre until it reaches the Equator where it disappears by rapid mixing with north origin waters.

In the southeast corner of the main anticyclonic gyre, near the tip of South America, some water leaves the gyre and passes through Drake Passage, entering the South Atlantic Basin. This motion is confirmed by the dynamic height (500/1500) chart at that location. A measure of the thickness of a Mode Water is the inverse of the Brunt-Vaisala frequency for a density interval of .02, i.e., the Brunt-Vaisala period. At a given depth, the larger is this period, the more homogeneous is the water at that level. McCartney (unpublished manuscript) charted the Brunt-Vaisala period at different depths

Fig. 3.   AAIW equivalent thickness.
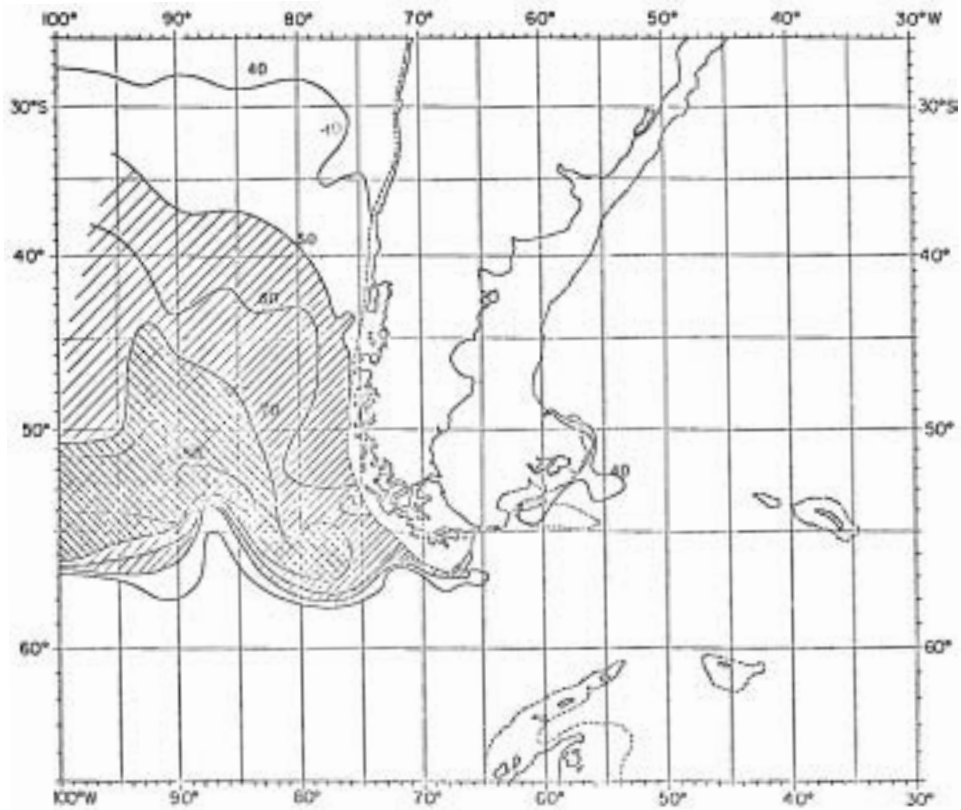
Fig. 4a. Contour of the Brunt–Vaisala period in minutes, for light
modes (350m, in the South East Pacific).
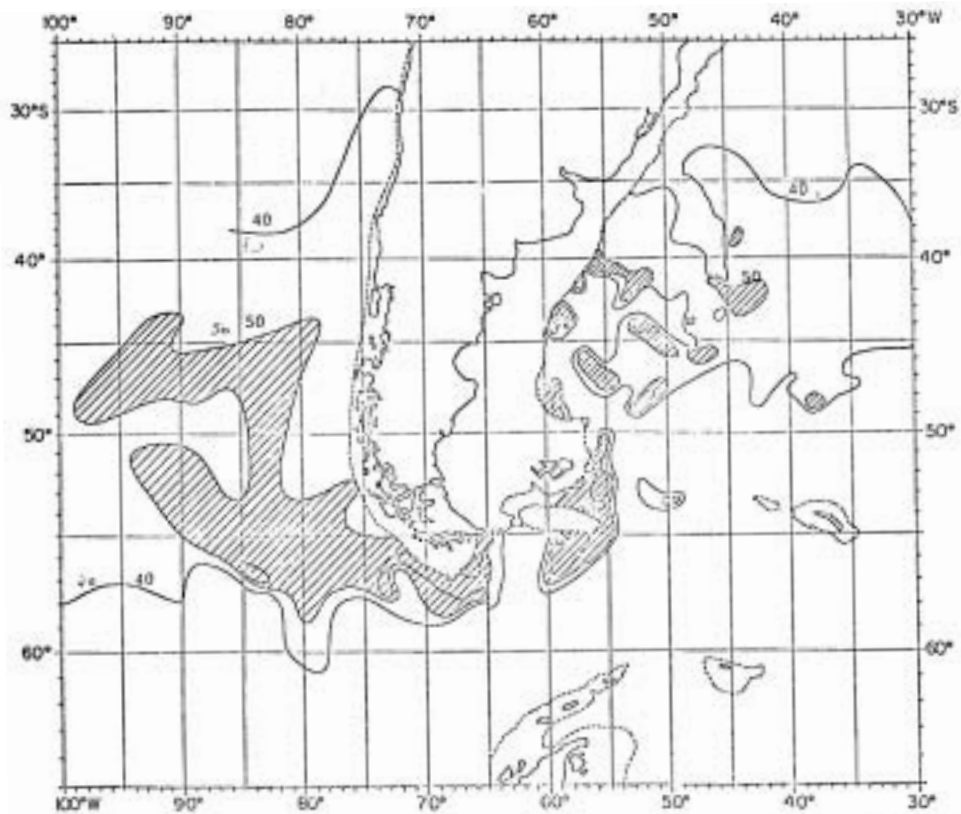
Fig. 4b. Contour of the Brunt-Vaisala period in minutes, for light
modes (350m, in the South East Pacific).
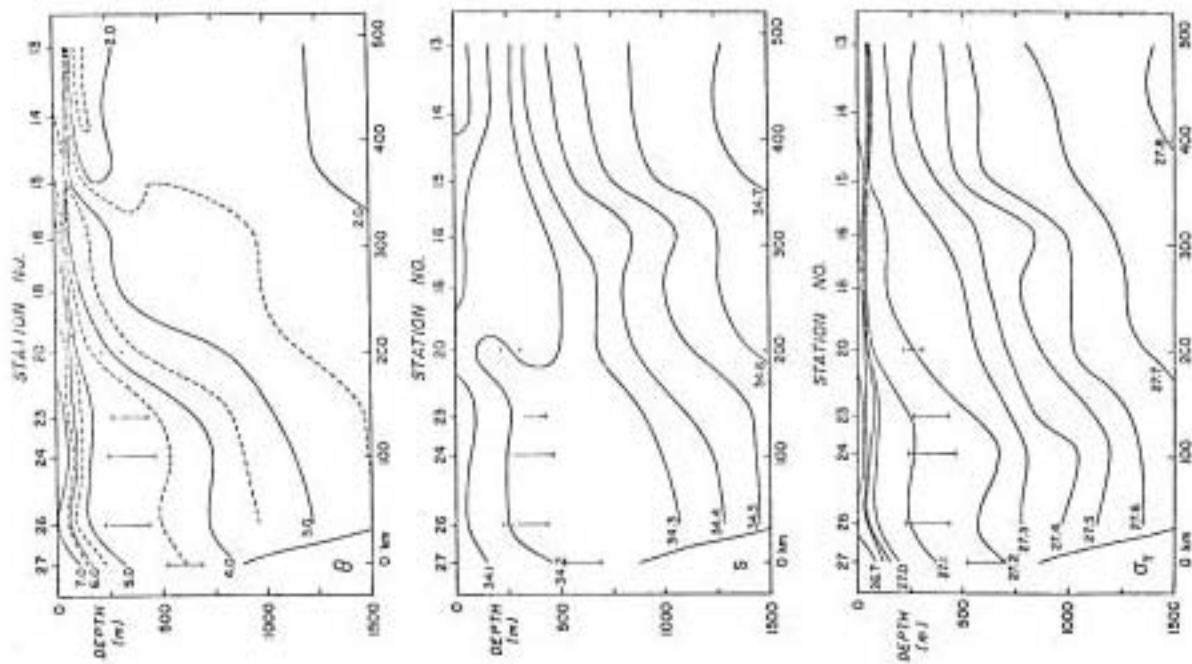
Fig. Section through the Drake Passage
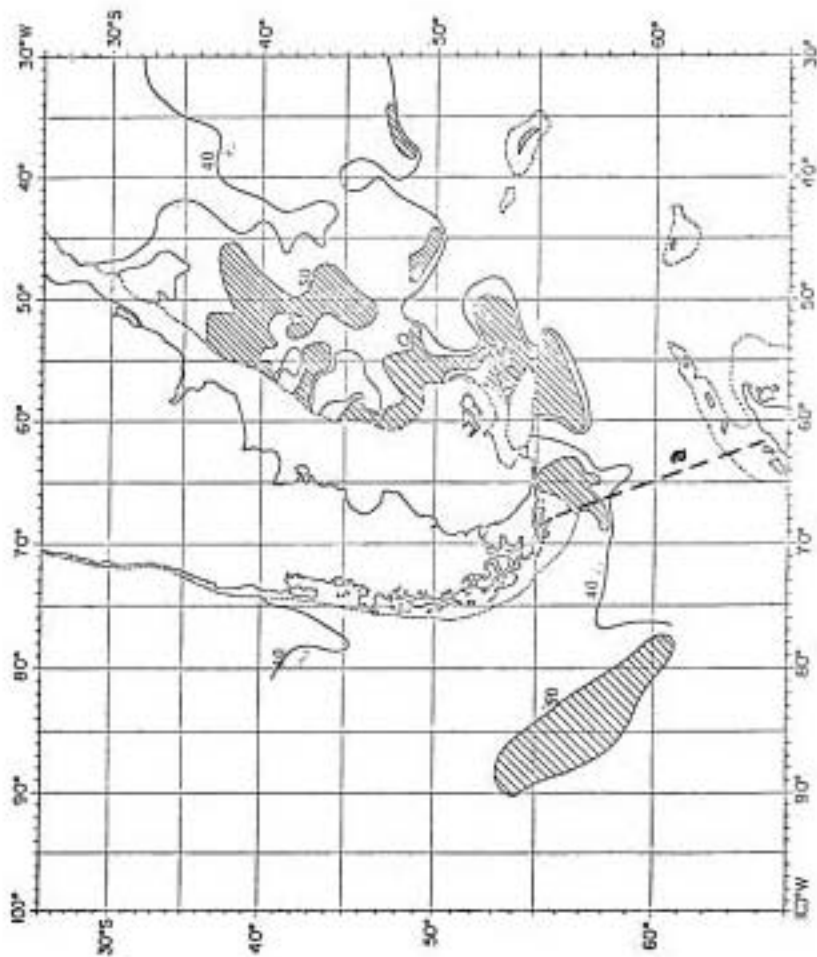
Fig. 4c. Contour of the Brunt-Vaisala period in minutes, for heavier modes (750m, in the South East Pacific).

in an area enclosing the South America tip (Fig. 4). From his charts it becomes apparent that the warmer upper water of the Mode Water family turns north and recirculates along the South Pacific anticyclonic gyre while the colder lower water goes straight through the Drake Passage and then, turns left as the Falkland Current in the South Atlantic Basin. Moreover, the section through the Drake Passage (Section A, Fig. 5) shows one essential mode ($4^{\circ}C < \theta < 5^{\circ}C$, S ~ 34.25 o/oo) to the north of the Subantarctic front, and a σ_{θ} – profile shows a well-defined pycnocline which precisely locates the Mode Water between 100 m and 800 m. The analog data for the East–West section in the Atlantic (Fig. 6) show a thickening of the density field around 27.10 and 27.20.

When moving equatorward along Argentina coast, the Falkland current encounters the Brazil Current. The result is an eastward deflection of both currents. In the turning process the warmer Subtropical Waters override the denser Subantarctic Water. The vertical profiles of 0_2, θ, S and σ_{θ} at a station there located (Geosecs Station 66) show the superimposition of these waters that the collision produces (Fig. 7). Above about 600 meters is the Subtropical Water influence, a low oxygen, very sharp main thermocline, with a higher oxygen pycnostad atop that marks the locally convectively–formed Subantarctic Mode Water of this part of the South Atlantic ($14^{\circ}C$, 35.5 o/oo). Below 600 meters is the thick, low salinity, high oxygen pycnostad that represents the Falkland Current Water. The AAIW from the Drake Passage has thus been injected into the Subtropical Gyre, and a corresponding amount of western boundary current water has been ejected from the gyre into the circumpolar Subantarctic Zone. The overriding has isolated the AAIW from the sea surface,
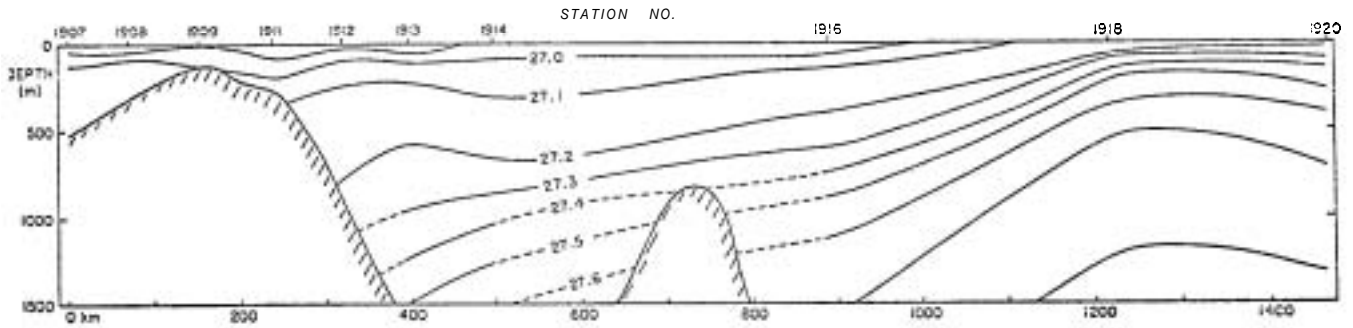
Fig. 6.   East-West section in the Southern Atlantic, off South America, at 54°S.
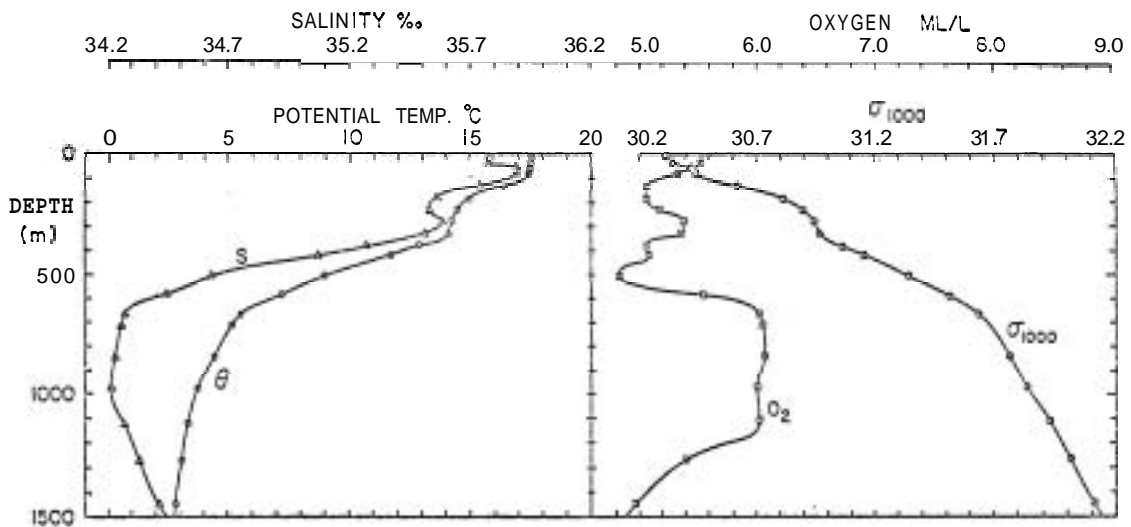
Fig. 7.   Profiles showing the overriding of the Falkland and Brazil Currents.

so on the rest of the circumpolar path it gradually gains salinity and loses oxygen (Fig. 2.). The progressively mixed water recirculates in the South Atlantic along several anticyclonic gyres of different sizes, embedded in one another, and again, a part does not recirculate, but passes south of the Cape of Good Hope (South Africa) and enters the Indian Ocean where the same pattern is more or less reproduced (McCartney, 1979).

Drake Passage Situation

Although heavier modes leave the South Pacific anticyclonic gyre and pass through the Drake Passage, there is a location, north of the exit of the Passage, where observations showed a gap of Subantarctic Mode Water (Fig. 8). This feature is not well understood and two likely explanations are equally possible. Topography may locally block the heavier deeper modes and force them to circle east around the ridge contour, or the Subantarctic Front may meander north and so prevent finding Subantarctic Mode Water at a location which is then south of the front.

General Theory of the Southern Hemisphere AAIW Circulation

From the previous description merges an analogy between the three different basins: South Pacific, South Atlantic and Indian Oceans. It is therefore possible to interpret the three situations by a single theory. This theory must be' able to explain the eastward progression of decreasing temperature and salinity of the Subantarctic Mode Water and the slight eastward increase of salinity of AAIW. This attempt was done by McCartney (1979) and may be summarized in Fig. 9.

In the southwest of the basin a collision occurs between the southward flowing western boundary current and the eastward flowing Subantarctic Zone
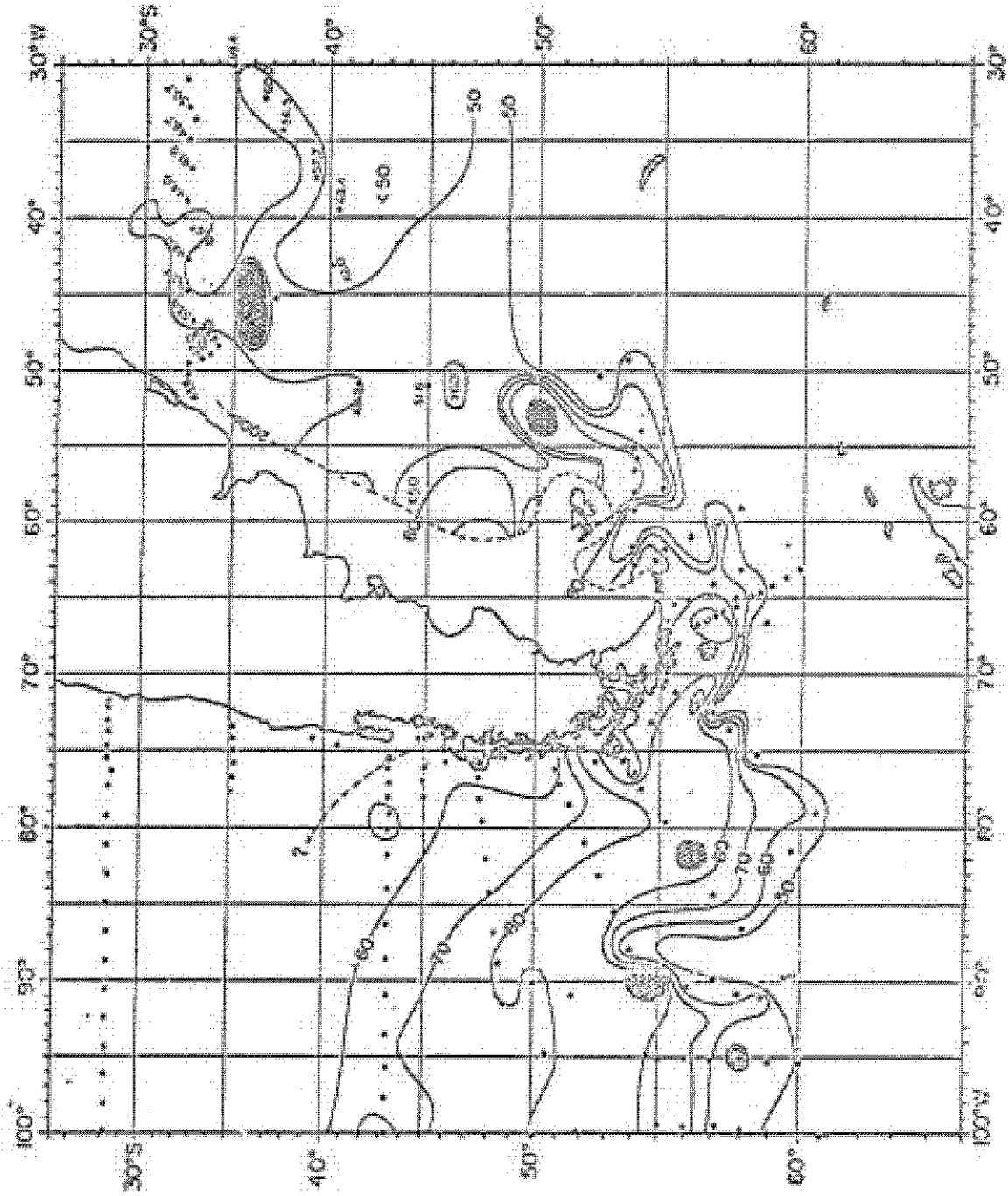
Fig. 8a. Evidence of a lack of Subantarctic Mode Water North-East of the Drake Passage.
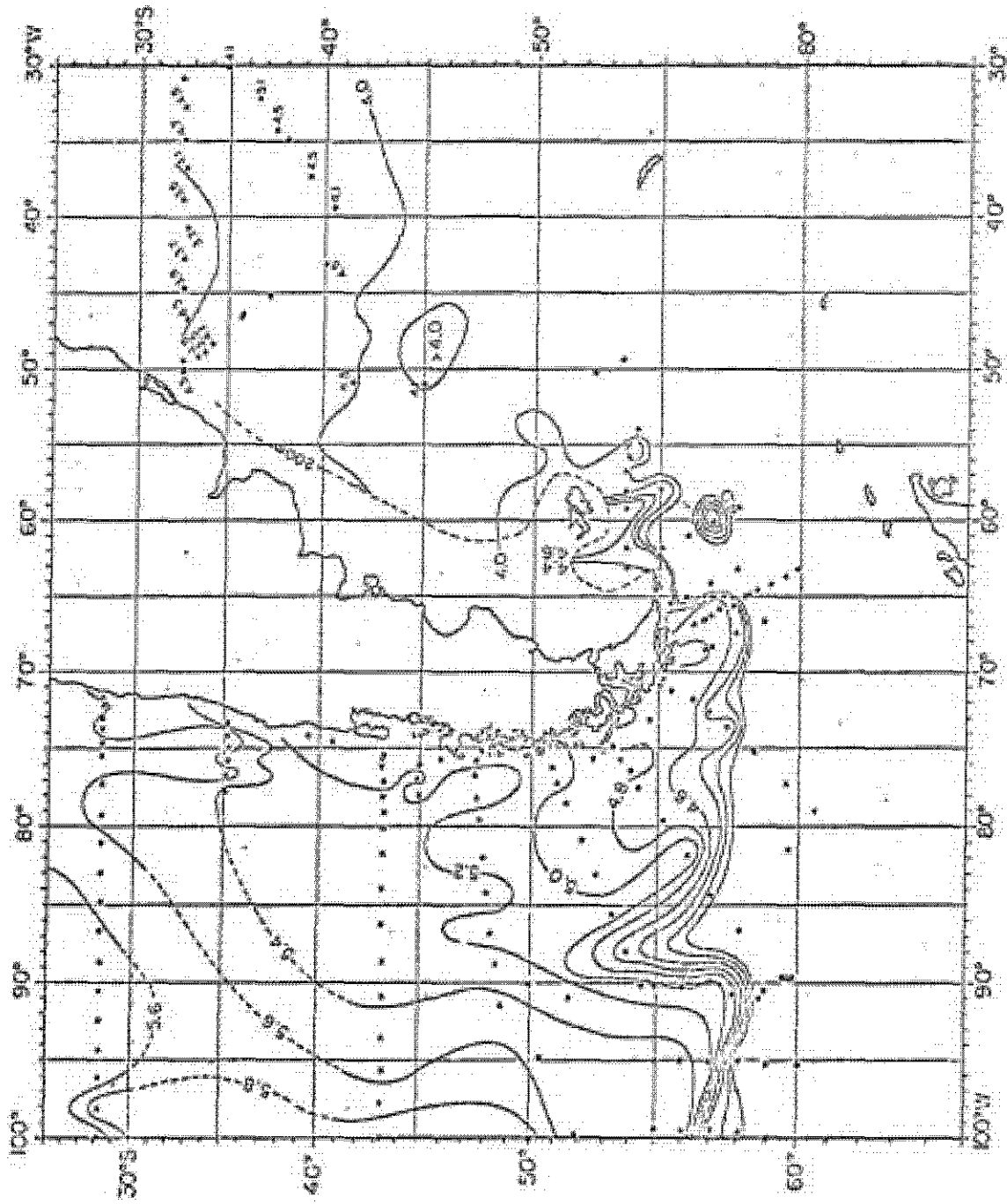
Fig. 8b   Evidence of a lack of Subantarctic Mode Water North-East of the Drake Passage.

current. The western boundary current separates and turns eastward with the circumpolar flow. In the turning process the warmer Subtropical waters over-ride the denser Subantarctic waters. There is clear evidence of this Subtropical Water injection in the southwest of each southern hemisphere basin. This is discussed in more detail in connection with the circulation of AAIW in McCartney (1979).

Excluding the overriding region, the figure is intended to suggest that the flow in the Subantarctic Zone is otherwise columnar. One is hard pressed to detect any systematic departures from unidirectionality of density surface in the upper 1500 meters or so of the Subantarctic Zone away from the southward corner. There still could be a spiraling of the horizontal velocity vector that would tend to move the warmer upper water southward relative to the waters at 500 and 1500 meters, that is, a meridional cell superimposed on the dominant zonal flow.

The best indication that a net exchange is affected with each Subtropical gyre is the presence of AAIW in all three southern hemisphere Subtropical gyres. Observational evidence (McCartney, 1977, 1979; Figs. 1 and 2) suggests that AAIW originates as a particular lowest salinity type of Subantarctic Mode Water formed in the southeastern Pacific and Drake Passage. Its presence in the Subtropical gyres of all the southern hemisphere oceans can be explained only by such net exchange processes as described above.

This circulation model predicts the structure of the Subantarctic Mode Water at Subtropical latitudes. If we were to cross zonally a gyre such as in the previous figure, what would we see? Crossing on a line such as A-A , south of the gyre center, the entire range of Mode Water should be seen, manifested as a pycnostad showing an east-west range similar to that found in the

Subantarctic Zone convective formation region further south. Such distribu-
tions have already been discussed in McCartney (1977). Crossing on a line such
as B-B', north of the gyre center, the range of densities of the pycnostad
should decrease, with only the denser ones formed in the central and eastern
longitudes of the Subantarctic being found.

Variations of Properties of AAIW Around the Globe

For stations around the globe at the Subantarctic Zone, where AAIW is
found, McCartney (unpublished manuscript, 1979) plotted the density, salinity,
and oxygen concentration at the salinity minimum, that is, at depth where AAIW
is expected to be found (Fig. 2). A main feature of this diagram is the effect
of collision with the western boundary current at the entrance of each basin;
each collision is clearly pointed out by a rapid slight change of properties,
especially at the entrance of the Atlantic Ocean where AAIW meets the Brazil
Current of completely different origin. In the Atlantic, salinity and density
rapidly increases eastward while the oxygen content decreases. This is an
artifact of the section location; it is too far north, and crosses the central
Subtropical gyre rather than its southern edge. When travelling around the
Indian Ocean, the Mode Water conserves its properties; the section runs along
the Subantarctic Front. Near New Zealand, a shallow plateau (1000 meters deep)
constraints the deeper heavier modes to pass south of $50^{o}S$, strengthening
the Subpolar Front, whose location is there predicted by topography, following
the isobaths. In the Pacific Ocean, the initial properties are progressively
restored by production of new AAIW in the southeastern Pacific, followed by an
anticyclonic gyre recirculation. The newly formed AAIW that recirculates anti-
cyclonically meets off New Zealand this old AAIW which is completing its "tour

du monde". The two water masses override each other east of a shallow plateau (Fig. 10). The newer mode has the salinity minimum and is represented by open circles on Fig. 2. The older AAIW coming from Australia has a density near 27.2 - 27.3 and is slightly more saline. It is plotted by black squares on Fig. 2. The continuity of the open circles west off South America and of black squares off New Zealand clearly indicates a production of AAIW in the southeast Pacific and the anticyclonic recirculation.

Comparison with the North Atlantic Ocean Circulation

As was shown in Lecture 5 the North Atlantic Ocean Circulation is a smaller version of the entire South Hemisphere circulation. Indeed, north of the Gulf Stream system is observed a large cyclonic gyre; a cold fresh water circulates along British Islands, Greenland, and Labrador Sea, then hits the Gulf Stream gyre, and with it, turns east. This later gyre is the analog of the anticyclonic gyres in the three basins of the South Hemisphere. On the other hand, the T–S diagrams for north and south gyres exhibit parallel straight lines. This confirms the analogy despite the differences in temperature and salinity of the Mode Waters involved.

The major difference between the two gyre systems is the salinity influence due to the Mediterranean Sea. This source of highly saline water drastically reduces the meridional extent of Mode properties in the North Atlantic. Moreover, the mixing of Mediterranean Water with Labrador Sea Water is enhanced by the fact that both waters have the same density and easily penetrate one
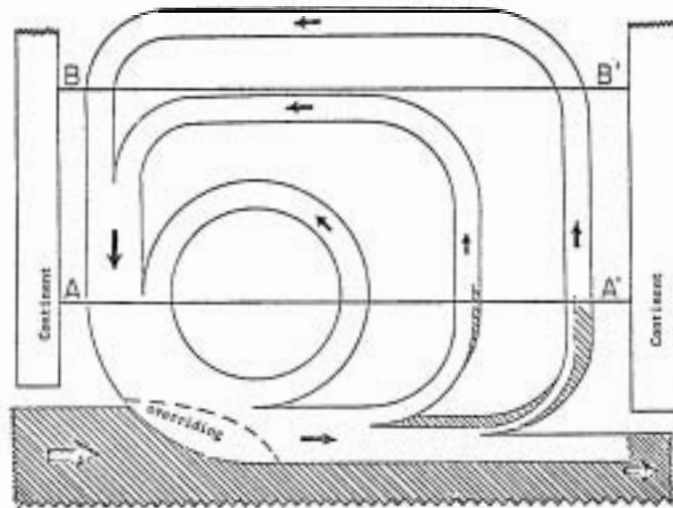
Fig. 9.   Schematic anticyclonic circulation in the southern oceans.

GEOSECS   Pacific   Station No. 296
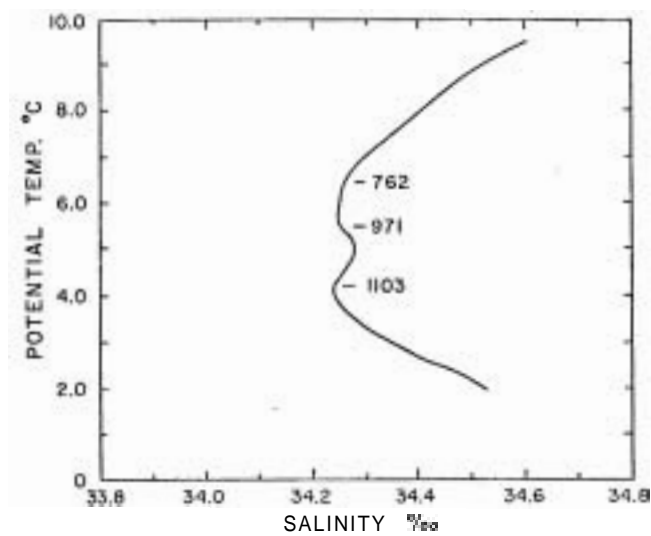
Fig. 10.   θ-S diagram showing the two AAIW Modes off New Zealand.   The
           warmer lighter mode is the newly formed AAIW after circulation
           across the Pacific.

REFERENCES

Johnson, R. E., 1973. Antarctic Intermediate Water in the South Pacific
    Ocean. Internal Symposium on Oceanography of the South Pacific,
    Wellington, New Zealand, Feb. 1972. Proceedings, UNESCO, 55-69.

McCartney, M. S., 1977. Subantarctic Mode Water. A voyage of discovery.
    Ed., M. Angel, 103-119.

McCartney, M. S., 1979. The Subtropical recirculation of Subantarctic Mode
    Water in the South Pacific and South Indian Oceans. (submitted)

Keid, J. L., 1965. Intermediate Waters of the Pacific Ocean. John Hopkins
    Oceanographic Studies, 2, 85 pp.

SUPPLEMENTARY READING

Georgi, D. T., 1979. Modal properties of Antarctic Intermediate Water in the
    Southeast Pacific and the South Atlantic. J.P.O. 2(3), 456-468.

Joyce, T. M. and S. L. Patterson, 1977. Cyclonic ring formation at the polar
    front in the Drake Passage. Nature, 265, (5590), 131-133.

 McCartney, M. S., 1979. The subtropical recirculation of Subantarctic Mode
    Water in the South Pacific and South Indian Oceans. Sub. Judis.

McCartney, M. S. and L. Talley, 1979. The upper water thermostad family of
    the subpolar North Atlantic Ocean. (In preparation)

Reid, J. L., Jr., W. D. Nowlin, and W. C. Patzert, 1977. On the characteris-
    tics and circulation of the Southwestern Atlantic Ocean. J.P.O., 7, 62-91.

Talley, L. and M. S. McCartney, 1939. The circulation of Labrador Sea Water.
    (In preparation)

Wright, W. R. and L. V. Worthington, 1970. The water masses of the North
    Atlantic Ocean - A volumetric census of temperature and salinity. Serial
    Atlas of the Marine Environment, Folio 19, Amer. Geogr. Soc.

Wüst, G., 1935. Die stratosphäre des Atlantischen Ozeans. Wissenschaftliche
    ergebnisse der Deutscher Atlantischen Expedition auf der Forschungs und
    Vermessungsschitz, Meteor 1925-1927, Gruyter and Company.

Notes submitted by
Benoit R. Roisin

I.   North Atlantic Circulation - Some Concluding Remarks

The intermediate produces of the Subpolar and Mediterranean Water circulation in the eastern North Atlantic are relatively saline. At 6°, 8° and $10^{o}C$, the saltiest waters extend northward from the Straits of Gibraltar as well as westward. As a consequence, salinity on these temperature surfaces is higher in the Rockall Channel than in either the Sargasso Sea or the Denmark Straits. This high salinity inflow into the Norwegian Sea may be important for Bottom Water formation. The water which does not flow into the Norwegian Sea, but which flows westward to the south of Iceland, becomes progressively cooler and less saline as a result of excess precipitation and convective homogenization. The pycnostads above the thermocline in the $4^{o} - 12^{o}C$ temperature range along this path are what we will term N. Atlantic Subpolar Mode Water. The Mode Water path ends in the Labrador Sea where the Labrador Sea Water (LSW), a low salinity Intermediate Water mass, is formed from the Mode Water.

If we construct a mean O-S curve from the horizontal properties of the North Atlantic Mode Water and compare it with a similarly constructed curve for the Subantarctic Mode Water, we see a surprising similarity in slope of the two curves. The major difference is an offset in salinity, the North Atlantic being much saltier. There appear to be no satisfactory explanations of this similarity, although we can look for similarities in possible formation scenarios. The path of Mode Water in both oceans is from a warm region to a colder one, into and through a region of excess precipitation, as seen in the graph of zonally averaged precipitation and evaporation (Lecture 2, Fig. 7).

Thus, the Mode Water of both oceans becomes progressively colder and less saline. It should also be noted that the Mode Water θ-S curves generally cross isopycnals at only a small angle: the temperature-salinity variations nearly cancel each other in their effect on density.

The final product of Mode Water circulation in both cases is a low salinity Intermediate Water mass. Some idea of how much water is involved in this circulation can be estimated by determining the net production of Intermediate Water from the inflow of Mode Water with a simple heat flux calculation. Based on net heat flux north of 50°N, we calculated in lecture 5 an estimate of the net production of Labrador Sea Water, allowing for a flow of 8 Sv of 8°C water into the Norwegian Sea. With the rest of the heat flux involved in producing 3.5°C water from 10.5°C water, we obtained a production volume flux estimate for Labrador Sea Water of 10.4 Sv.

Heat flux calculations in the Southern Ocean are much less well known due to the small number of observations. We could make an estimate of net production of Antarctic Intermediate Water by assuming that all heat flux in a 5°C latitude band at 45°S is involved in producing Antarctic Intermediate Water from the warmer Mode Waters. That is, if a heat flux of 25 $kcal/cm^2/yr$ is assumed over an area of 1.5 x $10^{17} cm^2$ with a temperature difference of 10° between the initial (14°C) and final (4°C) states, the net volume flux of AAIW would be 12 Sv. Unfortunately we do not have much idea of the actual heat flux: the use of 25 $kcal/cm^2/yr$ is just a guess.

An independent estimate of AAIW production may be obtained from the evaporation-precipitation chart (Lecture 2, Fig. 7) since the salinity of AAIW, the end product, is lower than the salinity of the initial 14° water. Assuming again a latitude of 45°S and 5° band, the net volume flux of fresh water

into the ocean is 2.6 x $19^5 m^3$/sec. Assuming that the initial salinity is

35.5 o/oo and that the final salinity is 34.2 o/oo, the net volume flux is

about 7 Sverdrups, a somewhat lower estimate. We see then that net produc-

tions of Intermediate Waters are not high compared with the net transport of

major currents. The actual observed transport of Mode Water may be substan-

tially higher due to recirculation.

A final point to be observed about North Atlantic circulation is that the

Subpolar Influence of the Labrador Sea Water is limited in its southern extent

by the highly saline Mediterranean outflow. An interesting feature of the

juxtaposition of these two water masses is the "Katz" gap in θ-S properties in

the temperature range 5° - 10°C in the North African Basin as seen in the

volumetric θ-S diagram of Wright and Worthington (1970). A possible interpre-

tation of the diagram is that a) the freshest branch is due to South Atlantic

(AAIW) influence, b) the middle branch is the θ-S relation for the Subpolar

Mode Waters, followed along their path from warm saline to cooler and less

saline and c) the saltier branch is due to mixing of Labrador Sea Water and

Subarctic Intermediate Water (3.9° - 4.0°C, 34.9 - 35.0 o/oo) north of the

North Atlantic Current with Mediterranean Sea Water (8°C, 35.5 o/oo) south

of the current. Since the only direct lateral (icopycnal) connection between

the surface Mode Waters and the saline LSW-Med Water mixture is the Labrador

Sea Water, there is a gap in salinity in the temperature range 6° - 8°C.

II. North Pacific Circulation: Intermediate Water

Since the Subpolar regions of the North Atlantic and Southern Oceans

produce low salinity Intermediate Water masses, we might ask if a similar

water mass is formed in the North Pacific. Reid's (1965) meridional section

of the Pacific at 155°W shows a striking salinity minimum in the North

Pacific with its deepest axis at about 600 m at $20^O N$ which we will take to be the North Pacific Intermediate Water. Its axis rises to the north and comes closest to the surface under an extremely well stratified low salinity layer which is also apparent in sections farther to the west.

The density surface which most nearly intersects the Intermediate Water is σ_T = 125 cl/ton so an idea of the distribution and properties of the Intermediate Water can be obtained from plots of salinity, oxygen and other properties on the σ_T = 125 cl/ton surface. Figures 1 and 2, from Reid (1965), show salinity and oxygen on this surface. The lowest salinity is seen to occur near the Kamchatka Peninsula and coincides with the region of maximum oxygen. If the tongue of low salinity and relatively high oxygen (4.0 m/l) to the east is an indicator of the circulation in this region, it seems that the Intermediate Water is fairly well confined to a cyclonic gyre north of $+40^O N$ and does not extend very far to the south. It appears that the net amount of Intermediate Water is quite a bit less than the net amount of Antarctic Intermediate Water (AAIW) (on the σ_T = 80 cl/ton surface, not shown here) judging from the very small region in which oxygen has its highest values, the limited extent of the Intermediate Water to the south and the low values of oygen in the east and south.

What are other similarities and differences between the North Pacific Intermediate Water and the AAIW and LSW? All three water masses are low salinity Intermediate Waters which seem to be formed in the Subpolar regions and are marked by high oxygen value in the assumed renewal area. All three water masses are formed in cyclonic gyres, as may be expected for dense water mass formation from other discussions in this series, since the inhibiting stratification is weakened in the center of a cyclonic gyre. Both LSW and
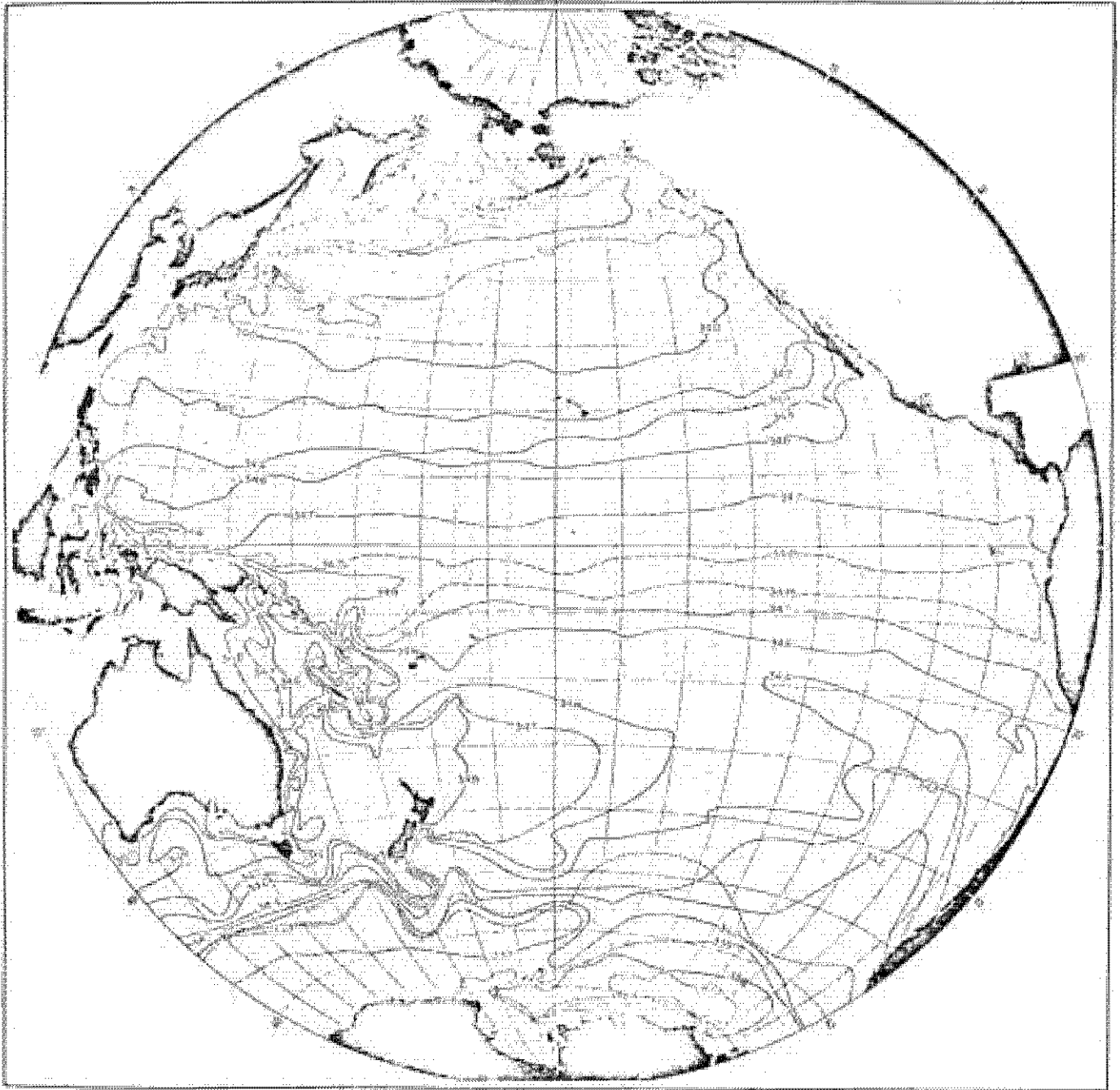
Fig. 1. Salinity on $\tilde{\delta}_T = 125$ cl/ton in the **Pacific** Ocean (from Reid, 1965).
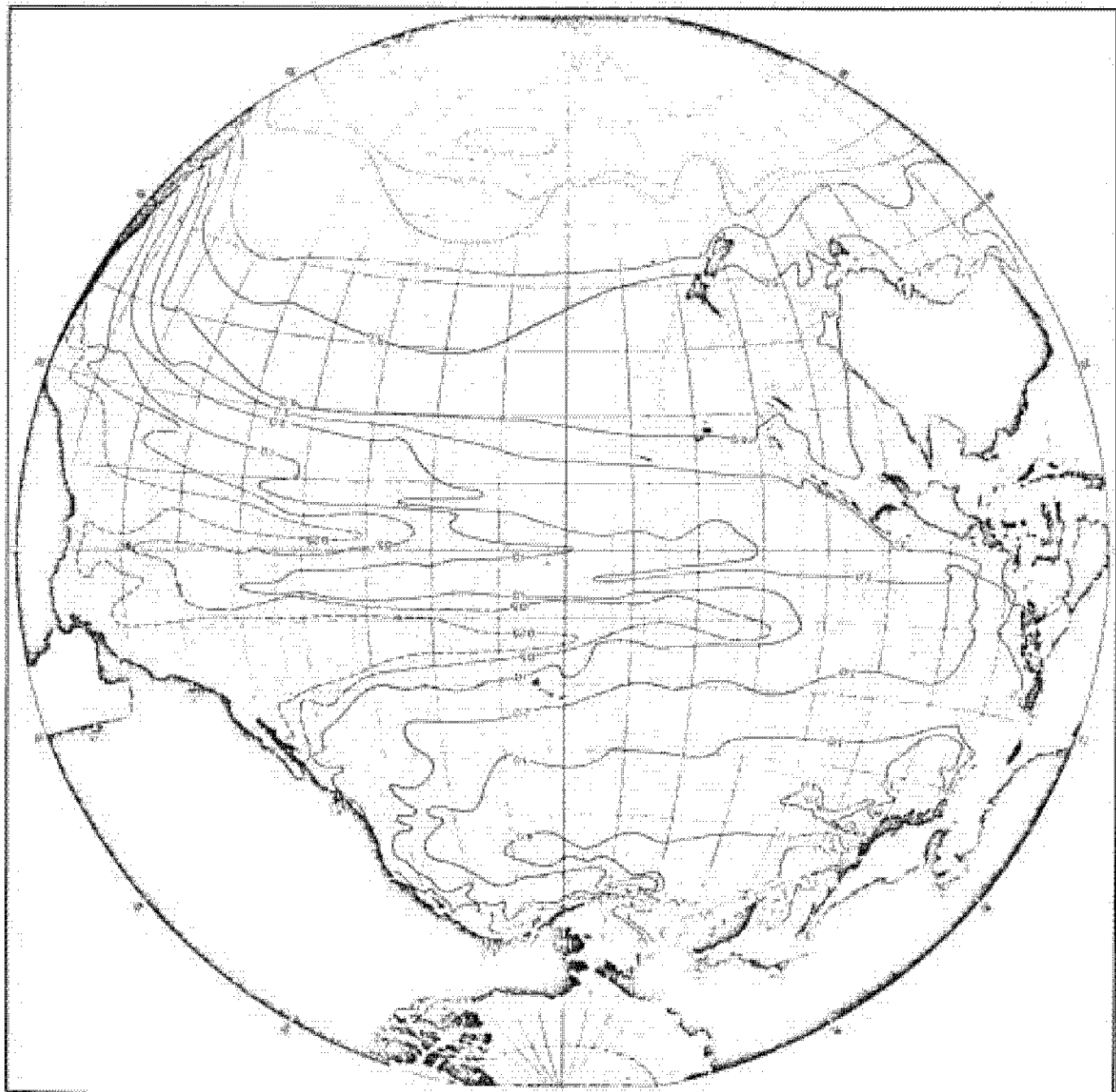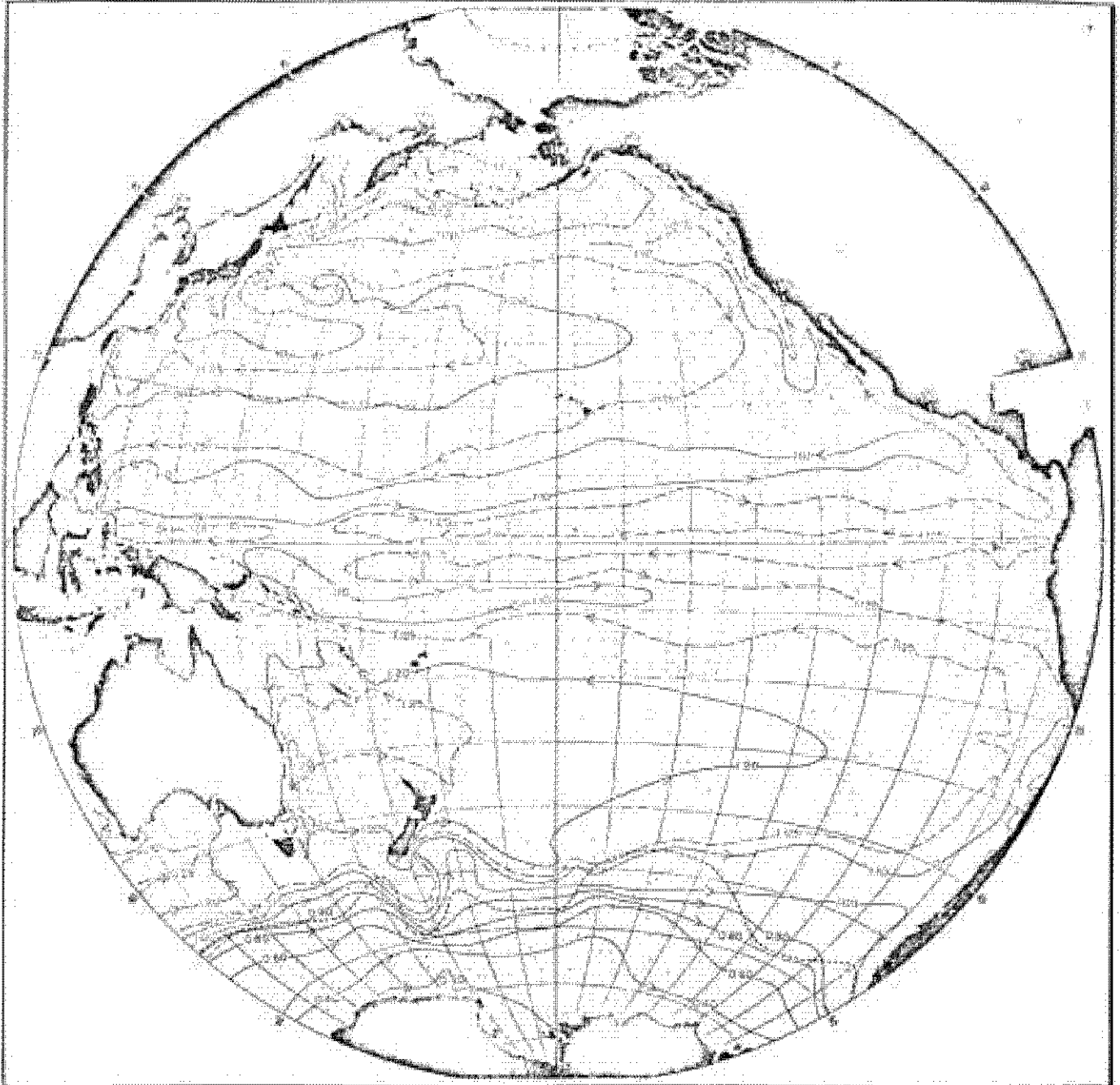
Fig. 3.   Acceleration potential for $\delta_T = 125$ cl/ton relative to 2000 db (from Reid, 1965).

North Pacific Intermediate Water are formed in the northwest corners near continental land masses where heat flux out of the ocean due to polar continental air may be very large. The Labrador Sea is, however, a much more confined basin than the open ocean region where North Pacific Intermediate Water may be formed.

The AAIW and LSW are well defined pycnostads as well as salinity minima whereas the North Pacific Intermediate Water appears to be only a salinity minimum and not a thick layer of water. Also, the presence of a sequence subpolar surface Mode Waters around Antarctica and in the North Atlantic has suggested that the AAIW and LSW are the final products of a sequence of cooling and homogenization processes. There does not appear to be a well defined sequence of subpolar Mode Waters leading into the Kanchatka region.

The surface layer in the northern North Pacific is well stratified in salinity and temperature (but not necessarily in density). It has been suggested that this low salinity surface layer may inhibit deep convection.

The problem is then: a particular sequence of events has been suggested for formation of a low salinity Subpolar water mass which seems to account for the situation in the North Atlantic and Southern Ocean. What is happening in the North Pacific?

Qne suggestion is that renewal of North Pacific Intermediate Water simply does not occur since the small pycnostad strengths at the salinity minimum and in the Subpolar surface region suggest that the Mode Water sequence does not occur. However, there is a salinity minimum layer with high oxygen values ,in a small region which suggests that some renewal, even if intermittent and of low production rate, must occur.

A second suggestion is that surface renewal of the salinity minimum does not occur but that it is formed beneath the surface in some sort of mixing process from upper layer water that is cooled and freshened as it moves westward in the northern side of the gyre. A temperature maximum beneath the surface layer, at intermediate salinity, mixes with cold fresh water above and cold saline water beneath and the product finally sinks as a relative salinity minimum beneath the warmer, more saline, surface water to the south when it turns to the south and east (Reid, 1973). Reid proposes this model because of his conclusion that the salinity minimum is not renewed at the surface, based on 1) the absence of directly observed renewal, 2) the fact that the $\sigma_T = 125$ cl/ton density surface did not outcrop at the surface during the winter of his observations and 3) the extremely low oxygen values found at the salinity minimum during the winter of observation, in comparison with summer data which showed high oxygen values at the salinity minimum.

Drawing on the second and third points above, there could be a third possibility, namely, that surface renewal of the water mass could occur, but at very low rates (suggestion and following description are L. Talley's). It is fairly well known that convective renewal of Intermediate and Bottom Water masses is an extremely local event and that the probabilities of actually observing its occurrence are slight. Secondly, it is known from the density at the axis of the Labrador Sea' Water that density is progressively higher downstream than in the formation region. It therefore may follow that the proper density surface to be observing in the North Pacific Intermediate Water formation region is not necessarily the same surface which intersects the salinity minimum considerably to the south and east (along 155°W) and that, in fact, renewal (or formation) may occur at lower density. Finally, the progression from high

oxygen values at the salinity minimum in the formation region in the summer to low values in the winter (Reid, 1973) may indicate formation of Intermediate Water in the late winter (giving rise to the observed high values in the summer). Subsequent advection away to the southeast of the newly formed water and advection in from the northeast old Intermediate Water with very low oxygen would give rise to the low oxygen values observed in winter.

If we take Reid's suggestion of cooling and freshening of the surface layer along the cyclonic gyre until some winter when it reaches the Kamchatka region, cool it and mix it, perhaps with the incoming old Intermediate Water, along a density surface (δ_T = 130–140 cl/ton) and then let it flow out of the region, increasing in salinity as it goes (perhaps by mixing with the under-lying high salinity water) until it reaches the δ_T = 125 cl/ton surface, we have a mechanism for direct surface renewal of North Pacific Intermediate Water, not at all unlike the process which occurs in the North Atlantic. The main difference may be in the amount of Intermediate Water which is produced-

Circulation rates for the North Pacific Intermediate Water can be estimated from oxygen values along the path of the gyre, again assuming that the tongue of high oxygen in Fig. 2 is indicative of the axis of the current. In the absence of other reliable estimates of oxygen consumption rates we use Jenkins (1979) consumption rates for the Sargasso Sea, based on tritium–helium measurements. The utilization rate decreases exponentially from 15 ml/l/year near the surface to 4×10^{-3} ml/l/yr at 1800 m. At a consumption rate of .1 ml/l/yr, the NPIW requires 30 years to go from an oxygen content of 6 ml/l near Kamchatka Peninsula decreasing to 3 ml/l, along a path of 5400 km length eastward to 140°W, approximately delineated by the acceleration potential (Reid, 1965). This implies an average velocity of .5 cm/sec which could be

higher or lower depending on the actual circulation rate and path length. Regular renewal with open ocean velocities of this order could therefore produce the observed pattern. (Approximate velocities calculated from the acceleration potential relative to 2000 db in the open ocean, far from the boundary current, are of order 1 cm/sec which compares favorably with the rough estimate from oxygen consumption.)

If there is fairly regular renewal of the North Pacific Intermediate Water, why are the rates so low? Several possibilities to be explored are a) the geometry of the formation region which is itself in the open ocean where a tight cyclonic circulation may not be possible and which includes adjacent seas which may dissipate some of the convective potential of the winds before they reach the open North Pacific and b) the presence of a low salinity surface layer arising from the Kamchatka current from the Bering Sea. It may also be noted that no Bottom Water is produced in the North Pacific although it is not clear what effect this may have on the Intermediate Water. (It may be that the low oxygen values in the Pacific deep water help to deplete the oxygen in the Intermediate Water through vertical advective-diffusive processes.)

It has already been noted that the LSW is formed in the center of a tight cyclonic gyre whose tightness is possibly aided by the semi-confined Labrador Sea Basin. No such topographical aid is present in the North Pacific, nor does it occur in the AAIW formation rgion. (It as noted in Section I that the net production of AAIW may be slightly less than LSW.) This alone cannot explain the low production rate of course although it may help. Since Intermediate and Bottom Water mass renewal in the North Atlantic seems to occur predominantly in the adjacent Labrador and Norwegian-Greenland Seas rather than in the open ocean, we might ask if the same is true of the North Pacific. Convective

renewal occurs regularly in the Sea of Japan, a Mediterranean-type sea with warm inflow at the surface from the south and production of dense deep water. The deep water produced has very homogeneous characteristics, most of it lying within a very narrow range of temperature and salinity (34.05 - 34.09 o/oo and 0.0° - $0.4^{\circ}C$). Because of extremely shallow sills, the deepest of which is 150 m (Sverdrup, Johnson and Fleming, 1942), the deep water is more or less isolated in the Sea of Japan and has little influence on the open ocean. A contrast to the Sea of Japan is the Okhotsk Sea which has a very well stratified salinity layer at the surface, inflow at depth and outflow in the upper layers. Because of the presence of the low salinity cap, winter convection does not penetrate very deeply or produce a deep water mass. The same is true of Bering Sea in which low salinity water introduced by the current flowing around the Aleutians is cooled and further diluted by excess precipitation and runoff and returns to the south as the cold Kamchatka current (ibid). Thus, in the North Pacific there is no source of Bottom Water for the open ocean and no adjacent sea source of Intermediate Water. If an Intermediate Water is to be formed, it must be formed in the open ocean, but we may perhaps expect it to be weaker than dense water masses formed in adjacent seas. Even so, this may not be enough to explain the low production rate since the boundaries in the northwest Pacific may be sufficient to help cause dense water production.

The extremely apparent low salinity layer on the surface almost everywhere in the northwest Pacific (Reid, 1973) may be the predominant reason for the low production rate since it would inhibit convection renewal to very great depth. Thus, no distinct progression of surface Mode Water of great thickness can occur with subsequent large production of Intermediate Water. Because the stratification is weakened in the center of the cyclonic gyre near Kamchatka,

there is a possibility for some production of Intermediate Water but not at the rates that would occur if there were significant Mode Water feeding into the region.

Thus, a possible conclusion is that there is a low salinity North Pacific Intermediate Water which may be renewed on a fairly regular basis but in very iow amounts, possibly because of the low salinity surface layer over the Subpolar North Pacific.

III. Southern Ocean Circulation

1. Topography

There is a great deal of variety in the topography of the Southern Ocean (Fig. 4). One of the most striking features is the constriction of the Drake Passage with maximum sill depth of about 3000 m. Moving eatward from Drake Passage and on around Antarctica, there are several notable features, the first of which is the complex Scotia Ridge. Zonal flow to the east of the Argentine Basin must then pass over the Mid-Atlantic Ridge, the Crozet Plateau, and the mid-ocean ridge in the Indian Ocean which it first crosses and then parallels. South of New Zealand, the Macquarie Ridge and Campbell Plateau influence the flow direction. In the Pacific the flow must cross yet another mid-ocean ridge before continuing on to Drake Passage in a wide basin which seems to diffuse the flow.

2. Nomenclature

We first wish to define several large-scale features of the Southern Ocean circulation in terms of identifiable temperature, salinity, oxygen and density features in horizontal and vertical sections and in vertical profiles. We proceed from north to south and use Figs. 5-7.
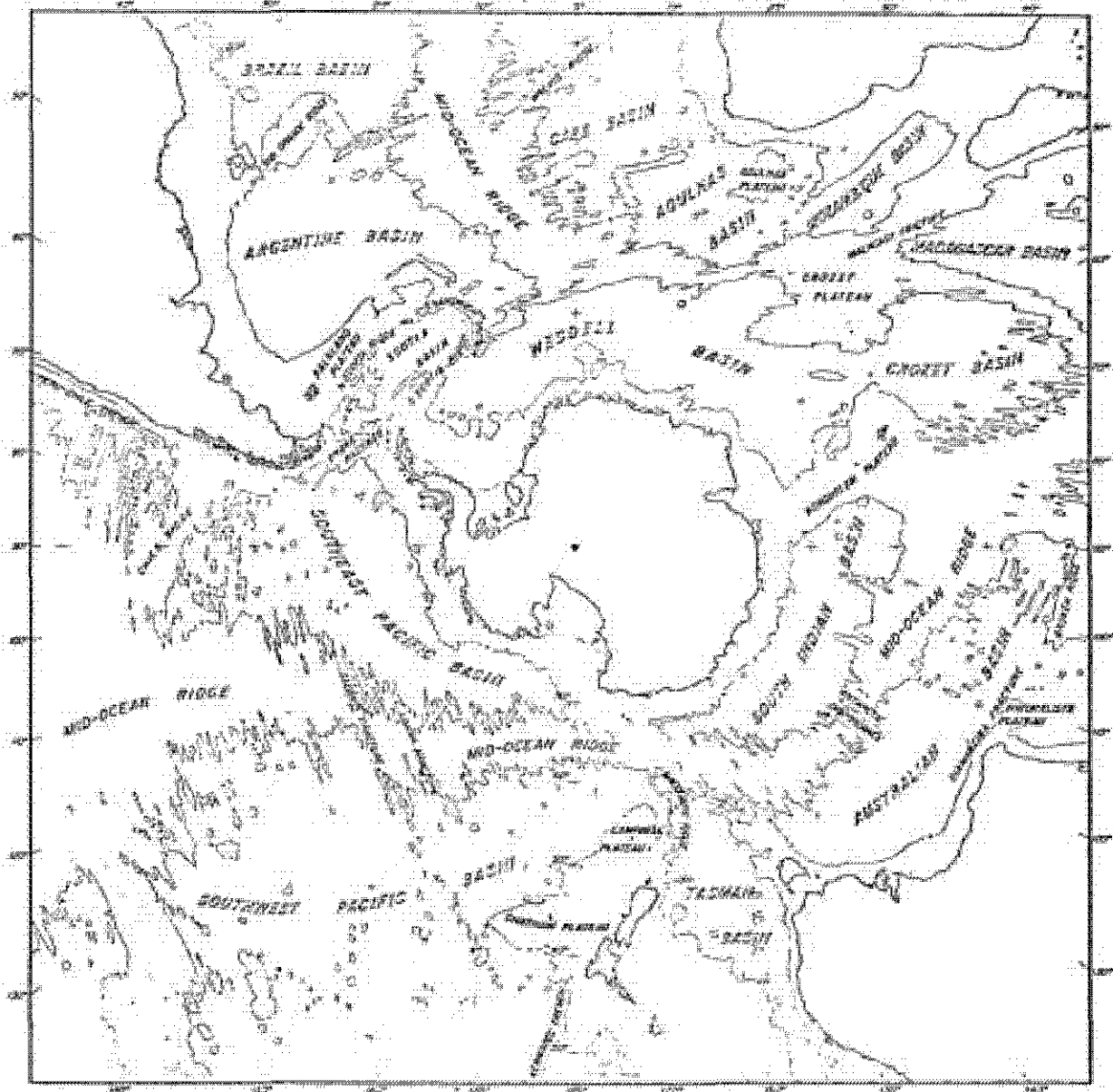
Fig. 4. Southern Ocean bathymetry. The 4000 m contour is from Heezen et. al. (1972).

Temperature
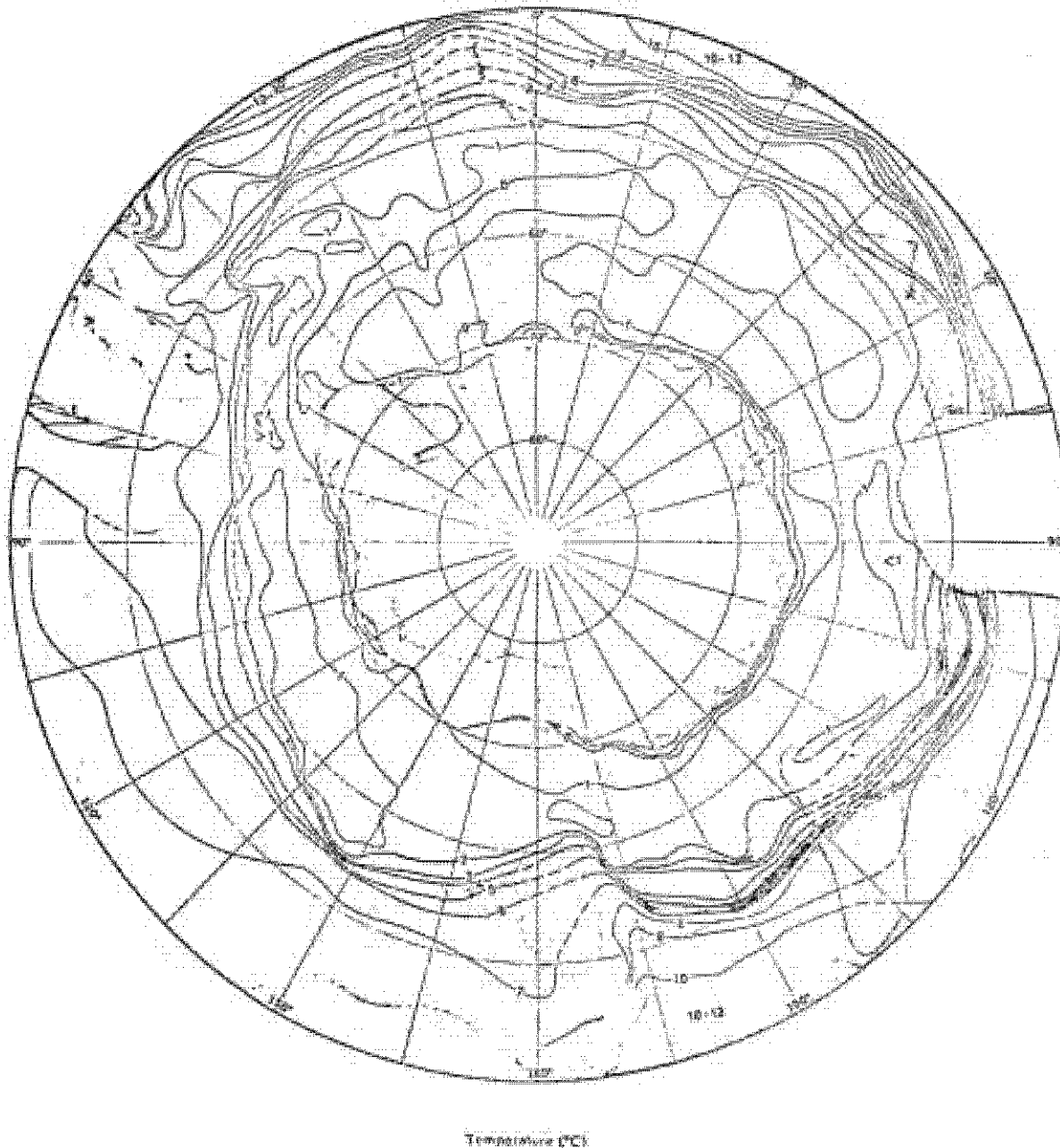
Fig. 5.   Temperatures at 200 m with the region of large temperature
          gradient shaded to mark the Polar Frontal Zone.   The Sub-
          antarctic Front is the northern side of this region.
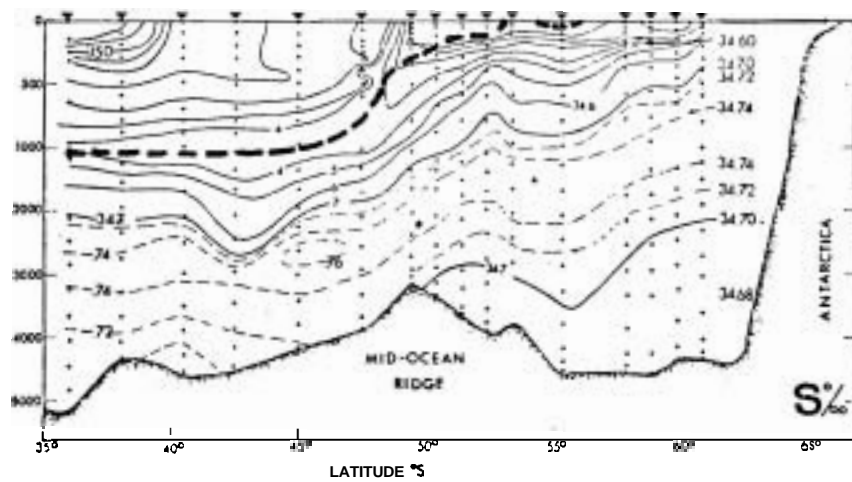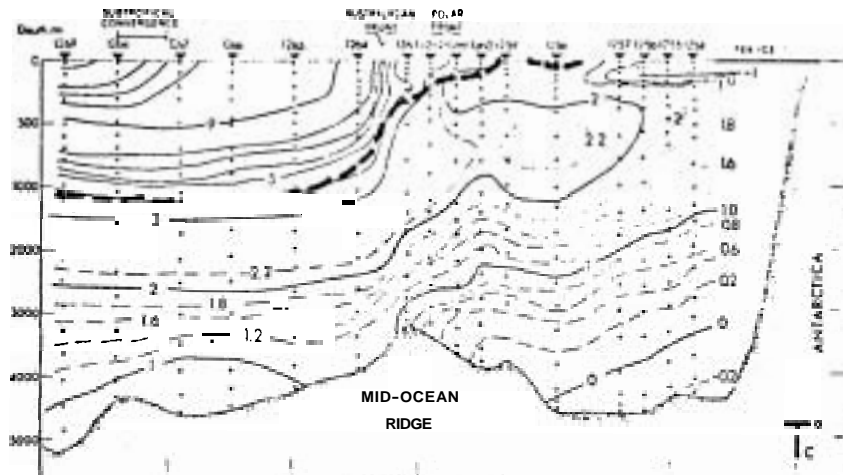
Fig. 6. Meridional temperature section along 115°E (from Gordon, Taylor and Georgi, 1977).

a) <u>Subantarctic Zone</u>: region north of the Subantarctic Front, as defined below. It is usually characterized (except in the S. E. Pacific) by a salinity minimum near 1000 m (indicative of Antarctic Intermediate Water), temperature which decreases more or less monotonically with depth, a deep oxygen minimum, a deeper salinity maximum (both due to NADW influence), and the presence of a thermostad in or above the thermocline.

b) <u>Subantarctic Front</u>: marked by the northernmost extent of intense meridional temperature gradients, as illustrated by temperature on the 200 m surface (Fig. 5). The front is well defined except in the eastern Pacific where the zonal flow is diffuse. No single isotherm can be used to trace the axis of the subantarctic Front but the gradient region is fairly continuous (shaded region in Fig. 5). A second definition in terms of vertical profiles is the northernmost occurrence of multiple inversions in temperature and salinity, characteristic of the polar frontal zone. These two definitions do not always select the same region for the Subantarctic Front since there may occasionally be a region of water of the sort that occurs in the Subantarctic Zone between the latitude of the most intense temperature gradients and the latitude of the onset of interleaving.

c) <u>Polar Frontal Zone</u>: between the Subantarctic and Polar Fronts. It is characterized in a vertical profile by multiple temperature and salinity inversions in the upper water columns which are density compensating for the most part. A vertical section taken across the PFZ shows isolated temperature and salinity maxima and minima. The multiple inversions are usually interpreted as indications of interleaving of cold fresh water masses of southern origin with warmer, more saline water masses from the north. (The meridional motion which this implies is of course much slower than the zonal flow whose

bifurcations may be the principal agent for interleaving.) The deep oxygen
minimum and salinity maximum are shallower than in the Subantarctic Zone.

d) Polar Front: the southern boundary of the PFZ. It is character-
ized by the onset of a distinct temperature minimum in the upper water column
and more precisely (and somewhat arbitrarily) defined as the northernmost
extent of the $2^{\circ}C$ isotherm in the upper waters. (In Fig. 5 the $2^{\circ}C$
isotherm seems to indicate the approximate southern extent of the large
meridional temperature gradient discussed above the Subantarctic Front.)
Ostapoff (1960) defines the polar front as the axis of the meridional salinity
minimum at 200 m.

e) Antarctic Zone: south of the Polar Front. It is characterized in
austral summer by a distinct temperature minimum layer (which may reach the
surface in winter) and an extremely sharp thermocline. The "deep" oxygen
minimum and salinity maximum are shallowest in the Antarctic Zone.

Figure 6 is a meridional temperature section along $115^{\circ}E$ (to a depth of
500 m) crossing the fronts and zones defined above (Gordon, Taylor, and
Georgi, 1977). The temperature minimum layer of the Antarctic Zone, multiple
inversions of the PFZ and the sharp temperature gradients of the Subantarctic
Front are readily observable.

Figure 7a shows examples of vertical temperature, salinity, oxygen and
density from the three zones and illustrates the more monotonic properties of
the Subantarctic Zone, the jumbled inversions of the PFZ and the presence of a
temperature minimum layer characteristic of the north Antarctic Zone. (This
station is not far enough south to show the extremely sharp thermocline.)

Definition of the various zones can also be made in terms of θ-S curves in
the upper water column while definitions of the fronts can be made in terms of

sharper merodional density gradients throughout the water column, marking geo-strophic currents. (Note that this is the only definition which involves currents directly and which can be used in the deep water.) θ-S curves for the upper water column progress from warm fresh surface water and colder saltier deep water (with a salinity minimum) to cold fresh surface water and deep salty water (with a salinity minimum) to cold fresh surface water and deep salty water (with a temperature minimum). Figure 7b shows θ-S curves for the CTD stations used in Fig. 7a. Figure 8a shows a meridional density section across Drake Passage with identifiable bands of higher density gradients marking stronger geostrophic currents (Nowlin, Whitworth and Pillsbury, 1977). With the aid of θ-S curves, it can be shown that these bands mark the fronts separating the various zones. One additional zone to the south is also present.

It is evident from the above discussion that most of the variation in properties seems to be restricted to the upper 600 m. Below 600-700 m the entire Southern Ocean is filled with Circumpolar Deep Water, characterized by an oxygen minimum, decreasing temperature and almost homogeneous salinity, with the possibility of a salinity maximum. The axis of the CDW, as marked by the oxygen minimum or salinity maximum (which may not coincide), is shallower to the south, as would be expected of a geostrophic current.

Disagreement with the above definitions is largely restricted to the use of the term "Subantarctic Front". Gordon (1975 and personal communication) also defines an "Australasian Subantarctic Front" north of the Subantarctic Front in the Indian Ocean. He defines the Subantarctic Front as the northern extent of multiple inversions in temperature and salinity and the Australasian Subantarctic Front as the northernmost large temperature gradient in order to differentiate between flow which is a zonal extension of the Agulhas Current and water which flows eastward from the Atlantic.
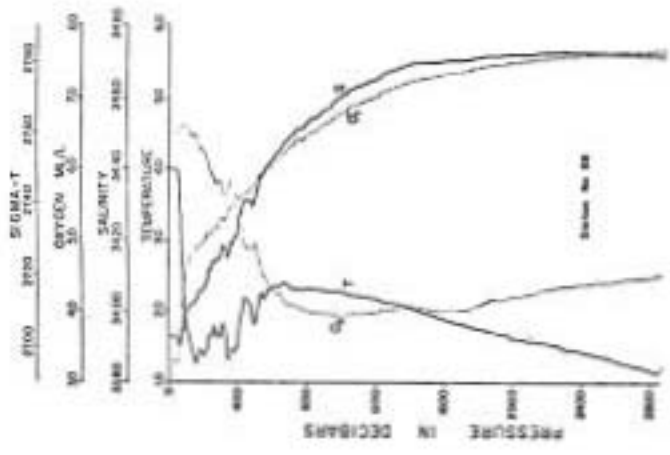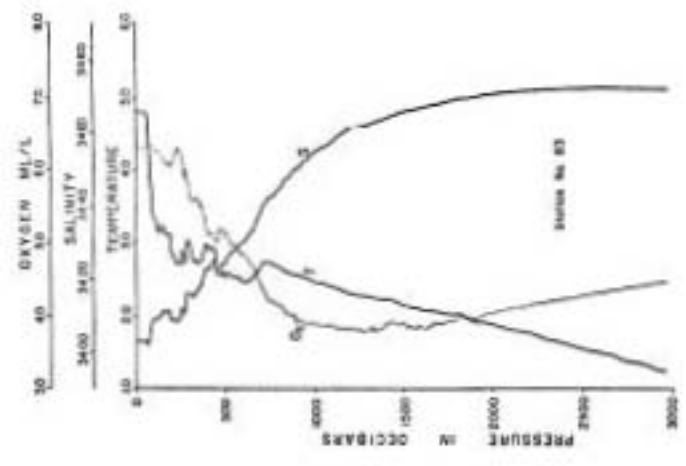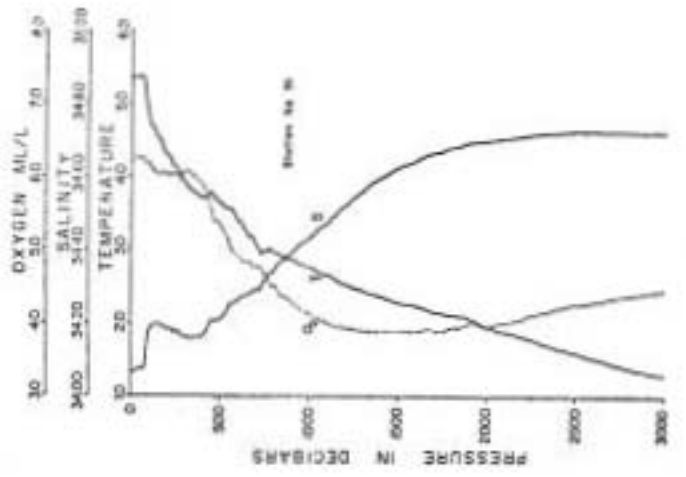
Fig. 7a   CTD profiles in the subantarctic, polar frontal and antarctic zones

(1)

(2)

(3)
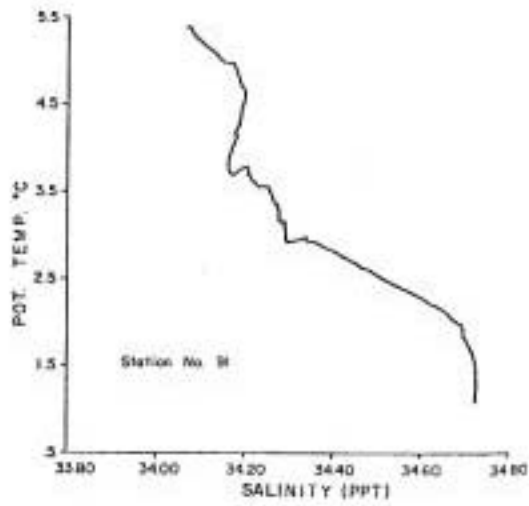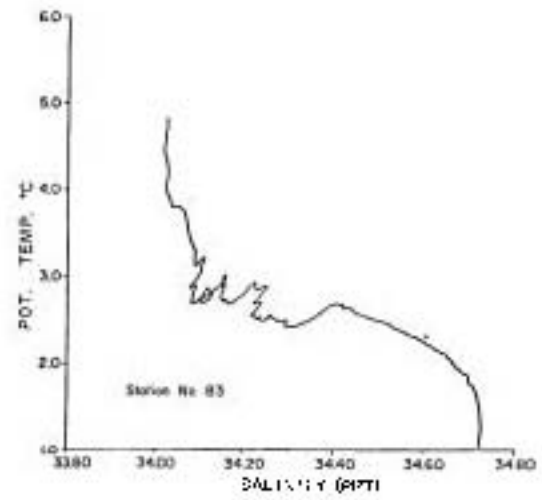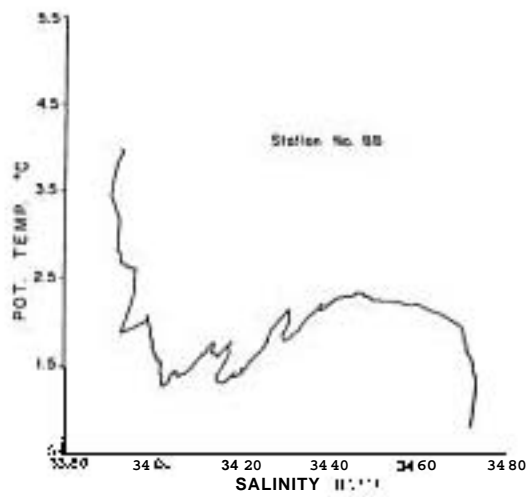
Fig. 7b. θ-S curves corresponding with the CTD profiles.
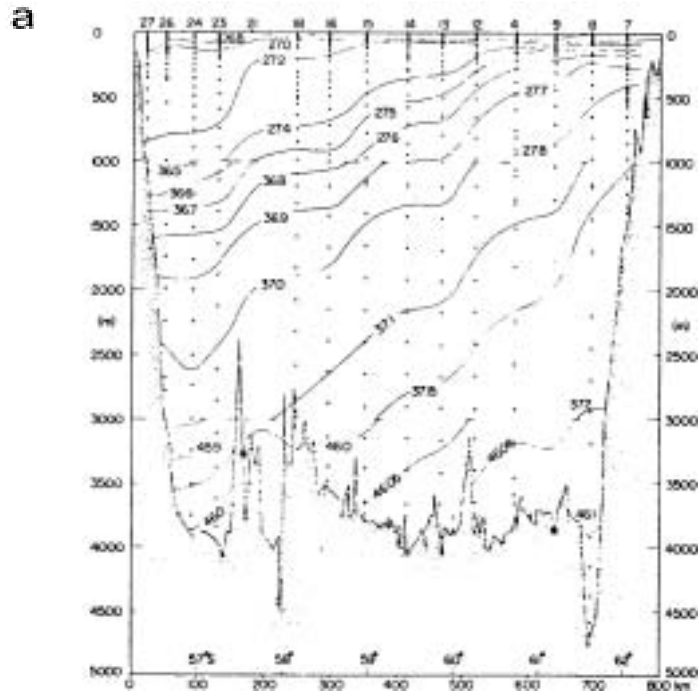
Fig. **8a.** Meridional density section from 60-68°W across Drake Passage (Nowlin, Whitworth and Pillsbury, 1977)
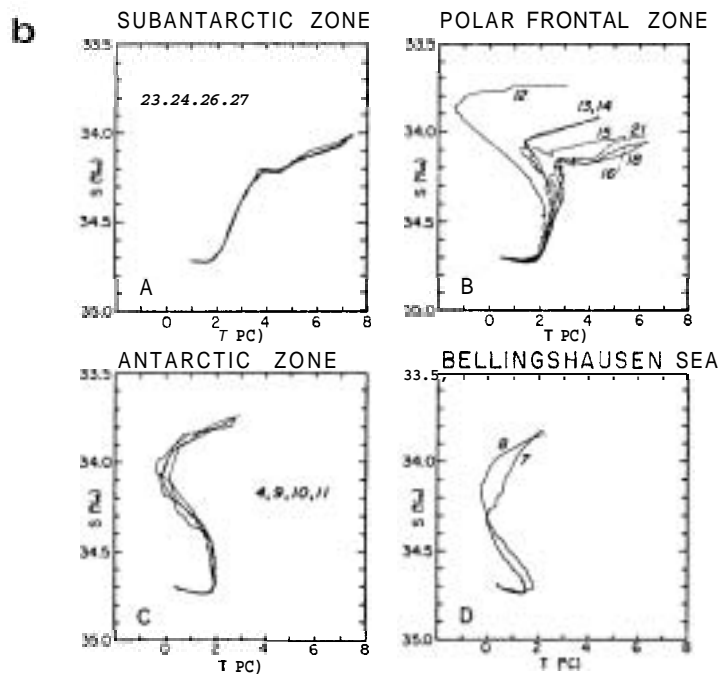
Fig. 8b. 8-S curves from the various zones from 60-68°W across Drake Passage (ibid.).

In the South Atlantic and Southwest Indian Ocean, the front defined above as the Subantarctic Front has traditionally been called the Subtropical Convergence.

3. Some Aspects of the Circumpolar Circulation

Meanders of the fronts may pinch off to form rings. Formation of a cyclonic cold core ring has been observed in Drake Passage as a result of meandering of the polar front, as defined by the position of the $2^{0}C$ isotherm (Joyce and Patterson, 1977). The observed ring had a diameter of 60-90 km and reached to the bottom. (The ring thus was several times larger than the Rossby radius, which is 10-20 km.) Velocities were 30-40 cm/sec as monitored by neutrally buoyant floats, four of which were placed in the vicinity of the ring. (Three floats remained with the ring and one float was apparently unaffected by its presence and moved off to the northeast.)

The Antarctic Circumpolar Current is strongly affected by topography, as mentioned at the beginning of this section. Figure 9 shows dynamic topogrzphy in the Southern Ocean, relative to 1000 db (Gordon, Molinelli and Baker, 1978). A few of the apparent effects of topography (Fig. 4) on the dynamic topography are:

1) South of Australia, the ACC parallels the zonal mid-ocean ridge and appears to be guided by it.

2) East of New Zealand the current splits into two branches, one following the edge of the Campbell plateau to the northeast and the other paralleling the zonal ridge to the south.

3) The two branches thus formed are forced to rejoin where the Pacific mid-ocean ridge turns to the north.

4) The zonal current is extremely diffuse over the Southeast Pacific Basin.
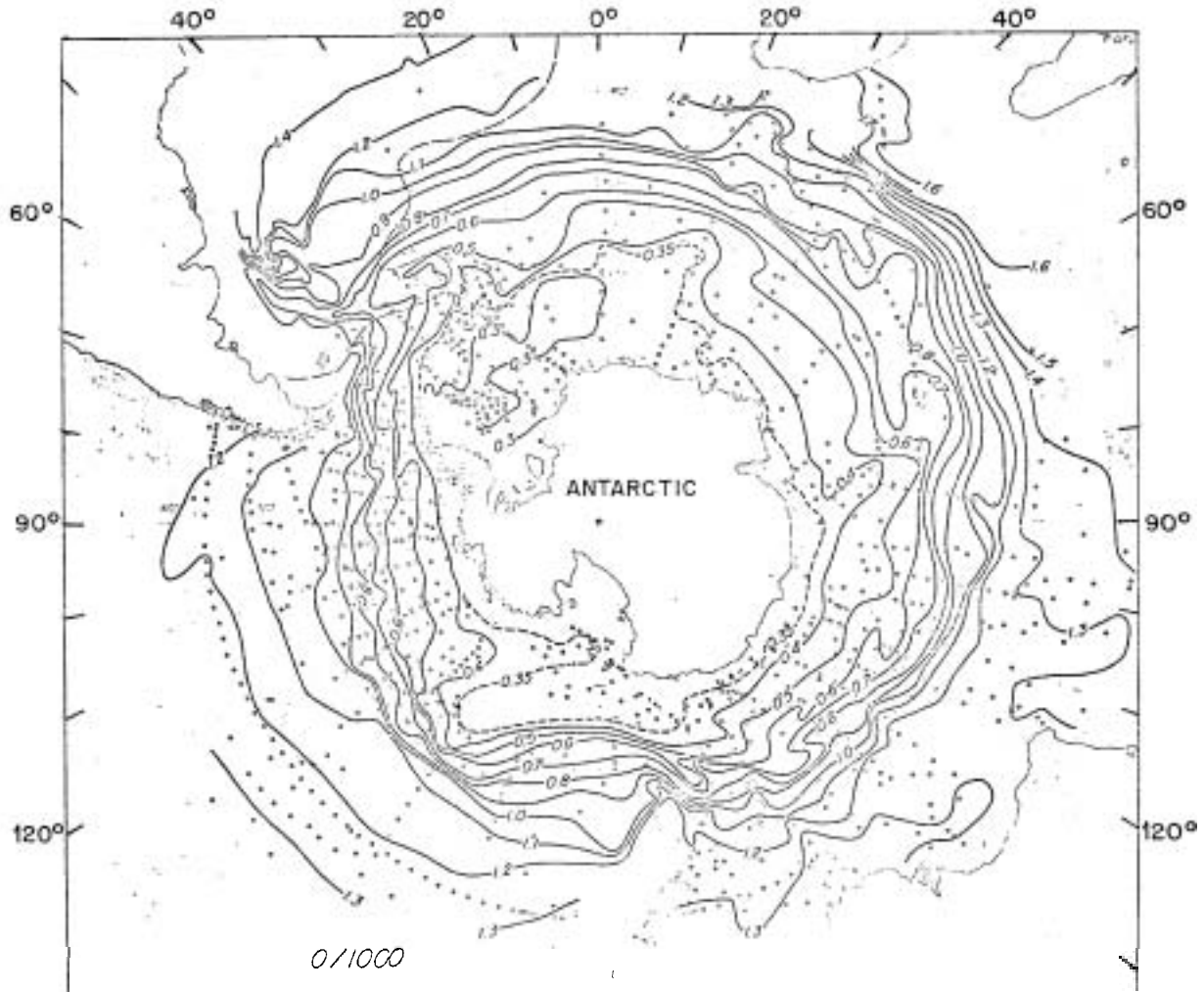
Fig. 9. Dynamic topography of the Southern Ocean relative to 1000db.
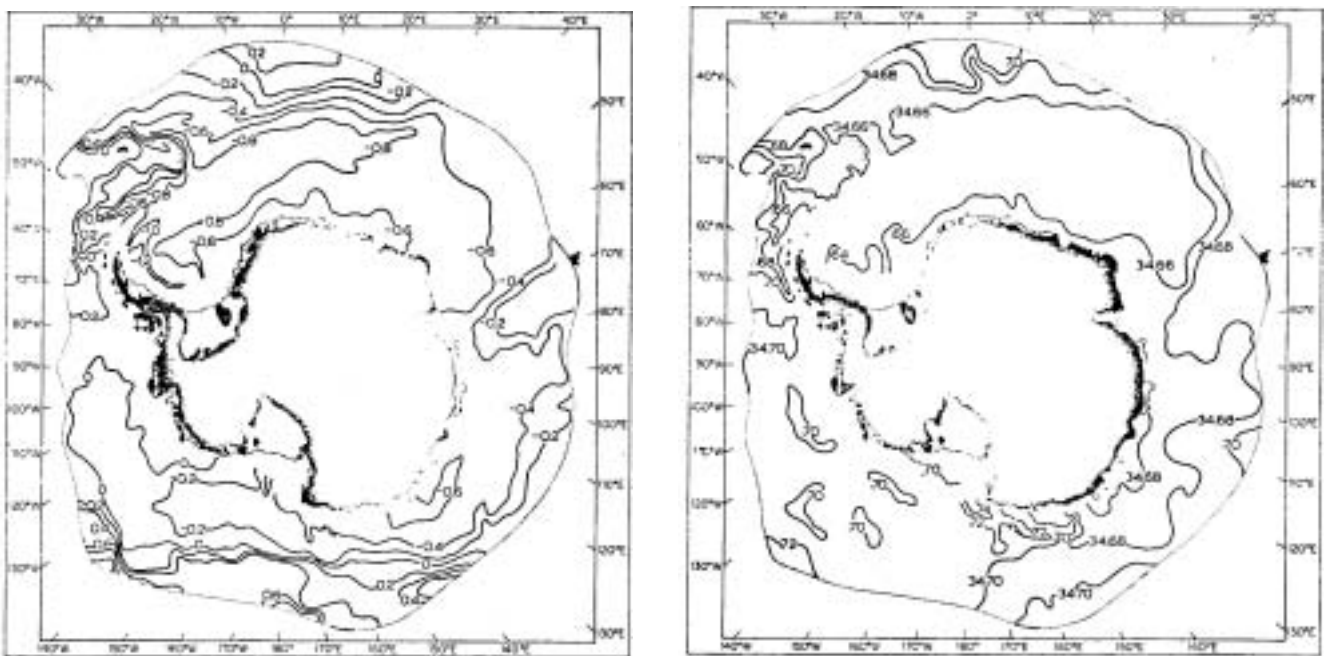
Fig. 10. Distribution of T and S at the bottom around Antarctica.
ABW is fresher and colder than surrounding water.

5) The current seems to be drawn in at Drake Pasage, becoming narrower and more intense.

6) The island archipelagos to the east of Drake Pasage apparently force a northward turn of the current.

7) Bottom Water distribution around Antarctica is strongly influenced by topography (and the position of the Antarctic Circumpolar Current) (Fig. 10).

'Transport calculations across Drake Passage have been collected by Nowlin, Whitworth and Pillsbury (1977). The present estimate of the transport is about i40 Sv of which 100 Sv are from the apparently steady baroclinic field and 40 Sv from the barotropic field.

REFERENCES

Gordon, A. L., 1975. An Antarctic oceanographic section along $170^{\circ}E$. Deep-Sea Kes. 22, 357-377.

Gordon, A. L., E. Molinelli and T. Baker, 1978. Large-scale relative dynamic topography of the Southern Ocean. J.G.K. 83 (c6), 3023-3032.

Jenkins, W. J., 1979. Tritium and ^{3}He in the Sargasso Sea. submitted to Jour. Geophys. Res.

Joyce, T. M. and S. L. Patterson, 1977. Cyclonic ring formation at the polar front in the Drake Passage. Nature 265 (5590), 131-133.

Nowlin, W. D., T. Whitworth, and R. D. Pillsbury, 1977. Structure and transport of the Antarctic Circumpolar Current at the Drake Passage and short-term measurements. J. P. O. 7, 788-802.

Ostapoff, F., 1962. The salinity distribution at 200 meters and the Antarctic Frontal Zones. Deut. Hydrograph. Zeitschrift. 15, 133-142.

Reid, J. L., 1965. intermediate waters of the Pacific Ocean. Johns Hopkins Oceanograpnic Studies 5, 96 pp.,

Sverdrup, Johnson and Fleming, 1942. The Oceans, Prentice Hall, New York.

Talley, L. D. and M. S. McCartney, 1979. The circulation of Labrador Sea Water (to be submitted to J.G.R.).

Worthington, L. V., 1972. Negative oceanic heat flux as a cause of water mass formation. J. P. O., 2, 205-211.

Worthington, L. V., and J. Kawai, 1972. Comparison between deep sections across the Kuroshio and Florida current and Gulf Stream. In: Kuroshio. H. Stommel and K. Yoshida, eds., University of Tokyo Press.

Wright, W. R. and L. V. Worthington, 1970. The water masses of the North Atlantic Ocean - A volumetric census of temperature and salinity. Serial Atlas of the Marine Environment, Folio 19, American Geographical Society.

Notes Submitted by
Lynne Talley

Lecture #8. THEORIES OF THE ANTARCTIC CIRCUMPOLAR CURRENT (ACC)

With the theories of Sverdrup, Stommel, and Munk, by the 1950's, the cause of the observed ,transports in the Subtropical gyres was considered almost closed. There were some discrepancies between observed transport estimates and theoretical wind driven prediction, but these were thought to be due to the difficulties in the assignment of level of no motion, and misestimation of wind stress. These theories were able to explain the circulation in enclosed basins (such as tor the Gulf Stream gyre), where the mean currents are circular and flow in direction oblique to the winds and where the motive balance is an interior Sverdrup balance of vorticity.

The basic difference for the Southern Ocean is that it is zonally un-bounded and shows an open basin regime. The mean currents in the ACC, unlike the enclosed basin regime, may be rectilinear and more directly driven by mo-mentum transfer from the wind. Since there are no meridional barriers, no Sverdrup flow can develop because of the impossibility of an east-west pres-sure gradient that would be supported by the boundaries and would balance the wind force. Therefore other types of balances seemed needed. The first idea was to use friction to balance the wind-supplied momentum.

Hidaka & Tsuchiya (1953) consider the case of an ACC which is purely zonal, and where the direct wind driving is balanced locally by eddy momentum airfusion. In order to get a realistic value for the ACC transport, they

needed a lateral diffusion coefficient A on the order of $10^{10} cm^2/sec$ compared to the $10^7 cm^2/sec$ that had been found for the Subtropical gyres. Bottom friction models give a similar discrepancy.

Munk and Palmen (1951) investigated the possibility of a pressure drag on topographic features that would result from a systematic offset between pressure field and topography. They find that a pressure change of 4 dyn. cm. at the leeside of a topographic feature (such as Mid Ocean Ridge or Drake Passage sill) is sufficient to dominate the bottom friction and pick up the torque.

Stommel (1957), in a survey of ocean current theory, emphasized the non-zonal aspect of the Southern Ocean because of the existence of ridges and constrictions (such as Drake Passage) which may play the role of meridional barriers. There exists no latitudinal circle in the ACC with a free passage below 1000 m. He, therefore, suggests the possibility of constructing a Sverdrup type solution, with all the resistance being concentrated at the Drake Passage. Using plausible wind-stress forcing a solution was sketched with a spiralling tendency of the ACC towards Antarctica (Fig. 1), and a meridional shift back north at the Passage.

Schulmann's (1970) numerical model deals with a barotropic, time dependent ocean flow in the Southern hemisphere to study the effects of bottom topography and non-linearity in the ACC. He shows that topography (Fig. 2) has very strong effects on the asymmetry and transport of circumpolar current and its interaction with the major ocean gyres. A large portion of the current is deflected to the North into the Falkland current. The presence of a sill across Drake Passage reduces drastically the transport by a factor of 5. Inclusion of topographic features such as Scotia Ridge shows the importance of topography in guiding the transport streamlines (Fig. 2). Inertial acceleration causes an overshooting of South America upon passing through the Drake Passage before it rejoins the coast as a western boundary layer.
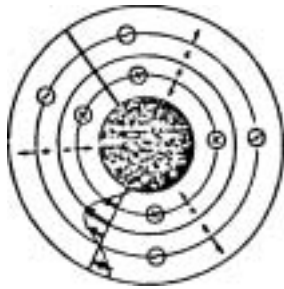
a. The schematic Southern *Ocean.* Antarctica **is the** solid. black circle. The meridional barrier extending northward from Antarctica is represented by the solid heavy black vertical line. The schematic wind system (purely zonal) is depicted by the **heavy** arrows on the lower left. The concentric circles are latitude circles. Latitudes of EKMAN convergence **and sinking** at the surface are indicated by minus signs, latitudes of EKMAN divergence and upwelling are indicated by plus signs. The direction of the required meridional geostrophic flow is. indicated by light radial arrows.
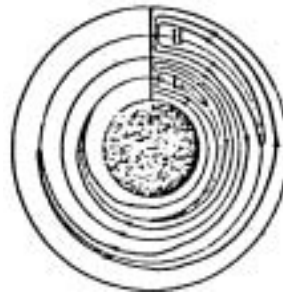
b. **Transport lines** of the solution for the model depicted in a. The western boundary currents are to be interpreted schematically.
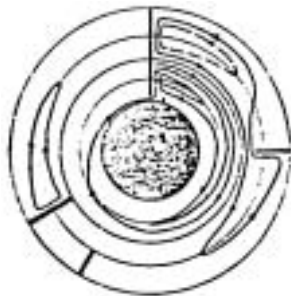
C. Modification of the transport field produced by introduction of other. meridional barriers corresponding to Africa, Australia, and New Zealand, and by breaking the American-Antarctic barrier so as to admit a very constricted Davis Straits.
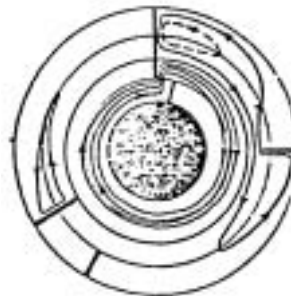
d. Hypothetical form of the solution that results from rupturing the American-Antarctic barrier in such a way as to permit water to flow through, but to obstruct all latitude circles.

Fig. 1
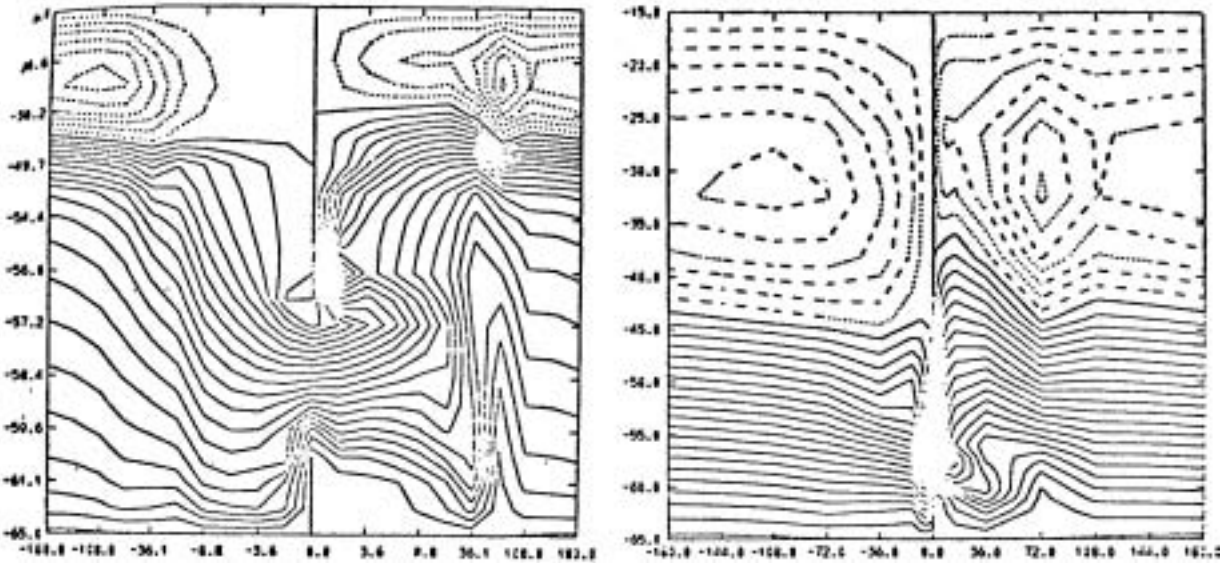
Streamlines for Scotia Ridge topography,
$\delta = 0.1$, $R_o = 0$. $H = 3$ for $\lambda \geq 35^\circ$, $\theta =$
-56.5°, -61°; $H = 1$ at $\lambda = 35^\circ$, $-61.0^\circ \leq \theta$
$\leq -56.5^\circ$; $H = 5$ elsewhere. Transport $= 90$
Sverdrups.
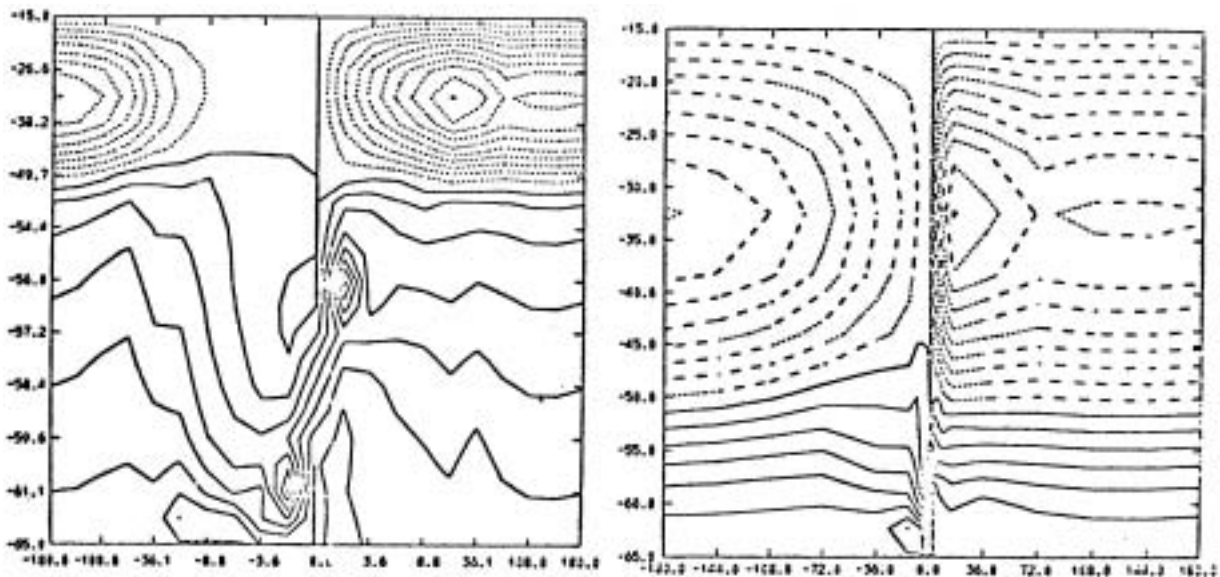
Streamlines for Drake Passage topography,
$\delta = 0.1$, $R_o = 0$. $H = 2 + 3/5^\circ |\lambda|$, $|\lambda| \leq 5^\circ$,
$-61.0^\circ \leq \theta \leq -56.5^\circ$; $H = 5$ elsewhere.
Transport $= 25$ Sverdrups.

Fig. 2

(a) $\epsilon = l/\ell = \frac{1}{2}$

(b) $\epsilon = l/\ell = 1$
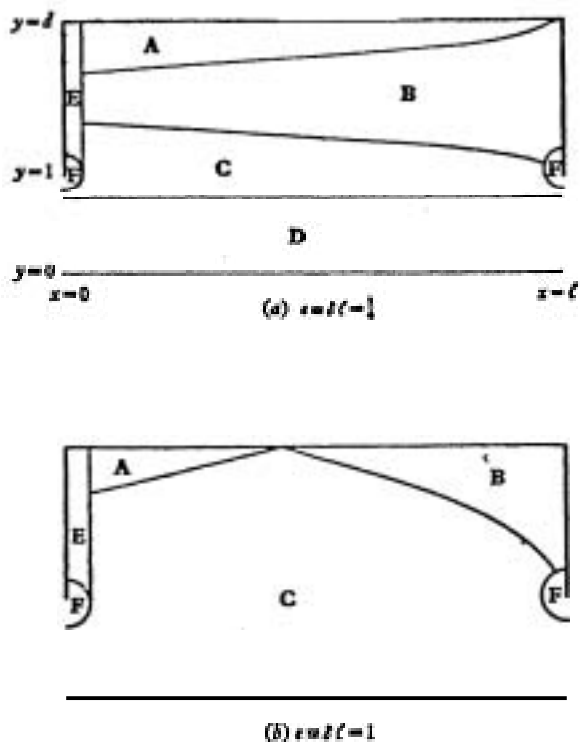
FIGURE 3. A schematic picture of the boundary layers that exist mhcn the friction **parameter** δ is small. (a)is the case where the product $\delta\ell$ is also small, (b) the case where $\delta\ell$ is of order unity. The layers E and F are of thickness δ while A and C have average thickness of order $(\delta\ell)^{\frac{1}{2}}$. The Sverdrup (or in case (b) the modified Sverdrup) solution is valid in B while the zonal solution in valid in D. The western boundary current flows in E. The behaviour of the transport lines in F is shown in figure 4.
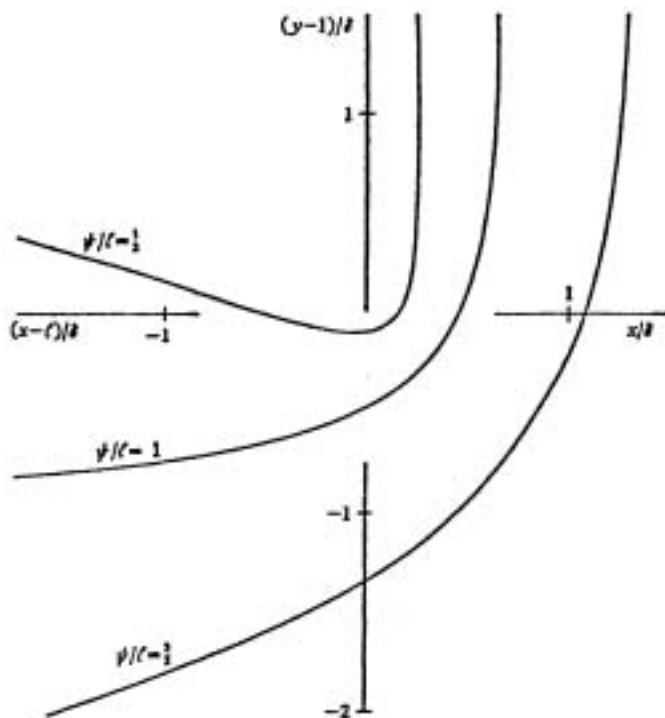
FIGURE 4. Transport lines, as given by (5.28), near the tip of the peninsula which cormponds in the model to Cnpe Horn. There is a transport of $2\sigma_0$ which goes into a 'western boundary current' seen hero to the right of the diagram. There is no exaggeration of the north–south scale.

Bryan & Cox (1972) in their numerical model of a homogeneous, flat bottom world ocean circulation, obtained a transport for the ACC of 600 Sv. The inclusion of a scaled down topography (for a grid size of 2° lat. x 2° lat) reduces the transport to 45 Sv; the interaction of broadscale wind fields and small scale ridge systems increase the horizontal gradients. The scale contributing to the horizontal velocity gradient is being defined by the topography scale, therefore the effects of lateral friction (with A ∼ $10^8 cm^2/sec$) are more important.

Gill (1968) studied a linear model of the ACC in which the geometry includes meridional barriers and where bottom friction is used to control the model. For small friction and both small western lateral boundaries effects (δ) and short zonal length (1) of the ocean (so that $\varepsilon = \delta 1 \sim 1/41$ the flow pattern is given by Fig. **3**. North of the Drake Passage there is an important Sverdrup region, and in the Southern Ocean the flow is zonal (other frictional boundary layers are also present).

The results suggest values of the frictional parameter ε between 4 and 6. As ε increases, a strong coupling between the currents at different latitudes occurs (Fig. 3b: broadening of the boundary region c). A large proportion of the water going through Drake Passage is directed into the western boundary and moves north of the latitude of Cape Horn (Fig. 4), and the currents tend to concentrate at the north end of the passage. This feature remains common to all models related to the ACC.

Large values of Fig. 5, resulting from large values of the zonal length, implies that the western boundary current goes well to the North of the passage, resulting in a strong east-west asymmetry of the meridional boundaries
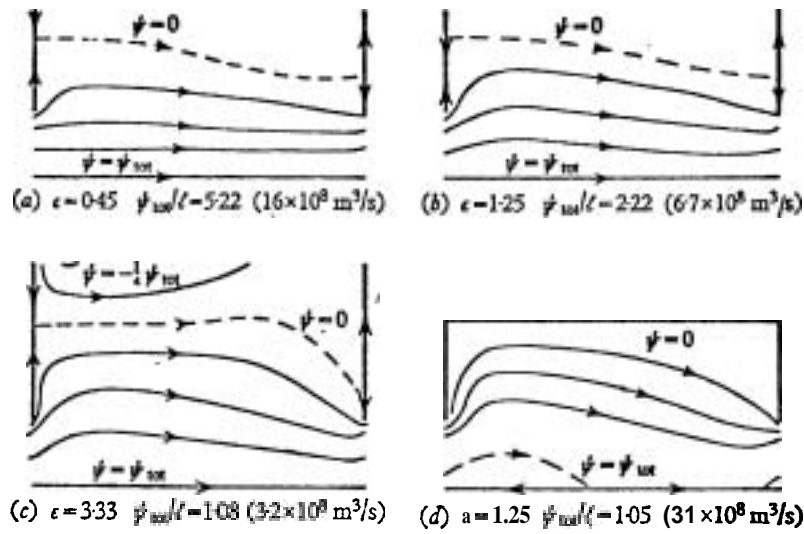
FIGURE 5. Some numerical solutions showing the dependence on the friction parameter ϵ [(a), (b),(c)] and on the wind stress distribution $X(y)$ [(b)and (d)]. X is given by (4.1) in cases (a),(b)and (c) and by (4.2) in case (d),X_0 being zero. The maximum wind stress is further north in the case (d). The contour interval for ψ is $\frac{1}{4}\psi_{tot}$.
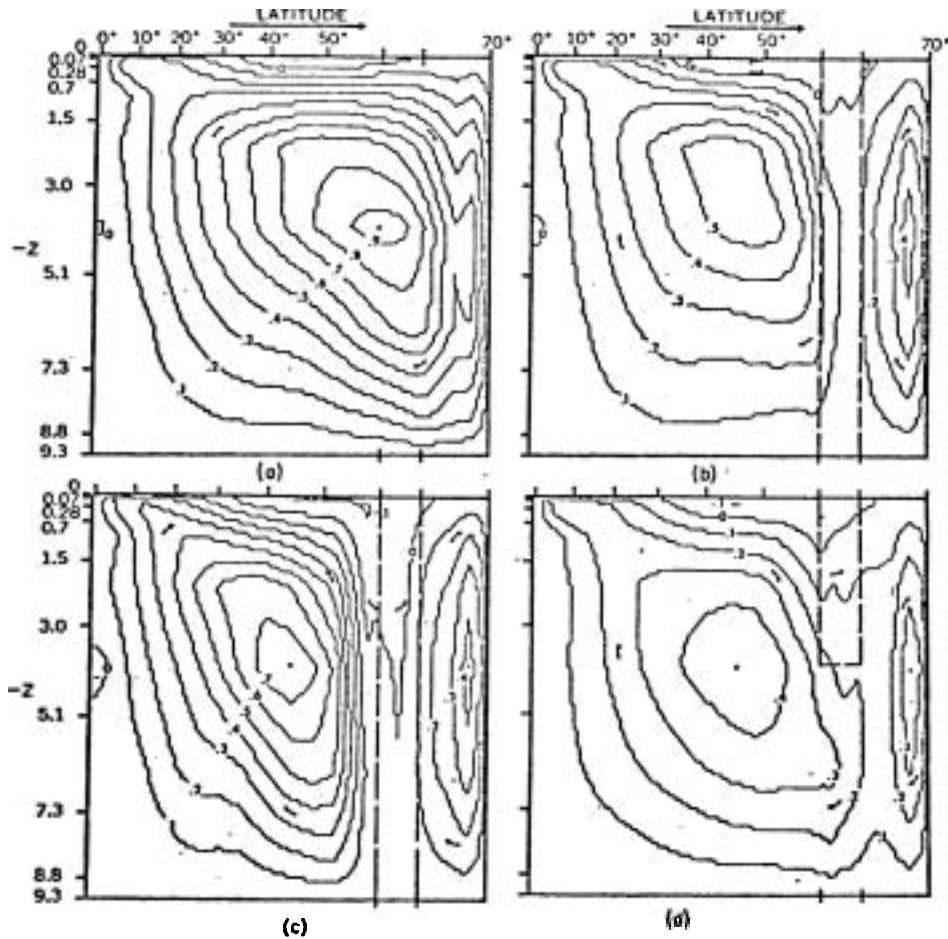
Fig. 6. Meridional circulation in the model ocean for cases (a) 14-1 (closed basin), (b) 15-1 (deep gap, linear surface-temperature distribution), (c) 16-1 (deep gap, curved surface-temperature distribution), and (d) 18-1 (shallow gap, linear surface-temperature distribution). Contours of the mass transport stream function, ψ, are shown in non-dimensional units. ψ is zero on the boundaries.
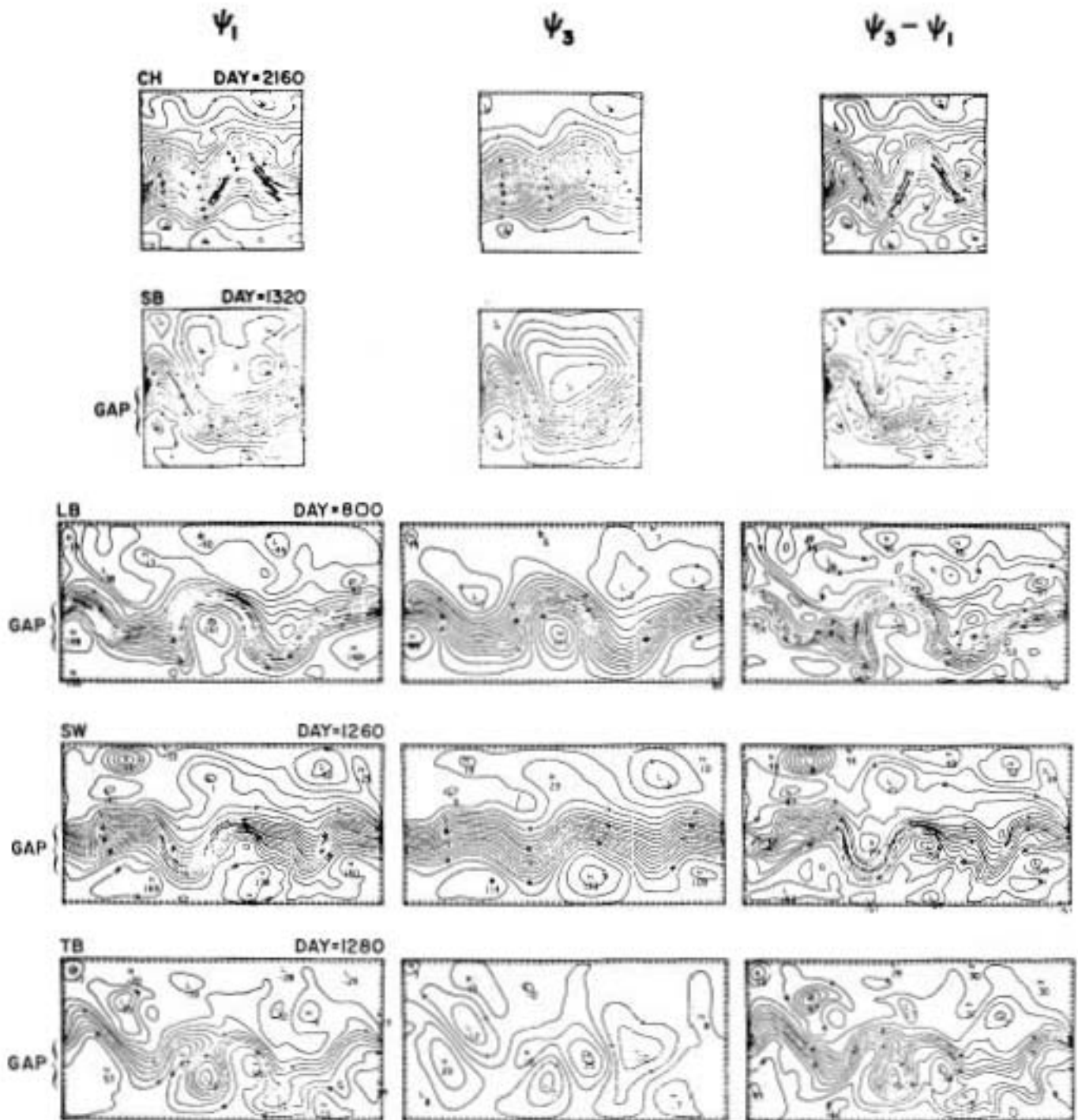
Fig. 7 Instantaneous streamfunction patterns on selected days during the equilibrium periods for the different cases. Shown for each case are the upper and lower streamfunctions and their difference, which, when multiplied by $f_0/g' = -0.55 \cdot 10^{-2}$ s m^{-1}, yields the interfacial displacement. The contour intervals are 10^4 m^{2}s^{-1} for ψ_1 and $0.6 \cdot 10^4$ m^{2}s^{-1} for $\psi_3 - \psi_1$; the labels are in units of 10^3 m^2 s^{-1}. The range of ψ values in each of these figures (from left to right, top to bottom) is 292, 165, 132, 199, 105, 108, 205, 116, 103, 230, 126, 116, 117, 37, and $104 \cdot 10^3$ m^2 s^{-1}, respectively.

regime, in agreement with Welander (1976) who found, for closed basins circu-
lations, that though large zonal extensions tend to give a zonally uniform
interior regime, the E-W asymmetry near the meridional boundaries always
persists, and only disappears when $\beta \rightarrow 0$.

Gill and Bryan (1971), in a thermally and wind-driven model, study the
effects of a sill in the gap of Drake Passage (no other topographic feature).
The effect of a deep sill is to effectively emphasize the isolation of the ACC
from the rest of the ocean (very small meridional transport across the ACC;
(Fig. 6). For a shallower sill, the transport increases three times due to
the fact that there exists a pressure difference across the barrier which acts
in the same direction as the wind-stress and which is of thermal origin. In
Holland's et al (1978) paper, the authors investigate a quasi-geostrophic
two-layer model in a β -plane channel, where the grid size is actually eddy
resolving. Mesoscale eddies can develop from fluid instabilities of the mean
geostrophic currents and may, in turn, provide significant Reynolds stresses
upon these currents. It is assumed that small-scale (sub grid scale physics)
diffusion is weak. Their results show the partially barotropic nature of the
HCC and also the existence of large vertical momentum transfer by interfacial
pressure drag induced by the eddies. The presence of a partial meridional bar-
rier and a topographic obstacle are found to strongly influence the equilibrium
solution, while neither a change in the basin length nor the presence of a
transient wind component appears to importantly alter the solution. In the
gap latitudinal barrier the pressure torque is resistive and is the major
resistive term. The topographic barrier in the gap creates the appearance of
standing eddies (Fig. 1) that dominate the zonal mean flow and reduces greatly
the transports and energies. No vestige of zonal symmetry remains and the
region downstream of the barrier is much more energetic than upstream.
Weddell gyre and Falkland current analogs are present in the model results.

A long period of oscillation of the order of three years of the transport is present in the run including a topographic barrier (TB) and seems to originate in an oscillation of strength of the standing eddies downstream of the Drake Passage siii (Fig. 8); the energy cycle (Fig. 9) involved is the building of potential energy while the kinetic energies decay and the peak potential energy is followed by rapid decay with rising kinetic energies.

In Bryan & Lewis's (1978) time-dependent model of the water masses of the world ocean, climatological wind-stress, temperature and salinity fields are imposed as surface boundary conditions and equilibrium state is reached after a period of 1000 years.

The model is able to reproduce the major observed differences between water mass features in the Atlantic and the Pacific and between the northern and southern oceans. The equivalent of Antarctic Intermediate Water is formed northward of the ACC in a small region of intense salinity off Chile in consistency with the mechanism proposed by McCartney (1977). The source is a mode type water which is formed by late winter deep convection in the same way that $18^{\circ}C$ water forms in the Sargasso Sea. This water cools as it moves along the ACC and sinks when it reaches its most poleward position near the Drake Passage off Chile and spreads from that point around the globe. Its salinity minimum is due to the excess of precipitation in the region north of the Subantarctic Polar Front.

Figure 10 a-c illustrate that mechanism. Intermediate level velocity vectors show flow through the Drake Passage with a branch current flowing to the North and West off of Chile and vertical downward velocities maximum is present off Southern Chile. The salinity pattern indicates a tongue of fresh water at the lower level originating near Chile and extending westward in a counterclockwise arc. A possible explanation for the renewal of the AIIW is

Fig. 9.
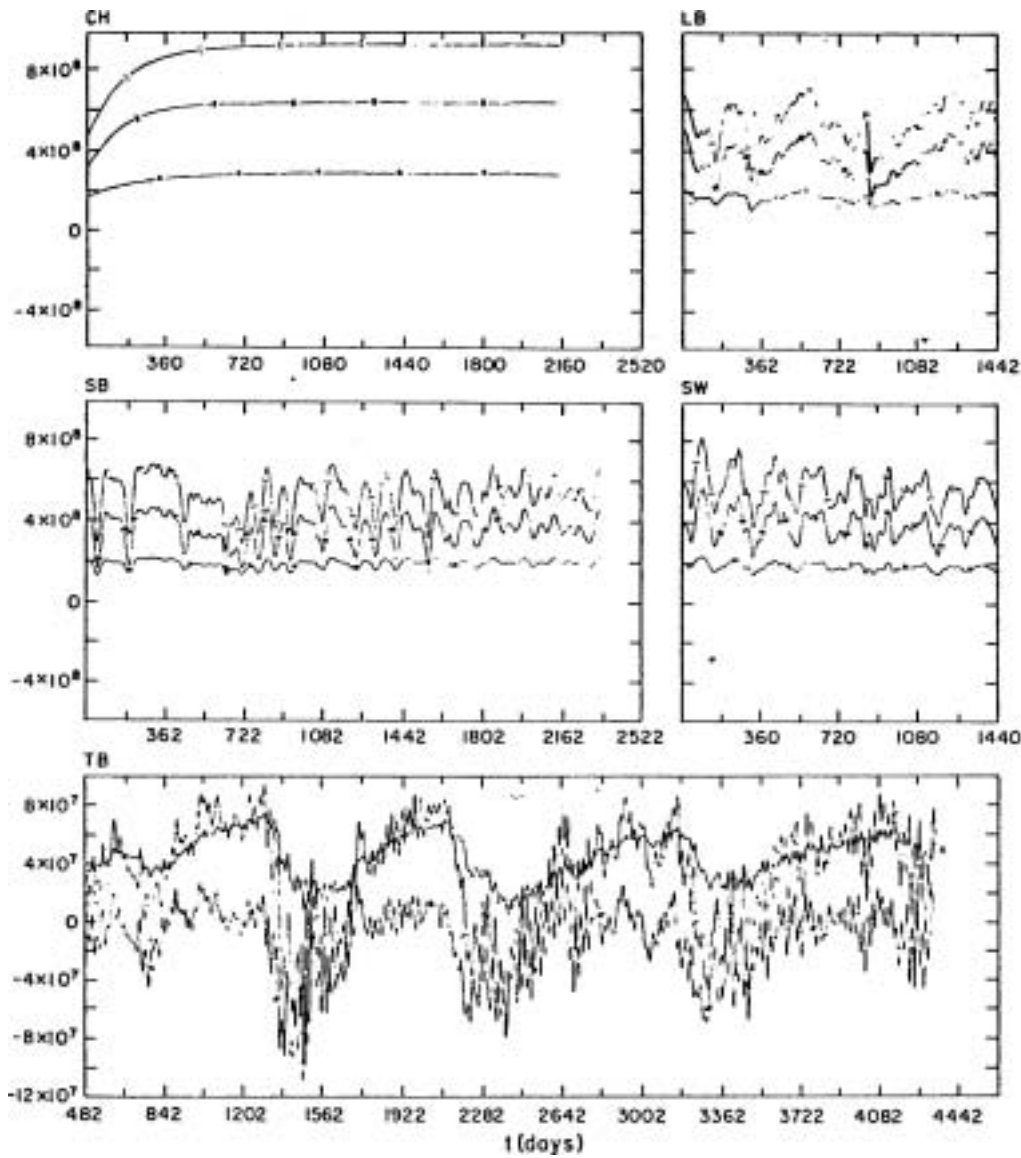
Fig. 8. The time histories of transport through the gap (m^3 s^{-1}). The three curves in each case are (a) upper layer $H_1(\psi_1(0) - \psi_1(L_y))$, (b) lower layer $H_3(\psi_3(0) - \psi_3(L_y))$, and (c) total transport. For TB only days 482—4320 are shown, since initial transients are off-scale for this graph (n.b. the scale for TB is different from the other cases).
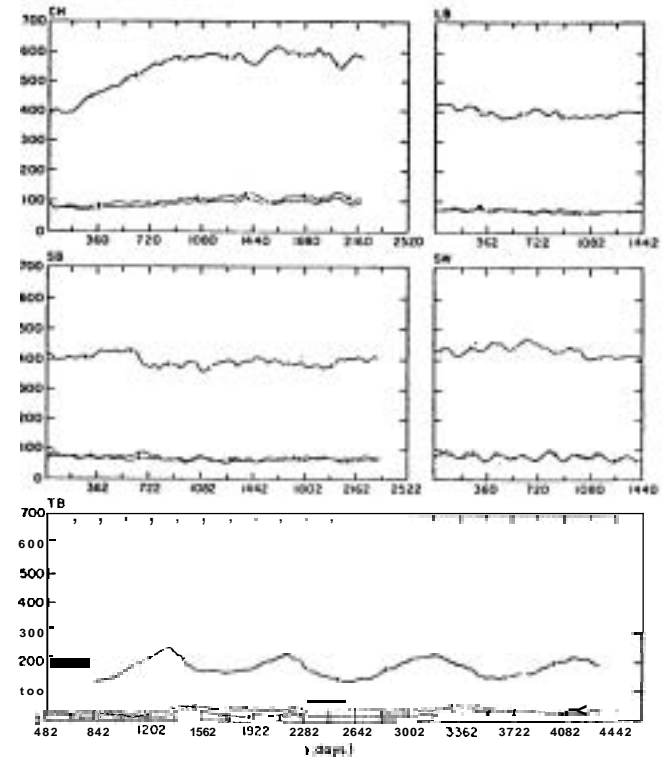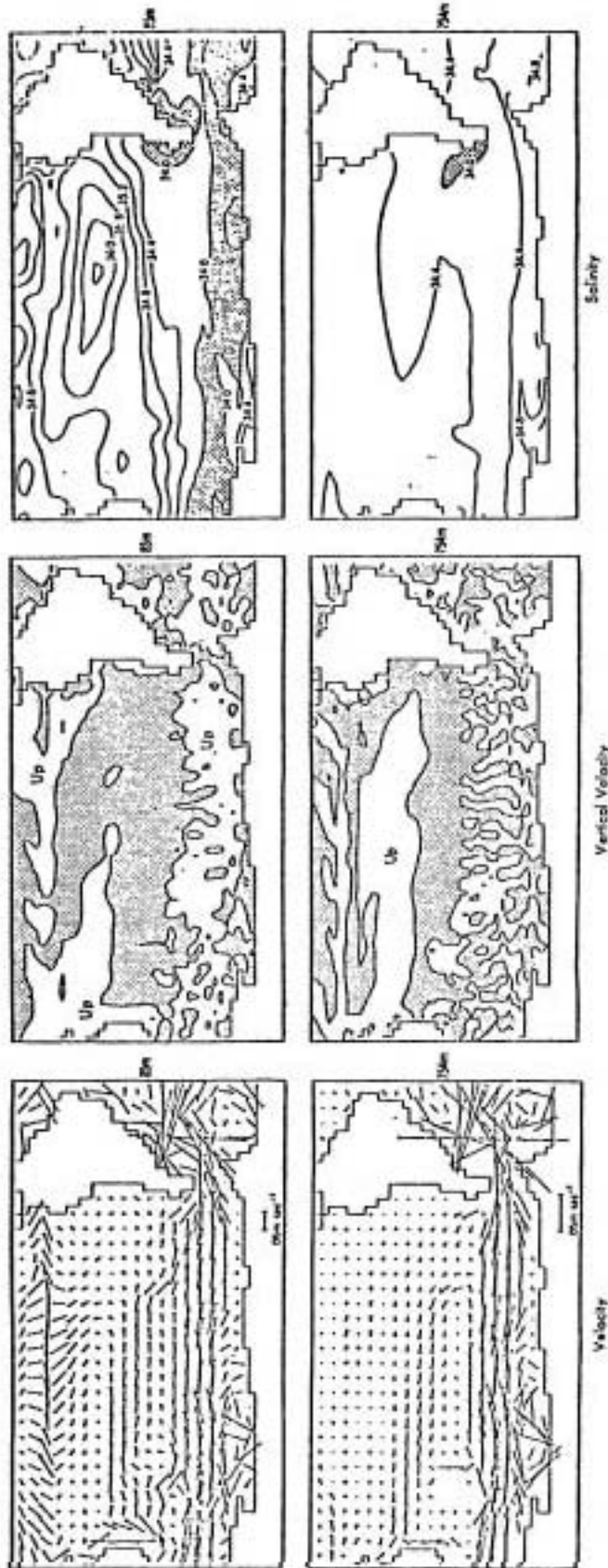
Fig. 10. a) South Pacific velocity vectors computed in Experiment III,

b) vertical velocity, c) salinity patterns.
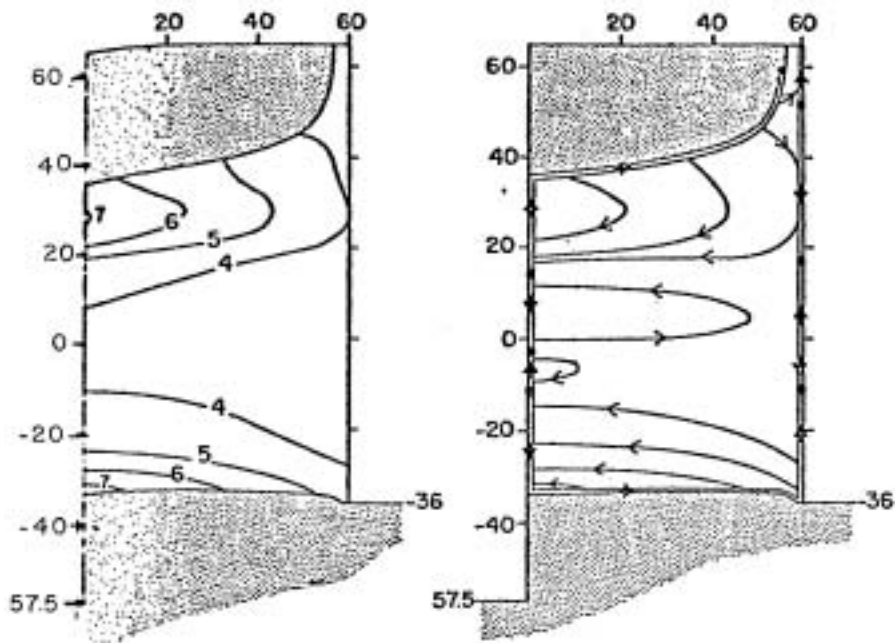
(left) Calculated thermocline depth (in hectometers) in Atlantic Ocean. Lower layer of surface in stippled regions.

      (right) Schematic of upper-layer transport for Atlantic.

Fig. 11

that it is formed along the ACC and sinks down to the 1000 m level and spreads equatorward. The associated salinity minimum is present in the globally averaged salinity profile of the model.

In a model of world ocean circulation, Veronis (1973, 1976, 1977) considered a two-layer representation of a wind and thermally driven ocean.

The Subtropical gyre system of the North Atlantic (Fig. 11) is well reproduced and the main features of the polar and subpolar masses are also present in the lower layer of the model. McCartney suggests a possible generalization of the model to a three-layer system to represent the polar, subpolar and subtropical layers and therefore allow for regions of downwelling where upper layer is converted to lower (formation of Subtropical and Subantarctic Mode Water).

REFERENCES

Bryan, K. and M. D. Cox, 1972. The circulation of the world ocean: a numerical study. Part I, a homogeneous model. JPO 2, 319-335.

Bryan, K. and A. Lewis, 1978. A water mass model of the world's oceans. published manuscript.

Gill, A. E., 1968. A linear model of the Antarctic Circumpolar Current, JFM, 32., 465-688.

Gill, A. E. and Bryan, 1971. Effects of geometry on the circulation of a three-dimensional southern hemisphere ocean model. DPS, 18, 635-721.

McCartney, M., 1977. Subantarctic Mode Water -- A voyage of DISCOVERY.

McWilliams, J. C. and Al, 1978. A description of numerical Antarctic circumpolar currents. Dy. Atm. Oceans, 2, 213-291.

Munk, W. H. and Palmén, E., 1951. Note on the dynamics of the Antarctic circumpolar current. Tellus, 3, 53-55.

Schulman, E. E., 1970. The Antarctic circumpolar current. Proc. Comput. Sinul. Conf., 6-12 June, 1970, Denver, Colorado, 955-968.

Stommel, H. M., 1957. A survey of ocean current theory. Deep-Sea Res. 4, 149-184.

Veronis, G., 1973. Model of world ocean circulation. **I.** Wind-driven two-layer. **J.M.R.**, 31(3), 228-287.

Veronis, G., 1976. Model of world ocean circulation. **II.** Thermally driven, two-layer. J.M.R., 34, 199-216.

Veronis, G., 1977. Model of world ocean circulations. **III.** Thermally and wind-driven. J.M.K., 36(1), 1-44.

Welander, P., 1976. A zonally uniform regime in the oceanic circulation. JPO, 6(2), 121-124.

FURTHER READING

Holland, W. R., 1978. The role of meso-scale eddies in the general circulation of the ocean-numerical experiments using a wind-driven quasi-geostrophic model. JPO, 8(3), 363-392.

Stommel, H. M., 1948. The westward intensification of wind-driven ocean currents. Trans. Am. Geophys. Un., 29, 202-206.

Stommel, H. M., 1962. An anology to the Antarctic circumpolar current. JMR, 20, 92-96.

Notes Submitted by
Bach-Lien Hua

THE NORTHERN SEA

Knut Aagard

Bathymetry

The northern sea may be regarded as a Mediterranean Basin. Its communications with the Atlantic are fairly broad and deep, > 2000 m between Greenland and Spitsbergen and 400-500 m in Barents Sea between Spitsbergen and Franz Josefs land. The outer sills, connecting Greenland, Iceland and Faeroe Islands, the Shetland Islands and Scotland are not quite that deep ~ -600 - 800 m. This is in stark contrast to the narrow and shallow 60 m connection with the Pacific through Berings Strait. The topography contains a few ridges, the most conspicuous being the Lomomosov Ridge running roughly along the $140°E$ meridian across the north pole, dividing the deep 4000 - 5000 m polar basin.

The shelves are very large and shallow; especially conspicuous is the 40 - 50 m deep shelf area off the East Siberian coast, which is one of the largest in the world.

Water Masses

The Northern Sea is characterized by a cold and low saline homogeneous surface layer reaching a depth of 40–50 m. Underneath the surface layer lies a strong 250–300 m thick pycnocline. The stratification is due to a marked salinity increase. Below the pycnocline we can identify the inflow of warm high-saline Atlantic Water. The signal is strong north of Spitsbergen, but it is transformed fast as it moves towards the east along the continental slope. The density appears to be conserved and the layer can be traced as a temperature maximum across the basin. The thickness varies between 400–750 m.

At depth we have a cold high salininity deepwater mass. The origin of this water has traditionally been thought to be the Greenland Sea. However, a transformation of Atlantic waters into deepwater in the Arctic basin may not be altogether ruled out. The source, however, must be on the Atlantic side of the basin as can be seen from the higher bottom temperature on the Pacific side of the Lornomosov Ridge.

Freshwater Discharge

The strangely estuarine appearance of the Arctic Sea is due to the high freshwater discharge from mainly the Siberian rivers. The discharge is about 0.1 (Sverdrup) but is highly variable both seasonally and over a longer time period. The surface salinity shows a marked gradient from the source area off Siberia towards the passage between Greenland and Spitsbergen. The high input of freshwater probably accounts for the permanent three-meters thick ice cover which covers the Arctic Sea. The ice, which is mostly formed over the shelf areas effectively insulates, due to its high albdeo, the subsurface layer from

incoming solar radiation. The appearance of rifts and polynyas in the ice cover will enhance the absorption of solar radiation, heating the water near the ice. The melting increases and a low saline surface water will form. This layer does not communicate with the water below and its temperature tends to a climatological limit balancing radiation and heat required for melting. The ireshwater input, due to the melting of ice, is around 1 Sv. and is clearly the seasonally most important freshwater contribution. The other sources, precipitation–evaporation +0.01 Sv and net inflow of freshwater as ice, through the Bering Strait, +0.02 Sv are clearly negligible.

During ice formation, the conviction due to an outfreezing of salt will homogenize the upper layer creating the upper homogeneous lid mentioned above.

Estimation of the residence time in the upper layer gives a value of ten years. Since fluctuation of river discharge occurs at the same time scales, these might conceivably produce some time variation in the depth and structure of the homogeneous layer.

Circulation

a) Surface Layer

The circulation in the upper homogeneous layer may be deduced from a study of ice drifts combined with the dynamic topography.

The picture that evolves consists of a small inflow through the Bering Strait, a drift across the basin and a large outflow between Spitsbergen and Greenland in the East Greenland current. There are also some small outflows through the Canadian Archipelago. The mean circulation is anticyclonic, with a rather tight gyre formed north of Alaska - the Beaufort gyre.

b) The pycnocline circulation will not be considered in any detail. We only note that occasionally strong eddy motion with velocities around 20–25 cm/s occurs in the pycnocline at a depth of 200 m.

c) <u>The inflow of Atlantic Water</u> takes place in the west Spitsbergen current. The current is narrow, meandering and shows great fluctuation in time, both in heat and mass transports. The mean transport is 6 Sv with fluctuations of 40% apart from the even greater seasonal variations. The flow appears to be tightly topographically controlled, both west of Spitsbergen and on its way eastward along the continental slope. There is evidence of Atlantic Water flowing into and out of submarine canyons. The Atlantic Water may be followed eastward by tracing its T-S characteristics. The circulation is cyclonic and covers the whole basin. Possibly some of the water makes a tighter turn following the Lomomosov Ridge. Based upon calculation of the heat content of the Atlantic Water and the inflow of heat from the west Spitsbergen current one gets a time estimate of 6 years for the flow to reach the Beaufort Sea.

The T-S signature of the Atlantic Water changes rapidly while it passes along the slope between Spitsbergen and Franz Josefs Land soon showing only as a temperature maximum. Vertical profiles taken north of Spitzbergen show interesting microstructure suggesting the existence of double-diffusive processes. A knowledge of the occurrence of these processes and other mechanisms, by which the heat carried by the inflowing Atlantic Water may be available to the Arctic, is of prime importance; especially considering the great heat fluxes involved. We may note that in the Atlantic layer there is enough heat to melt an ice cover of a thickness of 20 m.

The recent estimates of the global heat flux across 80°N show that the oceans account for 10-20%, even at this high latitude. The bulk of this heat is carried by the Atlantic Water in the west Spitsbergen current, the transport of latent heat in the form of ice by the East Greenland current accounting for most of the remaining balance.

A traditional way to approach the problem of the transformation of the Atlantic Water is to plot the inflowing and outflowing Atlantic Water on a T-S diagram and look for the needed mixing "partner" for straight line mixing. We find then, assuming the other water to be at its freezing point, that we need two parts of water T = 1.9, S = 34.79 o/oo to 3 parts of Atlantic Water. Any water of these properties has not yet been found. We will, therefore, turn to the possible mixing processes that may occur in the Arctic Ocean to see if we can find anything that may produce water of this T-S signature.

Exchange Processes

We find in Fig. 1 a rather complete schematic description of various mixing mechanisms. Apart from the transformation of the Atlantic layer we are interested in the maintenance of the 100 m deep cold layer with temperature near the freezing point as well as the maintenance of the pycnocline. The stirring and the convection in the open sea does not reach that deep. We need to turn to the shelves to find a mechanism that may produce the waters that are required.
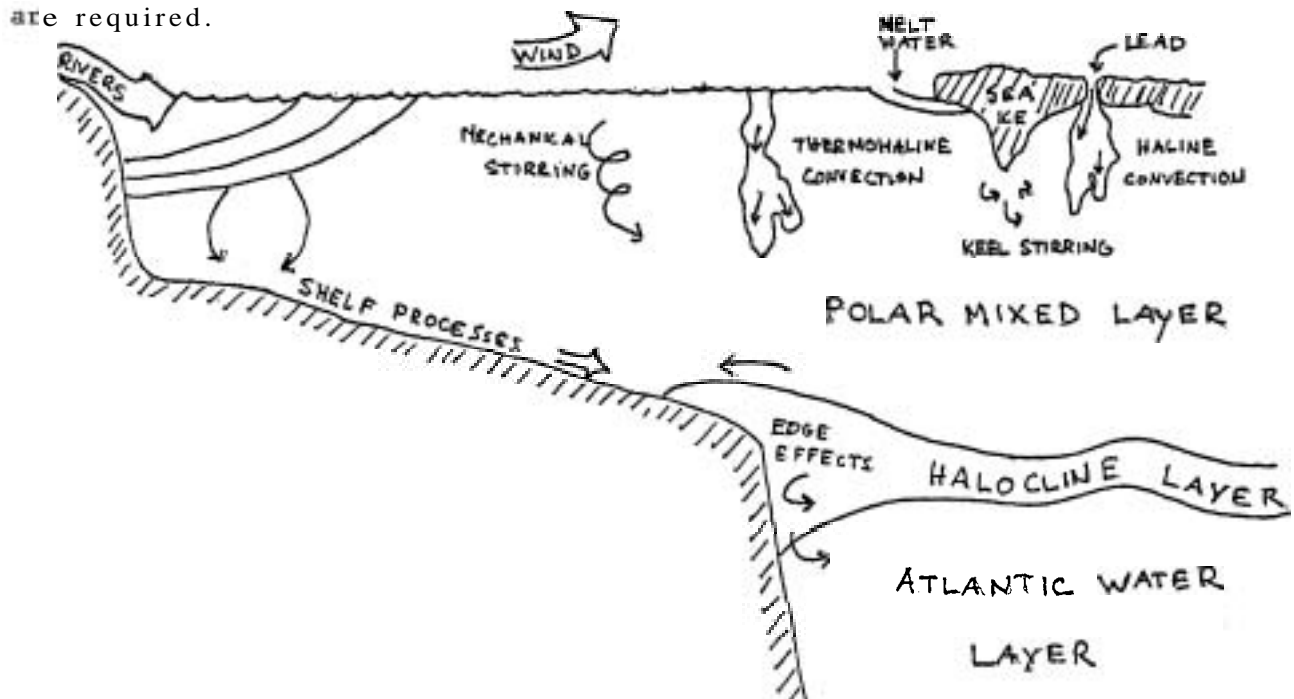
Fig. 1. Exchange Processes in the Arctic Sea.

Traditionally, the shelves have been considered to be able to produce a large amount of ice and cold dense water due to their high area to volume ratio. Water moves over the shelves, cools, freezes, and sinks, due to an increase in salt content. This mechanism may be effective in producing the waters in the upper few 100 ms. To reach further down we most probably require a higher initial salinity value. This may be affected by a circulation in the opposite sense, where high salinity water is forced up on the shelf and mixes its salt upward. A subsequent freezing may then produce cold, high saline water capable of sinking to the bottom.
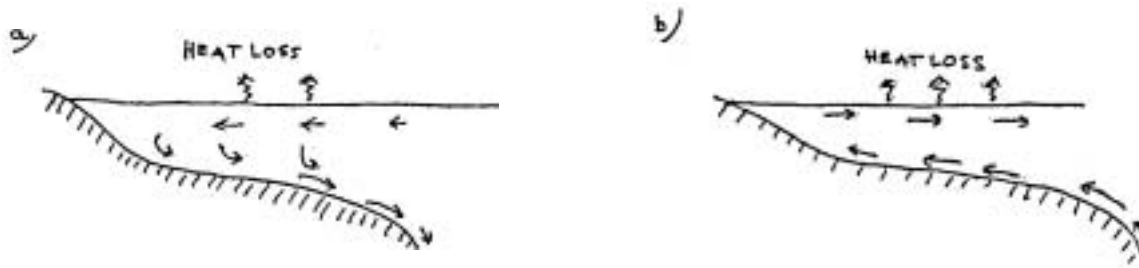
Fig. 2.   Shelf Circulations

One winter section taken across the Chukchi Sea shows the whole shelf near the freezing point and extremely dense saline water at the bottom. This water is denser than any observed outside isolated lagoons. To produce the amount of dense water observed in the Chukchi Sea a formation of 2.4 m of ice should be needed. This is a rather high figure due to the low heat conduction through the ice. However, on a shelf with open water and a circulation driving the ice off the coast, this amount of ice may be produced in little over three weeks. Assuming a rather continuous production of ice over the shelves during the whole winter, one may, given the shelf areas in the region, consider it possible to produce the observed amount of high saline water through the mechanism described above. The question remains, as to how the Subsurface Water

is forced up the shelf. One possibility is long periodic topographically trapped waves travelling along the continental slope. Observations of the lifting of relatively warm saline water onto the shelf have been made in the Beaufort Sea.

Summary

The key area to the Arctic basin seems to be the continental slope east of Spitsbergen towards Franz Josef Land and the Kara Sea. There the great transformation of Atlantic Water takes place and there are most probably the missing water masses formed.

This may also include deep water formation. The deep water in the Arctic is usually regarded as coming from the Greenland Sea. The salinity of the Arctic deep water is, however, a bit higher than the water observed in the Greenland Sea. Tracer studies indicate an unexpectedly fast vertical exchange rate and some T–S curves taken northwest of Spitsbergen show increasing salinity and decreasing temperature with depth. This. is a T–S relation rarely found in the deep ocean. Such T–S curves have, however, been observed in the Ross Sea and have been taken as signs of deep water formation. These thoughts on deep water formation in the Arctic must, however, remain speculations.

Notes Submitted by
Bert Rudels

THE AMPLITUDE OF CONVECTION

Willem V. R. Malkus

As the ubiquitous source of motion, both astrophysical and geophysical, convection has attracted theoretical attention since the last century. In the ocean, many different scales are called convection; from the deep circulation due to seasonal production of Arctic Bottom Water to the mixing by salt fingers. In the atmosphere, convection dominates the flow from sub-cloud layers to Hadley "cells". It is proposed that convection in the earth's core powers the geomagnetic field. The non-periodic reversals of that field, captured in the rock, define the evolution of the ocean basin. Recent recognition that this latter process is caused by convection in the mantle has produced a new geophysics.

In the past, understanding the central features of convection has come from the isolation of "simplest" mechanistic examples. Although large scale geophysical convection never quite provides the idealized simplest problem, these examples (e.g., Lord Rayleigh's study of the Benard cells) have generated much of the formal language of inquiry used in the field. In the past it has served the dynamic oceanographer to follow developments in understanding of these bits of the overall geophysics.

Speculations beyond these mathematically accessible problems take the form of hypotheses, experiments and numerical experiments in which one seeks to isolate the central processes responsible for the qualitative and quantita-tive features of fully evolved flow fields. The many facets of turbulent

convection represent the frontier. This talk will review only a narrow path towards that frontier. This path is aimed at an understanding of the elementary processes responsible for the amplitude of convection, in the belief that quantitative theories permit the theorist the least self-deception.

Of course the heat flux due to a prescribed thermal contrast, like the flow due to a given stress, has been observed for a century. The relationship between "force and flux" has been rationalized with models emerging largely from linear theory and kinetic theory - in particular the use of observationally determined "eddy conductivities", (estimated for the oceans in Sverdrup, Johnson and Fleming, 1942). Early theoretical interpretations of oceanic transport processes which go beyond these simple beginnings were explored by Stommel (1949), while current usage and extensions of "mixing" theory are commonplace in the literature.

Central to the most recent of such proposals is the idea that some large scale of the motion or density field is steady or statistically stable, while turbulent transport due to smaller scales can be parameterized. Changing the amplitude of the small scale transports is presumed to lead to a new equilibrium for the large scale, hence the statistical equilibrium is marginally stable. This view lurks behind most traditional oceanic model building and its quasi-linear form is used on small scale phenomena as well - from inviscid marginal stability to quantify aspects of the wind mixed layer (Pollard, Rhines and Thompson, 1973) to viscous marginal stability to quantify double-diffusion (Linden and Shirtcliffe, 1978).

It has not been possible yet to establish either the limits of validity or generalizability of this quasi-linear use of marginal stability in the geophysical setting. There can be little doubt that it is "incorrect" - that fluids typically are destabilized by the extreme fluctuations - yet it appears

to be the only quantifying concept of sufficient generality to have been used in oceanic phenomena from the largest to the smallest scales. Of course, our idealizations in the realm of geophysics all are "incorrect". One returns to observation to establish in what sense and in what degree these idealizations are good "first-order" descriptions of reality.

This talk explores the hierarchy of quantifying idealizations in convection theory. The quasi-linear marginal stability problem is drawn from the full formal statement for stability of the flow. A theory of turbulent convection based on marginal stability is presented, incorporating both the qualitative features determined by *inviscid* processes and the quantitative aspects determined by dissipative processes.

Observations provide better support for both the quantitative and qualitative results from quasi-linear marginal stability theory than might have been anticipated, encouraging its continued application in the oceanic setting.

REFERENCES

Linden, P. F and T. G. L. Shirtcliffe, 1978. The diffusive interface in double diffusive convection. J. Fluid Mech. 87, 417-32.

Pollard, R. T., P. B. Rhines, R.D.R.Y. Thompson, 1973. Deepening of the Wind-Mixed Layer. Geo. Fluid Dyn. 3, 381-404.

Stommel, H., 1949. Horizontal diffusion due to oceanic turbulence. J. Mar. Res. 4, 149-84.

Sverdrup, H. V., Johnson, M. W., Fleming, R. H., 1942. The Oceans. Prentice Hall, Inc. New York.

OCEAN SIGNATURES OF DOUBLE-DIFFUSION

Ray Schmitt

Theory and laboratory experiments are reviewed to delineate the conditions under which salt fingers are expected to be an important oceanic mixing process. The nondimensional density ratio $R_\rho = \alpha \Delta T / \beta \Delta S$, is the controlling parameter; Schmitt (1979a) finds that the finger e-folding time becomes less than a local buoyancy period for $R_\rho \leq 2$. The theory is an exact Boussinesq solution in a region of constant gradients of T and S, and assumes only Newtonian drag, Fourier heat conduction, and Fickian diffusion. The heat to salt density flux ratio of the fastest growing finger agrees well with data in both the heat-salt and sugar-salt systems; so there is good reason to trust the model. The increasing finger growth rates as approaches the singular case of $R_\rho = 1$ suggests an increasing dominance of the fingers. The Laboratory experiments (Schmitt, 1979b) show a similar trend; with the coefficient of the 4/3 power law for the salt flux increasing as $R_\rho \to 1$.

In rhe upper thermocline of the 'Central Waters', R_ρ tends to be constant and is about 2 for the Atlantic, 3 for the North Pacific and about 1.9 for the Southern Oceans. These are sufficiently low that we expect salt fingers may play a significant role in the mixing of the upper thermo-halocline.

Direct observations of salt fingering in the ocean have been by Williams (1975) and Magnell (1976) on the high gradient sheets separating adjacent mixed layers in the staircase regions where $R_\rho < 1.7$. No clear evidence for fingering has been found in the irregular steppy Central Water when $R_\rho > 2$. Indirect evidence of double diffusion has been found by Gargett (1976) and Gregg (1975) in the-increased microstructure activity where the local gradients are in the correct sense for double-diffusion (especially at the edges of isopycnal intrusions).

Two classes of oceanic finestructure can be attributed to double-diffusion. One is the thermo-haline staircase, which is found when T and S decrease monotonically with depth. A survey of the observations shows that strong staircases are found only when $R_\rho < 1.7$; irregular steppiness is found for $R_\rho > 1.8$. The other finestructure phenomena due to double-diffusion requires horizontal gradients as well; and is characterized by the propagation of lateral intrusions across density surfaces. This appears to occur at fronts (Joyce, Zenk and Toole, 1978) and surface mixed layers (Gregg, 1979). Stern (1967) suggests that the rising (sinking) of warm, salty (cold, fresh) intrusions across isopycnals provides a mechanism for keeping the T-S relationship tight; any T-S anomaly will cross density surfaces until reaching a surface with the same T and S.

Large scale signatures of salt fingering can be seen by tracing the core properties of water masses. The Antarctic Intermediate Water gains more salt than heat as it propagates northward in the Atlantic. The heat/salt flux ratio is in excellent agreement with salt finger theory and experiment.

Ingham (1966) found that most 'Central Water' T-S plots fit a curve of constant R_ρ better than a straight line. This argues against the traditional notion of equal eddy diffusivities for heat and salt and suggests that a double-diffusive explanation must be sought. The theory of Schmitt (1979a) and use of laboratory flux laws with observed ΔS'S from ocean staircases, both suggest that the finger mixing intensity is a strong function of R_ρ. (The effective eddy diffusivity for salt may drop 2 or 3 orders of magnitude as R_ρ varies from 1 to 2). Thus, any variation of R_ρ in the vertical will be a site for strong flux divergence or convergence that acts to smooth the anomaly in R_ρ because of the difference in the heat and salt transport rates.

Thus, **it** is proposed that active double diffusion in (1) regions where R_ρ < 1.7, (2) on the lateral intrusions at water mass boundaries and (3) where R_ρ varies with depth, all serve to keep the T–S relationship tight and give **it** a pronounced shape (R_ρ = constant) without requiring strong mixing in the interior. This is consistent with recent tracer and microstructure studies which find that the main thermocline is dominated by advection rather than ver-tical mixing.

REFERENCES

Gargett, A. E., 1976. An investigation of the occurrence of oceanic turbu-lence with respect to fine structure. **J. Phys. Oceanogr.**, 6(2), 139-i56.

Gregg, M. C., 1975. Microstructure and intrusions in the California current. **J. Phys. Ocean.**, 5(2), 253-278.

Gregg, M. C. and J. H. McKenzie, 1979. Cross-isopycnal intrusions. Submitted to Nature.

Ingham, M. C., 1966. The salinity extrema of the world ocean. Ph.D. dissertation, Oregon State University, Corvalis, Oregon.

Joyce, T. M., W. Zenk and J. M. Toole, 1978. The anatomy of the Antarctic Polar Front in the Drake Passage. **J. Geophys. Res.**, 83, (c12), 6093-6014.

Magnell, B., 1976. Salt fingers observed in the Mediterranean outflow region (34 N, 11 W) using a towed sensor. Jour. Phys. Oceanogr 6, 511-523.

Schmitt, R. W., 1979a. The growth rate of supercritical salt fingers. Deep-Sea Res., 26(1), 23-40.

Schmitt, R. W., 1979b. Flux measurements on salt fingers at an interface. J. Marine Res., 37(3).

Stern, M. E., 1967. Lateral mixing of water masses. Deep-Sea Res., 14, 747-753.

Williams, A. J., III, 1975. Images of ocean microstructure. Deep-Sea Res., 22, 811-829.

CRITICAL CONTROL THROUGH OCEAN PASSAGES

John A. Whitehead, Jr.

The concept of the effects of rotation upon critical flow in channels of various geometries is reviewed. For many geometries it is found that the upstream height h of the fluid adjusts itself so that $h \approx \left(\rho f Q / g \Delta \rho \right)^{1/2}$ when rotation is important, where f is two times the angular rotation, Q is volumetric flux, ρ is the density, and $\Delta \rho$ is the density difference between the flowing fluid and any still fluid which might lie above it.

Critical control will be discussed in conjunction with two distinct topographic regions in the oceans.

The first, which will be called a sill region, has unidirectional flow from one benthic basin to the next. Features of well known critical flows from sill regions such as the Denmark Strait, Faeroe overflow region, Anagada Jungfern Passage, Strait of Sicily, and Samoan Passage were given. Emphasis was made to recent observations over the Ceara Abyssal Plain (approximately $4^{\circ}N$) where water of Antarctic origin must move northward over an abyssal plain at approximately 4400 meters depth if it is to enter the western North Atlantic. Currents and profiles near the critical point were shown. Evidence will be given that the flows in such sills contribute significantly to the water mass which fills the downstream basin, and that theory allows one to obtain a fairly accurate estimate of the volumetric flux in such sill regions.

The second general type of region in which critical flows occur will be called a strait region. It has a flow and counterflow, and occurs when two large seas are connected by a relatively small passage. The well known examples of the Strait of Gibraltar, other connecting passages to the Mediterranean, and the Red Sea were reviewed. Generally, one basin contains denser water than the other -- dictated by the climate over the individual basins. The

water that flows out of the dense water basin sinks to some level, and forms
an easily identified water mass. Evidence that critical control applies at
the mouth of large gulfs and bays such as Spencer Gulf, South Australia, and
Chesapeake Bay in North America was given. Finally, evidence that one can
estimate volumetric fluxes in straits through critical control principles as
given in Whitehead, Leetmaa and Knox (GFD 6, 101-125, 1974) will be given.

LARGE SCALE STRUCTURE IN THE TURBULENT MIXING LAYER

Fred Browand

Consider the turbulent region formed between parallel streams moving at
different speeds. This mixing zone grows linearly with the downstream distance
(in the mean) and is found to contain large vortex structures aligned with axes
parallel to the axis of the mean vorticity. Initially the structures arise
from an instability which redistributes the mean vorticity into a succession of
vortex cores. What is interesting is that the features persist with increasing
downstream distance, and maintain identity by merging or pairing with neighbor-
ing vortices. The interaction is essentially inviscid and has been observed in
laboratory flows at Reynolds numbers above 10^6, and also in computer (point
vortex) simulations. It appears that this characteristic lumping together of
the vorticity is fundamental to the dynamics of the turbulent mixing layer,
although the view is not universally held. One point of contention concerns
the "degree of two-dimensionality" displayed by these features. Some platform
visualizations show the structure to be remarkably two-dimensional while other
visualizations indicate a progressive deterioration of spanwise coherence.

We are presently investigating the spanwise structure of the large fea-
tures quantitatively by means of hot wire velocity measurements at many points
across the span. Two interesting results have been obtained. First, beyond

an initial development distance, the correlation between two points at fixed spanwise separation actually increases linearly with increasing downstream distance. Since the characteristic scale (thickness) of the mixing layer also increases linearly with downstream distance, the implication is that spanwise structure approaches an asymptotic scale when referenced with the local mixing layer thickness. The establishment of an asymptotic limit is strong evidence for the persistence and importance of these large scale vortex features.

When the structure is "visualized" by observing the instantaneous velocities at all span locations simultaneously, it is possible to conclude that the vortices are very long in spanwise extent -- much longer on average than the width of the wind tunnel. The features are often skewed or contain multiple branches. These effects decrease the time averaged correlation between two spanwise stations, and give an unrealistically low value for the coherence. If the spanwise skewness is not penalized, an estimate of the spanwise length of the features is twenty shear layer thicknesses.

MIXING PROCESSES IN THE SURFACE LAYERS OF ICE COVERED OCEANS

J. D. Smith

In an intermittent manner, considerable heat and momentum is exchanged between a polar atmosphere and the ocean beneath. Two main oceanographic processes control the nature and effectiveness of this transfer. They are (1) brine driven convection under leads and polynya and (2) storm indiced turbulence production in the mixed layer of the ocean. In order to provide a solid foundation for theoretical models of these two processes a series of detailed field experiments was undertaken in various parts of the Beaufort Sea between February 1970 and May 1976. Results from these investigations comprise one of the most comprehensive sets of ocean boundary layer data presently available and provide an opportunity to test various convection and mixed layer models.

Rapid heat loss under extended areas of open water or thin ice produces a brine plume that sinks to the pycnocline then runs out horizonally. This carries the most saline water to the base of the mixed layer and maintains the temperature at this level at the zero pressure freezing point. As a stable stratification is maintained, replenishment of water in the lead is accomplished by selective withdrawal at the base of the ice. The resulting convection cell has a very large aspect ratio, thus mixing due to the down flowing plume is localized and limited. The spreading fluid at the base of the mixed layer and the inflow jet under the ice quickly reach an equilibrium thickness governed by the critical Richardson number. This leaves the interior of the mixed layer away from the open water unaffected except for the slow vertical motion imparted to it. In leads, rapid brine production usually ceases before rotational effects need to be considered; however, a weak lateral density gradient persists for a substantially longer period of time inducing weak baroclinic flows. These are clearly seen in the available data.

Both the stable stratification and the baroclinic pressure gradients affect the velocity and stress fields that arise during storms. However, the observed response of the Beaufort Sea is not slab-like in character and the simple eddy viscosity model of Long and Smith (1979) gives good agreement with measured velocity, stress and eddy coefficient profiles. For the stably stratified case this model employs a nondimensional eddy coefficient of the form $\xi e^{-\xi}(1-\beta R_f)$ where ξ is the nondimensional vertical coordinate, β is a coefficient found in atmospheric boundary layer experiments to have a value of 4.7 and R_f is the local flux Richardson number, obtained from a measured or calculated density profile. The ratio of mass to momentum diffusion coefficients is as measured in the atmospheric surface layer multiplied by the nondimensional stress profile. Long and Smith show that a time independent

eddy coefficient is not only justified but preferable for an unsteady flow of infinite depth thus, their approach is sufficiently accurate for a zero order model of ice covered mixed layer response to a storm induced surface stress field.

In order to obtain the complete response of a mixed layer to the passage of a storm, the forced internal wave field driven by both surface stress and surface pressure must be calculated. Morison and Smith (unpublished) have done this and shown that such calculations accurately predict the response of the Arctic mixed layer to a small storm only when the buoyant convection in-duced pressure field, associated with the lead pattern, is included in them. In this case the lead related pressure field accounted for over 50% of the ob-served pycnocline depression.

A CLIMATE OSCILLATOR INVOLVING SEA ICE EXTENT

Barry Saltzman and Richard Moritz

An idealized, time and latitude dependent, nonlinear, basically thermo-dynamic model is developed for an equinoctial, all-ocean planet to illustrate the possible roles of a number of positive and negative feedbacks that are present in the earth's climatic system. The mean atmospheric properties (e.g., temperature and cloud cover) and the sea-surface temperature are treated as fast response parts of the total system that are coherent with the sea ice extent measured by the sine of the ice edge latitude, η . The mean depth- and latitude-average ocean temperature, $@$, is the other prognostic variable that can vary along with η over long time periods.

The model is based on a set of parameterizations for all the modes of heat transfer across the top of the sea water, some of which represent con-

siderable improvements over those incorporated in previous statistical dynami-
cal climate models. In particular, the sensible heat flux now includes the
'rectifier' effects associated with synoptic air mass exchanges that arise as
a consequence of the baroclinicity of the atmosphere. This introduces a strong
positive feedback leading to instability of the system, that can be viewed as
the physical manifestation of the more familiar "ice–albedo" feedback. Another
positive feedback included is due to longwave emissivity changes associated
with CO_2 changes that, in turn, are postulated to arise in response to the
variations of mean ocean temperature θ . Among the negative feedbacks is one
due to the insulating effect of sea ice on θ (which, in turn, influences the
ice edge extent through an upward subsurface heat flux at the ice edge), and
another due to the changes of the amount and path length of solar radiation at
the ice edge.

The model is expressed mathematically as a coupled autonomous polynomial
system of 6th degree governing the two state variables η and θ . Analyses
are made of the equilibria, sensitivity of the equilibria to changes in all the
parameters, linear stability and structural stability of the equilibrium paths
for changes in selected parameters of special interest (e.g., the solar cons-
t^{a}nt and CO_2 level) constituting climatic prediction of the "second kind".
Finally, some phase plane portraits for specified values of parameters are
presented showing the evolution of the system from arbitrary initial conditions
(prediction of the "first kind") and illustrating the time dependent properties
of the system. For one reasonable set of parameters, damped oscillations of a
period on the order of a thousand years are obtained, while for other possible
parameter values unstable behavior is manifest. Because of the instabilities
for large departures from equilibrium, this system cannot exhibit stable limit
cycles (i.e., auto–oscillatory behavior), but realistic modifications are sug-
sted that offer the possibilities of such behavior.

COUPLED AIR-WATER LOOPS

Pierre Welander

A single fluid loop consisting of two well-mixed reservoirs connected by two horizontal tubes, differentially heated and also subjected to a given stress, exhibits multiple steady states in the case the buoyancy torque opposes the given stress, as shown by H. Stommel and Claes Rooth, 1968. It always reaches a stable steady state when inertial effects are excluded.

It is of interest to learn if self-sustained oscillations can occur when the stress is not prescribed but determined by a second (air) loop, which has heat and momentum exchange with the first. Two cases are considered and depicted below. The symbol —— means heat transfer by a conduction law, ⇒ means a stress proportional to a velocity difference. In the case a) oscillations occur when the stress is larger than the buoyancy effect flow opposite to the buoyancy torque in the steady state. In the case b) the fluid system is heated from the top and cooled from the bottom; still it is convectively unstable.

In the case shown, the system oscillates, if the air loop is twisted to reverse the direction of the stress, steady convection results (the direction decided by an initial disturbance). The reader has to figure this one out himself. Remember that the fluid has low thermal expansion, the gas high thermal expansion (= large velocity and large stress action from small temperature effects). The equations describing the systems are simple, nonlinear ordinary equations which can be discussed by phase-plane methods. Examples of oscillations were calculated using an HP 97.

REFERENCE

Stommel, Henry and Claes Rooth, 1968. On the interaction of gravitational and dynamic forcing in simple circulation models. Deep-Sea Res. 15(2): 165-170.
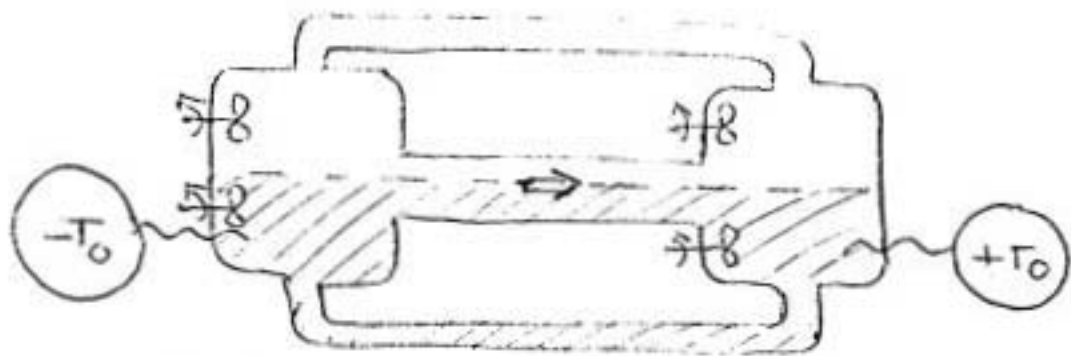
CASE a)
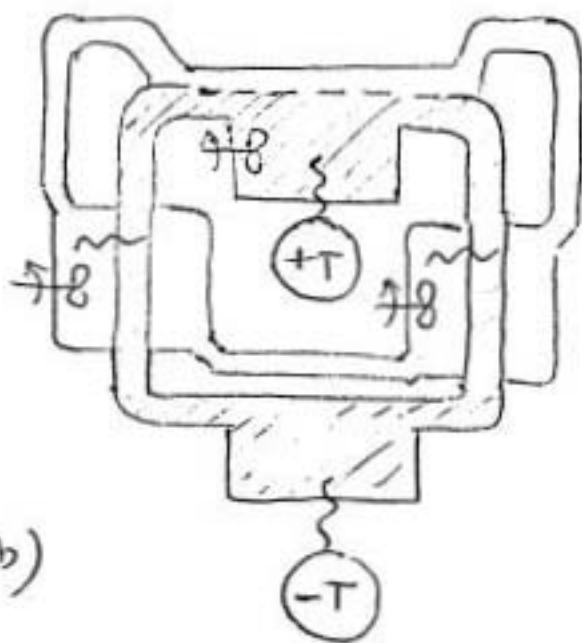
CASE b)

THE ASYMMETRIC SOUTHERN OCEAN

Arnold L. Gordon

Two types of zonally averaged meridional circulation patterns are proposed. There is a Deacon advective model in which southward and upward advection of the relatively warm-saline circumpolar deep water mass supplies heat and salinity to balance sea air heat and water flux. The deep water is converted into Antarctic Surface Water and Continental Shelf Water, which contributes to northward and downward motion of water across the polar front and at the continental slope. Another model is based on isopycnal mixing. The shallowing of isopycnals on approach to Antarctica, allows cold-low salinity Antarctic Surface and Slope Water to be exchanged isopycnally with relatively warm-saline northern waters. In this way, the thermohaline altered water near the sea surface may influence the entire water column rather than only the Antarctic Intermediate Bottom Water masses.

While patterns of the average meridional exchange patterns are important to study, we should not lose sight of the asymmetric nature of the Southern Ocean. The asymmetry begins with Antarctica itself, which is significantly shifted into the eastern hemisphere. The coast line of East Antarctica lies close to the Antarctic circle. About *15%* of the glacial ice cap is floating above sea water; these ice shelves comprise about *45%* of the coast line. The ice shelves offer a unique situation in that the sea water - glacial ice contact occurs at many hundreds of meters where the in situ freezing point is a few tenths of degrees below the freezing point at the sea surface. Hence, the ice shelves offer an opportunity to depress ocean temperatures below the sea surface freezing point. This influence has been observed adjacent to the ice shelves of the Weddell and Ross Seas.

The characteristic of the continental shelf water has important variations with longitude. In many sections the shelf water is dense (salty) enough to allow for deep continental slope convection and Antarctic Bottom Water formation. The most saline shelf water occurs in the Ross Sea, which also acts as the source of the most saline variety of Bottom Water. It is interesting to point out, however, that while saline slope plumes are observed in the western Ross Sea, low saline slope plumes are found in the eastern Ross Sea. The coldest variety of Antarctic Bottom Water found off the eastern coast of the Antarctic Peninsula is supplied from the southwestern Weddell Sea, though contributions from the east coast of the peninsula, even at its northern tip, is expected.

The wind field over the Southern Ocean is predominately from west to east, with a maximum near $50^{o}S$. Only in the regions of the Antarctica continental margins do easterly winds dominate.

The wind field induces a northward directed Ekman drift in the ocean surface layer. The Ekman drift is divergent between Antarctica and the maximum westerlies. The divergence results in significant upwelling velocities, up to 2.5 x 10^{-4} cm/sec near $60^{o}S$. The Ekman drift is most intense in the eastern hemisphere. Possibly the northern position of Antarctica on the eastern hemisphere intensifies the gradients in the thermal wind and the ocean.

The Southern Ocean sea ice undergoes very large seasonal variations, amounting to nearly 20 x $10^{6}Km^{2}$. The greatest degree of seasonality occurs in the western hemisphere, notably the Weddell Sea region. Sea ice is important to the sea air heat flux, due to the insulating effect of sea ice, and to the salinity budget, since sea ice salinity amounts to only 20% of the ocean water salinity. For each meter of sea ice formation 3 grams of salt is injected into the remaining sea water.

The seasonality of the Southern Ocean sea ice may be a wind effect or a cross pycnocline heat flux effect. The wind effect is associated with the generation of leads (breaks in the sea ice cover with scales of kilometers) which fill with new ice in winter, but which act as heat collectors (due to low albedo) in the summer period.

The cross pycnocline heat flux would be most important near the end of winter when the surface water is densest and the pycnocline weakest. The introduction of deep water heat into the surface layer removes the ice, accounting for the widespread waning of the winter ice cover.

The Polar Front Zone separating the Antarctic from Subantarctic zones, varies its latitudinal position with longitude. In the Atlantic Ocean it is near $50^o S$, but drops to near $60^o S$ in sections of the Pacific Ocean. In addition to these spatial variations, important transient shifts occurs as meanders and spin off eddies in the Polar Front Zone.

The Polar Front Zone (PFZ) is found in close proximity to the axis of the Antarctic Circumpolar Current (ACC); both the PFZ and ACC occur near the maximum westerly wind. The ACC is not composed of a simple well defined circumpolar jet; rather, it is composed of two or more axes of flow in some areas, broad diffuse drift in other areas. The ACC is well defined in the Indian Ocean, over the northern side of the mid-ocean ridge south of Australia, and near $145^o W$ at a Fracture Zone. The diffuse current of the Southeast Pacific Basin becomes a well defined axis in the Drake Passage and western Scotia Sea before a major northward ACC shift, amounting to 600 - 1000 km, takes place as the ACC enters the Argentine Basin. Important bifurcation occurs south of New Zealand as a well defined axis of flow follows the edge of the Campbell Plateau while another continues to follow the northern side of the mid ocean ridge.

The geostrophic ACC flow relative to the sea floor attains values of 130–180 x 10^6 m^3/sec. Often counter flows are found near the ACC axis. These may be manifestations of mesoscale eddies.

Coastal flow is directed to the west. Measurement is mostly confined to iceberg and ice locked ship drift. Northward deflection of the coastal flow into the general ACC drift occurs to the east of Antarctic Peninsula and over the eastern side of the submarine Kerguelan Plateau.

The deep water is advected eastward with the ACC. The warm–saline signal of the deep water is attenuated on eastward path from the Atlantic Ocean. The attenuation, induced by introductin of cold, relatively low salinity water from the surface and slope water to the south, is offset by the input of North Atlantic deep water.

The deep water signal is also attenuated as Antarctic is approached. Only remnants reach the continental margins; these remnants apparently supply the salt which initiates the convection associated with Antarctic Bottom Water formation.

At depths above the salinity maximum level of the deep water in the Atlantic Ocean sector of the Southern Ocean is a thick 2^oC layer. This 2^oC thermostad may be produced in the Argentine Basin where the Pacific Water may mix with the upper components of North Atlantic deep water. The 2^oC thermostad is advected eastward, where traces can be seen in the Pacific Ocean. The base is often marked by an abrupt gradient change in the vertical temperature profile. The cause of this abrupt gradient change is not clear.

MEDITERRANEAN DEEP WATER FORMATION BAROCLINIC
INSTABILITY AND OCEANIC EDDIES

J. C. Gascard

Since 1969 in studying formation of deep water in the North Western

Mediterranean Sea in winter, we discovered frequent cyclonic and anticyclonic

eddies genesis associated with processes of deep water formation. We are now

presenting such typical eddies observed in February-March 1975, during the

Medoc 75 cruise (Medoc area: $3^o30'E-6^oE$, and 41^oN-43^oN). Vertical

speed has also been measured in this area. Since several orders of magnitude

appear from these measurements, it may be supposed that several dynamical

processes are present in deep water formation. We will show that baroclinic

instability, which is one of these processes, is responsible for that part of

the slow (1 $mm.s^{-1}$) and aperiodic vertical motions, and corresponds to

meanders, eddies and fronts on the horizontal plane. Considering the

observations which allow us to use a quasi-geostrophic approximation, we will

propose a baroclinic instability model in order to explain the features of

these three-dimensional motions. We will evaluate the importance of the mixing

induced by this mechanism in the process of deep water formation between sur-

face and subsurface waters under the meteorological forcing.

MAINTENANCE OF ARCTIC T-S STRUCTURE AND ROLE OF SHELVES

Knut Aagaard

The classic water mass classification for the Arctic Ocean is surface,

Atlantic, and Bottom Water. A different taxonomy proves useful, one based on

the role of the various layers as transfer or reservoir fluids.

The polar mixed layer (PML) is a thin (50 m or less) layer of enhanced

vertical fluxes of buoyancy and momentum. Its overall importance lies in its

cumulative effect on the heat, mass, and momentum budgets of the Arctic Ocean.

Key questions relate to the dynamics of convective mixing.

The pynocline is a region of reduced vertical fluxes some 3-4 times the thickness of the PML. Its stability is due to a strong salinity gradient. It is, in effect, an insulating lid of reduced permeability.

The Atlantic Water (AW) is a very large reservoir of sensible heat and salt maintained by advection from the Norwegian Sea. It is isolated from effective atmospheric interaction by the pycnocline.

The role of the nearly homogeneous deep water, its circulation, and its residence time are essentially unknown. Presumably it is to some extent a heat sink for the AW.

An additional important factor in the maintenance of the PML is the cycling of fresh water. Total runoff into the Arctic Ocean is about 0.1 Sv, with an additional 0.05 Sv entering through Bering Strait as a salt deficit. The maximum input from precipitation less evaporation is 0.02 Sv. An overall fresh water residence time for the Polar Basin is about 10 years. The runoff is highly seasonal, producing local effects, but there are also variations with time scales comparable to regional residence times. The fresh water is important both to the growth and the decay of the ice cover, and there are several different kinds of feedback loops. Seasonally, the fractionation of fresh water by freezing and melting ice, cycles fresh water at a very large rate, of order 1 Sv. As the characteristic vertical mixing lengths of the freezing and melting processes differs, it is conceivable that the stratification can be maintained by these processes alone.

The advective input of AW is highly variable in both mass and heat flux on very long time scales (of order 50% year-to-year and much greater for a few months or less). Very large temperature and salt gradients, nearly compensating each other in density, have been observed in winter in a region of active

convection north of Spitsbergen, where the AW enters the Arctic Ocean, suggesting possible double-diffusive effects. The core of the AW appears bathymetrically steered during its subsequent transformation within the basin. The core transformation is nearly density-preserving, and the larger portion of the temperature and salinity changes occur relatively soon after the entry of the AW into the Polar Basin.

The T–S structure of the pycnocline points to advective renewal of about a 100 m-thick layer below the PML, by water conditioned by the freezing process; certain shelves are the indicated sources. Various considerations indicate a renewal rate of 2–3 Sv, the feed water being relatively salty (S > 34 o/oo) and near the freezing point. One mechanism by which such water may be formed is brine enrichment through ice formation on certain shelves, notably the Bering–Chukchi and the Barents–Kara. The mechanical removal of ice near boundaries, which allows large ice formation rates, appears to be an important factor in these considerations.

A second mechanism by which the cold, saline pycnocline feed water may be produced is the upwelling of saline water onto the shelves, subsequently to be cooled. Observational evidence of such events exists for the Kara, the Chukchi, and the southwestern Beaufort.

<u>Summary</u>

The classic water mass classification for the Arctic Ocean is surface, Atlantic, and Bottom Water. A different taxonomy proves useful, one based on the role of the various layers as transfer or reservoir fluids.

The polar mixed layer (PML) is a thin (50 m or less) layer of enhanced vertical fluxes of buoyancy and momentum. Its overall importance lies in its cumulative effect on the heat, mass, and momentum budgets of the Arctic Ocean. Key questions relate to the dynamics of convective mixing.

EDDIES IN THE ARCTIC OCEAN

Kenneth Hunkins

Observations in the Beaufort Sea (western Arctic Ocean) show a mean clockwise gyre with a diameter of about 2000 km and surface speeds of less than 5 cm/s. These mean speeds are geostrophic, based on hydrographic casts, and decrease with depth. During the Arctic Ice Dynamics Joint Experiment (AIDJEX) in 1972 and again in 1975-76, observations with current meters showed
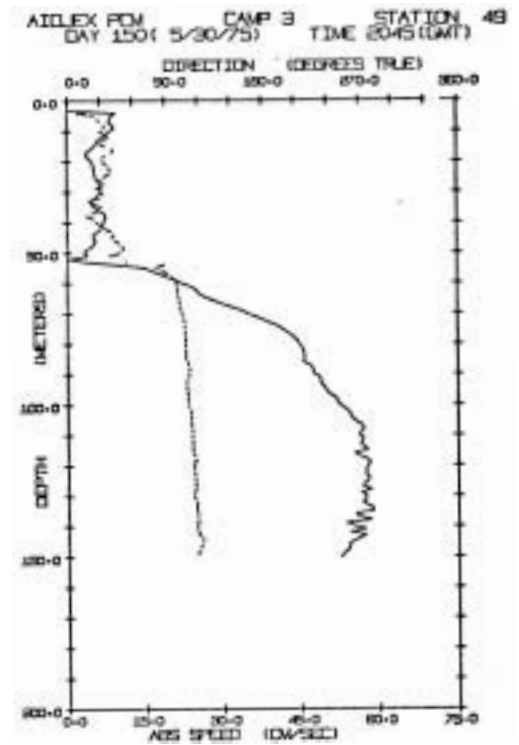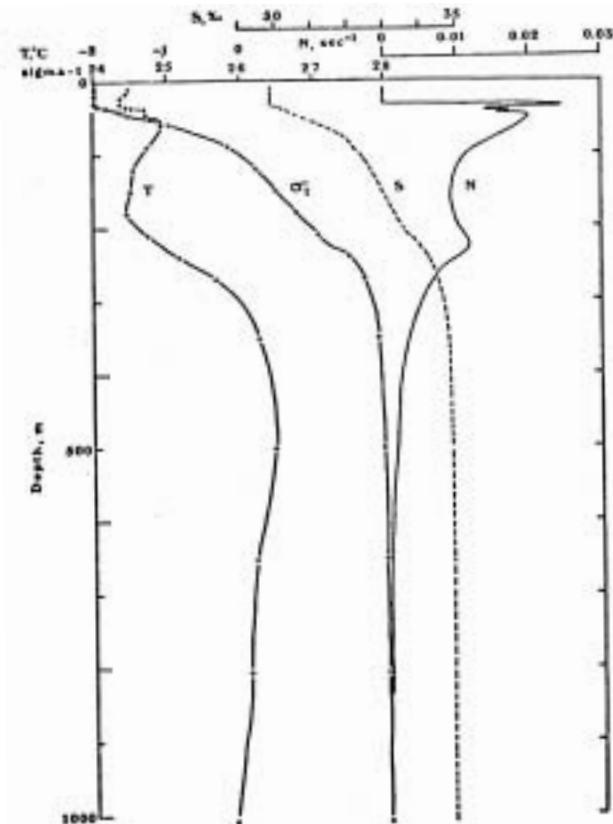
AIDJEX 75–76 CAMP SNOWBIRD

CURRENT VECTORS
130 m
50 cm/sec

DRIFT TRACK

SALINITY SURFACES, ppt

30.5
31.5
32.0
32.5

33.0

33.5

34.0

34.5

0   5   10
km

DEPTH, m
0
80
160
240
320
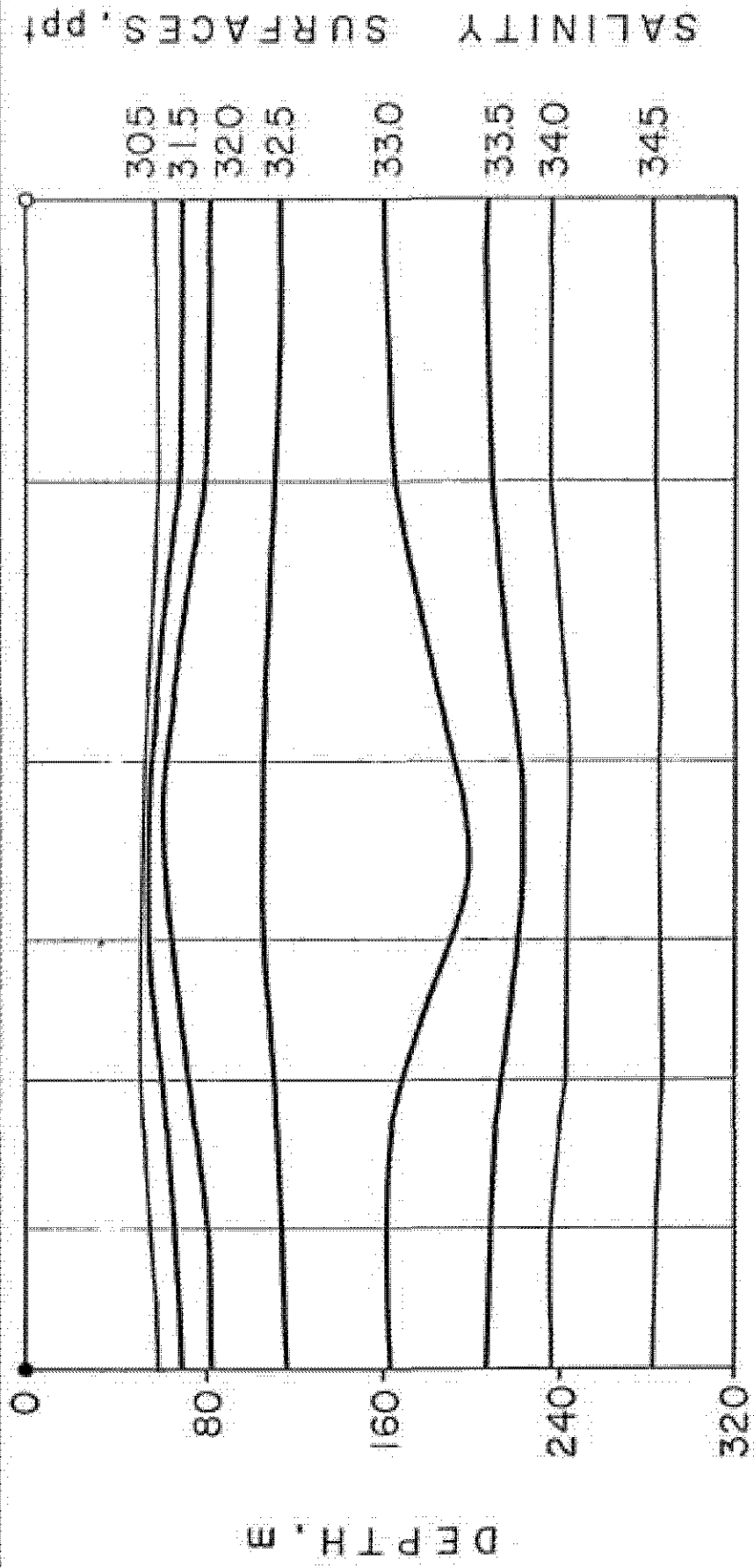
that swift transient undercurrents are superimposed on this slow mean flow (Hunkins, 1974; Newton et al., 1974). These undercurrents are **mesoscale** eddies with diameters of 10 to 20 km and maximum speeds of up to 60 **cm/s** at depths of 100 to 150 **m.** The pycnocline extends from the base of the mixed layer at 50 m to the top of the nearly isohaline deep layer at 400 m **(Fig. 1). It** is the region in which the flow in these eddies is concentrated as illustrated in (Fig. 2) where current speeds are represented by a solid line and directions by a dashed line. These eddies appear to be decoupled from the wind drift of the ice and of the water in the surface mixed layer. Th eddies translate slowly, probably being advected by the mean current. On occasion, the wind-driven ice moves over an eddy, giving a cross-section as current and hydro-graphic profiles are taken from the ice. An example is shown in Fig. **3.**

In 1975-76, STD profiles to 750 **m** and current profiles to 200 m were taken on a daily basis from an array of four drifting ice camps in the **Beaufort** Sea with horizontal spacing of about 100 km. A total of 55 eddies was observed from these camps over the course of one year. A predominant number of these, 53, showed clockwise rotation with a lens-shaped displacement of the isopycnal surfaces. Note that isohaline surfaces mirror isopycnal surfaces in the Arctic Ocean. Above the level of maximum velocity, the surfaces are displaced upward while below the maximum-speed level the surfaces are displaced downward. Surfaces are nearly level again at the base of the mixed layer and for levels below about 400 **m.** These features were encountered both in summer and winter. No clear correlation was seen between wind or pack ice movement and these eddies. The T-S characteristics of water within the eddies differs from the local water masses and suggests a source in Alaskan shelf waters.

Within the water column in this part of the Arctic Ocean, kinetic energy was found to reside in the fluctuating or eddy motions. An averaged kinetic energy profile based on one year of data from all four camps shows a maximum of 60 ergs/cm^3 at 110 m depth which is associated with the subsurface eddies. There is a secondary maximum of 45 ergs/cm^3 at the top of the water column just below the ice which is associated with the wind and ice driven currents. The kinetic energy contributed by the mean flow is only a few percent of the total.

There are a number of possible origins for these features including wind-generated Ekman divergence, freezing processes in leads and baroclinic instability. Of these baroclinic instability seems to be the most attractive. A general survey of baroclinic instability theory is given by Kuo (1973). It could occur either locally in the central Arctic Ocean where the eddies were found or in another distant region. The T-S characteristics suggest a distant origin.

An analytical baroclinic instability model was formulated with both mean shear and mean stability varying exponentially with depth, somewhat resembling actual Arctic Ocean conditions. The growth rate and wavelengths of small perturbations were examined for this generalized Eady-type model. Ekman pumping boundary conditions were introduced for a rigid bottom and for both rigid and free upper surfaces. No growth was found in the central Arctic Ocean in the observation. However, in the region north of Point Barrow, Alaska, there is sufficient shear near the shelf break under summer open-ocean conditions for small disturbances to grow, increasing by a factor of e every 28 days. The half wavelength of this fastest-growing wave is 64 km, somewhat larger than the observed eddy size.

Although this theory predicts maximum growth at the surface, the actual eddies have their swiftest currents at depth. It is possible that the eddies generated by the process outlined above in ice-free waters are advected north-ward under the ice by mean currents. There frictional dissipation against the ice would lead to a decrease in velocity near the surface. This effect is demonstrated with a calculation for the diffusion of vorticity against the ice. The initial vorticity profile decreases exponentially with depth, resem-bling the profiles of the growing waves resulting from the baroclinic insta-bility calculations. As the vorticity is dissipated, a subsurface maximum develops which stimulates the observed current profiles. The theory predicts that a period of time between 1 and 6 months would be required for the eddies to develop their observed current profile after being carried under an ice cover.

REFERENCES

Hunkins, K., 1974. Subsurface eddies in the Arctic Ocean. Deep-Sea Res., 21, 1017-1033.

Kuo, H. L., 1973. Dynamics of quasigeostrophic flows and instability theory in: Adv. in Appl. Math., 13, ed. by C. S. Yih, 257-330. Acad. Press, New York.

Newton, J. L., K. Aagaard and L. Coachman, 1974. Baroclinic eddies in the Arctic Ocean. Deep-Sea Res., 21, 707-719.

ROTATING ANNULUS CONVECTION AND F-PLANE THERMOCLINES

Peter D. Killworth

The archetypal thermally driven ocean circulation problem, studied experimentally by Rossby, is discussed in both nonrotating and rotating regimes. The configuration consists of a rectangular box (or an annulus with rectangular cross-section) which has insulating top and sides, and is heated and cooled along its lower surface. It is found experimentally that all the heat exchange of the fluid with this lower boundary takes place in a thin

boundary layer, the flow in which was directed toward the hotter end of the cell. There it rises against the wall, flows along the upper surface in a thicker layer and returns in a broad interior region toward the lower boundary. The interior, in the nonrotating regime, is quiescent and homogeneous, with a temperature excess about 70% of the maximum temperature difference imposed at the bottom.

Analysis (with P. C. Manins) reveals that the thin thermocline-like layer is really two layers when the Prandtl number σ is large. The thinner, buoyancy layer, has thickness L $Ra^{-1/5}$; the fluid is homogeneous, and viscous and nonlinear terms balance in the vorticity equation.

The solution does not depend on the details of the sidewall boundary layers, although in general remaining highly nonlinear. A similarity solution is employed to yield specific solutions; the interior temperature and Nusselt number (a measure of heat transport) depend only weakly on Prandtl number but are strong functions of Rayleigh number.

The problem is extended to rotating annuli (with P. H. Hignett). Six different regimes occur, depending on the magnitude of a quantity Q (= $Ra^{-2/5}E^{-1}$), where E is the Ekman number. Q can be thought of as a linear measure of rotation rate. The similarity solution may be extended to this case, and comparison made with the experimental results of Hignett. Only one major discrepancy exists: the observations show the Nusselt number initially increasing with (weak) rotation, whereas theory predicts a decrease. This anomaly is currently under investigation.

BAROCLINIC INSTABILITY AND HEAT, SALT AND BUOYANCY
FLUX IN THE DRAKE PASSAGE

Roland A. deSzoeke

The "footprints" of baroclinically unstable eddies were reviewed: (1) the spatial scale, namely, the baroclinic Rossby radius of deformation; (2) the instability of the basic potential vorticity distribution vis-a-vis the Rayleigh-Charney-Stern criterion; (3) the downgradient buoyancy flux necessary for available potential energy conversion; (4) the retrograde phase lag (relative to the direction of shear) in the vertical of the fluctuating velocity.

The implications of directly-measured eddy heat flux $\overline{v'T'}$ in Drake Passage were discussed. Eddy salt flux is inferred from the consistency of the T-S relationship. The contribution of this inferred eddy salt flux to total buoyancy flux is 6 to 8 times that of the eddy heat flux above the Circumpolar Deep Water salinity maximum and is down-gradient.

The inferred eddy salt flux below the salinity maximum is small but countergradient. A "caricatured" model of the thermocline structure in the Drake Passage made to resemble the Eady model was discussed. The thermohaline structure implies a convergence of heat (lost to the atmosphere?) in the neighborhood of the Polar Front.

A model of the basic potential vorticity structure in the Drake Passage was proposed. The internal p.v. gradient is modelled as concentrated in an interface. A new kind of instability emerges at higher wave-number than the Eady instability representing a vorticity interaction between the concentrated p.v. gradient interface and the bottom. The implications of the model to buoyancy flux distribution were discussed.

THE OCEANIC T–S CURVE RELATED TO
GLOBAL HEAT AND WATER TRANSPORT

Henry M. Stommel

From historical data on the distribution of temperature and salinity on vertical sections across the oceans over complete latitude circles it is possible to test the compatibility of certain meteorologically determined meridional fluxes in the ocean of sensible heat and fresh water, as functions of latitude. It is also possible to check the proportion of this flux that each ocean basin carries separately.

The information from both these sources leads to estimates of the magnitudes and distribution of the meridional oceanic mass flux over the salinity-temperature plane, and yields some indication of the probably physical processes operating (e.g. isopycnal mixing vs. large–scale advective currents).

NORTHERN CONTRIBUTIONS TO THE DEEP CIRCULATION

Knut Aagaard

The only water mass of northern hemisphere origin which lies within the 50% frequency limit on the volumetric T–S ,diagram of the world ocean is the North Atlantic Deep Water (NADW). The deep water of the Arctic Ocean and the Greenland–Norwegian Sea appears as a tertiary mode isolated both in T–S space and in frequency space. There is no deep–reaching ventilation on the Pacific side, as convection in the Bering Sea does not extend below 150–200 m.

Following Lee and Ellett (1967) the NADW appears to be formed by a mixture of Northeast Atlantic Deep Water (NEADW) and Northwest Atlantic Bottom Water (NWABW). The former is derived from overflow of the Iceland–Scotland Ridge by Norwegian Sea Deep Water (NSDW) and the latter from overflow through Denmark Strait.

About 2.5 Sv NSDW pours over the Iceland–Scotland Ridge and another 2.5 Sv of somewhat warmer and slightly less saline water flows out through Denmark Strait.

Deep water is not formed in the Norwegian Sea, but is probably instead supplied from the Greenland Sea. The NSDW is slightly saltier and warmer than the Greenland Sea deep water; its residence time is probably in the vicinity of 100 years.

Deep water is formed in the Greenland Sea at an apparent rate of about 3 Sv. Its turnover time is a few decades. The earlier ideas of a large–scale deep–reaching overturn in the central Greenland Sea do not appear to be applic–able. Alternate explanations have been sought to double–diffusive mechanisms and in small preconditioned chimneys generated by a baroclinic instability.

Essentially nothing is known about the ventilation of the Polar Basin. Local convection is confined to a thin upper layer, and the basin is probably primarily supplied from the NSDW reservoir to the south.

An Intermediate Water mass is formed in the Iceland Sea during winter. Surface cooling produces a low–temperature layer which subsequently mixes with water of Atlantic origin found at intermediate depths. It is this mixture which forms the principal dense component of the Denmark Strait overflow; its characteristics are a typical salinity of 34.8 o/oo and recent tritium values of 4–5 TU. The formation rate is probably over 30,000 km^3 per year, giving a residence time of about two years.

Downstream from the sill, the Denmark Strait overflow is composed of a strong mean flow of about 1 knot, upon which are superimposed various low–frequency variations. The mean flow is driven from an upstream reservoir of apparently nearly constant density and pressure head. This flow is baroclinic

and increases with depth; it is directed nearly along the isobaths. Frictional effects are apparent at least 25 m from the bottom. Modulations of the mean flow on time scales of weeks to months are random and do not exceed about 20%; there is, for example, no seasonal modulation. By far, the largest of the low-frequency variations is a persistent signal with a time scale of 1.5 - 2.5 days and amplitude comparable to the mean flow, probably representing a baroclinic instability. The statistics of this band are non-stationary.

BAROCLINIC INSTABILITY IN DRAKE PASSAGE

Harry Bryden

Predictions of baroclinic instability theory are compared with observations of current and temperature in the Antarctic Circumpolar Current in Drake Passage. Observed vertical profiles of current shear and Brunt Väisälä frequency satisfy the necessary condition for instability because of the presence of current shear at the bottom boundary which has the same sign as the meridional gradient of potential vorticity in the interior water column. Poleward eddy heat flux, which is directed down the mean horizontal temperature gradient, is observed for all current and temperature records and provides the predicted conversion of available potential energy into eddy kinetic and potential energies. Vertical phase lags such that deeper events lead shallower events, which have been proposed as signatures of the instability process, are observed for velocity components but not generally for temperature. Finally, the observed frequency, phase speed (and hence horizontal wave number) and derived critical level for observed eddies are in good agreement with those predicted by infinitesimal amplitude instability theory.

MERIDIONAL HEAT FLUX IN THE SOUTHERN OCEAN

ARNOLD L. GORDON

The Ekman divergence south of the Polar Front Zone induces upwelling of about 40 Sv into the surface Ekman layer. In the southern half of the Antarctic zone the pycnocline is shallow and may be considered to form the base of the Ekman layer. In a steady state situation, the mean Ekman upwelling of the pycnocline of 1.2 x 10^{-4} cm/sec, would introduce about 11 kcal/cm^2/yr into the surface layer, which would be subsequently lost to the atmosphere. This provides an estimate of sea–air heat flux. An independent estimate may be made using radiation 'balance and bulk aerodynamic equations. Values of total sea-air heat flux for the zone 60°- 70°S for ice free, complete ice cover and realistic ice cover concentrations are provided in Table I. An average annual value of sea to air heat flux of 27 kcal/cm^2/yr for the 60° - 70°S is suggested.

The influence of sea ice cover to the attenuation of sea–air heat flux is very apparent. Uncertainty in ice cover extent and concentration are very important factors in introducing uncertainty in heat flux.

At 60°S estimate of sea air heat flux for ice free and complete sea ice cover have been made by Fletcher (1969). Using realistic values of ice cover concentrations, an average annual sea to air heat flux of 6.4 kcal/cm^2/yr for 60°S is determined. Between the polar front zone (average position of 53°S) and 60°S the heat flux is into the ocean at a rate of 10 kcal/cm^2/yr, while just north of the front an equal heat flux into the atmosphere is determined (Zillman, 1972, for the area South of Australia and Bunker p.c. for the South Atlantic).

The anomaly to the large scale latitude pattern of sea–air heat flux is the oceanic heat loss north of the front. This may be a product of the high sensible and latent heat flux occurring during cold air outbreaks, across the polar front, over the relatively warm Subantarctic Surface Water.

TABLE I. Total Sea–air Heat Flux $60°-70°S$, Q_T

(Values in cal/cm^2. day, positive indicates

atmosphere to ocean heat transfer)

	A	B	C*	D**
Month	No-Ice	100% Ice Cover	Realistic Ice–Ocean Ratio	Same as c but with 30% Leads
Jan	+177	+64	+132	+145
Feb	+ 66	+18	+ 56	+ 59
Mar	−128	−26	−108	−114
Apr	−201	−46	−139	−158
May	−329	−56	−193	−233
Jun	−449	−54	−212	−283
Jul	−452	−54	−173	−257
Aug	−377	−34	−120	−195
Sep	−297	−21	− 76	−142
Oct	−130	− 20	− 53	− 76
Nov	− 84	−12	− 41	− 54
Dec	+ 55	+15	+ 35	+ 41
Average	−179	−19	−74	−106 $cal/cm^2 day$
	− 65	−6.9	−27	− 39 $kcal/cm^2 yr$

NOTES: $Q_T = (Q_s + Q_b) + Q_E + Q_h$

= Radiation balance + evaporation + sensible heat loss

Q_s from Sasamori et al., 1972. An albedo of 4 is used for the direct beam and 6.6% for the indirect short wave radiation.

wind speed: 5 m/sec

relative humidity 85%

50% middle cloud cover

T^oC sea: -2^oC May - November

             0^oC May, October - November

             $+2^oC$ January - March

T^oC air: -13^oC June - September

             -8^oC May, October - November

             -5^oC April, December

             -3^oC March

             $+1^oC$ January - February

* Estimate of percent ice cover taken from ice charts.

** Percentage of leads varies greatly; 30% may be upper limit. The Weddell Polynya not explicitly included in these calculations.

Table II gives the total average annual sea-air heat flux south of the polar front and south of 60^OS which represents the area covered at least for some time by sea ice. The area south of the polar front, but north of the sea ice field, does not extract oceanic heat; the total heat loss is south of 60^OS.

The meridional exchange of heat must satisfy the sea-air heat flux. The two patterns of meridional exchange are the advective model and the isopycnal spreading model (discussed in A. Gordon's previous lecture). In addition, a simple lateral turbulent heat flux model can be presented in which K_y dT across 40° - 60^OS (where sea-air heat flux averages near zero) of the water column above the crest of the mid-ocean ridge near 2.5 km transfers the necessary heat flux.

A K_y of 2 x 10^7 cm^2/sec* is determined (using a mean temperature difference between 400 - 60^OS for the upper 2.5 km of $3^O C$). If the term "lateral" is taken as isopycnal the meridional gradient is much reduced (close to $1^O C$) requiring a K_y value of 6 x 10^7 cm^2/sec. These values are in the "acceptable" range.

Should the Deacon advective model be accepted, it is possible to calculate the amount of deep water required to supply the necessary heat into the surface water south of the polar front zone (a value of 32 Sv is suggested; also see Gordon, 1975), with about half going into cross polar front flux of surface water and the other half going into Antarctic bottom water. The deep water heat is derived mainly from downward heat flux across the main thermocline of the world ocean.

---

*In the lecture a K_y value of 10^{10} cm^2/sec was presented. The correct value given above agrees with the value determined by Bryden and Joyce (personal communication) for the Drake Passage meridional temperature gradients.

TABLE II. Net Sea-Air Heat Flux
(Positive Values Represent Heat from Atmosphere to Ocean)

Zone	Latitude	Area $10^6 km^2$	Q_T kcal/cm^2/yr
Sea Ice Zone	60°-70°S	16	-27 (Table I, Calculations)
Northern Ice Fringe	60°S	--	-6.4 (Fletcher, 1969)
South of PFZ	53°-60°S	20	+10 (Zillman, 1972; Bunker, p.c.)
North of PFZ	45°-53°S		-15 (Zillman, 1972; Bunker, p.c.)

SUMMARY OF TOTAL HEAT FLUX:

1. South of Polar Front Zone: -7.4×10^{13} cal/sec

2. South of 60°S: -13.0×10^{13}

South of 60°S with 30% less ice: -20×10^{13} cal/sec

(a nearly 50% increase in ocean heat loss).

Attenuation of the warm-saline North Atlantic Deep water with increasing eastward distance from the Atlantic Ocean along the polar front and as Antarctica is approached along nearly all longitudes suggests the advective model cannot be completely correct; meridional diffusion has some impact.

An interesting and possibly important aspect of sea-air heat flux is the large (.5 to $.8 \times 10^6$ Km^2) ice free region which occurs in some winter near the Greenwich meridian and 66°S: the Weddell Polynya.

It is unreasonable to consider the polynya as solely a wind induced feature, since the wind could not remove newly formed ice fast enough to keep a 0.5 to 0.8×10^6 Km^2 area ice free. Upward Flux of deep water heat (the deep water is nearly 2.5°C above freezing) is required. A pycnocline characteristic value of K_z of 20 cm^2/sec is needed to match the winter sea-air heat flux for ice free condition. However, the associated salt flux is

strongly destabilizing and convection would quickly ensue. Salt flux would be greatly reduced if the cross pycnocline heat transfer is carried out by double diffusive means (pointed out by S. Turner after the GFD presentation).

Evidence of convection is presented by Gordon (1978) and discussed further by Killworth (1979).

The winter (June - September) heat loss in the polynya amounts to 2.64×10^{20} cal, which is enough to cool the 3000 meters of Weddell deep water in the entire Weddell gyre by $0.02^{o}C$. Since the historical data does not indicate significant variations in deep water temperature the polynya must reoccur with a time scale of less than 5 to 10 years. Perhaps the build-up of deep water heat during non-polynya years increases the potential for polynya occurrence in the following year. Cooled deep water, after a polynya occurrence, would decrease the potential. In this way an oscillating polynya may occur.

The position of the polynya and perhaps its oscillatory nature may be related to large scale cyclonic Weddell gyre circulation. It is proposed that Weddell circulation is a combination of a nearly barotropic Sverdrup transport and a baroclinic thermocline cyclonic gyre west of Maud Rise.

FINESTRUCTURE IN THE ANTARCTIC POLAR FRONT

Terrence Joyce

The Antarctic Polar Front represents the northern boundary of surface and near surface waters of Antarctic origin. To the south of the front waters are colder and fresher due to air-sea exchanges around the continent. Within the upper 800 meters of the Polar Front vertical profiles of temperature and salinity will contain numerous inversions of vertical scale 100 meters and less

in which warm, salty water found to the north is interleaved with the colder,
fresher Antarctic Waters. A closely spaced section across the front confirms
that the water mass boundary is highly convoluted with these medium scale
interleaving layers produced by cross-frontal mixing processes. The "energy"
source for the medium scale layers $y \sim O(\tilde{L})$, is the lateral variation of the
temperature/salinity field associated with the overall water mass transition,
$y \sim O(\tilde{L})$, across the front. Small-scale transfers, predominantly in the verti-
cal, act to attenuate the characteristics of the intrusions. A steady state
model, Joyce (1977), invoking a balance between the above two processes pro-
duces the following relation

$$- \overline{\tilde{v}'\tilde{T}'} \, \frac{\partial \overline{T}}{\partial y} = - \overline{\widetilde{w'T'} \, \frac{\partial \overline{\tilde{T}}}{\partial z}}$$

between the rate of production of medium scale variability (l.h.s.) and its
rate of dissipation. If the small scale fluxes of temperature and salinity
$\widetilde{w'T'}$, $\widetilde{w'S'}$ are known over the interleaving layer region, then the cross frontal
fluxes of heat and salt can be estimated.

An intensive three dimensional survey of the Antarctic Polar Front was
made in the Drake Passage as part of the International Southern Ocean Studies
(1505) program in March 1976. The front was imbedded within one of the high
velocity cores of the circumpolar current. The spatial and temporal persis-
tence of the variability was studied by analysis of continuous vertical pro-
files of horizontal velocity, temperature, salinity, and dissolved oxygen.
Results from a paper by Joyce, Zenk, and Toole (1978) show that the thermo-
haline variability was not internal wave induced but was associated with nearly
isotropic advection of different water masses across the front. Cold, fresh

and warm, salty intrusions did not conserve potential density, however, and double-diffusive transfer across intrusions are strongly suggested.

Laboratory studies have not yet provided quantitative estimates on small scale fluxes of heat and salt due to salt fingering and convective instabilities simultaneously acting on both sides of intrusions. In order to obtain estimates of the effect of the interleaving upon the large scale field using the above equation, the assumption is made that

$$- \widetilde{w'T'} = A_v \frac{\delta \bar{T}}{\delta z}$$

where A_v is a constant equal to 1 cm^2/sec. Using the observed variance of the intrusions with wavelengths in excess of 3 meters, and estimating large-scale gradients along density surfaces, poleward heat and salinity fluxes are obtained of

$$- \overline{\widetilde{v} \widetilde{T}} = .086 \ ^oC \ cm/sec$$

$$- \overline{\widetilde{v} \widetilde{S}} = .069 \ o/oo \ cm/sec$$

Combining the heat and salt fluxes an up gradient buoyance flux is obtained. The lowest, or most conservative estimate is

$$- \overline{\widetilde{v} \widetilde{\rho}} = 2 \times 10^{-6} \ gm \ cm^{-2} sec^{-1}$$

This estimate is most sensitive to instrumental problems and therefore somewhat suspect.

The overall effect upon the large scale field is to run down the existing horizontal temperature and salinity differences while increasing the existing density difference across the front. While data collected south of New

Zealand in December 1978 has yet to be completely digested the above fluxes are judged to be significant when compared to Southern Ocean wide salt and to a lesser extent heat budgets. The up gradient buoyancy flux could account for the increased vertical shear within the region of the polar front.

REFERENCES

Joyce, T. M., 1977. A note on the lateral mixing of water masses. J. Phys. Oceanogr. 7(4), 626-629.

Joyce, T. M., W. Zenk, and J. Toole., 1978. The anatomy of the Antarctic Polar Front in the Drake Passage. J. Geophy. Res., 83(C12), 6093-6113.

DOUBLE DIFFUSIVE INTRUSIONS AND MIXING ACROSS FRONTS

J. Stewart Turner

Over the past twenty years, there has been a close interaction between theoreticians, laboratory experimenters and observers investigating double-diffusive processes. The introduction to new theoretical ideas has run in parallel to the development of instruments capable of measuring fine- and microstructure, and there is now a wide acceptance that phenomena observed in the laboratory actually occur and can be found in the ocean. Most of the work to date, however, has concentrated on cases where the flow is horizontally uniform. There are still important one-dimensional processes to be studied more closely, particularly the transport of multiple components through double-diffusive interfaces.

The lecture emphasized recent laboratory experiments which have considered two-dimensional effects, and films of three of them were shown. The first was the effect of melting ice in a salinity gradient, investigated with Herbert Huppert in Canberra and Cambridge. Suggestions have been made that the plume of melt water along the sides of melting icebergs could be

responsible for raising nutrients from the deeper layers to the surface in Antarctic Waters. It has, on the contrary, been suggested by those proposing towing icebergs that fresh water will collect at the surface when icebergs melt, which implies that there is little mixing with the surrounding salt water. Our experiments have shown that in the presence of a salinity gradient in the environment neither picture is correct. Convection occurs in nearly horizontal layers, driven by the buoyancy associated with the horizontal temperature difference; the fresh water gets mixed into these layers and little reaches the surface.

The second type of experiment discussed was the intrusion of one fluid into a gradient of another. A source of salt solution in a salinity gradient just spreads out in a thin layer at its level of neutral buoyancy. Sugar solution (the analogue of hot, salty water) released into a salinity gradient (colder, fresher water) behaves very differently. There is rapid vertical convection produced by double diffusion, followed by extension in many layers, with "diffusive" interfaces above, and fingers below. The layers tilt upwards across isopycnals as they extend, due to the more rapid buoyancy flux in the fingers. A source of salt solution in a sugar gradient produces layers with properties in the inverse sense - diffusive interfaces below and fingers above, and tilted downwards.

The uncontrolled mixing in this type of experiment has been eliminated by the technique adopted by Barry Ruddick at ANU. He has filled two sides of a tank, separated by a dam, with identical stable density gradients, but using salt solution on one side and sugar solution on the other. When the barrier is removed, there is a rapid wave-like adjustment of any small density anomalies. When these motions die away, a nearly vertical front remains, across

which there are large anomalies of T and S but no horizontal density gradient. Intruding layers spontaneously develop and propagate, driven by the quasi-vertical fluxes through the interfaces which form above and below. Both the length scale and velocity of these layers are proportioned to depth, and thus to the horizontal property anomalies. This mechanism provides a means whereby molecular effects cannot only influence the fine structure (i.e., layer scales) but larger scale motion as well, through the changes they produce in the properties of the water masses on either side of a frontal surface.

Finally, some current experiments on intrusions in a rotating system were discussed briefly. It has been demonstrated that steady double-diffusive intrusions can persist at a geostrophically balanced front across which there is a shear, in a geometry which remains axisymmetric. In a different parameter range, instabilities have also been observed which are related to, but seem different in detail from, a baroclinic instability. Individual layers move spirally out in persistent confined "noses", and we have speculated that this behavior is influenced by the continuing density changes associated with double-diffusive transports.

THEORETICAL MODELS OF DEEP WATER FORMATION

Peter D. Killworth

In this talk, observations of bottom water formation were discussed in an area-by-area fashion, and theoretical models then presented which each focussed on some physical point or points.

The survey began with the "continental margin" formation regions. In such areas (as typified by the Antarctic, in the Weddell and Ross Seas, and off Adelie Land) there is a continental shelf-slope system. Dense water is formed

on the shelf by saline rejection from freezing sea ice. This water falls **down-slope**, mixing with the surrounding water as it goes, producing dense bottom water at the foot of the slope. This water then moves slowly away from the coast and into the world's ocean.

Such an observational description raises several important theoretical questions, namely:

(a) What is the source for the several million cubic meters of water which are involved in this motion downslope?

(b) Why does Bottom Water occur preferentially in such a few areas in the Antarctic, even with an enclosed area like the **Weddell** Sea, where production is confined to the western side?

(c) What controls how the dense water falls down the slope - a simple balance between buoyant and **Coriolis** forces would imply horizontal motion? and

(d) What happens to the water thereafter; specifically, can the dense water affect its own environment?

Problem (a) was examined by a two-dimensional(north and vertical) stratified model. The effects of both southward Ekman flux at the surface, due to westward winds near the coast and a southward Ekman flux due to vertical shear produced by thermal effects were discussed. Both fluxes impinge on the shelf and are returned downslope as a descending bottom flow. However, the magnitude of the wind-driven flux is order of magnitude larger than the thermally-driven flux, even with nonlinearity included. Hence wind driving appears to be responsible for the _flux_ of dense water, but not its properties.

A two-level model of a continental shelf was used to examine problem (b). Greater sea-ice production close to the edge of the ice shelves, and reduced production further north, was used to drive the motion via a surface buoyancy input. This yields a north-south pressure gradient, and a resulting geostrophic circulation which is eastward at the surface and westward at depth. When this flow impinges on the coastlines there is downwelling on the eastern coastline and upwelling at the west. This induces an east-to-west density gradient (as observed), and therefore a northward flow of deeper (dense) water out of the shelf region on the western side. Wind effects, neglected here, may well add to this effect.

A variety of models for problem (c) were discussed. All are of the turbulent piume or thermal variety, with effects of rotation added. It turns out to be impossible to bring dense water to the bottom with a flux of the observed magnitude. (This involves increasing frictional drag to combat Coriolis force, and increasing entrainment; but this causes the plume or thermal to asymptote to a very shallow depth.) If the correct equation of state is included, however, the situation becomes different. The change in thermal expansion coefficient with depth allows a dense parcel of fluid to become denser relative to its surroundings as it sinks in a stably stratified fluid (a source of internal energy).* With this modification, the two disposable parameters (entrainment and friction) can be tuned to reproduce the observed situation.

A critical test of such a model was provided by observations of anomalous lenses of water at 2000 m off Wilkes Land. Application of the model, with parameters set by the previous calculation, does indeed yield an asymptotic plume depth of 2000 m. This suggests that the lenses may be a variety of "not-quite-bottom-water" which was insufficiently dense to reach the bottom.

---

*This effect is unnecessary and negligible in the Norwegian and Mediterranean outflows.

These results apply to problem (d). The sideways outflow of water
sinking around Antarctica will tend, in time, to set up a stratified ocean
around the coastline. Since the buoyancy of the plumes varies seasonally, at
times the plumes will spread near the surface and at times at depth. The
resultant stratification has been produced in a laboratory model, and
reproduced on a computer-generated film from equations for a filling-box model.

Time did not allow a discussion of open-ocean convection, as observed in
the Mediterranean, Labrador and Weddell Seas and assumed to occur in the Green-
land Sea, although several models of these processes also exist. The models
discussed here include work by E. C. Carmack, P. Smith, J. S. Turner, J. M.
Smith and J. Venn, in addition to the author.

TRANSPORT CALCULATIONS IN THE TASMAN AND CORAL SEAS

George Veronis

The inverse method (Wunsch, 1978) has been used to determine the flow
for a closed-box region in the Tasman and Coral seas. The object of the study
was to determine the large scale transport through the region, and in particu-
lar, to obtain an updated estimate of the amount of water carried by the East
Australian Current. We conclude that there was no evidence of an East Austral-
ian Current in late March, 1960. During the latter period the only strong,
identifiable feature was a cyclonic gyre in the Coral Sea. Since an East
Australian Current has been identified at other times, the flow appears to be
transient. A series of experiments testing various aspects of the use of the
inverse method in such problems is also reported. Transports in the bottom

layer are shown to be sensitive to noise and to the procedure adopted for extrapolating available data to the bottom, particularly in regions of large topographic variations. The importance of working with synoptic, as opposed to climatological, data is demonstrated by the experiments. **It** is also shown that local eddies can affect the solution at relatively distant points.

ICE IN THE MARGINAL SEAS: FIELD OBSERVATIONS IN THE BERING SEA

Seelye Martin

During winter, strong northeast winds dominate the Bering Sea ice motion. Two kinds of ice form in this air flow. The first forms in the lee shore regions around the Bering such as the waters south of Cape Prince of Wales, and St. Lawrence and St. Matthews Islands; the second forms at the ice edge.

In the lee shore regions, the winds sweep the old ice several kilometers away from the shore, several times during the winter, so that seawater at its freezing point is exposed to cold winds. On the open water, the winds generate waves and the cold air creates freezing, so that because of the agitated water, the ice grows as small platelets, measuring about 1 mm in diameter and 10-100 um in thickness. These crystals, which form on the water surface and are also observed at depths up to 8 m, are herded into Langmuir streaks parallel to the wind. Related laboratory experiments on this ice, termed "grease ice" by the World Meteorological Organization, show that it forms an ice-seawater slurry consisting of approximately 40% ice crystals and 60% seawater. Because the crystals tend to sinter together at low rates-of-shear, the grease ice has a non-Newtonian viscosity, where the viscosity increases with decreasing rates-of-shear. This leads to a very efficient wave damping, which may intensify the

Langmuir circulation observed in the Bering Sea. Finally, because of the wave agitation, the grease ice initially grows in thickness very rapidly; in our tank at $-20^{o}C$, the equivalent of 10 cm of solid grows in 1 hour; in still water, this growth takes 24 hours. The grease ice in the lee-shore regions, then, is associated with high rates of ice growth and an intense Langmuir circulation, the combination of which leads to flows of saline bottom water from these regions.

The nature of the Bering Sea ice edge was investigated from the NOAA ship SURVEYOR in March 1979. One purpose of the cruise was to study both the interaction of ocean swell with the ice edge, and the formation of the ice bands which are nearly perpendicular to the wind, measure about 1 km in width and 10-20 km in length, and are located ahead of the main pack. The results of the cruise showed that the swell caused the pack ice to be divided into three zones. The first, which measured 5-10 km in width from the ice edge, consisted of heavily rated and ridged floes of 20 m diameter, with sail heights of 1 m, and keel depths of 4-5 m. These floes were heavily worked by the predominantly 8 seconds swell. Adjacent to this first region, there was a 5 km wide zone of recently broken ice consisting of near-rectangular floes, measuring 20x40 m^2 and about 0.6 m deep. These floes were organized in a regular tiled or "checkerboard" pattern with their long axis parallel to the crests of the swell. Finally, the ice adjacent to this second region consisted of large floes of kms in extent and with thicknesses of 0.3 m through which the swell propagated without breaking the ice.

We also observed from the placement and tracking of targets in the first zone when the wind blew off the ice, because of the extreme aerodynamic roughness of these floes, they moved out ahead of the rest of the pack to form the

observed bands. Over a 24-hour tracking period, in a 10 m/s^{-1} wind, a band formed from the outer region and moved about 15 km south of the pack into warmer water, where it began to disintegrate. This suggests that one mechanism for control, of the ice edge position is the continuous wave-induced rafting and ridging of the ice at the edge, its removal by the winds into warmer water, and the subsequent exposure of the inner region to intense rafting and ridging, wherein the process begins again.

BOTTOM WATER FORMATION IN THE WEDDELL SEA

Theodore D. Foster

Surrounding Antarctica are three large ocean basins; the largest of these, the Atlantic-Indian Basin, extends from the Antarctic Peninsula at about 60^oW to the Kerguelen Plateau at about $80^oE.$ The presence of a nearly permanent band of low atmospheric pressure around Antarctica results in an average surface wind pattern of eastern winds along the coast, intensified by the katabatic effect of the cold, high continent, and westerly winds north of about $60^os.$ In the Atlantic sector the Antarctic Peninsula has a blocking effect that causes strong southerly winds in the eastern Weddell Sea. The oceanic surface currents are largely wind driven and thus we have the Antarctic Circumpolar Current north of about 60^os and the Antarctic Coastal Current along the coast. In between there are a series of eddies. Most of these are ill defined with the exception of the large cyclonic gyre over the Weddell Sea which is stabilized by the presence of the Antarctic Peninsula as its western boundary. The Weddell Gyre is the only gyre around Antarctica that shows up strongly in the long term averaged surface temperature field. Further effects of the Weddell Gyre may be seen in the great northern extent of sea ice in the

Atlantic sector and in its being the chief source region for Antarctic Bottom Water. The principal evidence for this latter assertion is the pattern of bottom potential temperature (lowest values are found in the northwestern Weddell Sea) and the pattern of bottom oxygen (highest values are found in the northwestern Weddell Sea).

The International Weddell Sea Oceanographic Expedition (IWSOE) was organized to investigate the formation of Antarctic Bottom Water in the Weddell Sea in 1968 and has continued to this day. After an initial general survey by icebreakers from the United States and Argentina from 1968 to 1971, the second phase of IWSOE from 1973–1976 concentrated on making closely-spaced sections of hydrographic stations orthogonal to the general flow around the Weddell Sea. This work showed that Bottom Water forms near the shelf break in the Weddell Sea west of about $35^{\circ}W$ up to nearly the tip of the Antarctic Peninsula. In addition, it was found that a modified form of Warm Deep Water, which had mixed with the overlying Winter Water, intruded onto the shelf and then mixed with high salinity Shelf Water to form bottom water. This newly-formed Bottom Water flows down slope at a small angle to the slope mixing with the overlying Warm Deep Water and then flows out of the Weddell Sea as a contour current. Eventually the newly-formed Bottom Water attains characteristics typical of the classically defined Antarctic Bottom Water. Figure 1 shows a potential temperature–salinity diagram which depicts this three–step mixing process.

In order to look at the variability of the formation of Bottom Water we repeated a section in the northern Weddell Sea across the outflow of Bottom Water in 1975 and 1976. Large differences in the characteristics in the Bottom Water were found which were consistent with a higher proportion of

shelf water taking part in the mixing process in 1976 than in 1975. A
year-long record of current velocity and water temperature was obtained from a
meter moored near the bottom along this section between 1975 and 1976. Besides
tidal motion, energy was found in motions with periods near 20 days. Both tem-
perature and velocity showed much less activity in winter than in summer.

Detailed examination of the 1976 section from the center of the Weddell
Sea up onto the shelf just east of the tip of the Antarctic Peninsula shows
that there is probably formation of water near the shelf break that does not
have sufficient density to sink all the way to the bottom and thus intrudes
above the bottom as deep water. Since this deep water is somewhat less salty
than the Bottom Water, it probably formed from less salty shelf water. This
variation is also consistent with the model shown in Fig. 1.
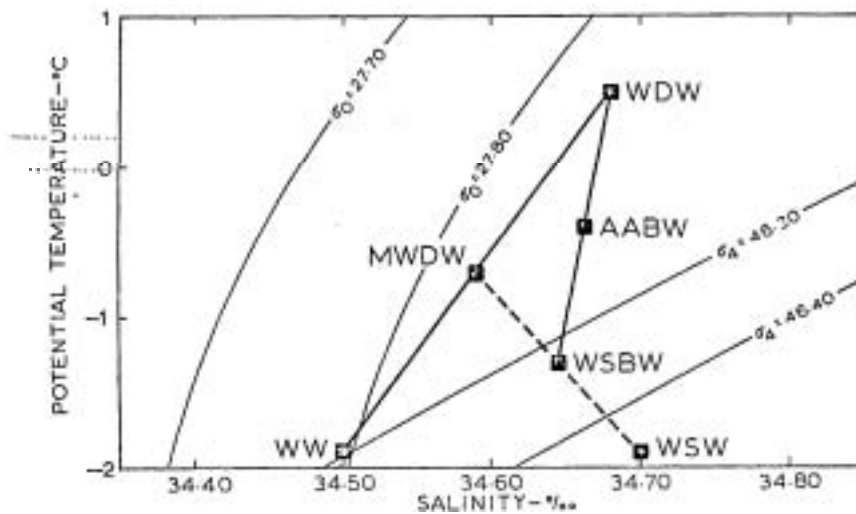
Fig. 1. Mixing Processes Leading to Antarctic Bottom Water (AABW), WW =
Winter Water, WDW = Warm Deep Water, WSW = Western Shelf Water, MWDW =
Modified Warm Deep Water, WSBW = Weddell Sea Bottom Water.

BOUNDARY LAYERS BENEATH ARCTIC SEA ICE

Kenneth Hunkins

Although the theory of the Ekman spiral has existed for three-quarters of a century, relatively few observations of spirals have been made in the ocean. Perhaps the majority of observed spirals have been seen in the Arctic Ocean beneath drifting sea ice. The first arctic spiral appeared in a set of averaged current measurements taken during summer stratified conditions. A model with an Ekman layer of constant eddy viscosity surmounted by a surface boundary layer of constant stress fitted the observations reasonably well. The Ekman layer was 16 m thick corresponding to an eddy viscosity of 24 cm^2/s and the constant-stress layer was 1 m thick (Hunkins, 1966). More recent current profiles from the 1975-6 Arctic Ice Dynamics Joint Experiment (AIDJEX) generally show a right-handed spiral in the upper layer although the exact shape does not always take the form predicted by the theory with constant eddy viscosity. Other observations of Ekman spirals have been made by Brennecke in the Weddell Sea, Gonella in the Mediterranean and by Swallow and Bruce in the Indian Ocean.

It has been shown by analysis and rotating tank experiments that the Ekman spiral solution for a homogeneous fluid is unstable in the Reynolds number range usually encountered in the ocean. Secondary flows develop which destroy the spiral pattern and observed Langmuir circulations are often cited as evidence for such secondary flows in the ocean. How is it then that the Ekman spiral is observed at all? It seems that the spiral develops best under stable stratification such as that produced by fresh water runoff in the Arctic Ocean during summer. This was also noted by Gonella in the Mediterrnean where spirals were seen under summer thermally-stratified conditions but not in the winter homogeneous upper layer. A stable platform such as ice is also helpful

since many open ocean measurements in the upper layers are contaminated by mooring motion induced by surface waves. So an Ekman layer beneath sea ice is a reality even down to details of the structure.

A numerical model of sea ice was developed by the AIDJEX project. The oceanographic part of this project sought a practical measure of water drag on the bottom of the ice, to be used as input for this model. Since Ekman spirals do not always develop or are not always readily interpreted other methods for finding stress were developed. The most direct technique is eddy correlation using current meters with rapid response. Another is a profile of mean currents in the logarithmic layer. Both techniques have been used under Arctic sea ice. Their limitation is that they must be used in the constant-stress layer which is only about 1 m thick. The results only apply to a region, say 100 m, upstream of the measurement site. Arctic sea ice is marked by pressure ridges with underlying keels in roughly isostatic adjustment. It is desirable to have an average stress over a larger area than can be obtained in the logsrithmic or constant-stress layer so as to include the effect of these keels. Under-ice sonar from submarines reveals keels extending to 10 m depth with a spacing of 200 m on the average. These keels thus extend through the logarithmic layer and into the Ekman layer.

A more representative stress given by a momentum integral based on current profiles which sums all of the non-geostrophic momentum in the Ekman layer. For well-averaged observations, can be shown that this method includes the effects of pressure drag from the ridges as well as skin friction (Hunkins, 1975a).

The momentum integral method does not determine internal wave drag. Keels below the drifting ice must generate internal waves in the stratified layers below the mixed layer. Some check on the contribution of this drag was made by analysis and by scaled model experiments. The results were not conclusive but tended to show that internal wave drag was a small factor except at the highest rates of ice drift (Hunkins, 1974; Rigby, 1974).

Geostrophic drag coefficients were derived from the 1972 AIDJEX data for possible use in numerical modeling (Hunkins, 1975b). The drag coefficient is defined by $C_D = \tau_o / \rho G^2$ where τ_o is the water drag, ρ is water density and G is the relative velocity between ice and the geostrophic flow beneath the Ekman layer. Since geostrophic flow is often small relative to ice speed, G may in many cases be approximated by ice speed. At low drift speeds, there was considerable scatter in the data. Only at the largest drift speeds could reliable coefficients be determined. At G = 25 cm/s, C_D = 0.002 and the surface inflow angle, α_o = 30°. If these results are to be useful for a variety of speeds and ice types, a functional relationship is needed between C_D, α_o, and $R_s = G/fz_o$, a surface Rossby number. Such relationships have been established by similarity relations which match an inner layer with a length scale z_o and an outer layer with length scale, u_*/f, where $u_* = \sqrt{\tau_o/\rho}$. The AIDJEX data produce somewhat different universal constants for this theory than those found from atmospheric data over level ground surfaces (Deacon, 1973). It is not clear whether the difference is in the limitations of the data or in the fact that the AIDJEX under-ice topography was relatively rougher than the level ground surfaces over which atmospheric constants were measured.

REFERENCES

Deacon, E. L., 1973.   Geostrophic drag coefficients.   Boundary Layer Met., 5, 321-340.

Hunkins, K., 1966.   Ekman drift currents in the Arctic Ocean.   Deep-Sea Res., 13, 607-620.

Hunkins, K., 1974.   An estimate of internal wave drag on pack ice.   AIDJEX Bull., 26, 141-152.

Hunkins, K., 1975a.   The oceanic boundary layer and stress beneath a drifting ice floe.   J. Geophys. Res., 80, 3425-3453.

Hunkins, K., 1975b. Geostrophic drag coefficients for resistance between pack ice and ocean.   AIDJEX Bull., 28, 61-67.

Rigby, F., 1974.   Theoretical calculations of internal wave drag on sea ice. AIDJEX Bull., 26, 129-140.

OPEN OCEAN FRONTOGENESIS

A. D. Voorhis

Intense and intermittent frontogenesis in the surface waters of the North Atlantic subtropical convergence is associated with mesoscale and sub-mesoscale motions which advect and distort the large scale climatic surface temperature field into long tongues and plumes, thereby, greatly increasing lateral thermal (and density) gradients. This is very apparent in satellite infra-red imagery.

Frontogenesis has been directly observed along the boundaries of these features. Time scales appear to be one to three days. A surface drogue at a depth of 15 m drifted into a frontal jet and accelerated from 30 to 80 cm sec^{-1} over a distance of about 100 km in two days. These large speeds, however, occurred only near the surface. Another drogue at a depth of 75 m never exceeded a speed of 40 cm sec^{-1}. Such fronts would appear to be excellent mechanisms for the lateral transfer of heat and salt in the upper 50 to 100 meters.

BOUNDARY CURRENTS AND BOTTOM WATER FORMATION

Adrian E. Gill

This is a discussion of some GFD problems stimulated by a look at currents in the Norwegian-Greenland Seas. First, some transects by submarine (Wadhams, Gill and Linden, 1979, Deep-Sea Research) across the ice edge off East Greenland show the existence of a strong front located near the ice edge. Sometimes the front is crossed several times in a transect suggesting the presence of eddies. Some old sections taken in 1905 and 1906 (Kiilerich, 1945) show the front is the edge of a wedge-shaped cold fresh water mass from the Arctic which is associated with the E. Greenland current flowing southwards down the E. Greenland coast.

This suggested the following GFD problem. Suppose the Arctic Ocean were completely enclosed and was covered by a surface layer of cold fresh water which was less dense than the surface waters of the surrounding oceans. Then suppose a dam from Greenland to Norway was opened up. What would happen? My paper, "Adjustment in a Rotating Channel" (JFM, 1976) suggests that a Kelvin wave would propagate down the Greenland coast establishing a boundary current which would carry the outflow from the Arctic. No current would be formed on the Norwegian side. An experiment confirming this picture was reported in Ocean Modelling. The conclusion is that buoyancy forces alone would produce an East Greenland current. In practice, there are strong southward winds along the Greenland Coast which would tend to enhance this current.

Now consider another problem associated with the Norwegian Greenland Seas: Bottom Water formation. This creates (Worthington, 1970) a buoyancy-driven flow of about 5 Mts^{-1} having the form of an inflow of this magnitude of light warm water and a corresponding outflow of heavy cold water. The warm water flowing past the British Isles appears to be an important factor in producing a mild climate in Northern Europe.

Now consider simple methods for modelling buoyancy driving so that the currents produced by this means can be calculated. One method is to use a two-layer model (Gill, Smith, Cleaver, Hide and Jonas, 1979). The Bottom Water formation being represented by upper layer fluid being converted to lower layer fluid. Thus, the forcing term appears in the continuity equation. In the linearized version, if h is the upward displacement of the interface, H_i the undisturbed layer depths and u_i, v_i the velocity components, the continuity equation for layer 2 (the lower one) takes the form

$$h_t + H_2 (u_{2x} + v_{2y}) = Q$$

where Q represents a source of fluid from the upper layer. The corresponding equation for layer 1 (the upper layer) is

$$-h_t + H_1(u_{1x} + v_{1y}) = -Q$$

The sum of these two equations gives continuity for the barotropic mode, with no forcing. Thus all the motion is baroclinic. The equation for the baroclinic mode is obtained by subtracting $1/H_2$ times the fluid equation from $1/H_1$ times the second, giving

$$-\left(\frac{1}{H_1} + \frac{1}{H_2}\right)h_t + \hat{u}_x + \hat{v}_y = -\left(\frac{1}{H_1} + \frac{1}{H_2}\right)Q,$$

$\hat{u}, \hat{v}$ being the difference between the layer velocities.

A simple solution can be constructed for cases where there is no y-dependence. In non-dimensional coordinates with time scale f^{-1} and space scale the Rossby radius, the continuity equation above becomes

$$-h_t + \hat{u}_x = -Q \tag{1}$$

and the momentum equations are

$$\hat{u}_t - v = h_x \tag{2}$$

$$\hat{v}_t + \hat{u} = 0 \tag{3}$$

The potential vorticity equation is obtained by substituting the expression for $\hat{u}$ from (3) in (1) to give an equation which integrates to give

$$h + \hat{v}_x = Qt$$

It follows that there is a solution where v and h are proportional to t but u, because of (3), is independent of time. In this case (2) reduces to the geostrophic relationship $v = h_x$ and so (4) becomes

$$h - h_{xx} = Qt \qquad (5)$$

An interesting special case is the one where the source Q is localized, so has the form of a delta function (at x = 0 say). For x > 0, Q = 0 and the solution of (5) is

$$h = Ae^{-x}t \qquad \text{for } x > 0$$

By symmetry, the solution for x   0 is

$$h = Ae^{x}t \qquad \text{for } x < 0$$

The value of A can be determined by volume conservation or by calculating the jump in h_x required at x = 0 by integrating (5) across x = 0. This shows that Bottom Water formation causes the interface to rise over a distance of the order of the Rossby radius, and geostrophic currents are associated with this interface slope. Similar solutions can be found for axisymmetric forcing. Laboratory experiments to illustrate the doming effect which is associated with Bottom Water formation are reported in the GAFD paper cited above. Similar doming is found in the Greenland Sea.

In the absence of boundaries, a point source of Bottom Water would just create a swirling flow with fluid spiralling into the upper layer sink in a cyclonic sense, as required by conservation of angular momentum. What effect would a boundary have? A linear numerical experiment shows that influence spreads from the nearest point of the boundary in the form of a Kelvin wave. After the wave has passed, a boundary current is established with upper layer

flow toward the sink. Since Kelvin waves in the northern hemisphere travel with the coast on their right, influence will ~~not~~ spread down the Norwegian Coast to produce an inflow past the British Isles if only buoyancy forces are acting.

However, wind driving can rescue the situation for us, because strong winds against the Norwegian Mountains generally blow northwards and so produce a boundary current in the same direction because they cause downwelling of the pycnocline against the coast (such is observed along the continental slope). If the wind is introduced into the model calculation, it is possible for the wind-driven boundary current to provide the inflow into the upper layer sink. This suggests the wind plays a part in keeping the inflowing warm current running up the Norwegian coast, but perhaps the model is oversimplified? The situation seems to be an interesting and worthwhile one to try and understand by means of model studies.

REFERENCES

Gill, Adrian, 1979. Seminar de dynamique des fluides geophysiques et du model-isation numerique apliquee a l'oceanographie, CNEXO, Paris.

Gill, A.F., J. M. Smith, R. P. Cleaver, R. Hide and P. R. Jonas, 1979. The vortex created by mass transfer between layers of a rotating fluid. Geophys. Astrophys, Fluid Dyn., 12, 195-220.

Kiilerich, A., 1945. On the hydrography of the Greenland Sea. Meddelelser Om Gronland, 144(2).

Worthington, L. V., 1970. The Norwegian Sea as a Mediterranean Basin. Deep-Sea Research, 17, 77-84.

CONVECTIVE PROCESSES IN THE ANTARCTIC

Theodore D. Foster

Buoyancy driven convection takes part in two of the mixing processes leading to the formation of Antarctic Bottom Water: (1) Haline convection induced by sea ice formation produces the high salinity shelf water, and (2)

the caballing instability leads to mixing between Winter Water and Warm Deep Water.

Haline convection occurs when sea ice forms since the salt is mostly excluded from the ice matrix and increases the salinity of the boundary layer just beneath the ice. The resulting instability can be very closely described using the time-dependent mean field equations during the initial stages of convection while the ice layer is relatively thin and flat. The only nonlinear term that is considered in the mean field approximation is that in the horizontal averaged diffusion equation:

$$\frac{\partial \bar{S}}{\partial t} + \frac{\partial}{\partial z}(\overline{wS}) = D \frac{\partial^2 \bar{S}}{\partial z^2} \quad , \qquad S(x,y,z,t) = \bar{S}(z,t) + s(x,y,z,t)$$

where $\bar{S}$ is the horizontally averaged salinity, s the salinity fluctuation, w the vertical velocity, and D the diffusivity. The nonlinear terms in the momentum equation are neglected since the Schmidt number, $\sigma = \nu/D$, is large. The salinity Rayleigh number for a salinity difference ΔS:

$$R = \frac{\gamma g \Delta S\, h^3}{D \nu}$$

where γ is the expansivity due to salt, D the kinematic viscosity, and h the total depth of the fluid, or for constant salt flux F:

$$R_F = \frac{g\, F\, h^4}{D^2 \nu \rho}$$

The initial behavior of the system is the formation of convection cells with a horizontal wavelength about twice the l/e boundary layer thickness at instability. If the water below the ice is neutrally stable, the convection will become highly elongated vertically. Under these conditions usually in cells encountered in the polar regions the cell spacing will be of the order of 1 to 2 mm and cell height several tens of cm. This gives the appearance of salt "fingers" or "streamers" under the growing sea ice sheet.

If the flux Rayleigh number is larger than about 10^8, the convection becomes intermittent.   The phenomenon is further complicated by the tendency of the convective streamers to coalesce and give rise to fewer, larger con-vective elements as they move away from the boundary layer.   The study of these secondary convective effects has only just begun.

The caballing instability occurs when two water types of nearly equal density but different temperatures and salinities are superimposed.   Then the nonlinearity of the equation of state of sea water with respect to temperature can cause mixtures of the two water types to be more dense than the underlying water.   Since the equation of state is most nonlinear at low temperatures, the caballing instability may be especially important in the polar regions. Examination of the temperature and salinity profiles at the interface between the near surface Winter Water and the Intermediate Warm Deep Water in the Weddell Sea shows that the interface can be quite sharp yet with little density difference between the two water masses.   When the interface is sharp, there are usually very large isohaline and adiabatic layers beneath the interface up to 500 m thick.   These layers have density ratios ($\alpha \Delta T / \beta \Delta S$) very close to unity (0.97 to 1.03) indicative of turbulent mixing and are nearly just unstable to the caballing instability.   Any slight increase in salinity in the top layer would make the caballing instability quite active. In addition, the conditions for instability vary with pressure, and since the interfaces of the large layers are found at depths varying from about 100 to 600 m, the salinity and temperature differences at the interfaces should vary with depth if the caballing instability is active.   Approximately the correct variation with depth is observed.

Numerical modeling of the caballing instability shows that the resulting convection is one-sided with flow only occurring in the lower layer. The lower layer gradually thickens until the salinity and temperature difference across the interface cannot support the caballing instability. The interface remains quite sharp. Laboratory experiments using mixtures of alcohol and water to simulate the nonlinear equation of state of sea water at low temperatures show that the one-sided convection modeled numerically does occur as predicted. Further numerical modeling and laboratory experiments will be needed to sort out the relative importance of the cabling instability and the diffusive instability which may be competing processes under certain oceanic conditions.

THE GROWTH AND DESALINATION OF FIRST-YEAR SEA ICE

Seelye Martin

Sea ice formation begins from the freezing of sea water. When the ice initially forms, following Martin (1980), there is an upward salt transport so that a highly saline layer with salinities of order 100% forms on the ice surface. Because of the cold surface temperatures, the salt remains on the surface throughout the winter. The ice below this layer has salinities of 5-10%.

When the ice warms in the spring, the surface salt forms a concentrated brine solution which drains down through the ice, leading to the formation of top-to-bottom brine channels. Around the cold brine outflow from these channels, fragile tubes of ice called stalactits occasionally form.. Martin (1974) describes a laboratory study of these stalactites, and summarizes the field observations. In McMurdo Sound, the stalactites have been observed to grow as long as 5 m in length. As the ice continues to warm in the summer fresh water melt ponds form and grow on the ice surface to cover as much as

40% of the Arctic pack ice surface. Some of this water drains into the ocean, to form the low salinity surface layer of the summer arctic. Some fresh water also flows under the ice where it refreezes into fragile crystals and eventually into horizontal ice sheets from the temperature difference between the -1.6^{o} sea water and the 0° fresh water. Martin and Kauffman (1974) describe this refreezing process in detail. Finally, in the fall, the remains of the first-year ice refreeze into the hard, low salinity multi-year ice.

REFERENCES

Martin, S., 1980. A field study of brine drainage and oil entrainment in the first-year sea ice. J. Glaciology (in press).

Martin, S., 1974. Ice stalactites: comparison of a laminar flow theory with experiment. J. Fluid Mech., 63, 51-79.

Martin, S. and Kauffman, P., 1974. The evolution of under-ice melt ponds, or double diffusion at the freezing point. J. Fluid Mech., 64, 507-527.

A WATER MASS MODEL OF THE WORLD OCEAN

Kirk Bryan

A model of the world ocean is solved to investigate the formation of water masses in response to the observed distribution of temperature, salinity and wind-stress at the ocean surface. An initial-value problem is solved starting with uniform temperature and salinity throughout the world ocean. After a numerical integration over the equivalent of 1000 years, a near equilibrium is obtained. Using this solution as a standard, a series of shorter numerical experiments are carried out to test the sensitivity of the model to different levels of the closure parameters which represent the effects of motions of mesoscale eddies and smaller scale motion in redistributing heat, salinity and momentum.

The distribution of temperature and salinity in the standard case is surprisingly realistic. North-South, vertical sections indicate the simulation of the major water mass types such as NADW (North Atlantic Deep Water) and AAIW (Antarctic Intermediate Water). The poleward transport of heat and water are in good qualitative agreement with observations, but the heat transport appears to be low in comparison with recent estimates by Oort and Vonder Haar (1978). The parameter tests show that the overall depth of the thermocline is closely related to the available potential energy which in turn is proportional to kinetic energy. In the range of parameter space of the model only an increase of vertical diffusion increases the available potential energy and deepens the thermocline. Increasing horizontal diffusion and viscosity, and vertical viscosity all tend to decrease total energy, and cause a thinning of the overall thermocline depth. The close relation between total large-scale energy and thermocline depth is interpreted to mean that the structure of thermocline in the real ocean is critically dependent on the level of baroclinic instability generating mesoscale motion.

A parameter study shows that the transport of the circumpolar current is proportional to the level of large-scale potential energy, and overall thermocline depth. This result is dictated by the fact that the circumpolar current marks the boundary between the main thermocline, and the region of very low vertical stability around Antarctica.

REFERENCES

Bryan, K. and L. J. Lewis., 1979. A water mass model of the World Ocean. J. Geophys. Res., 84, C5.

Oort, A. H. and T. H. Vonder Haar, 1976. On the observed annual cycle in the ocean-atmosphere heat balance over the Northern Hemisphere. I. Phys. Oceanogr., 6, 781-800.

LABORATORY MODELLING OF OCEANIC RESPONSE TO MONSOONAL WINDS

Ruby Krishnamurti

1. Introduction

A laboratory model of wind–driven ocean circulation is described in which various wind–stress patterns are simulated which drive fluid in a tank whose depth variation is used to model the β-effect. Both homogeneous and two-iayer fluids were used. The following three experiments are described:

(i) measurement of northward transport in the western boundary current as it varies with magnitude of wind–stress.

(ii) conditions for surfacing of the lower layer and separation of the western boundary current from the boundary.

(iii) periodic forcing of a two–layer model.

The first of these was motivated by the observation that the oceans effect a major portion of the transport of heat from equator to pole. However, unlike the atmosphere which is primarily thermally driven, the upper oceans are to a large extent driven by the atmospheric winds. These winds change, not only with the seasons, but also with the changing climate. For example, T. N. Krishnamurti (1979) shows major changes in air flow pattern from years of normal rainfall to years of drought over India and North Africa. It would be interesting to know the change in oceanic transport for a given change in the winds. Not only does this change in the poleward heat transport by the oceans directly affect the climate at a given latitude but it is also an important factor in the question of maintenance of the permanent cryosphere.

The second experiment, related to surfacing of the lower layer, was performed to test a theory due to Professor George Veronis (1973b, 1977). For a two–layer model with quiescent lower layer, his argument proceeds as follows.

In a region of anticyclonic wind-stress curl (such as the subtropical North Atlantic), the Sverdrup transport is to the south. Mass balance across a latitude line requires an equal northward transport in the region near the western boundary. This would require, for the geostrophically balanced part of the transport alone, that the height of the interface at the western boundary be equal to that at the eastern boundary. To this consideration, one must add the Ekman transport. In the Trade Wind regions, the Ekman transport is to the north. Thus the return transport on the west must be less than that required by the geostrophic flow alone, so the interface must be <u>lower</u> at the western than at the eastern boundary. If surfacing occurs at these latitudes, it would occur first on the eastern boundary. However, in the anticyclonic part of the Westerlies, the Ekman transport is to the South, adding to the geostrophic transport to the south. The interface at the western boundary must therefore be <u>higher</u> than at the eastern boundary. At these latitudes, surfacing would occur first on the western boundary. A similar argument has also been presented by Parsons (1969).

The third experiment was performed to simulate, in a very rough way, the response of a sea (such as the Arabian Sea) to time varying winds (such as the south-west and north-east monsoons). The spin-up time of a two-layer laboratory model can be adjusted to resemble the response time of a tropical ocean basin.

2. <u>Laboratory Model</u>

Certain gross features of the general circulation of the oceans can be modelled in laboratory experiments, as has been shown by Stommel, Arons, & Faller (1958), Pedlosky & Greenspan (1967), Beardsley (1969), Baker & Robinson

(1969), Veronis (1973a), Hart (1975) and others. For example, a constant wind stress curl can be simulated by a rotating lid in contact with the fluid, and variation of Coriolis parameter with latitude (β – effect) can be simulated by variation of fluid depth with location in the tank.

A circular cylindrical tank is divided into three separate basins: a 180° basin, a 120° basin, and a 60° basin. The lid is cone-shaped with slope tan δ , the base with slope tan δ_λ . In the first experiment, the center of the cylinder is shallowest; in the second experiment the center is deepest. The tank is placed on a rotating table whose angular velocity is Ω . The lid rotates relative to the tank at an angular velocity $A\Omega$. As in Beardsley's (1969) experiments this model possesses a western boundary. It differs from his homogeneous experiments in that these are two-layer experiments. In this respect, it is similar to Hart's two-layer models. However, in Hart's studies there was no western boundary.

The physical basis for the model lies in the analogy between the vortex stretching by flow across constant depth contours, and the relative vorticity produced by the oceanic flow to latitudes of different Coriolis force. Greenspan (1968) has elucidated the difference in the flows that may arise in closed containers having or not having closed geostrophic (constant depth) contours. Each of the three basins possesses no closed contours of constant depth. The nature of the steady driven flow is completely different from the case with closed geostrophic contours. The interior flow is a slow, order $E^{1/2}$ (where E is the Ekman number) drift across depth contours.

Since the speed on the top boundary is a linear function of radial distance, the top Ekman layer has a constant divergence with a vertical velocity w_E of order $E^{1/2}$. Because the interior flow is order $E^{1/2}$, the bot-

tom Ekman layer, for the case of a homogeneous fluid, has a much smaller flux of order E. However, if the interior flow would be across depth contours at just the right speed v so that the orographically induced vertical velocity w = v tan α balances the Ekman flux w_E, then the interior velocity can be depth independent. In case Ω is counterclockwise and $\Delta\Omega$ is clockwise, this is a constant flow to greater depths (or southwards flow) and is the equivalent of the Sverdrup balanced solution.

Mass is returned to the north by a fast current along the western wall. Beardsley (1969) shows that in case tan $\alpha \ll E^{1/4}$, a Stommel (1948) type geostrophic western boundary layer of thickness $E^{1/2}/tan \alpha$ forms in which vortex shrinking is balanced by Ekman suction. When tan α approaches $E^{1/4}$, the western boundary layer thins down towards the Stewartson $E^{1/4}$ layer. In this case the diffusion of vorticity from the side wall is balanced by orographic vortex stretching as well as by Ekman-layer suction. When tan α $\gg$ $E^{1/4}$ the flow is analogous to the Munk and Carrier (1950) model with lateral friction.

Rotating a rigid lid simulates a constant wind-stress curl, with uniform vertical velocity out of the top Ekman layer. This effect could as well have been simulated by a uniform distribution of sources of mass at a non-rotating top boundary (Baker, 1971). Wind-stress patterns are not always describable by a constant curl. Any jet such as the Findlater or 'low-level' jet over the Arabian Sea could better be described as a concentrated region of anticyclonic curl adjacent to another concentrated region of cyclonic curl. Such a wind-stress pattern is simulated by a line of sources adjacent to a line of sinks in a porous upper boundary.

In the case of a two layer fluid **it** was found in these experiments that the lower layer has mean velocities approximately two orders of magnitude smaller than the upper layer velocities. Thus, the assumption made in many theories that there is no stress transmitted across the interface appears to be most reasonable. A Sverdrup interior and a Stommel type western boundary layer is then a possible solution for the upper layer. The interface becomes distorted in such a way as to prevent pressure gradients in the lower layer, the slope of the interface being proportional to the interior velocity of the upper layer in accordance with the Witte-Margules formula. The change in upper layer depth produced by such distortion of the interface does not affect the vorticity of the upper layer since the geostrophic flow is perpendicular to the depth gradient. This being the case, distortions of the interface should not be thought of as contributing to the " β - effect".

Lower layer motions are, however, possible in the western boundary layer even for steady flow. Welander (1968) shows a recirculating flow confined to the western boundary lower layer if the northward gradient of f/h is positive, where f is the Coriolis parameter, h is the lower layer depth.

3. Theoretical basis for the two-layer model

For steady linear flow, the vorticity equation in each layer can be shown to be (Hart, 1972)

$$\underset{\sim}{V_1} \cdot \underset{\sim}{\nabla} H_T - \frac{E_1^{1/2}}{2} (\nabla^2 P_1 - 2) + \frac{E_1^{1/2}}{2} \frac{\chi}{1+\chi} (\nabla^2 P_2 - \nabla^2 P_1) = 0 \qquad (1)$$

$$\underset{\sim}{V_2} \cdot \underset{\sim}{\nabla} H_{\bullet} - \frac{E_2^{1/2}}{2} \nabla^2 P_2 - \frac{E_2^{1/2}}{2} \frac{1}{1+\chi} (\nabla^2 P_2 - \nabla^2 P_1) = 0 \qquad (2)$$

where $\underset{\sim}{V_1}$, $\underset{\sim}{V_2}$, are the upper, lower layer velocities respectively, P_1, P_2 are the upper, lower layer geostrophic stream functions respectively, H_T is the shape function of the top lid, H_B of the bottom. Here $\chi = \nu_1/\nu_2$ and we shall take

$$H_T = -y \tan \alpha_1$$

$$H_B = y \tan \alpha_2$$

The first term in equation (1) represents the orographically induced vertical velocity resulting from geostrophic flow along the top boundary. The second term is the Ekman suction at the top associatd with interior vorticity, the third is the vertical velocity resulting from Ekman layer divergence. The fourth and fifth terms represent Ekman suction at the interface associated with the interior vorticities of the lower and of the upper layers. The Froude number is assumed to be small and vortex stretching as columns of fluid move over the parabolic mean interface is neglected. For a 10 cm radius tank rotating at 20 rpm, the interface is only approximately 1 mm higher at the rim than at the center. This may be compared to the change in height of 2 cm due to the slope of the lid.

If we take $\nu_1 = \nu_2$ the above equations become

$$\left(\nabla^2 + \beta_1 \frac{\partial}{\partial x} \right) P_1 \; - \; 1/3 \nabla^2 P_2 = 4/3 \tag{3}$$

$$\left(\nabla^2 + \beta_2 \frac{\partial}{\partial x} \right) P_2 \; - \; 1/3 \nabla^2 P_1 = 0 \tag{4}$$

where we have defined

$$\beta_1 = 4/3 \ \frac{\tan \alpha_1}{E_1^{1/2}}$$

$$\beta_2 = 4/3 \ \frac{\tan \alpha_2}{E_2^{1/2}}$$

For a flat-bottomed ocean we would chose a model with $\beta_1 = \beta_2$.
However, β_2 could be varied to represent different bottom topographies. For
example, if β_2 is chosen zero, we find the upper layer equation reduces
to Stommel's equation for a homogeneous fluid, while the lower layer is motion-
less everywhere.

4. Observations

The following are typical observations of the first experiment related
to northward transport.

Case 1: Homogeneous Fluid

(i) A radial component of flow across constant depth contours over
much of the tank, from shallow to deep for clockwise rotation of the lid is ob-
served. This is analogous to the Sverdrup interior flow to the south.

(ii) This flow is diverted to the west in the rim boundary layer
which is several millimeters thick at the eastern part of the rim and becomes
several centimeters thick near the western part of the 180° basin.

(iii) The return flow to the north occurs in a fast narrow current
along the western boundary. The center of the gyre is far to the west of the
center of the basin.

(iv) A stationary topographic Rossby wave is observed where the
western boundary current enters the interior. Associated with this is a region
of weakly cyclonic flow. There are no instabilities and no time dependence.
All of these features are in agreement with Beardsley's homogeneous flows.

Case 2:   Two-Layer Fluid

For the same slopes and Rossby number, a two-layer fluid shows similar features, but baroclinic instabilities are now possible.   Typical features are:

(i) A westward intensified anticyclonic gyre, with the center of the gyre shifted to the southwest of the location for the homogeneous case.

(ii) The region of cyclonic flow as the western boundary current enters the interior is more pronounced.

(iii) There is instability and time dependence in primarily two scales. There are small waves of wavelength approximately 5 mm, which is the baroclinic radius of deformation for this experiment.   There is also a larger scale instability, with wavelengths several centimeters.   This is evident in the movies, and the conditions for its occurrence have been summarized in a regime diagram.

(iv) There is a counter-current in the rim boundary layer.   This is a highly depth-dependent flow which is strongest just above the interface and which vanishes rapidly with distance above the interface.   This counter-current becomes increasingly stronger to the east.   It continues along the eastern wall as a northward current and finally enters the interior by flowing cyclonically around the low formed by the topographic Rossby wave.

A movie was shown of one example of flow in the two-layer model.

The measured northwards volume transport T in the western boundary current was measured and is plotted against Rossby number for both homogeneous and upper layer of the two-layer model.

(i) With the tank shallow in the center and with the lid rotating in a clockwise sense, as in the Trade Wind regions, surfacing first occurs on the eastern boundary near the weak cyclonic flow associated with the stationary topographic Rossby wave.

(ii) With the tank deep in the center and with the lid rotating in a clockwise sense, as in the anticyclonic part of the Westerlies, surfacing of the lower layer occurs on the western boundary, and the fast western boundary current separates from the western boundary before it is forced to do so by the rim. The conditions for this surfacing are in qualitiative agreement with Professor Veronis' theory.

5. Conclusion

This two-layer laboraoty model of wind-driven ocean circulation appears to be capable of simulating some of the gross features observed or expected from theories of the oceanic general circulation. It also produced some unexpected features such as the deep countercurrent along the eastern boundary. Certainly the model allows features not observable in a homogeneous model of ocean circulation.

REFERENCES

Baker, D. J., 1971. A source-sink laboratory model of the ocean circulation. Geophys. Fluid Dyn., 2, 17.

Baker, D. J., and A. R. Robinson, 1969. A laboratory model for the general ocean circulation. Phil. Trans. Roy. Soc. London Ser. A, 265, 533.

Beardsley, R. C., 1969. A laboratory model of the wind-driven ocean circulation. J. Fluid Mech., 38, 255.

Greenspan, H. P., 1968. The theory of rotating fluids. Cambridge University Press.

Hart, J. E., 1972. A laboratory study of baroclinic instability. Geophys. Fluid Dyn., 3, 181.

Hart, J. E., 1975. The flow of a two-layer fluid over topography in a polar ocean. J. Phys. Oceanogr., 5, 615.

Krishnamurti, T. N., 1979. Northern summer tropical circulations during drought and normal rainfall months. Monsoon Dynamics. Sir James Lighthill and R. P. Pearce, Editors, Cambridge University Press.

Munk, W. H. and G. F. Carrier, 1950. The wind-driven circulation in ocean basins of various shapes. Tellus, 2, 158.

Parsons, A. T., 1969. A two-layer model of Gulf Stream separation. J. Fluid Mech., 38, 511.

Pedlosky, J. and H. P. Greenspan, 1967. A simple laboratory model for the ocean circulation. J. Fluid Mech., 17, 291.

Stommel, H., 1948. The westward intensification of wind-driven ocean currents. Trans. Am. Geoph. Un., 29, 202.

Stommel, H., A. B. Arons, and A. J. Faller, 1958. Some examples of stationary planetary flow patterns in bounded basins. Tellus, 10, 179.

Veronis, G., 1973a. Large scale ocean circulation. Advances in Applied Mechanics, 13, 1.

Veronis, G., 1973b. Model of world ocean circulation: 1. wind-driven, two-layer, J. Mar. Res., 31, 228.

Veronis, G., 1977. Personal communication.

REGULAR BAROCLINIC WAVES: SOME RECENT WORK

Raymond Hide

Regular baroclinic waves have evidently now been found in nature (in certain planetary atmospheres) nearly thirty years after they were discovered and their main properties elucidated during the course of laboratory experiments on thermal convection in a rotating fluid subject to a horizontal temperature gradient. They have been the subject of a great deal of research by several groups and their investigation and related work on other aspects of the dynamics of rotating fluids continue to provide insight into basic processing atmospheres and oceans.

Regular (i.e., spatially and temporally periodic) baroclinic waves, with their fully-developed jet-streams and their tendency under certain conditions to "vacillate" in amplitude, shape or wavenumber, occur when the dimensionless parameter

$$\Theta = g d \alpha \, \Delta T / \Omega^2 (b-a)^2$$

lies within a certain range $\Theta_R > \Theta > \Theta_I$. (Here g is the accel-

eration of gravity, d the depth of the fluid, $\alpha\Delta T$ the fractional density contrast associated with the impressed horizontal temperature gradient, b and a are the radii of the outer and inner side-walls of the annular container and Ω the angular speed of rotation of the container about a vertical axis, where $\Omega^2 b \ll g$. Thus, over a wide range of a second dimensionless parameter, the so-called Taylor number $\mathcal{T} = 4\Omega^2(b-a)^5/\nu^2 d$ greater than about 3×10^5 (where ν is the kinematic viscosity), regular baroclinic waves disappear when $\Theta > \Theta_R(\mathcal{T})$ giving way to axisymmetric flow, and also when $\Theta < \Theta_I(\mathcal{T})$ giving way to a second non-axisymmetric flow, namely irregular (i.e., spatially and temporally aperiodic) baroclinic waves, which constitute a form of geostrophic turbulence. These findings and the tendency for the regular regime to persist at the highest values of $\mathcal{T}$ attained in the experiments, around 10^{10}, show that the high degree of order that character izes the regular regime is due largely to nonlinear effects and not to vis- cosity (thus, incidentally, casting doubt on the ergodic assumption used in theories of atmospheric predictability). As Θ is decreased from Θ_R to Θ_I the dominant azimuthal wavelength λ decreases in steps from about 2 to 0.7 times the radial scale of the waves. When decreases in Θ are achieved by increasing Ω and keeping other parameters fixed the net heat transfer within the range $\Theta_R > \Theta > \Theta_I$ remains roughly constant and some 20% less than that found when $\Omega = 0$ (i.e. $\Theta^{-1} = \mathcal{T} = 0$). Regular waves are intransitive in the sense that several values of λ are possible at a given point $(\Theta, \mathcal{T})$ in parameter space although the most probable value of seems to be uniquely determined by Θ and $\mathcal{T}$. Transitions between differ-

ent values of λ are subject to hysteresis effects the transition to **axisym-**metric flow at $\Theta = \Theta_R$ also exhibits strong hysteresis when the upper surface is free, but not when the surface is in contact with a rigid lid. This result can be interpreted (Hide and Mason, 1978) in terms of the effect of potential vorticity gradients in the main body of the fluid on baroclinic instability of the basic axisymmetric flow.

Recent and current research includes investigations of effects due to non–axisymmetric boundaries and to varying the configuration of the impressed temperature field on the bounding-surfaces of the system (Hignett 1979). It also includes an attempt to construct a numerical model capable of reproducing various phenomena discovered through detailed laboratory studies of non–linear interactions between the main wave and its harmonics and various side-bands (Hide, Mason and Plumb, 1977; James and Farnell, 1977; James and Jonas, 1979), For reasons which are not yet clear, vacillation is less pronounced and more difficult to produce in the numerical model than in a laboratory system. In another recent laboratory study of thermal convection in a rotating fluid annulus, the effect of sloping boundaries on the radial scale of baroclinic waves has been determined (Macfadyen and Mason, 1979).

Baroclinic waves can be produced mechanically (rather than thermally) in a system consisting of two superposed immiscible fluids, and extensive work with such cases has been reported by J. E. Hart. Recent laboratory work with two-layer systems includes studies of side-band interactions, topographic effects and effects due to non-steady forcing (King, 1979; Appleby, 1979). Related theoretical work includes the discovery that the quasi-geostrophic

equations governing weakly nonlinear behavior of the two layer system can be transformed into the complex sine-Gordon equation (Gibbon, James and Moroz, 1979), which has soliton-type solutions. Attempts are now being made to find corresponding soliton solutions for systems with continuously variable density.

The parameterization of heat flow by baroclinic waves is of practical importance in the development of climate models. Several workers have carried out relevant laboratory experiments although much more remains to be done and great care has to be exercised in the interpretation of the experimental results (Pfeffer and Barcilon, 1978; Hide, 1979).

REFERENCES

Appleby, J. C., 1979. Baroclinic waves in a two-layer system subject to a cyclically-varying imposed shear. Internal Report, Geophysical Fluid Dynamics Laboratory, Meteorological Office.

Gibbon, J. D., I. N. James, and I. M. Moroz, 1979. Solitons and the sine-Gordon equation; application to a rapidly-rotating fluid. Proc. Roy. Soc. London A (in press).

Hide, R., 1979. Heat flow by baroclinic waves (in preparation).

Hide, R., P. J. Mason 1978. Thermal convection in a rotating fluid annulus at very high Taylor number: hysteresis effects at the upper transition and instabilities beyond the Eady cut-off. Geophys. Astrophys. Fluid Dyn., 10, 123.

Hide, R., P. J. Mason, and R. A. Plumb, 1977. Thermal convection in a rotating fluid annulus; spatial and temporal characteristics of fully-developed baroclinic waves. J. Atmos. Sci., 34, 930.

Hignett, P., 1979. Experiments on thermal convection in a rotating fluid annulus driven by non-uniform heating from below. PhD. thesis. Geophysical Fluid Dynamics Laboratory, Meteorological Office.

James, I. N. and L. Farnell, 1977. Where have all the side-bands gone? Internal Report, Geophysical Fluid Dynamics Laboratory, Meteorological Office.

James, I. N., and P. R. Jonas, 1979. Combined laboratory and numerical studies of baroclinic waves in a rotating fluid annulus (in preparation).

Julka, J., 1971. Eddy fluxes of heat and temperature variances. M. S. thesis, Florida State University.

King, J. C., 1979. An experimental study of baroclinic wave interactions in a two-layer system. Geophys. Astrophys. Fluid Dyn. (in press).

Macfadyen, M. R. and P. J. Mason, 1979. On the radial scale of fully-developed baroclinic waves in a differentially-heated rotating fluid annulus. (in preparation)

Pfeffer, R. L. and A. Barcilon, 1978. Determination of eddy fluxes of heat and eddy temperature variasn es using weakly nonlinear theory. J. Atmos. Sci., 35, 2099.

ON THE FUZZINESS OF ISOPYCNAL SURFACES AND THE CONSEQUENCES FOR MIXING AND MOVEMENT IN THE DEEP OCEAN

J. G. Shepherd

Careful consideration of the nature of isopycnal movements in the ocean shows that neutral surfaces cannot be unambiguously defined. The presence of both systematic gradients and random (microstructure) variations of temperature and salinity on isopycnal surfaces, ensures that neutral surfaces must be to some extent "fuzzy". As a direct consequence of this fuzziness, transport in the oceans cannot be solely along any unique set of neutral surfaces, but both random (diffusive) and systematic (advective) transport normal to neutral sur-faces must occur. A tentative estimate of the magnitude of these diapycnal effects is made. Both the diapycnal diffusivity and velocity arising from this mechanism can vary greatly from place to place in the oceans. They could be as high as 10 cm^2/sec and 10^{-3} cm/sec in active regions (or even more in the vicinity of fronts) but more normal figures for the deep oceans would be 0.1 cm^2/sec and 10^{-5} cm//sec. In many places such transport rates would represent a significant component of the diapycnal transport.

ICEBERG MELTING: RATES INFERRED FROM OBSERVATIONS AND LABORATORY EXPERIMENTS: AND A TEMPERATURE FIELD MEASURED AROUND A MELTING ICEBERG

Steven Neshyba

A Comparison of Melt Rate Inferred from Observations with Extrapolation from Laboratory Experiments

Morgan and Budd (1978) estimate the average sidewall melt rate of Antarctic icebergs as a function of the mean temperature of the upper 200 m ocean layer around Antarctica. Their method uses (1) reported observations of iceberg concentrations within latitudinal bands and meridional sectors around Antarctica together with (2) iceberg size distribution to obtain (3) the minimum length of bergs which can be dispersed to successive distances from their continental origin. These data are combined with reported estimates of dispersion rate and the field of mean temperature of the upper 200 m layer of Antarctic Ocean to obtain iceberg sidewall melt rate as a function of far-field water temperature. The results are shown in Fig. 1 as a series of points in a melt-rate vs thermal driving domain, the latter variable defined at $T_d = T_{far\ field} - T_{freezing}$.

A plausible interpretation of these point data would be first that their derivation implicitly combines iceberg size erosion by both sidewall melting and by sidewall volume loss by mechanical processes such as calving following erosion by surface waves or fracturing due to stresses induced by flexure or thermal shock. Thus a curve fitted to these data points need not pass through zero value at zero T_d; to the contrary, the zero T_d intercept value is logically a measure of mechanical wastage in the absence of, or independent of, the thermal melting. Second, thermal melt rate is likely to show a non-

linear dependency upon thermal forcing because the heat transfer from ocean water to the vertical ice wall is by turbulent diffusion since the Grashoff number typical of large vertical ice walls is extremely high, of order 10^{18}. Accordingly, we fit a quadratic curve to the observed data points (Fig. 1a) and translate the curve to the origin under the assumption that mechanical wastage is independent of thermal driving (Fig. 1b). This interpretation yields a mechanical wastage rate of *40* m yr^{-1}; a sidewall thermal melt rate of equal magnitude is found only for icebergs subjected to seawater whose thermal driving is $7°C$ or more. Considering that Antarctic surface waters south of the Polar Front are at lower temperatures than $7°C$, one infers that the dominant process of iceberg size deterioration is mechanical rather than thermal.

On the other hand, several laboratory experiments on the melting of ice are reported (Sandstrom, 1914; Huppert and Turner, 1978; Josberger, 1979) and a comparison of results with those given above should be made. The Josberger data were obtained in cold but unstratified saline water, conditions which approximate the upper layer conditions in the Antarctic where stratification is very weak. He found a dependency of melt rate upon the *1.63* power of T_d and the 1/4 power of distance above the bottom of the melting ice block. In Fig. 1, curve M shows his average sidewall melt rate and curve M_{200} is an extrapolation to the typical *200* m draft iceberg wall. These data are obtained with bubble–free ice. Characteristically, glacier ice contains an average of about *200* air bubbles per cc of ice; these vary in diameter from about 1 mm near the ice surface to about *0.3* mm at *250* m ice depth, the latter reflecting adjustment to hydrostatic pressure. Upon release during melting these bubbles contribute to the buoyant forcing within the melt–water diluted and vertically

convected boundary fluid adjacent to the ice wall; in magnitude, the additional buoyant forcing by bubbles exceeds that due to dilution by melt water at levels higher than about 150 m above the base of the iceberg (Josberger, 1979b). In Fig. 1c the M_{200} curve of melt rate has been adjusted for the bubble effect, using the criterion that turbulent heat transfer across a vertically convecting boundary layer scales with the third root of the buoyant forcing (Chapman, 1960).

Curves (b) and (c) in Fig. 1 are coincident within the errors of laboratory experiments and field observations from which they derive, a result which suggests that these are accurate estimations of ice wall melt rates under varying ambient thermal conditions. So far only one independent check point is available; this is marked by an asterisk in Fig. 1 and is a result of measurement of the subsidence of an iceberg which froze fast to pack ice in D'Iberville Fjord, Northwest Territory, Canada, at the beginning of the winter season and gradually distorted the surface of the pack ice as its submerged portion melted (D. Topham, personal communication).

Measurements of the Temperature Field around a Grounded Iceberg

In an effort to quantify melt rate of real icebergs we have begun a field project with the objectives of (1) estimating melt rate by assessing the thermal field around an iceberg and (2) establishing the nature of the convection layer adjacent to a large vertical wall of glacier ice in sea water. In June 1979 we obtained a series of XBY profiles close to a grounded iceberg in Conception Bay, Newfoundland, and a sampling of these is given in Fig. 2. The iceberg was grounded in 100 m of water and extended 35 m above the sea surface; at water line it extended about 135 m in length and 80 m in width. The berg is sketched in Fig. 2a along with the approximate locations of the casts whose profiles of temperature are compared in Fig. 2b; this line of
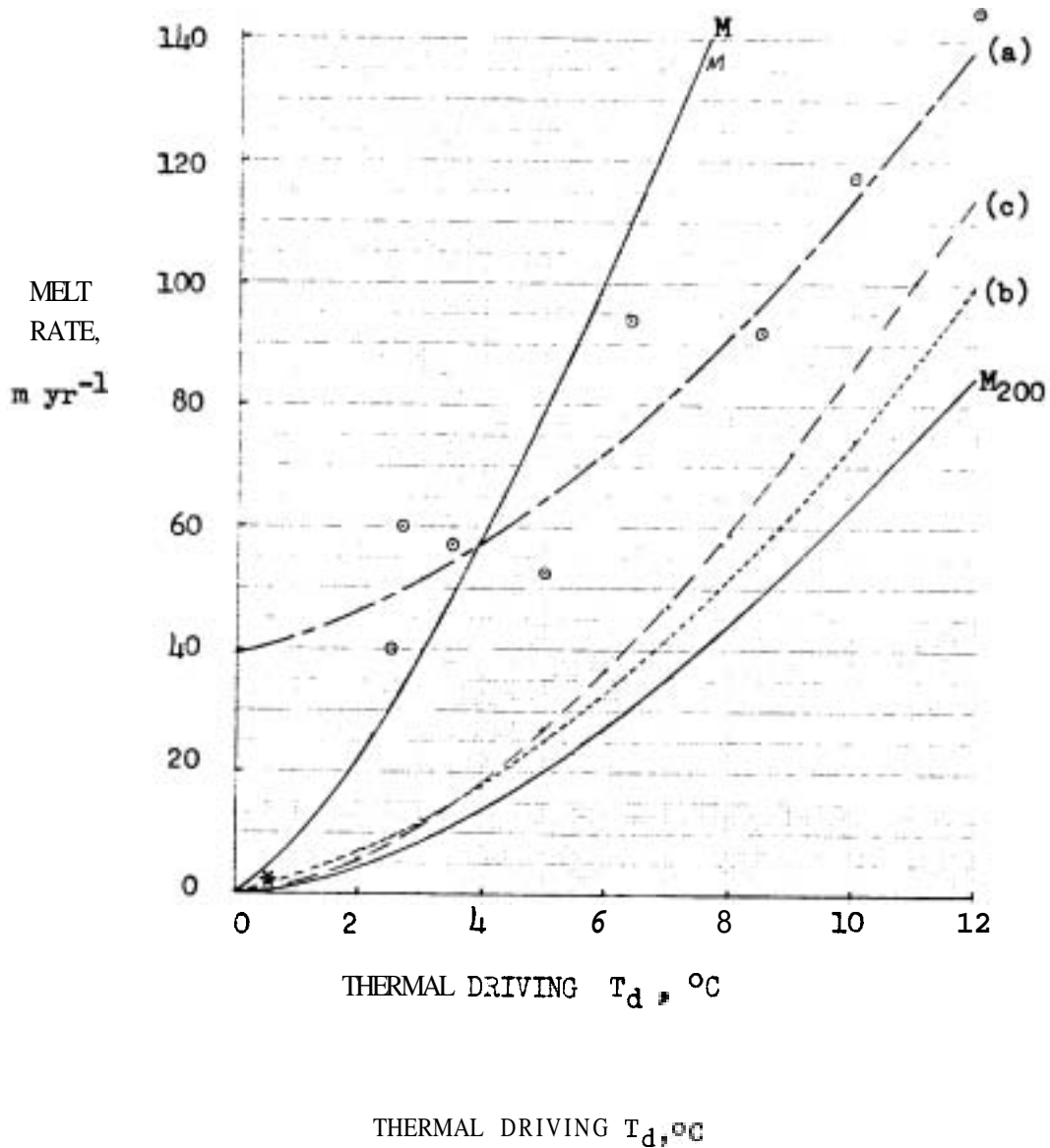
Fig. 1. Estimates of iceberg melt rates as a function of thermal driving:

⊙   from Morgan and Budd (1978).

M   unweighted average melt rate from Josberger (1979a).

M_{200} weighted average melt rate for iceberg of 200 m draft.

(a)   quadratic regression to M&B data: $y = 39.29 + 2.78T_d + 0.47T_d^2$.

(b) regression line transposed to zero melt at zero thermal driving.

(c) M_{200} modified for effects of bubble discharge from glacier ice.

※   Field observation of melt rate of an Arctic iceberg in D'Iberville Fjord, Northwest Territory, Canada (D. Topham, pers. comm.).

casts coincided roughly with axis of a low temperature surface feature which is assumed to have been the plume.

Casts 4 and 5 are respectively within 50 and 100 m of the iceberg. The profiles are quite similar in structure and both show (1) sharp vertical gradients at the 29 and 22 m levels and (2) temperature inversions in the 60 to 80 m zone. The profile at cast 7,300 m from the berg, is considerably smoother above the 40 m level, suggesting that the sharp gradient zones of casts 4 and 5 reflect convection cells which weaken with distance from the berg. The inversion at 60 m, on the other hand, is present in both casts 7 and cast 1, the latter taken about 4 km from the berg and on the other side from casts 4, 5, and 7 and is assumed to be representative of the far field structure of temperature in this bay. This suggests that the deeper inversions are unrelated to the iceberg melt. It is clear that the average temperature above the 50 m level is successively higher with distance from the iceberg, a result found in each of five series of casts along different radii from the iceberg. However, the calibration of our instrument was not adequate for accurate assessment of the caloric contents of the water columns sampled in successive casts.

Summary

The fact that estimates of melt rate of icebergs obtained from global scale observation statistics and by extension of laboratory results agree as well as these suggests confidence in the results. Melt rate from 5 to 20 m yr^{-1} would be typical of Antarctic icebergs south of the Polar Front; 10 to 50 m yr^{-1} would be expected of icebergs in the Labrador Sea. These estimates should be checked by field measurements but the process will be a difficult one. A somewhat surprising outcome of this analysis is that the dominant iceberg deterioration is not by melting but rather due to mechanical
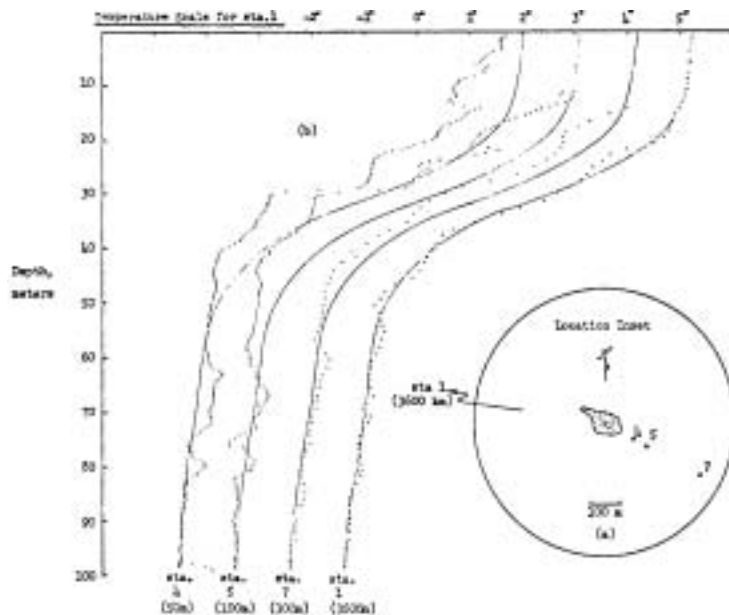
Pig. 2 XBT profiles of temperature taken near a grounded iceberg in Conception Bay, Newfoundland June 9, 1979. Station 1 represents the far-field profile; the solid curves are the smoothed station 1 profile superposed over other station profiles to show surface water, cooling near the iceberg.

REFERENCES

Chapman, A. J., 1960. Heat Transfer. Macmillan, London.

Huppert, H. E. and J. S. Turner, 1978. On melting icebergs. Nature, 271, 46-8.

Josberger, E. G., 1979a. Laminar and turbulent boundary layers adjacent to melting vertical ice walls in salt water. PhD. thesis, Univ. of Washington.

Josberger, E. G., 1979b. The effect of bubbles released from a melting ice wall on the melt-driven convection in salt water. Conf. Iceberg Dyn., Memorial Univ. of Newfoundland.

Morgan, V. I. and W. F. Budd, 1978. The distribution, movement and melt rates of Antarctic icebergs. Proc. First Intl. Conf. Iceberg Util; A. A. Husseiny ed. Pergamon Press.

Sandstrom, J. W., 1914. The hydrodynamics of the Canadian Atlantic Waters. Can. Fish. Expedition 1914-1915, Dir. of Fisheries for Norway.

INEQUALITIES AND VARIATIONAL PRINCIPLES
FOR TURBULENT DOUBLE DIFFUSION

Melvin E. Stern

An inequality pertaining to the energetics of the boundary layer in turbulent channel flow has been previously proposed (Stern, 1979) and generalized to the problem of turbulent thermal convection. The inequality is generalized further and applied to the double-diffusive convection problem (Linden and Shirtcliffe, 1978), wherein a semi-infinite layer of hot, salty water lies below a layer of lower density. The inequality implies that the smallest salt/heat flux ratio equals the square root of the ratio of molecular diffusivities. Comparison of this bound with experiment is given, and suggestions are made for further exploration of this line of turbulence theory.

REFERENCES

Linden, P. F. and T.G.L. Shirtcliffe, 1978. The diffusive interface in double-diffusive convection. J. Fluid Mech., 87, 417-432.

Stern, Melvin E., 1979. Inequalities and variational principles for turbulent transport. J. Fluid Mech., 91, (3), 513-540.

SOME IRREGULAR OSCILLATORS

Louis N. Howard

The suggestion of E. N. Lorenz (1963) that severely truncated models of thermal convection, whose behavior is described by autonomous systems of ordinary differential equations of order as low as three, may help us to understand better questions of predictability in meteorology which has in the past few years brought the remarkable properties of some such systems to the attention of geophysical fluid dynamicists. Indeed, Lorenz's penetrating investigation of one such system (actually suggested earlier by Platzman), which

showed that many of its solutions have an irregular character reminiscent of some features of turbulent flow, together with subsequent other studies (e.g., Baker, et al., 1971; Robbins, 1976), have raised hopes that at least some aspects of turbulence itself can be seen in such simple systems. This work has also attracted the interest of various mathematicians interested in the qualitative theory of differential equations (e.g., Guckenheimer, 1976).

That simple differential equations can have remarkably irregular solutions was already pointed out by Cartwright and Littlewood (1945) for the forced van der Pol equation, and particularly clearly by Levinson (1949).

Levinson considered the equation

$$\epsilon \ddot{x} + \phi(x)\dot{x} + \epsilon x = b \sin t$$

where

$$\phi(x) = \begin{cases} -1 & |x| < 1 \\ 1 & |x| > 1 \end{cases} \quad , \qquad \epsilon \text{ is small,}$$

and b is chosen from a certain set of intervals in $(0,1)$.

The behavior of solutions to this equation in the case b = 0 is particuiarly easy to understand if the equation is replaced by the equivalent system $(x_1 = x)$:

$$\epsilon \frac{dx_1}{dt} = x_2 - \Phi(x_1) - b\cos t$$

$$\frac{dx_2}{dt} = -\epsilon x_1$$

where

$$\Phi(x_1) = \int_0^{x_1} \phi(x)dx .$$

The graph of the curve $x_2 = \Phi(x_1)$ in the x_1, x_2 plane is shown in Fig. 1.
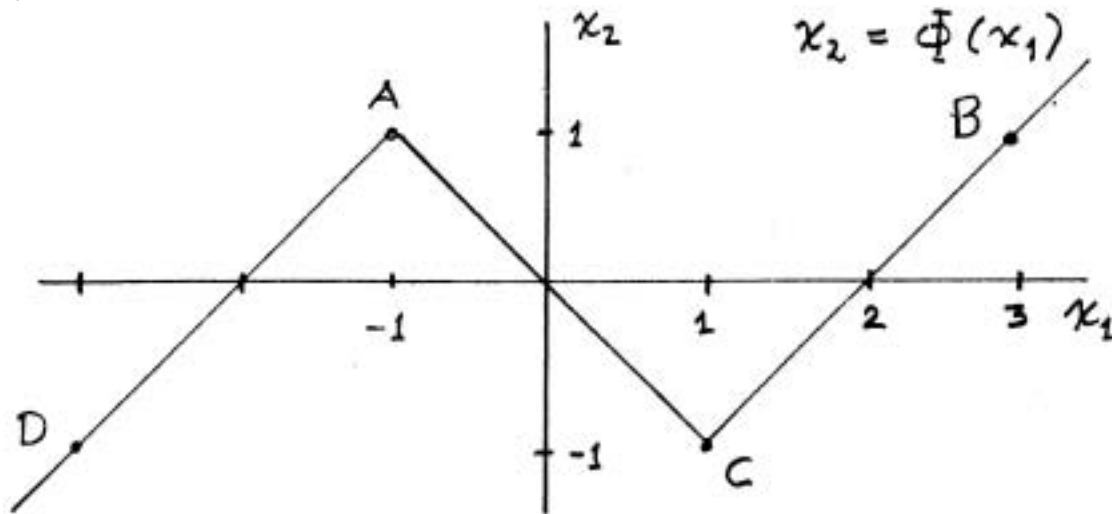

Figure 1.

Evidently, (when $b = 0$), if the phase–point is above this curve, the trajectory moves rapidly to the right, and only very slowly vertically, because $\varepsilon \; (>0)$ is small. Likewise, if it is below, it moves rapidly to the left. Thus, a trajectory starting practically anywhere is very soon attracted to one or the other of the upward sloping portions of the curve, where $x_2 = x_1 - 2$ if $x_1 > 0$, and $x_2 = x_1 + 2$ if $x_1 < 0$. If the trajectory reaches, say, the righthand portion this way it is forced (by the first equation) to remain near $x_1 = x_2 + 2$ so long as $x_2 > -1$; however, with $x_1 > 0$, x_2 will slowly decrease (cf. the second equation), essentially as a solution of the equation

$$\frac{dx_2}{dt} = - \varepsilon(x_2 + 2)$$

Thus, after a long but finite time, (of order $1/\epsilon$). x_2 will be reduced past -1, and the trajectory will then rapidly move across to the lefthand upward sloping portion of the curve $x_2 = \Phi (x_1)$, where $x_1 = x_2 - 2$. x_2 then slowly increases, essentially as a solution of

$$\frac{dx_2}{dt} = \epsilon (2 - x_2)$$

until after another long but finite time it reaches +1 and the trajectory snaps across to the neighborhood of the point $(3,1)$. It is clear from this description (and easily proved rigorously) that all solutions of the equation except the (unstable) critical point at the origin rapidly approach a stable limit-cycle whose trajectory is approximately a parallelogram with vertices at the points marked ABCD in the Fig. 1. The horizontal portions AB and CD are traversed rapidly, while BC and DA are traversed slowly.

It is now fairly easy to describe approximately the behavior of solutions, plotted in the x_1, x_2 plane, when the forcing term is included (it is helpful to think of b as a rather small positive number). If we start, say, at $t = 0$ with $x_1 = 0$, and x_2 near 1, the phase-point will move rapidly to the right until the righthand side of the first equation is nearly zero, which, since t will have changed little from 0, will be approximately where $x_2 = x_1 - 2 + b$, i.e., near $x_1 = 3 - b$. Now the phase point moves gen-erally down the segment BC as before, except that the forcing term causes it to ocillate back and forth, nearly parallel to the x_1 axis, as it does so, following essentially the curve $x_2 = x_1 - 2 + b \cos t$, or $x_1 = x_2 - b \cdot \cos t$. A sketch of such a path is shown in Fig. 2.
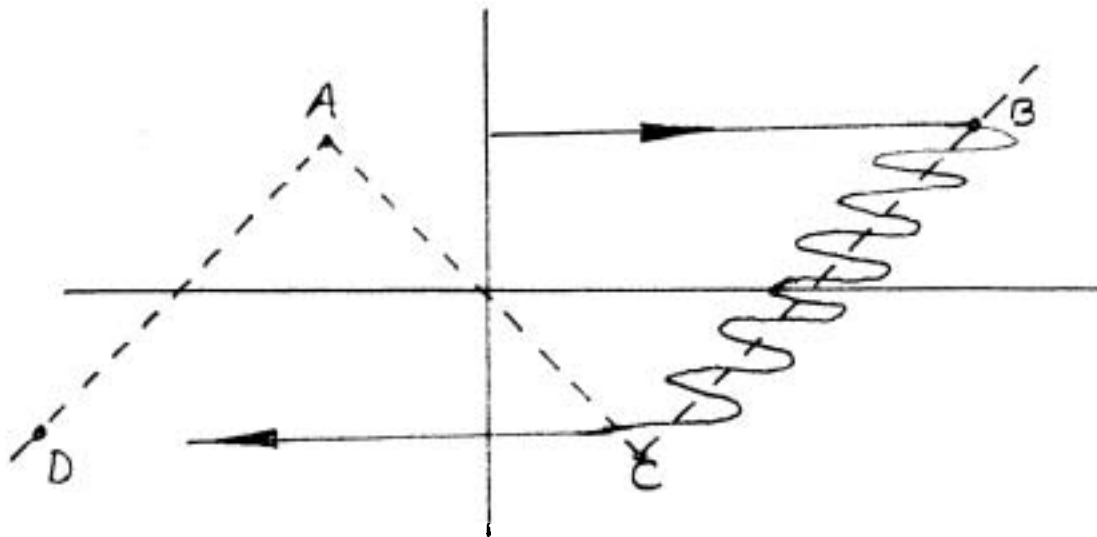
Figure 2

As x_2 approaches -1, there will be a time, normally close to an even integral multiple of π (at these times the excursion to the left produced by the forcing term is largest, as one sees from the formula $x_1 = x_2 + 2-b \cos t$), at which the trajectory once again enters a 'fast' phase, and jumps across to a point near -3, -1. After this the trajectory wiggles its way up the lefthand segment near DA in Fig. 1, and at some time near an odd integral multiple of π, x_1 will undergo another up-jump to the neighborhood of the point B again.

Now it is evident that trajectories which start at $x_1 = 0$ and x_2 near 1, at a time $\tau > 0$ but small, will be close to the one just described until the neighborhood of C is approached, but that then the time at which the down-jump occurs is likely to depend very sensitively on the initial conditions. This is because a small change in initial conditions can easily advance by one cycle the time at which the down-jump occurs. Levinson shows, by a somewhat lengthy analytical argument, that if b is chosen from a certain set of intervals contained in $(0,1)$ that this is in fact the case, and that some

trajectories crossing $x_1 = 0$ at a time in a short interval just to the right of $t = 0$ and with x_2 near 1 will cross $x_1 = 0$ going down at approximately $t = (2 n-2) \pi$, say, for a certain integer n, while others will do so at $t = 2 n \pi$. In fact, with suitable restrictions on τ and the initial value of x_2 only these two approximate times of down-jump occur. He then shows that of those trajectories which jump down near $(2 n-2) \pi$, some will reach the next up-jump at approximately $(4 n-3) \pi$, while others reach it at $(4 n-1) \pi$; of those which jump down near $2n \pi$, some jump up again near $(4 n-1) \pi$ and others near $(4 n+1) \pi$. Thus the interval between up-jumps and down-jumps is always near $(2 n-1) \pi$ or $(2 n+1) \pi$. Furthermore, Levinson shows that for *any* sequence a_k of -1 and $+1$, it is possible to find an initial value of x_2 and a τ , satisfying the "suitable restrictions" mentioned above, for which the successive intervals between up and down-jumps are spaced approximately by $(2n + a_k) \pi$. All of these solutions remain bounded, but since there are uncountably many sequences of -1 and $+1$ which are not periodic, most of these solutions of the differential equation are not periodic, and indeed not even anywhere near periodic.

Levinson shows also that the same conclusions can be drawn if the discontinuous function is replaced by a suitable smooth approximation, which may be, for instance , a polynomial.

It was in an attempt to understand Levinson's example in a more geo-metrical and more general context that Smale (1965) later invented the idea of the "horseshoe map". Levinson's example is a non-autonomous two-dimensional system, but it can be replaced by an autonomous three-dimensional system by introducing a new variable x_3 and writing:

$$\epsilon \frac{dx_1}{dt} = x_2 - \phi(x_1) - b \cos x_3$$

$$\frac{dx_2}{dt} = -\epsilon x_1$$

$$\frac{dx_3}{dt} = 1$$

In this form the trajectories do not remain bounded, but if x_3 is regarded as an angle rather than a number (which is appropriate since it only really enters as the argument of cosine), then they remain bounded. The 'phase space' of x_1, x_2, x_3 is no longer the Euclidean R^3, but the cartesian product of R^2 and a circle; however, this is of no great consequence apart from a minor difficulty in visualizing it. Solutions to the original problem starting at $x_1 = 0$ with various values of x_2 near 1 and at times $\tau \gtrless 0$ but near zero, which were mentioned briefly before, can now be regarded as solutions to this autonomous system starting at $t = 0$ on $x_1 = 0$ with values of x_2 near 1 and with $x_3 = \tau$ (i.e., x_3 an angle whose numerical measure is τ, or $\tau \pm 2 m\pi$). These solutions have trajectories in the phase-space which return after awhile to $x_1 = 0$, some of them with x_2 near -1 and x_3 in the first quadrant near 0; of these some return to $x_1 = 0$ (with x_1 now decreasing instead of increasing as at first) after x_3 has gone n-1 times around its circle, and others after n times around. Similarly, after a while some of the trajectories once again return to $x_1 = 0$ (now increasing again) with x_2 near 1 and x_3 again in the first quadrant near zero, after an additional n-1 or n revolutions in x_3. It was essentially by investigating these two successive mappings from parts of $x_1 = 0$ into itself, and subsequent iterations thereof, exploiting the splitting associated

with the n −1 and n revolutions of the angle x_3, that Levinson obtained his

results.   Smaie's horseshoe map is an abstraction (somewhat simplified) of

this idea.   We consider a one-to-one continuous mapping (homeomorphis m) of a

portion of some plane into this plane, which carries a (closed) rectangle onto

a horseshoe−shaped region which intersects the original rectangle in two
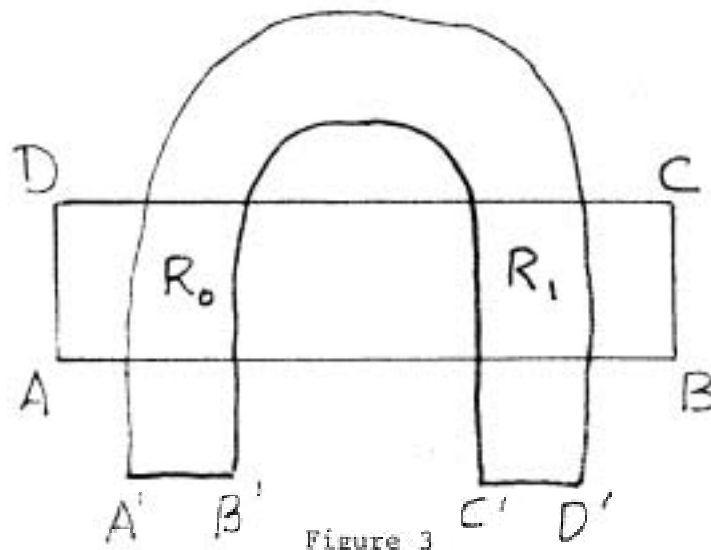
pieces, as shown in Fig. 3.

Figure 3

This mapping is to have the feature that the original rectangle is <u>contracted</u>

in the horizontal direction (parallel to AB and DC) and <u>expanded</u> in the verti-

cai direction (parallel to AD and BC), then being bent around into the horse−

shoe shape.   (Levinson's example, though similar, is somewhat more complicated;

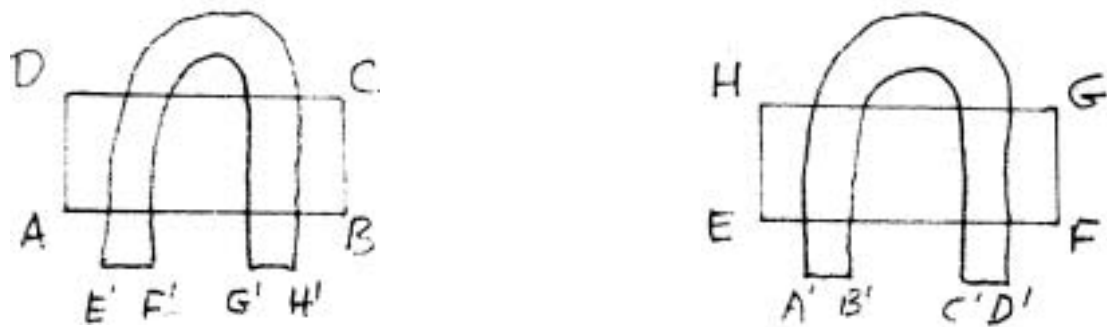it is more like the picture shown in Fig. 4).

Figure 4

Let the original rectangle ABCD be called R and the horsehoe T(R), and let the two pieces in which they intersect be R_o and R_1, as in Fig. 3. R_o can be regarded as a part of R; as such it is a strip joining AB to DC. Thus $T(R_o)$ is a thin horseshoe inside T(R) joining A'B' to D'C'. $T(R_1)$ is another such thin horseshoe -- see Fig. 5.
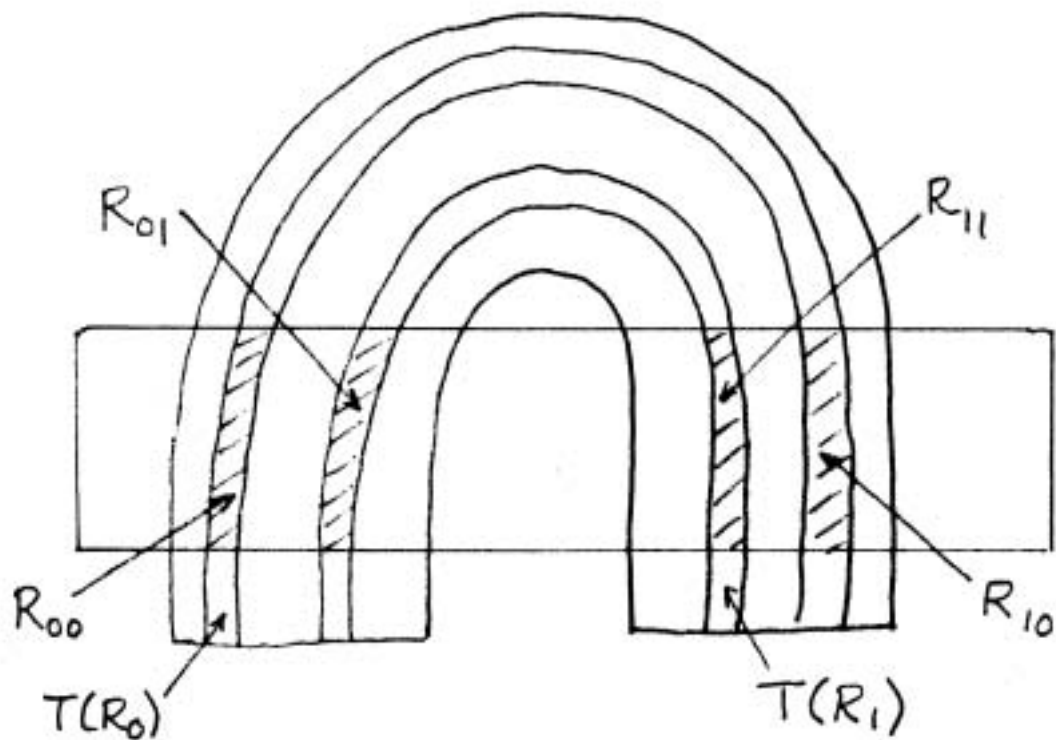

Figure 5

Let $R_0 \cap T(R_0) = R_{00}$, $R_1 \cap T(R_0) = R_{10}$, $R_0 \cap T(R_1) = R_{01}$ and $R_1 \cap T(R_1) = R_{11}$. We can proceed in this manner to consider the still thinner horseshoes $T(R_{ij})$ and their intersections $R_{0ij} = R_0 \cap T(R_{ij})$ and $R_{1ij} = R_1 \cap T(R_{ij})$ with R_0 and R_1, and so on, obtaining thinner and thinner "vertical" strips R_Δ labelled by finite binary sequences Δ. Note that if the sequence Δ is regarded as made of two pieces, $\Delta = \Delta_1 \Delta_2$, say, then $R_{\Delta_1 \Delta_2} \subset R_{\Delta_1}$. This can be seen for instance by induction on the length of Δ_1 ($R_{0\Delta_2} = R_0 \cap T(R_{\Delta_2}) \subset R_0$ and $R_{1\Delta_2} = R_1 \cap T(R_{\Delta_2}) \subset R_1$, hence true if Δ_1, contains just one symbol; if $R_{\Delta_1 \Delta_2} \subset R_{\Delta_1}$ for sequences Δ_1, of length N, then $T(R_{\Delta_1 \Delta_2}) \subset T(R_{\Delta_1})$ so $R_{0\Delta_1\Delta_2} = R_0 \cap T(R_{\Delta_1 \Delta_2}) \subset R_0 \cap T(R_{\Delta_1}) = R_{0\Delta_1}$ and likewise for $R_{1\Delta_1\Delta_2}$, hence true for sequences Δ_1, of length $N+1$). Also for any sequence $k\Delta_1$ of length $N+1$, say, ($k = 0 \text{ or } 1$, Δ_1 a sequence of length N) $R_{k\Delta_1} \subset T(R_{\Delta_1})$

Ultimately we obtain a set of infinitely thin strips (vertical arcs), R_Δ, one for each <u>infinite</u> binary sequence Δ; R_Δ is contained in each R_f where f is a finite sequence obtained from Δ by omitting some "tail", and is in fact, the intersection of the decreasing sequence of closed sets R_{f_N}, where f_N consists of the first N terms of Δ. Evidently, $R_{k\Delta} \subset T(R_\Delta)$ also for infinite binary sequences Δ ($k = 0 \text{ or } 1$). Thus any point on a vertical arc $R_{k\Delta}$ has as its inverse image under T a point on the arc R_Δ, i.e., the arc labelled by the original sequence with its first symbol omitted. Thus the set of all the vertical arcs is invariant under T^{-1}.

Now the original regions R_0 and R_1 can be thought of as parts of $T(R)$ as well as as parts of R, and as such they are "horizontal" strips joining $A'D'$ to $B'C'$. Thus $T^{-1}(R_0)$ and $T^{-1}(R_1)$ are thin horizontal

strips in R joining AD to BC ; the intersections of these with R_0 and $\overline{R}_1$ give horizontal sub–strips of R_6 and R_1 , which we call $_{ij}R$, writing the subscripts on the left of the symbol R ; see Fig. 6. Continuing to further inverse images we generate $_{ijk}R = R_{R} \; T^{-1}(_{ij}R)$, and so on, analogously to the previous construction. Ultimately we obtain a set of <u>hori</u>-<u>zontal</u> arcs, one for each left–going infinite binary sequence $_{t_2 t}R$.
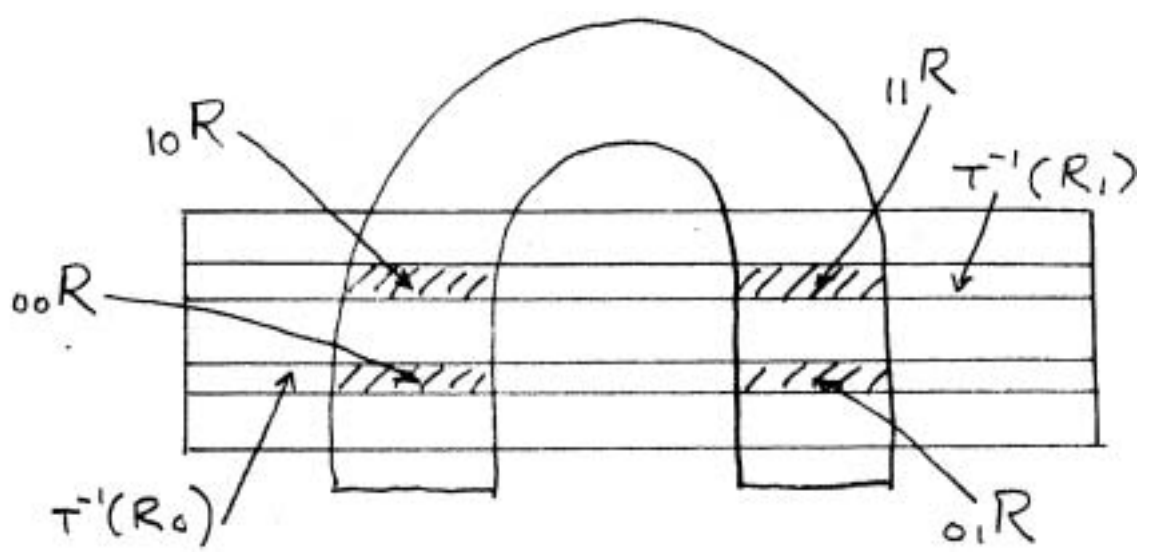

Figure 6

In this case we have $_{t_2 t_1}R \subset _{t_1}R$ and $_{sk}R \subset T^{-1}(_s R)$ $(k = 0 \text{ or } 1)$. Thus the set of all horizontal arcs is invariant under T, and any point on a horizontal arc $_{tk}R$ has as its image under T a point on the arc $_{t}R$.

Now consider a horizontal arc $_{tk}R$, $k = 0$ or 1 , and a vertical arc R_{js} . If k and j are the same, $_{tk}R$ and R_{js} intersect in a point in R_k , but if they are different $_{tk}R$ and R_{js} do not inter-sect at all. Thus the set C of intersections of horizontal and vertical arcs (which has the nature of a Cantor set) is made up of points which may be labelled by doubly infinite binary sequences with a distinguished element:

$t_k R \cap R_{k \ell}$ is specified by $t \underline{k} \ell$, the underline marking the element which is the right−most symbol in the sequence specifying the horizontal arc and the ieftmost in that for the vertical arc. Evidently C is invariant   under both T and $^{-1}$. Although R_0 and R_1 may well contain   many points for which repeated iterations of T and T^{-1} are not defined , they do contain the uncountable set C to which any number of such iterations may be applied.

Now consider a point $t \underline{k} \ell$ in C. Since it lies in $t_k R$, its image under T lies in $t R$, so if $t = t_i j$, $T(t \underline{k} \circ) = t_i \underline{j} \ell_1$, for some ℓ_1 . But since $t_i j \ell_1$ lies on $R_{j \ell_1}$, its inverse image (which is $t \underline{k} \ell$) must lie on R_{ℓ_1} , so in fact $\ell_1 = k \ell$. Thus $T(t_i j \underline{k} \ell)$ $= t_i \underline{j} k \ell$, i.e. the action of T on points of C can be described very simply in terms of their labels as a <u>shift</u> to the left of the underline by one symbol. The action of T^{-1} is similarly described as a shift to the right.   (Such transformations on doubly infinite sequences are sometimes called "Bernoulli Shifts.").   doubly infinite(marked) sequence is evidently then a periodic

A point of C corresponding to a <u>periodic</u>∧point of T; in particular ...○○○··· and ...|||||\... are fixed points,...|○|○|...is a point of period 2 etc. Thus C contains periodic points of <u>all</u> orders. However, since most sequences are <u>not</u> periodic, most points in C are not periodic.

To apply these ideas to differential equations, one imagines the mapping T to be obtained by taking a plane section (transverse to trajectories) in the phase space of a three−dimensional autonomous system, starting with some initial conditions in this section, and integrating the equation until the phase−point once again enters the section. Assuming this happens, this de− fines a mapping ("Poincaré Map") from the section, or part of it, to itself. If it turns out that this maps a "rectangle" into a "horseshoe" with the appropriate contraction and expansion properties, then one may conclude

that there must be an uncountable set C of initial conditions in the section, through which pass orbits bounded for all **t** on $(-\infty, \infty)$. Among these orbits are many different periodic orbits, but most of them are aperiodic.

Actually **it** is not necessary to havn the whole horseshoe; if one can show that T carries two "horizontal" strips into two vertical ones, each of which crosses both of the original ones, and that horizontal contraction and vertical expansion occur, then once again one gets a Cantor set on which T acts like a Bernoulli shift. If there are N horizontal strips crossing N vertical ones, the same general picture holds except that the sequences are not binary but contain N different symbols. These ideas provide one of the few available methods for demonstrating the existence of irregular oscillations in differential equations, but **it** is clear from the many "ifs" in the above that actually finding a horseshoe map in a particular case of a differential equation given by formulas -- especially one you are interested in for some other reason -- is not likely to be easy. For "practical purposes", and with sufficient attention to the numerical analysis also for proving things, this might in principle be done by numerical construction of the Poincaré map, explicitly exhibiting the "horizontal" and "vertical" strips. This does not appear to have been done much yet, but seems to have some real interest in certain applied problems. An example is given in (Kopell & Howard, 1980), where also singular perturbation methods are used to demonstrate the required properties of the Poincaré map. The contraction and expansion properties (in the mathematicians' terminology, the existence of a "hyperbolic structure on the tangent bundle") arise in that example because the trajectories of interest pass close to a saddle point. In that example **it** was, in fact possible, by choosing the small parameter of the singular perturbation small enough, to obtain a Bernoulli shift on as many symbols as desired.